PRECLINICAL ASSESSMENT OF NANOPARTICLE AND NEURAL STEM CELL-BASED THERAPIES IN ISCHEMIC STROKE

by

ERIN ELIZABETH KAISER

(Under the Direction of Franklin Delano West)

ABSTRACT

Although the National Institutes of Health and American Heart Association (AHA) have committed millions of dollars in research funding over decades, with AHA funding 838 new research endeavors worth more than $188.7 million in 2018-2019 alone, only two Food and Drug Administration (FDA)-approved therapies are available to stroke patients. Recently, transplanted induced pluripotent stem cell-derived neural stem cells (iNSCs) have shown particular therapeutic promise as these cells led to decreased ischemic lesion volumes and improvements in behavioral and sensorimotor functions by integrating into host neural circuitry and secreting trophic factors, thus replacing lost neural tissue and promoting endogenous protective pathways. To facilitate these effects, administration of a neuroprotectant agent prior to iNSC transplantation may be warranted to quail the cytotoxic stroke environment leading to increased cell survival and engraftment. Tanshinone IIA (Tan IIA) treatment has shown both antioxidative and anti-inflammatory effects in stroke and limits blood-brain barrier breakdown leading to improved outcomes in rodent models and human patients. An alternative agent, neural stem cell-derived extracellular vesicles (NSC EVs), may also ameliorate the secondary

injury cascade by modifying the activation of microglia and the release of inflammatory cytokines through the transfer of microRNAs and proteins. Individually, these neuroprotective agents have induced reductions in lesion size, hemorrhage, white matter damage, and functional deficits. However, further investigation in a large animal model with comparable anatomy and physiology to humans is warranted. Preclinical testing in a pig model may provide critical insight into iNSC, Tan IIA, and NSC EV therapeutic efficacy to determine if these treatments are suitable for translation into human clinical trials.

INDEX WORDS: Brain ischemia, Large animal model, Pig, Induced pluripotent stem cells, Neural stem cells, Tanshinone IIA, Extracellular Vesicles, Neural repair

PRECLINICAL ASSESSMENT OF NANOPARTICLE AND NEURAL STEM CELL-BASED THERAPIES IN ISCHEMIC STROKE

by

ERIN ELIZABETH KAISER

B.S.A, University of Georgia, 2013

A Dissertation Submitted to the Graduate Faculty of The University of Georgia in Partial Fulfillment of the Requirements for the Degree

DOCTOR OF PHILOSOPHY

ATHENS, GEORGIA

2019

PRECLINICAL ASSESSMENT OF NANOPARTICLE AND NEURAL STEM CELL-BASED THERAPIES IN ISCHEMIC STROKE

by

ERIN ELIZABETH KAISER

Major Professor:	Franklin D. West
Committee:	Elizabeth W. Howerth
	Simon R. Platt

Electronic Version Approved:

Ron Walcott
Interim Dean of the Graduate School
The University of Georgia
December 2019

ACKNOWLEDGEMENTS

I would like to thank my parents for assisting me in all of my academic endeavors. Every child grows up being told “you can be anything you want”, but you two made this dream a reality. Your collective hard work and sacrifices have provided me with more opportunities than I will ever be able to thank you for. Your unequivocal love and encouragement over the past twenty-nine years have proven to be invaluable to me as both your daughter and now as a doctor. Dad, thank you for being a continuous reminder of what can be accomplished with hard work and determination. Mom, thank you for your unwavering patience and wisdom through all of life’s ups and downs. To my brother Andrew, thank you for allowing me to coerce you into whatever scheme I had conjured up when we were kids and for being my trusted confidant now that we are grown. To my horse Brooke, thank you for always putting things into perspective and for teaching me the meaning of unconditional love. To Michael, thank you for always knowing what to say to bring a smile to my face and for being my rock at every opportunity.

I would also like to thank my committee Dr. West, Dr. Howerth, and Dr. Platt. Frank, I do not know how I will ever thank you enough for taking a chance on me all those years ago (it must have been Dr. Kinder’s salesmanship). Your guidance as a mentor has shaped me into a resourceful and ambitious scientist also known as “Wonder Woman”. Thank you for always having my back, even when it involved wrestling a pig out of a poop pit, and for always knowing what to say when my experiments went awry. I would not be where I am today without your support. Dr. Howerth and Dr. Platt, thank

you for investing your valuable time and expertise into my educational development. It has meant so much to me and your kindness will not be forgotten. Dr. Howerth, thank you for being so patient with my endless questions and naïve understanding of pathology. Dr. Platt, thank you for expanding my surgical skill set as well as my veterinary and magnetic resonance expertise.

I would also like to thank Dr. Kinder and Dr. Baker for supporting me through my first few years of graduate school. Although I relentlessly teased you about your "Homily" mannerisms, you two made this journey fun and together we had a good run as the "Golden Girls". To my West lab girls, I do not know how I would have made it this far without you. I will always remember our West lab days of fun, lunch dates, pranks, and family trips to conferences. We have shared so many laughs and tears, it is hard to imagine what this journey would have been without you. I will miss you very much and I wish all of you nothing but future success and statistical significance.

TABLE OF CONTENTS

Page

CHAPTER 1

INTRODUCTION

In patients experiencing a large vessel acute ischemic stroke, 120 million neurons, 830 billion synapses, and 714 km (447 miles) of myelinated fibers are lost each hour [1]. Compared to the rate of neuronal loss associated with normal aging, ischemic stroke ages the brain 3.6 years each hour patients go without clinical treatment [2, 3]. Lack of vital oxygen and nutrients to cerebral tissues due to an arterial blockage results in cellular death, neurological deterioration, functional impairments, thus substantial efforts have been made to develop new neuroprotectants that are capable of reducing cerebral damage [4]. Patient reperfusion potentials are largely dependent on 1) the duration of vascular occlusion (<4.5 hours), and 2) intracerebral/systemic hemorrhagic risk factors [5, 6]. Given these restrictions, tissue plasminogen activator (tPA) is received by 2-5% of patients [7]. Mechanical thrombectomy is associated with a number of intra-procedural complications including vasospasm, arterial perforation, hemorrhage, pseudoaneurysm, and post-operative infection [8]. These risk factors highlight the need for safer and more inclusive patient treatment options that not only prevent further tissue damage, but also possess regenerative potential.

A potential opportunity to hasten the speed at which novel therapeutics are developed is through the use of translational animal models that are predictive of the human condition. Animal models are an indispensable tool for the preclinical assessment of potential therapies due to the following reasons: 1) Human ischemic stroke is diverse

in its progression, localization, and severity whereas experimental stroke conditions are controllable with well-characterized and repeatable infarctions, thus allowing for more precise analysis of stroke pathophysiology and drug effects; 2) molecular, cellular, and biochemical physiological investigations often require invasive access to brain tissue; 3) collateral vascularization and reperfusion rates cannot be modeled in in-vitro models [9]. Rodent stroke models offer many translational advantages including low cost, a well-characterized physiological database, and the ability to investigate knockout genes and co-morbidities in conjunction with ischemic stroke pathologies. Specifically, middle cerebral artery occlusion (MCAO) rodent models have been found to be highly reproducible with penumbra development, controllable reperfusion, and preservation of the cranium and intracerebral dynamics [10]. Consequently, these rodent MCAO stroke models are an invaluable tool for the initial screening and testing of novel therapies.

Recently, intracerebral transplantation of stem cells has been considered a promising approach for treating stroke. Specifically, transplanted induced pluripotent stem cell-derived neural stem cells (iNSCs), have shown particular promise as these cells could be obtained from the stroke patient, thus avoiding both ethical concerns and the need for immunosuppression [11]. In a rodent model of ischemic stroke, iNSCs functionally integrated into host neural circuitry and differentiated into neurons, astrocytes, and oligodendrocytes at the site of injury [12, 13]. iNSC therapy has also led to decreased lesion volumes and Yuan et al. showed improved behavioral and sensorimotor functions at 3 weeks with improvement in beam walking, grasping tasks, and Morris water maze performance. Further investigation revealed iNSCs may also support post-stroke neuroregenerative and angiogenic processes by secreting trophic

factors (e.g. VEGF, BDNF, GDNF) to promote endogenous tissue repair [14, 15]. This dual therapeutic mechanism of action makes iNSCs a strong candidate for stroke therapy by both potentially replacing lost neural tissue and promoting endogenous protective pathways.

Regrettably, as it has been described for endogenous neural stem cells (NSCs) post-stroke, a majority of transplanted iNSCs (80%) do not survive or integrate long-term into the ischemic brain, thus leaving patients with persistent cognitive and physical morbidities [16-20]. Similar studies in the field have attributed the limited iNSC survivability to the cytotoxic stroke environment resulting from the secondary injury cascade [21, 22]. Mediated by the release of inflammatory cytokines and the production of reactive oxygen species (ROS), studies have shown the secondary injury cascade ultimately leads to significant cell death, increased infarction volumes, and consequent tissue atrophy [23-30]. To address this issue, supplemental administration of anti-inflammatory and antioxidant neuroprotectants like Tanshinone IIA (Tan IIA) prior to iNSCs transplantation may aid in the survivability and long-term integration of iNSCs. Recently published data suggests Tan IIA was effective in attenuating the formation of cerebral edema in response to ischemia and reperfusion injury, partly by Tan IIA's protective effect on blood brain barrier (BBB) permeability in rats [31, 32]. Furthermore, Tan IIA was found to have a neuroprotective effect by suppressing activation of glial cells and inhibiting caspase-3, caspase-8, and macrophage migration inhibitory factor (MIF) [33, 34]. By mediating post-stroke inflammatory responses and decreasing levels of endogenous cytotoxicity, pre-treatment with Tan IIA may improve iNSC cell

survivability, differentiation, and long-term integration to promote neurobehavioral and functional recovery in patients.

An alternative neuroprotective treatment, extracellular vesicles (EVs), may also ameliorate the cytotoxic effects of the secondary injury cascade by releasing a myriad of intracellular components that modify the release of inflammatory mediators and the activation of microglia through the transfer of microRNAs and proteins [35-39]. In particular, in-vivo rodent studies involving mesenchymal stem cell derived-extracellular vesicles (MSC EVs) administration resulted in increased angiogenesis and neurogenesis, reduction of infarct volume and inflammation, and neurological recovery [40-46]. Neural stem cell derived-extracellular vesicles (NSC EVs) influence the activity of recipient cells by favoring macrophage polarization toward anti-inflammatory M2 cells, increasing Treg cell populations, and decreasing pro-inflammatory TH17 cells [47]. Further comparisons between MSC EVs and NSC EVs revealed enhanced improvements in cellular, tissue, and functional outcomes in a murine stroke model. Acute differences in lesion volume following NSC EV treatment were corroborated by magnetic resonance imaging (MRI) analyses resulting in positive effects on motor function as indicated by beam walk, instances of foot faults, and grasping strength. Increased time spent with novel objects (NO) also indicated NSC EVs improved episodic memory formation in rodents [47]. NSC EVs significantly improved neural tissue preservation by significantly decreasing infarct volumes, protecting WM structures, and reducing cytotoxic edema in ischemic lesions [48]. These findings suggest a bidirectional relationship between secondary inflammatory responses and tissue-level and functional recovery post-stroke.

Despite the promising neuroprotective and regenerative effects of NSC products and NP therapies, assessment by the Stem Cell Therapy as an Emerging Paradigm for Stroke (STEPS) and Stroke Therapy Academic Industry Roundtable (STAIR) consortiums suggest after sufficient evidence of therapeutic efficacy has been collected in rodent models, large animal stroke models should be used to increase clinical predictive value [49-52]. The inherent interspecies differences between rodents and humans in terms of cerebral cytoarchitecture suggest the use of an intermediate species, such as the pig, may enhance preclinical translation given similarities in neuroanatomical structure to the human brain (i.e. gyral pattern, brain size, white matter composition) and an improved resemblance to the pathophysiological and clinical co-morbidities (i.e. hypertensive, diabetic) seen in humans [53-55]. These factors are critical to improving clinical translation as cerebral cytoarchitecture and composition is correlated to neuronal network complexity [56, 57]. Furthermore, clinical dosing of iNSCs, Tan IIA and NSC EVs can more accurately be assessed in an animal with similar body size to humans. This pig stroke model must be enlisted within the translational framework in order to successfully bridge the gap between preclinical studies and clinical trials in order to discover effective therapies for human patients.

The studies that comprise this dissertation sought to 1) characterize a novel pig ischemic stroke model with clinically-relevant assessments of stroke pathophysiology, and 2) test the therapeutic efficacy of iNSCs, Tan IIA, and NSC EVs in a pig ischemic stroke model. First, we characterize acute ischemic stroke in a translational pig model revealing that 1) hemispheric swelling, ischemic lesions, and intracerebral hemorrhage result in notable midline shift, while 2) decreased diffusivity and white matter integrity

correspond with functional deficits including reduced exploration in open field testing and impairments in spatiotemporal gait parameters. This novel, acute ischemia characterization provides important insights into tissue and functional level changes in a pig model that can be used to identify treatment targets and future testing of therapeutics and diagnostics. Next, we show that iNSC, Tan IIA, and NSC EV therapies mitigate neural tissue damage with decreased ischemic volumes and intracerebral hemorrhage as well as improved diffusivity, white matter integrity, and functional performance following treatment. Collectively, these studies strengthen preclinical therapeutic development strategies by evaluating a large animal stroke model with quantifiable deficits at tissue and functional levels while also confirming NSC-derived products and Tan IIA may be effective treatment modalities for future stroke patients.

References

1. Saver, J.L., *Time is brain--quantified.* Stroke, 2006. **37**(1): p. 263-6.
2. Prevention, C.f.D.C.a., *Underlying cause of death, 1999-2016*. 2013: Atlanta, Georgia.
3. Kochanek, K.D., et al., *Mortality in the United States, 2016.* NCHS Data Brief, 2017(293): p. 1-8.
4. Mackay, J., et al., *The atlas of heart disease and stroke*. 2004, Geneva: World Health Organization. 112 p.
5. Del Zoppo, G.J., et al., *Expansion of the time window for treatment of acute ischemic stroke with intravenous tissue plasminogen activator: a science advisory from the American Heart Association/American Stroke Association.* Stroke, 2009. **40**(8): p. 2945-8.
6. Barber, P.A., et al., *Why are stroke patients excluded from TPA therapy? An analysis of patient eligibility.* Neurology, 2001. **56**(8): p. 1015-20.
7. Gravanis, I. and S.E. Tsirka, *Tissue-type plasminogen activator as a therapeutic target in stroke.* Expert Opin Ther Targets, 2008. **12**(2): p. 159-70.
8. Balami, J.S., et al., *Complications of endovascular treatment for acute ischemic stroke: Prevention and management.* Int J Stroke, 2018. **13**(4): p. 348-361.
9. Fluri, F., M.K. Schuhmann, and C. Kleinschnitz, *Animal models of ischemic stroke and their application in clinical research.* Drug Des Devel Ther, 2015. **9**: p. 3445-54.
10. Liu, S., et al., *Rodent Stroke Model Guidelines for Preclinical Stroke Trials (1st Edition).* J Exp Stroke Transl Med, 2009. **2**(2): p. 2-27.

11. Amabile, G. and A. Meissner, *Induced pluripotent stem cells: current progress and potential for regenerative medicine.* Trends Mol Med, 2009. **15**(2): p. 59-68.

12. Jensen, M.B., et al., *Survival and differentiation of transplanted neural stem cells derived from human induced pluripotent stem cells in a rat stroke model.* J Stroke Cerebrovasc Dis, 2013. **22**(4): p. 304-8.

13. Yuan, T., et al., *Human induced pluripotent stem cell-derived neural stem cells survive, migrate, differentiate, and improve neurologic function in a rat model of middle cerebral artery occlusion.* Stem Cell Res Ther, 2013. **4**(3): p. 73.

14. Oki, K., et al., *Human-induced pluripotent stem cells form functional neurons and improve recovery after grafting in stroke-damaged brain.* Stem Cells, 2012. **30**(6): p. 1120-33.

15. Polentes, J., et al., *Human induced pluripotent stem cells improve stroke outcome and reduce secondary degeneration in the recipient brain.* Cell Transplant, 2012. **21**(12): p. 2587-602.

16. Kumar, S., M.H. Selim, and L.R. Caplan, *Medical complications after stroke.* Lancet Neurol, 2010. **9**(1): p. 105-18.

17. Schaapsmeerders, P., et al., *Long-term cognitive impairment after first-ever ischemic stroke in young adults.* Stroke, 2013. **44**(6): p. 1621-8.

18. Wolfe, C.D., et al., *Estimates of outcomes up to ten years after stroke: analysis from the prospective South London Stroke Register.* PLoS Med, 2011. **8**(5): p. e1001033.

19. Thored, P., et al., *Persistent production of neurons from adult brain stem cells during recovery after stroke.* Stem Cells, 2006. **24**(3): p. 739-47.

20. Arvidsson, A., et al., *Neuronal replacement from endogenous precursors in the adult brain after stroke.* Nat Med, 2002. **8**(9): p. 963-70.

21. Rosenblum, S., et al., *Timing of intra-arterial neural stem cell transplantation after hypoxia-ischemia influences cell engraftment, survival, and differentiation.* Stroke, 2012. **43**(6): p. 1624-31.

22. Darsalia, V., et al., *Cell number and timing of transplantation determine survival of human neural stem cell grafts in stroke-damaged rat brain.* J Cereb Blood Flow Metab, 2011. **31**(1): p. 235-42.

23. Alex, A.B., et al., *CGX-1007 prevents excitotoxic cell death via actions at multiple types of NMDA receptors.* Neurotoxicology, 2011. **32**(4): p. 392-9.

24. Jablonska, A. and B. Lukomska, *Stroke induced brain changes: Implications for stem cell transplantation.* Acta Neurobiol Exp (Wars), 2011. **71**(1): p. 74-85.

25. Rothwell, N., *Interleukin-1 and neuronal injury: mechanisms, modification, and therapeutic potential.* Brain Behav Immun, 2003. **17**(3): p. 152-7.

26. Simi, A., et al., *Interleukin-1 and inflammatory neurodegeneration.* Biochem Soc Trans, 2007. **35**(Pt 5): p. 1122-6.

27. Zou, J.Y. and F.T. Crews, *TNF alpha potentiates glutamate neurotoxicity by inhibiting glutamate uptake in organotypic brain slice cultures: neuroprotection by NF kappa B inhibition.* Brain Res, 2005. **1034**(1-2): p. 11-24.

28. Ceulemans, A.G., et al., *The dual role of the neuroinflammatory response after ischemic stroke: modulatory effects of hypothermia.* J Neuroinflammation, 2010. **7**: p. 74.

29. Gilgun-Sherki, Y., et al., *Antioxidant therapy in acute central nervous system injury: current state.* Pharmacol Rev, 2002. **54**(2): p. 271-84.

30. Wang, Q., X.N. Tang, and M.A. Yenari, *The inflammatory response in stroke.* J Neuroimmunol, 2007. **184**(1-2): p. 53-68.

31. Tang, C., et al., *The effects of Tanshinone IIA on blood-brain barrier and brain edema after transient middle cerebral artery occlusion in rats.* Phytomedicine, 2010. **17**(14): p. 1145-9.

32. Liu, L., et al., *The neuroprotective effects of Tanshinone IIA are associated with induced nuclear translocation of TORC1 and upregulated expression of TORC1, pCREB and BDNF in the acute stage of ischemic stroke.* Brain Res Bull, 2010. **82**(3-4): p. 228-33.

33. Zhoua, L., Bondy, SC, .Jian, L, Wen, P, Yang, F, Luo, H, Li, W, Zhou, J., *Tanshinone IIA attenuates the cerebral ischemic injury-induced increase in levels of GFAP and of caspases-3 and -8.* Neuroscience, 2015. **288**: p. 105-111.

34. Chen, Y., et al., *Neuroprotection of tanshinone IIA against cerebral ischemia/reperfusion injury through inhibition of macrophage migration inhibitory factor in rats.* PLoS One, 2012. **7**(6): p. e40165.

35. Robbins, P.D. and A.E. Morelli, *Regulation of immune responses by extracellular vesicles.* Nat Rev Immunol, 2014. **14**(3): p. 195-208.

36. Cantaluppi, V., et al., *Microvesicles derived from endothelial progenitor cells protect the kidney from ischemia-reperfusion injury by microRNA-dependent reprogramming of resident renal cells.* Kidney Int, 2012. **82**(4): p. 412-27.

37. Mokarizadeh, A., et al., *Microvesicles derived from mesenchymal stem cells: potent organelles for induction of tolerogenic signaling.* Immunol Lett, 2012. **147**(1-2): p. 47-54.

38. Arslan, F., et al., *Mesenchymal stem cell-derived exosomes increase ATP levels, decrease oxidative stress and activate PI3K/Akt pathway to enhance myocardial viability and prevent adverse remodeling after myocardial ischemia/reperfusion injury.* Stem Cell Res, 2013. **10**(3): p. 301-12.

39. Lo Sicco, C., et al., *Mesenchymal Stem Cell-Derived Extracellular Vesicles as Mediators of Anti-Inflammatory Effects: Endorsement of Macrophage Polarization.* Stem Cells Transl Med, 2017. **6**(3): p. 1018-1028.

40. Doeppner, T.R., et al., *Extracellular Vesicles Improve Post-Stroke Neuroregeneration and Prevent Postischemic Immunosuppression.* Stem Cells Transl Med, 2015. **4**(10): p. 1131-43.

41. Xin, H., et al., *Systemic administration of exosomes released from mesenchymal stromal cells promote functional recovery and neurovascular plasticity after stroke in rats.* J Cereb Blood Flow Metab, 2013. **33**(11): p. 1711-5.

42. Chen, K.H., et al., *Intravenous administration of xenogenic adipose-derived mesenchymal stem cells (ADMSC) and ADMSC-derived exosomes markedly reduced brain infarct volume and preserved neurological function in rat after acute ischemic stroke.* Oncotarget, 2016. **7**(46): p. 74537-74556.

43. Otero-Ortega, L., et al., *White Matter Repair After Extracellular Vesicles Administration in an Experimental Animal Model of Subcortical Stroke.* Sci Rep, 2017. **7**: p. 44433.

44. Xin, H., et al., *MicroRNA cluster miR-17-92 Cluster in Exosomes Enhance Neuroplasticity and Functional Recovery After Stroke in Rats.* Stroke, 2017. **48**(3): p. 747-753.

45. Xin, H., et al., *Secondary Release of Exosomes From Astrocytes Contributes to the Increase in Neural Plasticity and Improvement of Functional Recovery After Stroke in Rats Treated With Exosomes Harvested From MicroRNA 133b-Overexpressing Multipotent Mesenchymal Stromal Cells.* Cell Transplant, 2017. **26**(2): p. 243-257.

46. Kalani, A., et al., *Curcumin-loaded embryonic stem cell exosomes restored neurovascular unit following ischemia-reperfusion injury.* Int J Biochem Cell Biol, 2016. **79**: p. 360-369.

47. Webb, R.L., et al., *Human Neural Stem Cell Extracellular Vesicles Improve Tissue and Functional Recovery in the Murine Thromboembolic Stroke Model.* Transl Stroke Res, 2017.

48. Webb, R.L., et al., *Human Neural Stem Cell Extracellular Vesicles Improve Recovery in a Porcine Model of Ischemic Stroke.* Stroke, 2018. **49**(5): p. 1248-1256.

49. Fisher, M., et al., *Update of the stroke therapy academic industry roundtable preclinical recommendations.* Stroke, 2009. **40**(6): p. 2244-50.

50. Fisher, M., et al., *Recommendations from the STAIR V meeting on acute stroke trials, technology and outcomes.* Stroke, 2007. **38**(2): p. 245-8.

51. Fisher, M. and R. Stroke Therapy Academic Industry, *Recommendations for advancing development of acute stroke therapies: Stroke Therapy Academic Industry Roundtable 3.* Stroke, 2003. **34**(6): p. 1539-46.

52. Savitz, S.I., et al., *Stem Cell Therapy as an Emerging Paradigm for Stroke (STEPS) II.* Stroke, 2011. **42**(3): p. 825-9.

53. Bellinger, D.A., E.P. Merricks, and T.C. Nichols, *Swine models of type 2 diabetes mellitus: insulin resistance, glucose tolerance, and cardiovascular complications.* ILAR J, 2006. **47**(3): p. 243-58.

54. Li, D., et al., *A Novel Swine Model of Spontaneous Hypertension With Sympathetic Hyperactivity Responds Well to Renal Denervation.* Am J Hypertens, 2016. **29**(1): p. 63-72.

55. Lind, N.M., et al., *The use of pigs in neuroscience: modeling brain disorders.* Neurosci Biobehav Rev, 2007. **31**(5): p. 728-51.

56. Platt, S.R., et al., *Development and characterization of a Yucatan miniature biomedical pig permanent middle cerebral artery occlusion stroke model.* Exp Transl Stroke Med, 2014. **6**(1): p. 5.

57. Baker, E.W., et al., *Induced Pluripotent Stem Cell-Derived Neural Stem Cell Therapy Enhances Recovery in an Ischemic Stroke Pig Model.* Sci Rep, 2017. **7**(1): p. 10075.

CHAPTER 2

LITERATURE REVIEW:

LARGE ANIMAL ISCHEMIC STROKE MODELS: REPLICATING HUMAN STROKE PATHOPHYSIOLOGY[1]

[1]Kaiser, E.E., and West, F.D. *Neural Regeneration Research*. 2019. Reprinted here with permission of the publisher.

Abstract

The high morbidity and mortality rate of ischemic stroke in humans has led to the development of numerous animal models that replicate human stroke to further understand the underlying pathophysiology and to explore potential therapeutic interventions. Although promising therapeutics have been identified using these animal models, with most undergoing significant testing in rodent models, the vast majority of these interventions have failed in human clinical trials. This failure of preclinical translation highlights the critical need for better therapeutic assessment in more clinically relevant ischemic stroke animal models. Large animal models such as non-human primates, sheep, pigs, and dogs are likely more predictive of human responses and outcomes due to brain anatomy and physiology that are more similar to humans- potentially making large animal testing a key step in the stroke therapy translational pipeline. The objective of this review is to highlight key characteristics that potentially make these gyrencephalic, large animal ischemic stroke models more predictive by comparing pathophysiological responses, tissue-level changes, and model limitations.

Key words: brain ischemia, magnetic resonance imaging, stroke, large animal model, gyrencephalic, clinical translation

Introduction

Resulting in approximately 142,000 deaths a year, stroke ranks 5th among all causes of death in the United States (Benjamin, Muntner et al. 2019). Although the age-adjusted mortality rates for stroke decreased between 1990 and 2015, the absolute number of people who have strokes annually have increased worldwide (Benjamin, Muntner et al. 2019). Given the high morbidity and mortality of stroke, animal models have been developed over the last four decades to replicate various aspects of human stroke to further understand underlying pathophysiological responses and explore potential treatments. Ischemic stroke caused by a blockage in the brain vasculature leading to brain ischemia is the most common type of stroke, accounting for 85% of all clinical cases (Mackay, Mensah et al. 2004).

Due to ischemic stroke prevalence, a number of rodent ischemic stroke models (e.g. permanent middle cerebral artery occlusion and thromboembolic models) have been developed. Although current rodent models offer many advantages including low cost, well-characterized physiological responses, and the ability to investigate genetic manipulations and co-morbidities (e.g. diabetes, hypertension), the number of failed human clinical trials suggests additional testing in translational ischemic stroke models, more representative of the human condition, are needed for the assessment of novel therapies (Perel, Roberts et al. 2007, Hossmann 2009, Sicard and Fisher 2009). Stroke Therapy Academic Industry Roundtable (STAIR) meetings of leading stroke experts have recommended that after sufficient evidence of therapeutic efficacy has been collected in rodent models, large animal models of stroke should be used to increase clinical predictive value (Fisher and Stroke Therapy Academic Industry 2003, Fisher, Hanley et al. 2007,

Fisher, Feuerstein et al. 2009). The use of an intermediate species may enhance successful translation given similarities in neuroanatomical structures and clinical hallmarks relative to humans (**Figure 2.1**).

In order to advance our current understanding of human stroke pathophysiology, to develop novel therapies, and devices, numerous pre-clinical animal models are widely employed. In this review, we will compare relevant brain anatomical and physiological characteristics between humans, non-human primates (NHPs), sheep, pigs, and dogs as well as consequential neurologic and motor function deficits post-stroke. Clinically relevant magnetic resonance-based outcomes will also be evaluated in these large animal models to assess tissue-level changes across acute and chronic time points (**Figure 2.2**). Finally, clinical translatability and experimental practicality will also be considered.

Large animal ischemic stroke models

Non-human primate ischemic stroke models

The use of gyrencephalic NHP species for translational stroke research is an attractive alternative due to their remarkable anatomical similarity to the human brain. NHPs have comparable complex cortical organization with deep white matter (WM) tracts, white-gray matter composition (>60%), and cerebral vasculature that closely resembles humans (**Figure 2.1**) (Cook and Tymianski 2011). Furthermore, NHPs possess relatively thick cortices and numerous, high-velocity neurons thus allotting for superior cognitive and behavioral processing capacities during neurobehavioral testing (Cook and Tymianski 2012, Roth and Dicke 2012). These favorable anatomical similarities have led to the development of several NHP ischemic stroke models.

Historically, the primary NHP stroke model utilized to investigate cerebral ischemia was the baboon permanent middle cerebral artery occlusion (MCAO) model (Spetzler, Zabramski et al. 1983, Nehls, Cartwright et al. 1986). This model resulted in key stroke hallmarks such as ischemia, classical cytotoxic edema and lesioning of the brain. However, this model produces marked cerebral edema requiring prolonged intensive care of the animal and is associated with a high risk of mortality making it a challenging model to study. In addition, this permanent occlusion model did not allow for reperfusion, which is common in human patients, limiting its potential to assess key aspects of ischemic stroke like reperfusion injury. As a result, transient NHP models were developed in order to gain a better understanding of secondary reperfusion injury and successive microvasculature failure. Del Zoppo et al. describes a balloon transorbital reperfusion baboon model with increasing cortical lesion volumes observed between 10 days (3.2±1.5 cm^3) and 14 days (3.9±1.9 cm^3) post-stroke with functional deficits including contralateral hemiparesis, facial paresis, and mydriasis of variable degrees due to internal capsule, putamen, and caudate nucleus involvement (Del Zoppo, Copeland et al. 1986). In addition, microvascular clip reperfusion baboon models exhibit lesion volumes (30% of the ipsilateral hemisphere) and progressive temporal evolution similar to humans as assessed by magnetic resonance imaging (MRI) diffusion weighted imaging (DWI) and T2Weighted (T2W) structural sequences (Huang, Mocco et al. 2000, D'Ambrosio, Sughrue et al. 2004, Giffard, Young et al. 2005). Functional deficits including hemiparesis of the contralateral arm and leg were thought to arise from the loss of the tissue integrity in the striato-capsular area with internal capsule and basal ganglia involvement. In the context of human ischemic stroke, these results possess important implications for researchers given that many human studies

confirm this delayed evolution of ischemic areas with mean lesion volumes significantly ($p<0.0001$) higher at 7 days compared to 1-day post-stroke in patients (Pantano, Caramia et al. 1999, Saver 2006). Moreover, most stroke patients also exhibit hemiparesis with correlative asymmetries in arm, leg, trunk, and face movements due to internal capsule, putamen, and basal ganglia involvement in the complex communication and feedback loops between the areas of the cerebral cortex and the brainstem (Ng, Stein et al. 2007, Patterson, Parafianowicz et al. 2008). Restoring functional deficits in stroke patients is critical for improvements in patient quality of life and is an important measure of a treatment's therapeutic potential in animal models (Sofuwa, Nieuwboer et al. 2005, Liao, Wang et al. 2008, Veerbeek, Koolstra et al. 2011).

Macaque reperfusion models generated by transorbital and pterional craniotomy approaches have been characterized with both methods of cerebrovascular access while producing representative ischemic lesions. In addition to modeling the structural damage of stroke, these models mirror functional deficits including reduced strength and skilled movement of upper limbs with the loss or disruption of motor and sensory cortices, similar to the human condition (Nakayama, Jorgensen et al. 1994, Cirstea and Levin 2000, Nudo, Plautz et al. 2001). Chin et al. reported transient decreases in MRI WM fractional anisotropy (FA) values, suggesting loss of integrity of the ipsilateral motor pathways at the dorsal region of the internal capsule at 7 days post-stroke (Chin, Sato et al. 2010). This correlated with deficits in motor function including paralysis and weakness in upper and lower limbs as well as incoordination. However, motor function recovered to baseline at 6 weeks post-stroke. This gradual motor recovery observed in macaques has also been reported in chronic stroke patients where gradual motor recovery is also observed and

correlates with WM FA value changes (Pierpaoli, Barnett et al. 2001, Biesbroek, Weaver et al. 2017). West et al. characterized varying durations of microvascular clip occlusion and consequent mean lesion volumes at 45 minutes (1.983±2.51 cm^3), 60 minutes (2.381±6.54 cm^3), and 90 minutes (4.707±12.7 cm^3) as determined by T2W imaging in macaques (West, Golshani et al. 2009). Consequent ischemia encompassed portions of the frontal and parietal lobes, insular motor cortex, and cingulate cortex with the severity of hemiparesis in the extremities and face consistent with clinical stroke patients diagnosed with damaged neuronal motor cortex circuitries (Traversa, Cicinelli et al. 2000, West, Golshani et al. 2009). In a similar study by Murphy et al., a 90 minute occlusion produced infarcts extending from the caudate nucleus and putamen (basal ganglia), external capsule, and adjacent subcortical WM in macaques (Murphy, Kirsch et al. 2008). Multiple human clinical trials and large cohort studies have characterized these frontotemporal abnormalities with most involving both basal ganglia and WM compartments (Saver 2006). Final patient volumes in clinical trials range from 19 to 138 cm^3 (3.33 to 24.17% of the ipsilateral hemisphere), thus suggesting 45 minutes (19.0±0.98% of the ipsilateral hemisphere) and 60 minutes (22.1±4.6%) of clip application are more clinically relevant macaque models of ischemic stroke as compared to 90 minutes (44.4±4.0%) of temporary occlusion (Saver 2006).

Endovascular occlusion using an autologous blood clot, coil, or surgical suture has also been widely developed in macaques to induce focal ischemia. Advantages of these methods include 1) they are minimally invasive and avoid the need for enucleation and its associated loss of vision and impacts on neurobehavioral assessments, 2) they are capable of achieving reperfusion, and 3) they directly affect the intracranial vessels, thus avoiding

surgically induced damage to the endocranium and intracranial environment. Autologous blood clot models have induced ischemic lesions (28.3±12.4% of the ipsilateral hemisphere) affecting the caudate, globus pallidus, putamen, internal capsule, claustrum, and insular cortex (Hill, Millikan et al. 1955, Kito, Nishimura et al. 2001). Clinical signs compatible with selective occlusion of these middle cerebral artery (MCA) territories in humans were also observed in macaques exhibiting contralateral facial sensation, pinna and pain reflexes, and severe paralysis of contralateral hands and legs. Furthermore, significant correlations between macaque lesion volumes and total neurologic deficit scores were observed, with similar correlations commonly seen between acute ischemic stroke patient lesion volumes and the National Institutes of Health Stroke Scale (NIHSS) neurological scores (Kito, Nishimura et al. 2001, Furlanis, Ajcevic et al. 2018).

The ischemic penumbra is classically defined as potentially salvageable hypoperfused tissue and is the difference between the perfusion weighted imaging (PWI) lesion volume and the DWI lesion volume in stroked tissue (Astrup, Siesjo et al. 1981, Kakuda, Lansberg et al. 2008). This PWI/DWI mismatch is a key characteristic in both NHP and human stroke pathology and has prompted alterations in therapeutic targets and treatment windows (Hossmann 1994, Wey, Kroma et al. 2011). Alternative penumbra imaging concepts more technologically available have also been recently developed using diffusion tensor imaging (DTI) and associated FA values. For example, in a recent study by Neal et al., they demonstrated that patients with acute ischemic stroke (<6 hours) exhibited decreased FA values in regions of ischemic core, yet increased FA values in hypoperfused penumbra tissues (Nael, Trouard et al. 2015). This trend suggests DTI and FA related changes in humans could be used to differentiate penumbra and ischemic core

in addition to currently used PWI/DWI comparisons. Comparatively, NHP coil endovascular occlusion revealed a PWI/DTI mismatch with PWI lesion volumes being larger than DTI abnormalities at 1 hour post-stroke with the difference being penumbra (Guo, Zheng et al. 2011). A similar NHP suture model also identified penumbra evolution as detected by DWI and corresponding apparent diffusion coefficient (ADC) maps followed by T2W sequences (Rodriguez-Mercado, Ford et al. 2012). Liu et al. provided further evidence that the evolution of stroke in macaques is closer to what has been observed in humans than in rodent models by comparing ADC and FA maps with T2W and T2FLAIR sequences to establish the temporal profile of diffusion changes and to determine endpoint lesion volumes in permanent and transient MCAO models (Liu, D'Arceuil et al. 2007). In human studies, the mean time of pseudonormalized ADC (i.e. return to an apparently normal ADC value) was ~10–14 days, while in rodent studies a pseudonormalized ADC was often found much earlier at ~1–4 days post-stroke, likely due to inherent differences in cerebrovascular collateralization and cytoarchitecture (Eastwood, Engelter et al. 2003, Munoz Maniega, Bastin et al. 2004, Liu, D'Arceuil et al. 2007). Comparatively, NHP ADC pseudonormalized at ~8 days in lissencephalic marmosets and ~10 days in gyrencephalic macaques, providing further support for the use of gyrencephalic NHP species that more adequately replicate human penumbra evolution post-stroke (Liu, D'Arceuil et al. 2007, Bihel, Pro-Sistiaga et al. 2010). Wey et al. implemented arterial spin labeling (ASL) to characterize the spatial-temporal characteristics associated with perfusion-diffusion mismatch and provided evidence that reperfusion salvaged damaged penumbra tissue in a transient baboon model (Wey, Kroma et al. 2011, Wey, Wang et al. 2011). In humans, this perfusion-diffusion mismatch is often detected for up to 12 hours

post-stroke with the frequency of detection decreasing over time (Darby, Barber et al. 1999, Shen, Meng et al. 2003, Zhang, Tong et al. 2015). Comparatively, this mismatch volume has shown to be detectable for up to 6 hours in both baboons and macaques, whereas it is only detectable for up to 3 hours post-stroke in rodent models (e.g. intraluminal reperfusion models). The similarities in the manifestation, evolution and detection of the salvageable penumbra region between humans and primates provides researchers with valuable information on ischemic stroke pathophysiological changes and the ability to better assess drugs targeting the salvageable penumbra tissue (Astrup, Siesjo et al. 1981, Warach, Dashe et al. 1996).

Non-human primate ischemic stroke model considerations

Despite the translational potential of primate models, there are a number of important practical and scientific disadvantages that have limited the use of these models. Baboons exhibit a network of arteries that communicate between the bilateral anterior cerebral arteries (ACAs) rather than the single vessel found in humans, which may influence Circle of Willis collateralization (Kapoor, Kak et al. 2003). Additionally, some NHP species, sheep, and pigs demonstrate complete anterior communicating artery (CoA) hypoblastia, which may result in poor outcomes due to decreased cerebral blood flow (Combs, Dempsey et al. 1990, Sorby-Adams, Vink et al. 2018). Baboon MCAO models are associated with high premature mortality rates and prolonged intensive care (Nehls, Cartwright et al. 1986, Huang, Mocco et al. 2000, D'Ambrosio, Sughrue et al. 2004). Some permanent and transient occlusion methods in baboons and macaques require enucleation for transorbital access to the MCA and the ACA, thus limiting neurobehavioral assessments due to binocular vision loss (Nehls, Cartwright et al. 1986, Tagaya, Liu et al. 1997, Mack,

King et al. 2003, D'Ambrosio, Sughrue et al. 2004). Cynomolgus and rhesus macaque endovascular induction methods require substantial technological and surgical skill and may produce unreliable anterior circulation stroke patterns (Kito, Nishimura et al. 2001, Kuge, Yokota et al. 2001, de Crespigny, D'Arceuil et al. 2005, Wu, Chen et al. 2016). Reperfusion in autologous blood clot models is difficult to control, while microcatheter embolization methods utilizing metal coils or guide wires prohibits the use of MRI prior to reperfusion. The extensive limitations of cost, housing facilities, veterinary care, and ethical challenges associated with NHP models warrant further investigation of alternative large animal species for modeling ischemic stroke.

Ovine ischemic stroke models

Sheep are a highly promising surrogate for modeling human stroke due to inherent anatomical similarities including gyrencephalic cerebral structure with dense WM tracts (Bataille, Wager et al. 2007). A strong fibrous dura mater and tentorium cerebelli also play a significant role in modeling human ischemic stroke by confining post-stroke increases in intracranial pressure (ICP) to the supratentorial compartment (Klintworth 1968, Gabrielian, Willshire et al. 2011). Comparatively, rodents have a weak vestigial connective tissue membrane that enables distribution of ICP into other compartments. Increases in ICP in humans and large gyrencephalic animals post-stroke are therefore more significant and more common than in rodents and often leads to loss of consciousness, cerebral herniation, and premature death. Sheep cerebrovasculature also facilitates the development of sheep stroke models as the intradural internal carotid artery (ICA) supplies blood to a majority of the supratentorial structures and, like humans, the terminal intradural ICA bifurcates to the ACA and MCA (Ashwini 2008). Despite these similarities, sheep possess a reticulated

arterial anastomosis between the maxillary and internal carotids known as the rete mirabile (Daniel PM 1953, Hoffmann, Stoffel et al. 2014). This capillary network at the branch of the common carotid artery (CCA) renders endovascular models of cerebral ischemia virtually impossible due to the minute diameter of arterial vessels, thus transcranial stroke induction approaches are typically required.

Permanent occlusion in sheep via frontotemporal craniectomy boasts a number of advantages including preservation of post-operative binocular vision, unlike NHP transorbital models, as well as lesion reproducibility due to the length of the ICA which aids in proximal MCA accessibility (Kapoor, Kak et al. 2003). Boltze et al. reported DWI-based lesion volumes could be titrated, with complete MCAO lesion volumes being significantly greater than 2-branch and 1-branch-MCAO lesion volumes (16.3±5.2 vs. 8.7±3.9 vs. 5.6±3.6 cm^3, respectively) at 1 day post-stroke (Boltze, Forschler et al. 2008). These significant differences in lesion volumes were maintained between subgroups up to 42 days post-stroke. Lesion volume was found to be correlated with functional outcomes based on a novel sheep-specific neurobehavioral score system including important metrics such as unconsciousness, ataxia, fetlock flexion weakness, delayed hemistanding, circling behaviors, and impaired hopping reactions. Comparatively, complete proximal MCA occlusion in humans resulted in similar motor and somatosensory deficits including ataxia and hemiparesis of contralateral upper and lower extremities as well as loss of consciousness due to significant cerebral edema and swelling (Battey, Karki et al. 2014, Navarro-Orozco and Sanchez-Manso 2019). Furthermore, T2W sequences in sheep revealed significantly higher atrophy ratios for the complete MCAO group compared to the 2-branch-MCAO group, whereas 1-branch-MCAO resulted in significantly less

atrophy ratios compared with 2-branch-MCAO 42 days post-stroke (Boltze, Forschler et al. 2008). Although this model maintains clinically relevant tissue and functional-level deficits at acute and chronic time points, it also exhibits unrealistic survivability rates (100%) post-stroke. Researchers believe these survival rates are due to reduced ICP at the craniectomy site and is therefore a notable limitation of the model.

To address the translational limitations of the permanent sheep occlusion model, Wells et al. later developed a transient sheep occlusion model and performed a head to head comparison to more accurately assess intracranial dynamics and reperfusion mechanism differences between these models (Wells, Vink et al. 2012, Wells, Vink et al. 2015). As expected, lesion volumes were greater in permanent occlusion sheep compared to transient occlusion sheep (27.4-28.8% vs. 7.9-14.6% of the ipsilateral hemisphere, respectively) with ischemia affecting both cortical and subcortical structures in both models. DWI deficits were also greater in permanent occlusion sheep compared to transient occlusion sheep (25.4±6.8% vs. 10.7±3.9%, respectively) with restricted diffusion reported throughout the entire right MCA territory and basal ganglia in permanent occlusion sheep and throughout the right caudate head and genu of the internal capsule in transient occlusion sheep. T2W sequences revealed similar model differences in edema volume (25.0±4.9% vs. 5.4±4.1% of the ipsilateral hemisphere) resulting in increasing midline shift (MLS) (3.3±0.6 mm vs. 1.0±0.8mm).Sorby-Adams et al. recently reported significantly elevated ICP levels in excess of 20 mmHg at 5-6 days post-transient MCAO in sheep (Sorby-Adams, Leonard et al. 2019). These findings are comparable to human patients in which cerebral edema and ICP peak around 3-5 days following initial ischemic insult (Hewitt A. 2012). Clinically, ICP readings >20 mmHg warrant treatment intervention as

persistently elevated ICP following MCA infarction is commonly associated with rapid neurological deterioration (Treadwell and Thanvi 2010, Lavinio and Menon 2011, Battey, Karki et al. 2014). Death is common in the 78% of patients that experience herniation and consequent brainstem compression due to ICP (Hacke, Schwab et al. 1996, Wang, Nair et al. 2011). The sequela of herniation and comparative mortality rates observed in the transient sheep model further supports the use of this clinically relevant large animal model in order to study ICP related pathology and decompressive therapies.

Ovine ischemic stroke model considerations

Arguably the most notable disadvantage of sheep models is the rete mirabile. This dense network of small diameter arteries renders endovascular methods of ischemic induction unfeasible, thus necessitating rather complex transcranial surgical approaches to induce MCAO. Transcranial approaches disturb endocranium dynamics and may lead to hematomas or hemorrhagic transformation as seen in approximately ~12% patients with MCA infarctions that undergo decompressive craniectomies (Kenning, Gooch et al. 2012, Lee, Yang et al. 2012). Furthermore, surgical craniectomy permits the loss of CSF upon dural excision and minimizes the pathological development of elevated ICP following MCA occlusion (Boltze, Forschler et al. 2008). Common assessments of patient injury severity and prognosis in clinical settings are often based on neurological symptoms including pupillary dilation, anisocoria, consciousness, and paralysis which are caused by excessive ICP (Chen, Gombart et al. 2011). Without representative increases in ICP, craniectomy sheep occlusion models display notable alterations in stroke pathophysiology, thus decreasing this model's translational potential. Furthermore, with <30% WM, sensorimotor impairments commonly associated with WM injuries in stroke patients may

not be fully replicated in sheep models (**Figure 2.1**) (Sahin B 2001, Nitzsche, Frey et al. 2015, Wang, Liu et al. 2016). Perhaps similarities in other critical brain characteristics overcome this limitation, yet this remains to be determined.

Porcine ischemic stroke models

Pigs possess notable translational advantages due to inherent neuroanatomical similarities including gyrification, large intracranial vessel diameter, and a high white-to-gray matter ratio (Gralla, Schroth et al. 2006, Kobayashi, Hishikawa et al. 2012). Proportionally comparable cerebral volumes between humans and pigs (1273.6 cm^3 for men and 1131.1 cm^3 for women vs. 111.09 cm^3 for males and 103.15 cm^3 for females) allows for a more direct assessment of therapeutic dosing in a preclinical model (Allen, Damasio et al. 2002, Conrad, Dilger et al. 2012). In terms of cytoarchitecture, human and pig brains are composed of >60% WM (**Figure 2.1**) (Tanaka, Imai et al. 2008, Nakamura, Imai et al. 2009). These attributes are critically important as WM and gray matter (GM) demonstrate different metabolic needs due to neuroanatomical differences. Specifically, neuron-rich GM requires 2.5 times more ATP and consequently 3-5 times more vascularization than WM (Borowsky and Collins 1989, Nonaka, Akima et al. 2003, Peters, Schweiger et al. 2004). The increased vasculaturization of GM permits some protection following ischemic events, however the limited collateralization of WM leaves these tissues particularly susceptible to ischemic insult and is a critical factor to consider when modeling human ischemic stroke. Experimental pig stroke models have also been characterized with human MRI modalities and may help provide critical insight into the refinement of acute stroke detection (**Figure 2.2**). Lastly, high purchase and housing costs

as well as ethical challenges associated with other large animal models are less pronounced in pigs making them an attractive alternative (Kobayashi, Hishikawa et al. 2012).

Similar to sheep, the rete mirabile network in pigs makes endovascular methods of MCA occlusion challenging (Stroke Therapy Academic Industry 1999, Sakoh, Rohl et al. 2000, Watanabe, Sakoh et al. 2007, Ashwini 2008). Watanabe et al. developed a permanent pig MCAO model in which the proximal MCA was occluded via permanent electrocautery utilizing a transorbital approach (Watanabe, Sakoh et al. 2007). Although transorbital induction has been well characterized in NHP models as an efficient method of inducing focal cortical infarction, DWI analysis in pigs revealed varying lesion volumes in relation to the magnitude of residual flow following MCAO (Sakoh, Ostergaard et al. 2000, Watanabe, Andersen et al. 2001, Watanabe, Sakoh et al. 2007). Subsequent loss of binocular vision and limited neurobehavioral and gait assessments were additional limitations (Sakoh, Rohl et al. 2000). Comparatively, frontotemporal MCAO approaches avoid the need for enucleation and intraorbital decompression making it a favorable alternative over transorbital approaches (Imai, Konno et al. 2006, Platt, Holmes et al. 2014, Baker, Platt et al. 2017, Webb, Kaiser et al. 2018). This model provides increased visibility of the MCA and its associated branches, thus resulting in repeatable ischemic injury with consistent lesion volumes. Platt et al. showed pigs, like humans, exhibit a standard evolution of ischemic injury with cytotoxic edema primarily observed as hypointense ADC abnormalities followed by delayed vasogenic edema (Ho, Rojas et al. 2012, Platt, Holmes et al. 2014). Additionally, as pig cerebrums are approximately 7.5 times smaller than humans, the West Laboratory has recently confirmed pig DWI lesion volumes (9.91±3.14 cm^3; unpublished data) closely replicate patient DWI lesion volume thresholds of 72 cm^3,

which frequently correspond to major cerebral artery occlusions and poor neurological outcome (Sanak, Nosal et al. 2006, Gonzalez 2012).

T2W sequences in the pig MCAO model revealed acute hemispheric swelling (126.8±3.4% change from contralateral hemisphere), pronounced MLS, and cerebellar herniation with functional deficits in gait and behavior performance as well as premature death (Webb, Kaiser et al. 2018). T2W visualized hemispheric swelling and MLS in patients is also considered a robust predictor of cerebral herniations and patient death as rapid neurological deterioration often leads to 60-80% 30-day patient mortality rates (Ropper 1986, Hacke, Schwab et al. 1996, Berrouschot, Sterker et al. 1998, Walberer, Blaes et al. 2007, Treadwell and Thanvi 2010). Hemispheric swelling often instigates herniation leading to abnormal protrusion into adjacent neural structures or through rigid intracranial barriers (i.e. the foreman magnum) (Klintworth 1968, Kotwica, Hardemark et al. 1991, Gabrielian, Helps et al. 2013). The tentorium cerebelli in humans and large animal species is relatively strong, which limits and alters the displacement of the brain post-stroke. Comparatively, rodents possess a weak tentorium cerebelli that permit the displacement of the brain. This results in inconsistencies between rodent and human swelling responses post-stroke. DTI sequences have revealed permanent pig MCAO also replicates patient reductions in WM integrity of the internal capsule and corpus callosum at acute and chronic time points (Baker, Platt et al. 2017, Webb, Kaiser et al. 2018, Kaiser E.E. 2019). These reductions in WM integrity were coupled with deteriorations in pig spatiotemporal and relative gait pressure measurements including velocity, cadence, swing percent of cycle, stride length, cycle time, and mean pressure. Likewise, these deficits correlate with contralateral deteriorations in patient motor function, as studies utilizing

Functional Ambulatory Categories found patients with internal capsule lesions exhibited persistent (>6 months) motor deficits and required aids for balance and support during ambulation (Baltan, Besancon et al. 2008, Srikanth, Beare et al. 2009, Ahmad, Satriotomo et al. 2015, Lee, Kim et al. 2017). Understanding how brain ischemia leads to WM changes and consequent motor deficits, preferably in models with comparable WM content (>60%), is a research priority that will help advance strategies for WM repair and regeneration.

Consequential damage to the dura and disrupted ICP evolution in the pig craniectomy models has led to the development of an endovascular pig model. Cui et al. established an endovascular model of focal ischemic stroke in miniature pigs in which sodium alginate microspheres, a biodegradable material, were injected through the femoral artery to embolize the rete mirabile as confirmed by angiographic and DWI analysis (Cui, Tian et al. 2013). Signal abnormalities on T2W sequences revealed lesion volumes encompassing approximately 30% of the ipsilateral hemisphere with notable ischemia in the temporal and parietal lobes and the basal ganglia. Infarction in these regions prompted mild hemiplegia and associated ambulation impairments in balance and coordination as early as 12 hours post-stroke. Interestingly, stroke patients with confined basal ganglia and internal capsule injury exhibit persistently impaired balance and ambulation performance as well (Miyai, Blau et al. 1997). These observed motor memory deficits are likely due to persistent dysfunction in the cortico-basal ganglia-thalamo-cortical loop, an intricate neural circuit system responsible for facilitating voluntary movements while simultaneously inhibiting competing or interfering movements (Boyd, Edwards et al. 2009, Simonyan 2019).

Porcine ischemic stroke model considerations

Like the sheep, the rete mirabile necessitates transcranial approaches that damage the cranium and dura and result in uncharacteristic intracranial dynamics and cerebrovascular pathophysiological changes post-stroke (Imai, Konno et al. 2006). Although an endovascular occlusion method has been described, minimal sample size, short observation windows, and occlusion of the anatomical anastomosis the rete mirabile (a more distal vasculature structure), limits the clinical translatability of this model. Furthermore, the posterior CoA in the Circle of Willis in both pigs and sheep is comparable to the diameter of the anterior cerebral artery whereas in humans the posterior CoA is approximately half the diameter of the anterior cerebral artery. (Ashwini 2008, Deepthi S. 2016). These variations in vessel diameter are an important consideration when modeling ischemic stroke as equal blood volume flows through both divisions of internal carotid artery in animals whereas in man the blood flow through the posterior CoA is reduced, thus impacting collateral flow within the Circle of Willis. Pig plasminogen also displays high resistance to tPA activation due to unique plasminogen-streptokinase interactions (Yakovlev, Rublenko et al. 1995, Flight, Masci et al. 2006). As a result, investigation of combination therapies in conjunction with tPA are hindered, even if a clot model were available.

Canine ischemic stroke models

Similar to previously discussed large animal models, dogs demonstrate conserved gyrencephalic structure, well-established WM tracts, and large cerebrovascular diameter (Traystman 2003). Additionally, unlike sheep and pigs, dogs lack a rete mirabile. This anatomical similarity to humans favors endovascular approaches of stroke induction and is

one notable translational advantage of dog models (Gralla, Schroth et al. 2006, Howells, Porritt et al. 2010). Permittable endovascular access avoids the need for enucleation or invasive transcranial procedures to access the MCA thus preserving dura, cerebral spinal fluid volumes, and post-stroke ICP. The use of dogs also minimizes economic, housing, and handling difficulties commonly associated with NHP use, however ethical concerns remain a notable consideration (Hillock SM 2006).

First described by Hill et al., several studies have since reported on various endovascular methods for inducing MCAO in dog models (Hill, Millikan et al. 1955, Shaibani, Khawar et al. 2006, Rink, Christoforidis et al. 2008, Christoforidis, Rink et al. 2011). Permanent MCA, achieved via ICA injection of synthetic emboli, induced lesion volumes (32.13±11.98%) in the basal ganglia, left ventral cortex, left ventrolateral cortex, and left cortex of the cerebrum with swelling, MLS, and mass effect observed via T1W sequences (Kang, Lee et al. 2007). Kang et al. later reported a mean ADC ratio (0.77±0.08) that closely replicated human ADC ratios (0.5-0.8) at acute post-stroke time points (van Everdingen, van der Grond et al. 1998, Lee, Kang et al. 2005, Kang, Jang et al. 2009). Accumulation of cytotoxic and vasogenic edema were well-preserved within this model, thus presenting a significant advantage over photothrombotic rodent models (Carmichael 2005, Kang, Lee et al. 2007, Kang, Jang et al. 2009, Macrae 2011). Interestingly, dog cerebral spinal fluid (CSF) concentration of interleukin-6 (IL-6) positively correlated with the severity of neurological deterioration and death. This correlation has also been observed in several human stroke studies in which elevated CSF levels of IL-6 were found to positively correlate with ischemic lesion volumes and poor functional outcome (Tarkowski, Rosengren et al. 1995, Tarkowski, Rosengren et al. 1997). As CSF IL-6,

unlike serum IL-6, maintains significant predicative value in both dog and human stroke, further examination of this potential biomarker may help identify at-risk patients prior to onset of severe neurological symptoms and death.

Endovascular occlusion can also be achieved via coil placement in dogs through the vertebral artery (VA) in order to control for the variable intricacies of the ICA as previously mentioned (Atchaneeyasakul, Guada et al. 2016). Coil models offer a number of translational advantages as angiographic guidance in dogs is significantly superior when compared to rodent models where the relative size of the cranial arteries limits procedural evaluation and confirmation of occlusion (Flecknell, Flecknell et al. 2009). This method utilizes comprehensive imaging techniques to precisely position the coil encased within a microcatheter through the proximal M1 until appropriate permanent or transient occlusion of the MCA is achieved. Although the use of imaging guidance requires a complex understanding of dog cerebrovasculature, it enables specificity in coil placement that cannot be achieved by emboli injection via ICA. This yields definite and reproducible dog ischemic lesions of approximately 9.81-20.58 cm^3 (30.9±2.1% and 31.2 ±4.3%, as reviewed by two independent observers) as determined by T2 structural sequences 1-day post-stroke (Rink, Christoforidis et al. 2008, Rink, Christoforidis et al. 2011). DTI fiber tract projections from the region of the internal capsule to the corona radiata were dramatically reorganized with impaired connectivity in stroke dogs (Rink, Christoforidis et al. 2011). These corticospinal and corticobulbar tracts that descend through the corona radiata and posterior limbs of the internal capsule mainly originate in the primary motor cortex in humans and play an important role in recovery of motor deficits (Higano, Zhong et al. 2001, Kunimatsu, Aoki et al. 2003). These anatomical similarities may provide

important insights into the WM responses to hypoxia as well as necessary therapeutic measures to induce recovery of these WM structures.

The distal injection of autologous clots through the ICA accurately mimics human ischemia and is amenable to studies investigating the efficacy of novel thrombolytic therapies or thrombectomy devices. Despite clinical applicability, this model induces inconsistent lesion distribution as the precise site of occlusion cannot be controlled due to individual vascular variability, particularly of the ICA (Liu, Hu et al. 2012). Variations in emboli size have also contributed to variations in lesion volumes. Liu et al. reported clots 1.7 mm in diameter resulted in small, variable lacunar infarcts of 0.148±0.133 cm^3 at 6 hours (DWI), 0.150±0.154 cm^3 at 24 hours (T2W), and 0.095±0.115 cm^3 at 7 days post-stroke (T2W) affecting the internal capsule and caudate (Liu, Hu et al. 2012). Zu et al. reported clots 1.4-1.7 mm in diameter resulted in mean infarct volumes of 4.17±0.06 cm^3 at 24 hours (T2W) and 3.27±0.062 cm^3 at 7 days post-stroke (T2W) affecting the basal ganglia and cortex (Zu, Liu et al. 2013). Van der Bom described larger clots of 2.33 mm in diameter that induced extremely variable infarct volumes 4 hours post-stroke (0.12 to 12.53 cm^3, ADC) (van der Bom, Mehra et al. 2012). These discrepancies were suggested to be due to convoluted ICA and perfusion differentials from the extensive leptomeningeal collaterals and have contributed to heterogeneous strokes in dogs (Symon 1960, Harris, Kosior et al. 2009, Christoforidis, Rink et al. 2011).

In addition to MCAO models, vertebral artery occlusion (VAO) and basilar artery occlusion (BAO) models have also been developed. In VAO models, high vertebral artery blood pressure often prevents emboli from anchoring to the vessel wall, thus limiting experimental efficacy. To address this, a recent study utilized a preinstalled self-expanding

thrombus filter in the delivery catheter to allow for successful implantation of emboli (Zhang, Jin et al. 2015). Although further imaging and clinical outcome studies of this canine model are still needed, this model may be useful to evaluate novel endovascular therapy for acute VAO in humans. The BAO model comparatively is commonly used to test recanalization by intravenous versus intraarterial thrombolysis. Qureshi et al. reported significant lesion formation following autologous clot injection into the proximal portion of the basilar artery with intraarterial thrombolysis affording a recanalization rate similar to that of intravenous thrombolysis, but with a lower rate of intracerebral hemorrhage (Qureshi, Boulos et al. 2004). The most relevant disadvantages of BAO models are the exaggerated neurological deficits, prolonged intensive care, and premature mortality which limit longitudinal assessments of therapeutic efficacy, functional outcomes, and tissue recovery post-stroke.

Canine ischemic stroke model considerations

An appreciable concern in dog models is the low extent of WM (35%), similar to that observed in sheep (<30%) (Figure 1) (Krafft, Bailey et al. 2012). Limited WM in these models may hinder advancements in understanding WM pathophysiology and mechanisms involved in ischemic injury (Ahmad, Satriotomo et al. 2015). Conversely, NHPs and pigs display comparable WM to humans (> 60%) that results in similar prognosis and motor function decline commonly associated with human WM hyperintensities post-stroke (Debette and Markus 2010). Occlusion of the MCA is primarily achieved via ICA access, yet this procedure requires great surgical skill due to the intracavernous connection between the torturous ICAs as well as the small diameter of microcatheter administration systems (Nanda and Getty 1975, Rink, Christoforidis et al. 2008). A number of dogs exhibit

extensive leptomeningeal anastomoses branching from the posterior, middle, and anterior cerebral artery, potentiating variation in lesion volume due to differentials in collateralization (Symon 1960). Variation in vascular diameter, organization and physiological responses such as vasospasms between dog breeds may also limit reproducibility and experimental outcomes especially as mongrel dogs are commonly used (Rink, Christoforidis et al. 2008, Christoforidis, Rink et al. 2011). In the endovascular coil model, Christoforidis et al. reported the coil positioned to occlude the proximal MCA, ACA, and distal ICA resulted in premature mortality of ~38% of the dogs within 1 day post-stroke (Rink, Christoforidis et al. 2011). These experimental challenges in combination with pronounced ethical complications, limit the widespread use of canine species.

Conclusion

The stroke field agrees that a therapeutic breakthrough will most likely require a multifaceted approach including innovations in clinical trial design, consideration of systemic biomarkers, and optimization of therapeutic dosing. Large animal ischemic stroke models are a key part of this approach providing more predictive models for identifying potential treatment targets and testing novel therapeutics. While rodent models provide invaluable insight into the initial characterization and screening of potential therapeutic interventions, the significant failures of novel pharmacological agents in clinical trials may be partly due to the use of animal models that do not fully reflect stroke pathophysiology as it occurs in humans. As highlighted throughout this review, NHP, ovine, porcine, and canine ischemic stroke models possess significant advantages including comparative brain anatomy, similar tissue-level and functional responses, and compatibility with clinically

relevant MRI techniques. To further enhance the predictive power of these large animal models, advances need to be made to develop thromboembolic clot models that will more closely mimic patient vascular occlusion mechanisms, enable the study of reperfusion injury and evaluate the effects of novel combined therapies with thrombolytic agents. These large animal models must be enlisted as an important step in the translational framework in order to successfully bridge the gap between pre-clinical basic studies and effective therapies in human patients.

Author contribution statement

All listed authors made a substantial contribution to the concept and interpretation of the literature; drafted the review; revised it critically for important intellectual content; and approved the version to be published.

Acknowledgements

The authors would like to thank Dr. Kylee Duberstein, Dr. Holly Kinder, and Kelly Scheulin for their valuable editorial critiques of this review.

Funding

This work was also supported by the National Institutes of Health, National Institute of Neurological Disorders and Stroke grant R01NS093314.

Disclosures

We have no conflicts of interest, financial or otherwise, to declare.

References

Ahmad, A. S., I. Satriotomo, J. Fazal, S. E. Nadeau and S. Dore (2015). "Considerations for the Optimization of Induced White Matter Injury Preclinical Models." Front Neurol **6**: 172.

Allen, J. S., H. Damasio and T. J. Grabowski (2002). "Normal neuroanatomical variation in the human brain: an MRI-volumetric study." Am J Phys Anthropol **118**(4): 341-358.

Ashwini, C. A., Shubba, R., Jayanthi, K.S. (2008). "Comparative anatomy of the circle of Willis in man, cow, sheep, goat, and pig." Neuroanatomy **7**: 54-85.

Astrup, J., B. K. Siesjo and L. Symon (1981). "Thresholds in cerebral ischemia - the ischemic penumbra." Stroke **12**(6): 723-725.

Atchaneeyasakul, K., L. Guada, K. Ramdas, M. Watanabe, P. Bhattacharya, A. P. Raval and D. R. Yavagal (2016). "Large animal canine endovascular ischemic stroke models: A review." Brain Res Bull **127**: 134-140.

Baker, E. W., S. R. Platt, V. W. Lau, H. E. Grace, S. P. Holmes, L. Wang, K. J. Duberstein, E. W. Howerth, H. A. Kinder, S. L. Stice, D. C. Hess, H. Mao and F. D. West (2017). "Induced Pluripotent Stem Cell-Derived Neural Stem Cell Therapy Enhances Recovery in an Ischemic Stroke Pig Model." Sci Rep **7**(1): 10075.

Baltan, S., E. F. Besancon, B. Mbow, Z. Ye, M. A. Hamner and B. R. Ransom (2008). "White matter vulnerability to ischemic injury increases with age because of enhanced excitotoxicity." J Neurosci **28**(6): 1479-1489.

Bataille, B., M. Wager, F. Lapierre, J. M. Goujon, K. Buffenoir and P. Rigoard (2007). "The significance of the rete mirabile in Vesalius's work: an example of the dangers of inductive inference in medicine." Neurosurgery **60**(4): 761-768; discussion 768.

Battey, T. W., M. Karki, A. B. Singhal, O. Wu, S. Sadaghiani, B. C. Campbell, S. M. Davis, G. A. Donnan, K. N. Sheth and W. T. Kimberly (2014). "Brain edema predicts outcome after nonlacunar ischemic stroke." Stroke **45**(12): 3643-3648.

Benjamin, E. J., P. Muntner, A. Alonso, M. S. Bittencourt, C. W. Callaway, A. P. Carson, A. M. Chamberlain, A. R. Chang, S. Cheng, S. R. Das, F. N. Delling, L. Djousse, M. S. V. Elkind, J. F. Ferguson, M. Fornage, L. C. Jordan, S. S. Khan, B. M. Kissela, K. L. Knutson, T. W. Kwan, D. T. Lackland, T. T. Lewis, J. H. Lichtman, C. T. Longenecker, M. S. Loop, P. L. Lutsey, S. S. Martin, K. Matsushita, A. E. Moran, M. E. Mussolino, M. O'Flaherty, A. Pandey, A. M. Perak, W. D. Rosamond, G. A. Roth, U. K. A. Sampson, G. M. Satou, E. B. Schroeder, S. H. Shah, N. L. Spartano, A. Stokes, D. L. Tirschwell, C. W. Tsao, M. P. Turakhia, L. B. VanWagner, J. T. Wilkins, S. S. Wong, S. S. Virani, E. American Heart Association Council on, C. Prevention Statistics and S. Stroke Statistics (2019). "Heart Disease and Stroke Statistics-2019 Update: A Report From the American Heart Association." Circulation **139**(10): e56-e528.

Berrouschot, J., M. Sterker, S. Bettin, J. Koster and D. Schneider (1998). "Mortality of space-occupying ('malignant') middle cerebral artery infarction under conservative intensive care." Intensive Care Med **24**(6): 620-623.

Biesbroek, J. M., N. A. Weaver and G. J. Biessels (2017). "Lesion location and cognitive impact of cerebral small vessel disease." Clin Sci (Lond) **131**(8): 715-728.

Bihel, E., P. Pro-Sistiaga, A. Letourneur, J. Toutain, R. Saulnier, R. Insausti, M. Bernaudin, S. Roussel and O. Touzani (2010). "Permanent or transient chronic ischemic stroke in the non-human primate: behavioral, neuroimaging, histological, and immunohistochemical investigations." J Cereb Blood Flow Metab **30**(2): 273-285.

Boltze, J., A. Forschler, B. Nitzsche, D. Waldmin, A. Hoffmann, C. M. Boltze, A. Y. Dreyer, A. Goldammer, A. Reischauer, W. Hartig, K. D. Geiger, H. Barthel, F. Emmrich and U. Gille (2008). "Permanent middle cerebral artery occlusion in sheep: a novel large animal model of focal cerebral ischemia." J Cereb Blood Flow Metab **28**(12): 1951-1964.

Borowsky, I. W. and R. C. Collins (1989). "Metabolic anatomy of brain: a comparison of regional capillary density, glucose metabolism, and enzyme activities." J Comp Neurol **288**(3): 401-413.

Boyd, L. A., J. D. Edwards, C. S. Siengsukon, E. D. Vidoni, B. D. Wessel and M. A. Linsdell (2009). "Motor sequence chunking is impaired by basal ganglia stroke." Neurobiol Learn Mem **92**(1): 35-44.

Carmichael, S. T. (2005). "Rodent models of focal stroke: size, mechanism, and purpose." NeuroRx **2**(3): 396-409.

Chen, J. W., Z. J. Gombart, S. Rogers, S. K. Gardiner, S. Cecil and R. M. Bullock (2011). "Pupillary reactivity as an early indicator of increased intracranial pressure: The introduction of the Neurological Pupil index." Surg Neurol Int **2**: 82.

Chin, Y., Y. Sato, M. Mase, T. Kato, B. Herculano, M. Sekino, H. Ohsaki, N. Ageyama, F. Ono, K. Terao, Y. Yoshikawa and T. Hisatsune (2010). "Transient decrease in cerebral motor pathway fractional anisotropy after focal ischemic stroke in monkey." Neurosci Res **66**(4): 406-411.

Christoforidis, G. A., C. Rink, M. S. Kontzialis, Y. Mohammad, R. M. Koch, A. M. Abduljalil, V. K. Bergdall, S. Roy, S. Khanna, A. P. Slivka, M. V. Knopp and C. K. Sen (2011). "An endovascular canine middle cerebral artery occlusion model for the study of leptomeningeal collateral recruitment." Invest Radiol **46**(1): 34-40.

Cirstea, M. C. and M. F. Levin (2000). "Compensatory strategies for reaching in stroke." Brain **123 (Pt 5)**: 940-953.

Combs, D. J., R. J. Dempsey, S. Kumar and D. Donaldson (1990). "Focal cerebral infarction in cats in the presence of hyperglycemia and increased insulin." Metab Brain Dis **5**(4): 169-178.

Conrad, M. S., R. N. Dilger and R. W. Johnson (2012). "Brain growth of the domestic pig (Sus scrofa) from 2 to 24 weeks of age: a longitudinal MRI study." Dev Neurosci **34**(4): 291-298.

Cook, D. J. and M. Tymianski (2011). "Translating promising preclinical neuroprotective therapies to human stroke trials." Expert Rev Cardiovasc Ther **9**(4): 433-449.

Cook, D. J. and M. Tymianski (2012). "Nonhuman primate models of stroke for translational neuroprotection research." Neurotherapeutics **9**(2): 371-379.

Cui, Y., Y. Tian, Y. Tang, L. Jia, A. Wu, P. Peng, J. Yang, H. Du, X. Wang and L. Wu (2013). "Application of sodium alginate microspheres in ischemic stroke modeling in miniature pigs." Neural Regen Res **8**(16): 1473-1480.

D'Ambrosio, A. L., M. E. Sughrue, J. Mocco, W. J. Mack, R. G. King, S. Agarwal and E. S. Connolly, Jr. (2004). "A modified transorbital baboon model of reperfused stroke." Methods Enzymol **386**: 60-73.

Daniel PM, D. J., Prichard MML (1953). "Studies of the carotid rete and its associated arteries." The royal society **237**(645).

Darby, D. G., P. A. Barber, R. P. Gerraty, P. M. Desmond, Q. Yang, M. Parsons, T. Li, B. M. Tress and S. M. Davis (1999). "Pathophysiological topography of acute ischemia by combined diffusion-weighted and perfusion MRI." Stroke **30**(10): 2043-2052.

de Crespigny, A. J., H. E. D'Arceuil, K. I. Maynard, J. He, D. McAuliffe, A. Norbash, P. K. Sehgal, L. Hamberg, G. Hunter, R. F. Budzik, C. M. Putman and R. G. Gonzalez (2005). "Acute studies of a new primate model of reversible middle cerebral artery occlusion." J Stroke Cerebrovasc Dis **14**(2): 80-87.

Debette, S. and H. S. Markus (2010). "The clinical importance of white matter hyperintensities on brain magnetic resonance imaging: systematic review and meta-analysis." BMJ **341**: c3666.

Deepthi S., S. D., Pramod Kumar D., Saradadevi S. S., Subhadradevi V. (2016). "Comparative study of formation of Circle of Willis in human and sheep brain." J. Anat. Soc. **65**(Supplement 1): S16–S19.

Del Zoppo, G. J., B. R. Copeland, L. A. Harker, T. A. Waltz, J. Zyroff, S. R. Hanson and E. Battenberg (1986). "Experimental acute thrombotic stroke in baboons." Stroke **17**(6): 1254-1265.

Eastwood, J. D., S. T. Engelter, J. F. MacFall, D. M. Delong and J. M. Provenzale (2003). "Quantitative assessment of the time course of infarct signal intensity on diffusion-weighted images." AJNR Am J Neuroradiol **24**(4): 680-687.

Fisher, M., G. Feuerstein, D. W. Howells, P. D. Hurn, T. A. Kent, S. I. Savitz, E. H. Lo and S. Group (2009). "Update of the stroke therapy academic industry roundtable preclinical recommendations." Stroke **40**(6): 2244-2250.

Fisher, M., D. F. Hanley, G. Howard, E. C. Jauch, S. Warach and S. Group (2007). "Recommendations from the STAIR V meeting on acute stroke trials, technology and outcomes." Stroke **38**(2): 245-248.

Fisher, M. and R. Stroke Therapy Academic Industry (2003). "Recommendations for advancing development of acute stroke therapies: Stroke Therapy Academic Industry Roundtable 3." Stroke **34**(6): 1539-1546.

Flecknell, P. A., P. A. Flecknell and ebrary Inc. (2009). Laboratory animal anaesthesia. Amsterdam ; Boston ; London, Elsevier/Academic Press.

Flight, S. M., P. P. Masci, M. F. Lavin and P. J. Gaffney (2006). "Resistance of porcine blood clots to lysis relates to poor activation of porcine plasminogen by tissue plasminogen activator." Blood Coagul Fibrinolysis **17**(5): 417-420.

Furlanis, G., M. Ajcevic, L. Stragapede, C. Lugnan, M. Ridolfi, P. Caruso, M. Naccarato, M. Ukmar and P. Manganotti (2018). "Ischemic Volume and Neurological Deficit: Correlation of Computed Tomography Perfusion with the National Institutes of Health Stroke Scale Score in Acute Ischemic Stroke." J Stroke Cerebrovasc Dis **27**(8): 2200-2207.

Gabrielian, L., S. C. Helps, E. Thornton, R. J. Turner, A. V. Leonard and R. Vink (2013). "Substance P antagonists as a novel intervention for brain edema and raised intracranial pressure." Acta Neurochir Suppl **118**: 201-204.

Gabrielian, L., L. W. Willshire, S. C. Helps, C. van den Heuvel, J. Mathias and R. Vink (2011). "Intracranial pressure changes following traumatic brain injury in rats: lack of significant change in the absence of mass lesions or hypoxia." J Neurotrauma **28**(10): 2103-2111.

Giffard, C., A. R. Young, F. Mezenge, J. M. Derlon and J. C. Baron (2005). "Histopathological effects of delayed reperfusion after middle cerebral artery occlusion in the anesthetized baboon." Brain Res Bull **67**(4): 335-340.

Gonzalez, R. G. (2012). "Clinical MRI of acute ischemic stroke." J Magn Reson Imaging **36**(2): 259-271.

Gralla, J., G. Schroth, L. Remonda, A. Fleischmann, J. Fandino, J. Slotboom and C. Brekenfeld (2006). "A dedicated animal model for mechanical thrombectomy in acute stroke." AJNR Am J Neuroradiol **27**(6): 1357-1361.

Guo, J., H. B. Zheng, J. C. Duan, L. He, N. Chen, Q. Y. Gong, H. H. Tang, H. X. Li, L. Wang and J. Q. Cheng (2011). "Diffusion tensor MRI for the assessment of cerebral ischemia/reperfusion injury in the penumbra of non-human primate stroke model." Neurol Res **33**(1): 108-112.

Hacke, W., S. Schwab, M. Horn, M. Spranger, M. De Georgia and R. von Kummer (1996). "'Malignant' middle cerebral artery territory infarction: clinical course and prognostic signs." Arch Neurol **53**(4): 309-315.

Harris, A. D., R. K. Kosior, H. S. Chen, L. B. Andersen and R. Frayne (2009). "Evolution of hyperacute stroke over 6 hours using serial MR perfusion and diffusion maps." J Magn Reson Imaging **29**(6): 1262-1270.

Hewitt A., E. C. (2012). "Brain oedema, intracranial pressure and cerebral blood flow." Surgery **30**: 102-106.

Higano, S., J. Zhong, D. A. Shrier, D. K. Shibata, Y. Takase, H. Wang and Y. Numaguchi (2001). "Diffusion anisotropy of the internal capsule and the corona radiata in association with stroke and tumors as measured by diffusion-weighted MR imaging." AJNR Am J Neuroradiol **22**(3): 456-463.

Hill, N. C., C. H. Millikan, K. G. Wakim and G. P. Sayre (1955). "Studies in cerebrovascular disease. VII. Experimental production of cerebral infarction by

intracarotid injection of homologous blood clot; preliminary report." Proc Staff Meet Mayo Clin **30**(26): 625-633.

Hillock SM, D. C., Stefanacci JD, Fondacaro JV (2006). "Vascular encephalopathies in dogs: incidence, risk factors, pathophysiology, and clinical signs." Compendium on Continuing Education for the Practising Veterinarian **28**: 196-207.

Ho, M. L., R. Rojas and R. L. Eisenberg (2012). "Cerebral edema." AJR Am J Roentgenol **199**(3): W258-273.

Hoffmann, A., M. H. Stoffel, B. Nitzsche, D. Lobsien, J. Seeger, H. Schneider and J. Boltze (2014). "The ovine cerebral venous system: comparative anatomy, visualization, and implications for translational research." PLoS One **9**(4): e92990.

Hossmann, K. A. (1994). "Viability thresholds and the penumbra of focal ischemia." Ann Neurol **36**(4): 557-565.

Hossmann, K. A. (2009). "Pathophysiological basis of translational stroke research." Folia Neuropathol **47**(3): 213-227.

Howells, D. W., M. J. Porritt, S. S. Rewell, V. O'Collins, E. S. Sena, H. B. van der Worp, R. J. Traystman and M. R. Macleod (2010). "Different strokes for different folks: the rich diversity of animal models of focal cerebral ischemia." J Cereb Blood Flow Metab **30**(8): 1412-1431.

Huang, J., J. Mocco, T. F. Choudhri, A. Poisik, S. J. Popilskis, R. Emerson, R. L. DelaPaz, A. G. Khandji, D. J. Pinsky and E. S. Connolly, Jr. (2000). "A modified transorbital baboon model of reperfused stroke." Stroke **31**(12): 3054-3063.

Imai, H., K. Konno, M. Nakamura, T. Shimizu, C. Kubota, K. Seki, F. Honda, S. Tomizawa, Y. Tanaka, H. Hata and N. Saito (2006). "A new model of focal cerebral ischemia in the miniature pig." J Neurosurg **104**(2 Suppl): 123-132.

Kaiser E.E., W. E. S., Fagan M.M., Scheulin K.M., Platt S.R., Jeon J.H., Fang X., Kinder H.A., Shin S.K., Duberstein K.J., Park H.J., West F.D. (2019). "Acute characterization of tissue and functional deficits in a clinically translatable pig model of ischemic stroke." PLoS One.

Kakuda, W., M. G. Lansberg, V. N. Thijs, S. M. Kemp, R. Bammer, L. R. Wechsler, M. E. Moseley, M. P. Marks, G. W. Albers and D. Investigators (2008). "Optimal definition for PWI/DWI mismatch in acute ischemic stroke patients." J Cereb Blood Flow Metab **28**(5): 887-891.

Kang, B. T., D. P. Jang, S. H. Gu, J. H. Lee, D. I. Jung, C. Y. Lim, H. J. Kim, Y. B. Kim, H. J. Kim, E. J. Woo, Z. H. Cho and H. M. Park (2009). "MRI features in a canine model of ischemic stroke: correlation between lesion volume and neurobehavioral status during the subacute stage." Comp Med **59**(5): 459-464.

Kang, B. T., J. H. Lee, D. I. Jung, C. Park, S. H. Gu, H. W. Jeon, D. P. Jang, C. Y. Lim, F. S. Quan, Y. B. Kim, Z. H. Cho, E. J. Woo and H. M. Park (2007). "Canine model of ischemic stroke with permanent middle cerebral artery occlusion: clinical and histopathological findings." J Vet Sci **8**(4): 369-376.

Kapoor, K., V. K. Kak and B. Singh (2003). "Morphology and comparative anatomy of circulus arteriosus cerebri in mammals." Anat Histol Embryol **32**(6): 347-355.

Kenning, T. J., M. R. Gooch, R. H. Gandhi, M. P. Shaikh, A. S. Boulos and J. W. German (2012). "Cranial decompression for the treatment of malignant intracranial

hypertension after ischemic cerebral infarction: decompressive craniectomy and hinge craniotomy." J Neurosurg **116**(6): 1289-1298.

Kito, G., A. Nishimura, T. Susumu, R. Nagata, Y. Kuge, C. Yokota and K. Minematsu (2001). "Experimental thromboembolic stroke in cynomolgus monkey." J Neurosci Methods **105**(1): 45-53.

Klintworth, G. K. (1968). "The comparative anatomy and phylogeny of the tentorium cerebelli." Anat Rec **160**(3): 635-642.

Kobayashi, E., S. Hishikawa, T. Teratani and A. T. Lefor (2012). "The pig as a model for translational research: overview of porcine animal models at Jichi Medical University." Transplant Res **1**(1): 8.

Kotwica, Z., H. G. Hardemark and L. Persson (1991). "Intracranial pressure changes following middle cerebral artery occlusion in rats." Res Exp Med (Berl) **191**(2): 99-104.

Krafft, P. R., E. L. Bailey, T. Lekic, W. B. Rolland, O. Altay, J. Tang, J. M. Wardlaw, J. H. Zhang and C. L. Sudlow (2012). "Etiology of stroke and choice of models." Int J Stroke **7**(5): 398-406.

Kuge, Y., C. Yokota, M. Tagaya, Y. Hasegawa, A. Nishimura, G. Kito, N. Tamaki, N. Hashimoto, T. Yamaguchi and K. Minematsu (2001). "Serial changes in cerebral blood flow and flow-metabolism uncoupling in primates with acute thromboembolic stroke." J Cereb Blood Flow Metab **21**(3): 202-210.

Kunimatsu, A., S. Aoki, Y. Masutani, O. Abe, H. Mori and K. Ohtomo (2003). "Three-dimensional white matter tractography by diffusion tensor imaging in ischaemic stroke involving the corticospinal tract." Neuroradiology **45**(8): 532-535.

Lavinio, A. and D. K. Menon (2011). "Intracranial pressure: why we monitor it, how to monitor it, what to do with the number and what's the future?" Curr Opin Anaesthesiol **24**(2): 117-123.

Lee, D. H., D. W. Kang, J. S. Ahn, C. G. Choi, S. J. Kim and D. C. Suh (2005). "Imaging of the ischemic penumbra in acute stroke." Korean J Radiol **6**(2): 64-74.

Lee, K. B., J. S. Kim, B. Y. Hong, B. Sul, S. Song, W. J. Sung, B. Y. Hwang and S. H. Lim (2017). "Brain lesions affecting gait recovery in stroke patients." Brain Behav **7**(11): e00868.

Lee, M. H., J. T. Yang, H. H. Weng, Y. K. Cheng, M. H. Lin, C. H. Su, C. M. Chang and T. C. Wang (2012). "Hydrocephalus following decompressive craniectomy for malignant middle cerebral artery infarction." Clin Neurol Neurosurg **114**(6): 555-559.

Liao, F., J. Wang and P. He (2008). "Multi-resolution entropy analysis of gait symmetry in neurological degenerative diseases and amyotrophic lateral sclerosis." Med Eng Phys **30**(3): 299-310.

Liu, S., W. X. Hu, Q. Q. Zu, S. S. Lu, X. Q. Xu, L. Sun, W. Z. Zhou and H. B. Shi (2012). "A novel embolic stroke model resembling lacunar infarction following proximal middle cerebral artery occlusion in beagle dogs." J Neurosci Methods **209**(1): 90-96.

Liu, Y., H. E. D'Arceuil, S. Westmoreland, J. He, M. Duggan, R. G. Gonzalez, J. Pryor and A. J. de Crespigny (2007). "Serial diffusion tensor MRI after transient and permanent cerebral ischemia in nonhuman primates." Stroke **38**(1): 138-145.

Mack, W. J., R. G. King, D. J. Hoh, A. L. Coon, A. F. Ducruet, J. Huang, J. Mocco, C. J. Winfree, A. L. D'Ambrosio, M. N. Nair, R. R. Sciacca and E. S. Connolly, Jr. (2003).

"An improved functional neurological examination for use in nonhuman primate studies of focal reperfused cerebral ischemia." Neurol Res **25**(3): 280-284.

Mackay, J., G. A. Mensah, S. Mendis, K. Greenlund and World Health Organization. (2004). The atlas of heart disease and stroke. Geneva, World Health Organization.

Macrae, I. M. (2011). "Preclinical stroke research--advantages and disadvantages of the most common rodent models of focal ischaemia." Br J Pharmacol **164**(4): 1062-1078.

Miyai, I., A. D. Blau, M. J. Reding and B. T. Volpe (1997). "Patients with stroke confined to basal ganglia have diminished response to rehabilitation efforts." Neurology **48**(1): 95-101.

Munoz Maniega, S., M. E. Bastin, P. A. Armitage, A. J. Farrall, T. K. Carpenter, P. J. Hand, V. Cvoro, C. S. Rivers and J. M. Wardlaw (2004). "Temporal evolution of water diffusion parameters is different in grey and white matter in human ischaemic stroke." J Neurol Neurosurg Psychiatry **75**(12): 1714-1718.

Murphy, S. J., J. R. Kirsch, W. Zhang, M. R. Grafe, G. A. West, G. J. del Zoppo, R. J. Traystman and P. D. Hum (2008). "Can gender differences be evaluated in a rhesus macaque (Macaca mulatta) model of focal cerebral ischemia?" Comp Med **58**(6): 588-596.

Nael, K., T. P. Trouard, S. R. Lafleur, E. A. Krupinski, N. Salamon and C. S. Kidwell (2015). "White matter ischemic changes in hyperacute ischemic stroke: voxel-based analysis using diffusion tensor imaging and MR perfusion." Stroke **46**(2): 413-418.

Nakamura, M., H. Imai, K. Konno, C. Kubota, K. Seki, S. Puentes, A. Faried, H. Yokoo, H. Hata, Y. Yoshimoto and N. Saito (2009). "Experimental investigation of encephalomyosynangiosis using gyrencephalic brain of the miniature pig:

histopathological evaluation of dynamic reconstruction of vessels for functional anastomosis. Laboratory investigation." J Neurosurg Pediatr **3**(6): 488-495.

Nakayama, H., H. S. Jorgensen, H. O. Raaschou and T. S. Olsen (1994). "The influence of age on stroke outcome. The Copenhagen Stroke Study." Stroke **25**(4): 808-813.

Nanda, B. S. and R. Getty (1975). "Arteria intercarotica caudalis and its homologue in the domestic animals." Anat Anz **137**(1-2): 110-115.

Navarro-Orozco, D. and J. C. Sanchez-Manso (2019). Neuroanatomy, Middle Cerebral Artery. StatPearls. Treasure Island (FL).

Nehls, D. G., M. Cartwright and R. F. Spetzler (1986). "Experimental primate stroke model." Neurosurgery **18**(3): 388-389.

Ng, Y. S., J. Stein, M. Ning and R. M. Black-Schaffer (2007). "Comparison of clinical characteristics and functional outcomes of ischemic stroke in different vascular territories." Stroke **38**(8): 2309-2314.

Nitzsche, B., S. Frey, L. D. Collins, J. Seeger, D. Lobsien, A. Dreyer, H. Kirsten, M. H. Stoffel, V. S. Fonov and J. Boltze (2015). "A stereotaxic, population-averaged T1w ovine brain atlas including cerebral morphology and tissue volumes." Front Neuroanat **9**: 69.

Nonaka, H., M. Akima, T. Hatori, T. Nagayama, Z. Zhang and F. Ihara (2003). "The microvasculature of the cerebral white matter: arteries of the subcortical white matter." J Neuropathol Exp Neurol **62**(2): 154-161.

Nudo, R. J., E. J. Plautz and S. B. Frost (2001). "Role of adaptive plasticity in recovery of function after damage to motor cortex." Muscle Nerve **24**(8): 1000-1019.

Pantano, P., F. Caramia, L. Bozzao, C. Dieler and R. von Kummer (1999). "Delayed increase in infarct volume after cerebral ischemia: correlations with thrombolytic treatment and clinical outcome." Stroke **30**(3): 502-507.

Patterson, K. K., I. Parafianowicz, C. J. Danells, V. Closson, M. C. Verrier, W. R. Staines, S. E. Black and W. E. McIlroy (2008). "Gait asymmetry in community-ambulating stroke survivors." Arch Phys Med Rehabil **89**(2): 304-310.

Perel, P., I. Roberts, E. Sena, P. Wheble, C. Briscoe, P. Sandercock, M. Macleod, L. E. Mignini, P. Jayaram and K. S. Khan (2007). "Comparison of treatment effects between animal experiments and clinical trials: systematic review." BMJ **334**(7586): 197.

Peters, A., U. Schweiger, L. Pellerin, C. Hubold, K. M. Oltmanns, M. Conrad, B. Schultes, J. Born and H. L. Fehm (2004). "The selfish brain: competition for energy resources." Neurosci Biobehav Rev **28**(2): 143-180.

Pierpaoli, C., A. Barnett, S. Pajevic, R. Chen, L. R. Penix, A. Virta and P. Basser (2001). "Water diffusion changes in Wallerian degeneration and their dependence on white matter architecture." Neuroimage **13**(6 Pt 1): 1174-1185.

Platt, S. R., S. P. Holmes, E. W. Howerth, K. J. Duberstein, C. R. Dove, H. A. Kinder, E. L. Wyatt, A. V. Linville, V. W. Lau, S. L. Stice, W. D. Hill, D. C. Hess and F. D. West (2014). "Development and characterization of a Yucatan miniature biomedical pig permanent middle cerebral artery occlusion stroke model." Exp Transl Stroke Med **6**(1): 5.

Qureshi, A. I., A. S. Boulos, R. A. Hanel, M. F. Suri, A. M. Yahia, R. A. Alberico and L. N. Hopkins (2004). "Randomized comparison of intra-arterial and intravenous

thrombolysis in a canine model of acute basilar artery thrombosis." Neuroradiology **46**(12): 988-995.

Rink, C., G. Christoforidis, A. Abduljalil, M. Kontzialis, V. Bergdall, S. Roy, S. Khanna, A. Slivka, M. Knopp and C. K. Sen (2008). "Minimally invasive neuroradiologic model of preclinical transient middle cerebral artery occlusion in canines." Proc Natl Acad Sci U S A **105**(37): 14100-14105.

Rink, C., G. Christoforidis, S. Khanna, L. Peterson, Y. Patel, S. Khanna, A. Abduljalil, O. Irfanoglu, R. Machiraju, V. K. Bergdall and C. K. Sen (2011). "Tocotrienol vitamin E protects against preclinical canine ischemic stroke by inducing arteriogenesis." J Cereb Blood Flow Metab **31**(11): 2218-2230.

Rodriguez-Mercado, R., G. D. Ford, Z. Xu, E. N. Kraiselburd, M. I. Martinez, V. A. Eterovic, E. Colon, I. V. Rodriguez, P. Portilla, P. A. Ferchmin, L. Gierbolini, M. Rodriguez-Carrasquillo, M. D. Powell, J. V. Pulliam, C. O. McCraw, A. Gates and B. D. Ford (2012). "Acute neuronal injury and blood genomic profiles in a nonhuman primate model for ischemic stroke." Comp Med **62**(5): 427-438.

Ropper, A. H. (1986). "Lateral displacement of the brain and level of consciousness in patients with an acute hemispheral mass." N Engl J Med **314**(15): 953-958.

Roth, G. and U. Dicke (2012). "Evolution of the brain and intelligence in primates." Prog Brain Res **195**: 413-430.

Sahin B, A. H., Unal B, Canan S, Bilgic S, Kaplan S, Tumkaya L (2001). "Brain volumes of the lamb, rat and bird do not show hemispheric asymmetry: a stereological study." Image Analysis & Stereology **20**(1): 9-13.

Sakoh, M., L. Ostergaard, L. Rohl, D. F. Smith, C. Z. Simonsen, J. C. Sorensen, P. V. Poulsen, C. Gyldensted, S. Sakaki and A. Gjedde (2000). "Relationship between residual cerebral blood flow and oxygen metabolism as predictive of ischemic tissue viability: sequential multitracer positron emission tomography scanning of middle cerebral artery occlusion during the critical first 6 hours after stroke in pigs." J Neurosurg **93**(4): 647-657.

Sakoh, M., L. Rohl, C. Gyldensted, A. Gjedde and L. Ostergaard (2000). "Cerebral blood flow and blood volume measured by magnetic resonance imaging bolus tracking after acute stroke in pigs: comparison with [(15)O]H(2)O positron emission tomography." Stroke **31**(8): 1958-1964.

Sanak, D., V. Nosal, D. Horak, A. Bartkova, K. Zelenak, R. Herzig, J. Bucil, D. Skoloudik, S. Burval, V. Cisarikova, I. Vlachova, M. Kocher, J. Zapletalova, E. Kurca and P. Kanovsky (2006). "Impact of diffusion-weighted MRI-measured initial cerebral infarction volume on clinical outcome in acute stroke patients with middle cerebral artery occlusion treated by thrombolysis." Neuroradiology **48**(9): 632-639.

Saver, J. L. (2006). "Time is brain--quantified." Stroke **37**(1): 263-266.

Shaibani, A., S. Khawar, W. Shin, T. A. Cashen, B. Schirf, M. Rohany, S. Kakodkar and T. J. Carroll (2006). "First results in an MR imaging--compatible canine model of acute stroke." AJNR Am J Neuroradiol **27**(8): 1788-1793.

Shen, Q., X. Meng, M. Fisher, C. H. Sotak and T. Q. Duong (2003). "Pixel-by-pixel spatiotemporal progression of focal ischemia derived using quantitative perfusion and diffusion imaging." J Cereb Blood Flow Metab **23**(12): 1479-1488.

Sicard, K. M. and M. Fisher (2009). "Animal models of focal brain ischemia." Exp Transl Stroke Med **1**: 7.

Simonyan, K. (2019). "Recent advances in understanding the role of the basal ganglia." F1000Res **8**.

Sofuwa, O., A. Nieuwboer, K. Desloovere, A. M. Willems, F. Chavret and I. Jonkers (2005). "Quantitative gait analysis in Parkinson's disease: comparison with a healthy control group." Arch Phys Med Rehabil **86**(5): 1007-1013.

Sorby-Adams, A. J., A. V. Leonard, L. E. Elms, O. C. Marian, J. W. Hoving, N. Yassi, R. Vink, E. Thornton and R. J. Turner (2019). "Determining the Temporal Profile of Intracranial Pressure Changes Following Transient Stroke in an Ovine Model." Front Neurosci **13**: 587.

Sorby-Adams, A. J., R. Vink and R. J. Turner (2018). "Large animal models of stroke and traumatic brain injury as translational tools." Am J Physiol Regul Integr Comp Physiol **315**(2): R165-R190.

Spetzler, R. F., J. M. Zabramski, B. Kaufman and H. N. Yeung (1983). "Acute NMR changes during MCA occlusion: a preliminary study in primates." Stroke **14**(2): 185-191.

Srikanth, V., R. Beare, L. Blizzard, T. Phan, J. Stapleton, J. Chen, M. Callisaya, K. Martin and D. Reutens (2009). "Cerebral white matter lesions, gait, and the risk of incident falls: a prospective population-based study." Stroke **40**(1): 175-180.

Stroke Therapy Academic Industry, R. (1999). "Recommendations for standards regarding preclinical neuroprotective and restorative drug development." Stroke **30**(12): 2752-2758.

Symon, L. (1960). "Observations on the leptomeningeal collateral circulation in dogs." J Physiol **154**(1): 1-14 12.

Tagaya, M., K. F. Liu, B. Copeland, D. Seiffert, R. Engler, J. H. Garcia and G. J. del Zoppo (1997). "DNA scission after focal brain ischemia. Temporal differences in two species." Stroke **28**(6): 1245-1254.

Tanaka, Y., H. Imai, K. Konno, T. Miyagishima, C. Kubota, S. Puentes, T. Aoki, H. Hata, K. Takata, Y. Yoshimoto and N. Saito (2008). "Experimental model of lacunar infarction in the gyrencephalic brain of the miniature pig: neurological assessment and histological, immunohistochemical, and physiological evaluation of dynamic corticospinal tract deformation." Stroke **39**(1): 205-212.

Tarkowski, E., L. Rosengren, C. Blomstrand, C. Wikkelso, C. Jensen, S. Ekholm and A. Tarkowski (1995). "Early intrathecal production of interleukin-6 predicts the size of brain lesion in stroke." Stroke **26**(8): 1393-1398.

Tarkowski, E., L. Rosengren, C. Blomstrand, C. Wikkelso, C. Jensen, S. Ekholm and A. Tarkowski (1997). "Intrathecal release of pro- and anti-inflammatory cytokines during stroke." Clin Exp Immunol **110**(3): 492-499.

Traversa, R., P. Cicinelli, M. Oliveri, M. Giuseppina Palmieri, M. M. Filippi, P. Pasqualetti and P. M. Rossini (2000). "Neurophysiological follow-up of motor cortical output in stroke patients." Clin Neurophysiol **111**(9): 1695-1703.

Traystman, R. J. (2003). "Animal models of focal and global cerebral ischemia." ILAR J **44**(2): 85-95.

Treadwell, S. D. and B. Thanvi (2010). "Malignant middle cerebral artery (MCA) infarction: pathophysiology, diagnosis and management." Postgrad Med J **86**(1014): 235-242.

van der Bom, I. M., M. Mehra, R. P. Walvick, J. Y. Chueh and M. J. Gounis (2012). "Quantitative evaluation of C-arm CT cerebral blood volume in a canine model of ischemic stroke." AJNR Am J Neuroradiol **33**(2): 353-358.

van Everdingen, K. J., J. van der Grond, L. J. Kappelle, L. M. Ramos and W. P. Mali (1998). "Diffusion-weighted magnetic resonance imaging in acute stroke." Stroke **29**(9): 1783-1790.

Veerbeek, J. M., M. Koolstra, J. C. Ket, E. E. van Wegen and G. Kwakkel (2011). "Effects of augmented exercise therapy on outcome of gait and gait-related activities in the first 6 months after stroke: a meta-analysis." Stroke **42**(11): 3311-3315.

Walberer, M., F. Blaes, E. Stolz, C. Muller, M. Schoenburg, M. Tschernatsch, G. Bachmann and T. Gerriets (2007). "Midline-shift corresponds to the amount of brain edema early after hemispheric stroke--an MRI study in rats." J Neurosurg Anesthesiol **19**(2): 105-110.

Wang, D. Z., D. S. Nair and A. V. Talkad (2011). "Acute Decompressive Hemicraniectomy to Control High Intracranial Pressure in Patients with Malignant MCA Ischemic Strokes." Curr Treat Options Cardiovasc Med **13**(3): 225-232.

Wang, Y., G. Liu, D. Hong, F. Chen, X. Ji and G. Cao (2016). "White matter injury in ischemic stroke." Prog Neurobiol **141**: 45-60.

Warach, S., J. F. Dashe and R. R. Edelman (1996). "Clinical outcome in ischemic stroke predicted by early diffusion-weighted and perfusion magnetic resonance imaging: a preliminary analysis." J Cereb Blood Flow Metab **16**(1): 53-59.

Watanabe, H., F. Andersen, C. Z. Simonsen, S. M. Evans, A. Gjedde, P. Cumming and X. S. G. DaNe (2001). "MR-based statistical atlas of the Gottingen minipig brain." Neuroimage **14**(5): 1089-1096.

Watanabe, H., M. Sakoh, F. Andersen, A. Rodell, J. C. Sorensen, L. Ostergaard, K. Mouridsen and P. Cumming (2007). "Statistical mapping of effects of middle cerebral artery occlusion (MCAO) on blood flow and oxygen consumption in porcine brain." J Neurosci Methods **160**(1): 109-115.

Webb, R. L., E. E. Kaiser, B. J. Jurgielewicz, S. Spellicy, S. L. Scoville, T. A. Thompson, R. L. Swetenburg, D. C. Hess, F. D. West and S. L. Stice (2018). "Human Neural Stem Cell Extracellular Vesicles Improve Recovery in a Porcine Model of Ischemic Stroke." Stroke **49**(5): 1248-1256.

Wells, A. J., R. Vink, P. C. Blumbergs, B. P. Brophy, S. C. Helps, S. J. Knox and R. J. Turner (2012). "A surgical model of permanent and transient middle cerebral artery stroke in the sheep." PLoS One **7**(7): e42157.

Wells, A. J., R. Vink, S. C. Helps, S. J. Knox, P. C. Blumbergs and R. J. Turner (2015). "Elevated Intracranial Pressure and Cerebral Edema following Permanent MCA Occlusion in an Ovine Model." PLoS One **10**(6): e0130512.

West, G. A., K. J. Golshani, K. P. Doyle, N. S. Lessov, T. R. Hobbs, S. G. Kohama, M. M. Pike, C. D. Kroenke, M. R. Grafe, M. D. Spector, E. T. Tobar, R. P. Simon and M. P.

Stenzel-Poore (2009). "A new model of cortical stroke in the rhesus macaque." J Cereb Blood Flow Metab **29**(6): 1175-1186.

Wey, H. Y., G. M. Kroma, J. Li, M. M. Leland, L. Jones and T. Q. Duong (2011). "MRI of perfusion-diffusion mismatch in non-human primate (baboon) stroke: a preliminary report." Open Neuroimag J **5**: 147-152.

Wey, H. Y., D. J. Wang and T. Q. Duong (2011). "Baseline CBF, and BOLD, CBF, and CMRO2 fMRI of visual and vibrotactile stimulations in baboons." J Cereb Blood Flow Metab **31**(2): 715-724.

Wu, D., J. Chen, B. Wang, M. Zhang, J. Shi, Y. Ma, Z. Zhu, F. Yan, X. He, S. Li, D. Dornbos Iii, Y. Ding and X. Ji (2016). "Endovascular ischemic stroke models of adult rhesus monkeys: a comparison of two endovascular methods." Sci Rep **6**: 31608.

Yakovlev, S. A., M. V. Rublenko, V. I. Izdepsky and E. M. Makogonenko (1995). "Activating effect of the plasminogen activators on plasminogens of different mammalia species." Thromb Res **79**(4): 423-428.

Zhang, X., F. Tong, C. X. Li, Y. Yan, D. Kempf, G. Nair, S. Wang, E. C. Muly, S. Zola and L. Howell (2015). "Temporal evolution of ischemic lesions in nonhuman primates: a diffusion and perfusion MRI study." PLoS One **10**(2): e0117290.

Zhang, Y., M. Jin, B. Du, H. Lin, C. Xu, W. Jiang and J. Jia (2015). "A Novel Canine Model of Acute Vertebral Artery Occlusion." PLoS One **10**(11): e0142251.

Zu, Q. Q., S. Liu, X. Q. Xu, S. S. Lu, L. Sun and H. B. Shi (2013). "An endovascular canine stroke model: middle cerebral artery occlusion with autologous clots followed by ipsilateral internal carotid artery blockade." Lab Invest **93**(7): 760-767.

Figure 2.1: Major large animal models utilized to evaluate human ischemic stroke pathophysiology. Inherent white matter composition, stroke type, surgical occlusion methods, and magnetic resonance assessments provide a platform to investigate human ischemic stroke pathophysiology and consequent functional outcomes. Collectively, these clinically-relevant modalities enable researchers to characterize unique tissue-level and functional (e.g. sensorimotor) changes across acute and chronic time points. These tools possess indisputable value in identifying therapeutic targets and testing of novel treatments prior to clinical trials.

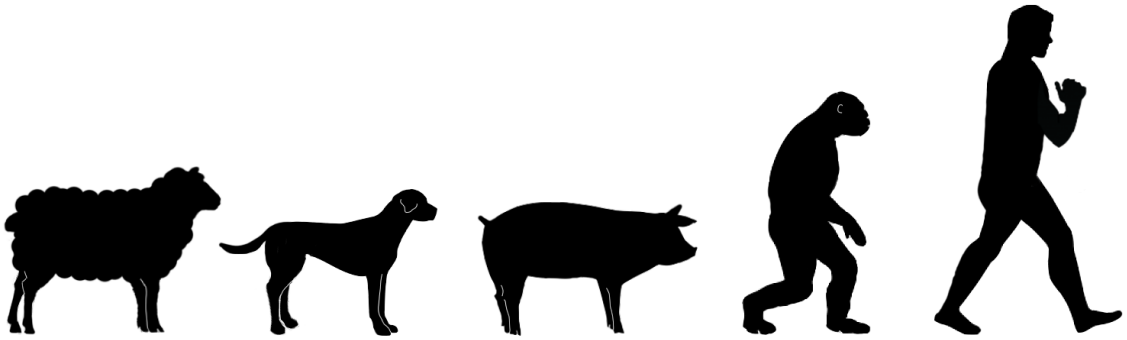

Ovine	Canine	Porcine	Primate	Human
• <30% white matter • Permanent/transient transcranial models • DWI lesion volume correlates with motor impariments • ICP induces cerebral herniation	• <35% white matter • Endovascular models • Clinically relevant acute ADC ratios • IL-6 levels correlate with neurological impairments	• >60% white matter • Permanent transcranial models • Endovascular models • T2W reveals swelling, MLS, and herniation • FA decreases correlate with motor impairments	• >60% white matter • Permanent/transient transcranial models • Endovascular models • Perfusion-diffusion mismatch • FA decreases correlate with motor impairments	• >60% white matter • Perfusion-diffusion mismatch • Lesion volume, FA values, and MLS correlate with motor and neurological impairments

Figure 2.2: Magnetic resonance assessment of a preclinical pig ischemic stroke model 1-day post-middle cerebral artery occlusion. Pathophysiological changes including increased hemispheric swelling, MLS, and hyperintense lesion formation are observed in T2W (**A**) and T2F (**B**) sequences. DWI (**C**) sequences showed hyperintense lesions indicative of territorial edematous injury, while corresponding hypointense lesions on ADC maps (**D**) confirmed restricted diffusion and cytotoxic edema. FA maps (**E**) revealed increased loss of WM integrity in the internal capsule (IC) and the corpus callosum (CC).

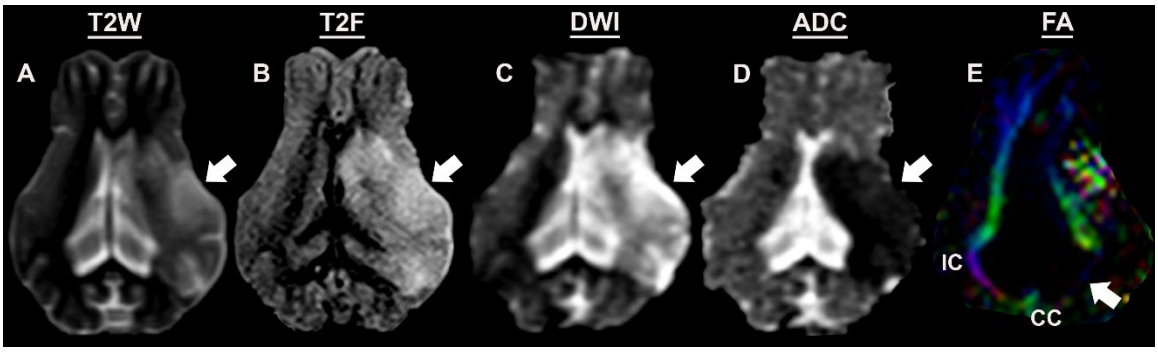
T2W
T2F
DWI
ADC
FA
A
B
C
D
E
IC
CC

CHAPTER 3

CHARACTERIZATION OF TISSUE AND FUNCTIONAL DEFICITS IN A CLINICALLY TRANSLATIONAL PIG MODEL OF ACUTE ISCHEMIC STROKE [1]

[1]Kaiser, E.E., Waters E.S., Fagan, M.M., Scheulin K.M., Platt S.R., Jeon J.H., Fang, X., Kinder H.A., Shin S.K., Duberstein K.J., Park H.J., and West, F.D. In review *Plos ONE*, 2019.

Abstract

The acute stroke phase is a critical time frame used to evaluate stroke severity, therapeutic options, and prognosis while also serving as a major target for the development of diagnostics. To better understand stroke pathophysiology and to enhance the development of treatments, our group developed a translational pig ischemic stroke model. In this study, the evolution of acute ischemic stroke tissue damage, immune response, and functional deficits were further characterized in the pig model. Stroke was induced by middle cerebral artery occlusion in Landrace pigs. At 24 hours post-stroke, magnetic resonance imaging revealed a decrease in ipsilateral diffusivity and an increase in hemispheric swelling and intracerebral hemorrhage resulting in notable midline shift. Stroke negatively impacted white matter integrity leading to decreased fractional anisotropy. Similar to acute clinical patients, stroked pigs showed a reduction in circulating lymphocytes and a surge in neutrophils and band cells. Functional responses corresponded with structural changes with reduced exploration in open field testing and impairments in spatiotemporal gait parameters. This novel, acute ischemia characterization provides important insights into tissue and functional level changes in a pig model that can be used to identify treatment targets and future testing of therapeutics and diagnostics.

Key words Brain ischemia, Gait analysis, Magnetic resonance imaging, Porcine, Acute stroke

Introduction

Every year, 6.2 million people worldwide die from stroke making it the leading cause of death in individuals over the age of 60 and the fifth leading cause of death in individuals ages 15-59 (1, 2). Of the patients that survive, approximately 5 million are left permanently disabled making stroke a global medical and socioeconomic problem (3). The acute phase of ischemic stroke is a critical time window to determine stroke severity, treatment options, and future prognosis in clinical patients. Specifically, the acute phase is a major target for the development of novel therapeutics and diagnostics as an early reduction in brain tissue loss is directly correlated with improvements in functional outcomes. In addition, all current Food and Drug Administrative approved treatments, tissue plasminogen activator (tPA) and thrombectomy, are only effective during this acute window (4-6). The acute phase of ischemic stroke has also been the focus of diagnostic and prognostic tool development; tools including magnetic resonance imaging (MRI) that can rapidly and accurately identify ischemic stroke and has demonstrated strong predictive value with respect to long-term patient outcomes (7-11). However, the development of therapies and diagnostic tools has been slower than desired particularly with respect to treatments with numerous failed clinical trials (12-15).

A potential opportunity to hasten the speed at which therapies and diagnostics reach patients is through the use of translational large animal models that are more predictive of human outcomes. Assessments by the Stem Cell Emerging Paradigm in Stroke (STEPS) and the Stroke Therapy Academic Industry Roundtable (STAIR) consortiums identified therapeutic testing in higher-order gyrencephalic species and in translational animal models more reflective of human pathology and physiology as major needs in pre-clinical

stroke studies to better predict therapeutic efficacy (6, 16-21). To address this unmet need, a pig ischemic stroke model has been recently developed by our research team with anatomy, physiology, and stroke pathology similar to human patients (22-25). The pig brain is similar in mass compared to humans being only 7.5 times smaller, whereas the rodent brain is 650 times smaller in comparison to humans (26). This allots for a more direct assessment of therapeutic dosing in a pre-clinical model. The pig's brain size is also an advantage in developing diagnostic tools as human 3T MRI scanners and coils can be used to develop new MRI sequences and analytical tools. In terms of cytoarchitecture, human and pig brains are gyrencephalic and are composed of >60% white matter (WM), while rodent brains are lissencephalic and are composed of <10% WM, making pig tissue responses potentially more predictive of human outcomes (27-30). These attributes are critically important as WM and gray matter (GM) exhibit differing sensitivities to hypoxia (30). Although the failure of pharmacological translation is multifactorial, the failure to ameliorate ischemic damage to WM is proposed to be a major factor (31). The similarities between pig and humans in brain size, cytoarchitecture, and WM composition collectively support the use of a pig ischemic stroke model to more accurately predict potential outcomes of human clinical trials. However, more in depth characterization of the acute ischemic stroke timepoint is needed in the pig model to better understand similarities and differences between human and pig acute stroke outcomes.

MRI is an excellent tool for use in the pig ischemic stroke model as it allows for bidirectional development of the pig model as well as MRI diagnostic and prognostics. MRI allows for the assessment of stroke evolution in the pig model and evaluation of novel therapeutic efficacy. In addition, new MRI sequences and post-processing tools can be

developed in the pig for use in clinical settings. Acute MRI assessment of ischemic stroke patients has become the standard of care in diagnosing and predicting patient clinical outcomes (8, 32). Clinically, diffusion-weighted imaging (DWI) has been shown to reliably enable early identification of the lesion size, location, and age with high sensitivity and specificity (7, 33-38). Moreover, acute stage DWI lesion volume measures have proven to be highly correlated with chronic lesion size and stroke severity as determined by Modified Rankin Scale (mRS) and National Institutes of Health Stroke Scale (NIHSS), suggesting DWI provides valuable prognostic information (7-9, 38-40). DWI derived apparent diffusion coefficient (ADC) maps have aided in further understanding the time course of acute ischemic brain damage by tracking the diffusion of water in the hypoxic brain parenchyma from extracellular to intracellular compartments (41, 42). In conjunction with other MR techniques, ADC hypointensities allow clinicians to differentiate between regions at risk for cerebral infarction and irreversibly damaged tissue in order to establish time windows for stroke treatment and to identify patients who are most likely to benefit from acute stroke therapies (7, 40, 43, 44). Disruption of WM structural integrity is also associated with poor early neurological outcomes in stroke patients (45). Diffusion tensor imaging (DTI) studies of human stroke reveal notable alterations in WM fractional anisotropy (FA) that correspond with the temporal evolution of stroke (10, 11). FA analysis has improved the identification of ischemic lesions at acute and subacute time points and has proved particularly useful in determining time of stroke onset, which is frequently unknown in clinical settings (11). Recently, progressive structural remodeling of contralateral WM tracts related to motor, cognitive, and sensory processing was positively associated with motor function recovery in the acute and sub-acute stages post-stroke as

well as 1, 4, and 12 weeks post-ischemic onset in patients (46, 47). Acute MRI analysis in the pig stroke model will allow for the characterization of clinically-relevant parameters and to assess for correlations with acute functional changes as observed in human patients.

Ischemic stroke leads to a wide array of acute deficits in behavior, cognition, and sensorimotor function in clinical patients thus resulting in poor mRS scale scores (48). Neurological deficits in executive function, episodic memory, visuospatial function, and language manifest within 48 to 72 hours in 33.6% of patients (49-52). Occlusions of the middle cerebral artery (MCA) and territorial infarction are regularly linked to acute limb paresis that is sustained long-term (52). Understanding these motor impairments are essential to planning rehabilitation efforts to restore ambulatory activity levels and balance deficiencies in stroke survivors (53, 54). Specifically, improvements in foot placement, stride length, and walking speed are recognized as powerful indicators of long-term recovery (55-59). Among these neurologic and functional consequences, post-stroke depression (PSD) is the most frequent psychiatric problem occurring in one-third of stroke survivors (60). PSD is strongly associated with further inhibition of recovery processes due to the combination of ischemia-induced neurobiological dysfunctions and psychosocial distress (61, 62). The pig stroke model offers a unique opportunity to study acute changes in behavior, cognition, and motor function due to anatomical similarities in the size of the prefrontal cortex and cerebellum in addition to somatotopical organization of the motor and somatosensory cortices which are critically important in modeling human motor function effects in the acute ischemic stroke phase (26, 63-65).

The objective of this study was to utilize clinically relevant assessment modalities to characterize acute ischemic stroke in a pig model that will provide a translational

platform to study potential diagnostics and therapeutic interventions. We present evidence pigs display an acute ischemic stroke response similar to human patients including brain lesioning, swelling, loss of WM integrity, and increased white blood cell (WBC) counts. These physiological changes correlated with aberrant behavior and worsened motor function. This compelling evidence suggests the pig stroke model could serve as a valuable tool in bridging the gap between pre-clinical rodent studies and human clinical trials.

Materials and methods

Animals and housing

All work performed in this study was approved by the University of Georgia Institutional Animal Care and Use Committee (IACUC; Protocol Number: 2017-07-019Y1A0) and in accordance with the National Institutes of Health Guide for the Care and Use of Laboratory Animals guidelines. 6, sexually mature, castrated male Landrace pigs, 5-6 months old and 48-56 kg were purchased from the University of Georgia Swine Unit and enrolled in this study. Male pigs were used in accordance with the STAIR guidelines that suggests initial therapeutic evaluations should be performed with young, healthy male animals (66). Pigs were individually housed in a Public Health Service (PHS) and AAALAC approved facility at a room temperature approximately 27°C with a 12-hour light/dark cycle. Pigs were given access to water and fed standard grower diets with provision of enrichment through daily human contact and toys.

Study design

The sample size for this study was determined by a power calculation based on our routine use of the middle cerebral artery occlusion model with lesion volume changes by MRI imaging being the primary endpoint (67). The power analysis was calculated using a

two-tailed ANOVA test, α=0.05, and an 80% power of detection effect size of 1.19 and a standard deviation of 44.63. This was a randomized study where 2 pigs were randomly assigned to each surgical day. All endpoints and functional measurements were prospectively planned and underwent blinded analysis. Predefined exclusion criteria from all endpoints included instances of infection at the incision site, self-inflicted injuries that required euthanasia, inability to thermoregulate, uncontrolled seizure activity, and/or respiratory distress. 1 pig was excluded from MRI collection as well as post-stroke blood and functional analysis due to post-operative complications and premature death. No outliers were removed from the data.

Middle cerebral artery occlusion surgical procedures

The day prior to surgery, pigs were administered antibiotics (Excede; 5 mg/kg intramuscular (IM) and fentanyl for pain management (fentanyl patch; 100 mg/kg/hr transdermal (TD)). Pre-induction analgesia and sedation were achieved using xylazine (2 mg/kg IM) and midazolam (0.2 mg/kg IM). Anesthesia was induced with intravenous (IV) propofol to effect and prophylactic lidocaine (1.0 mL 2% lidocaine) topically to the laryngeal folds to facilitate intubation. Anesthesia was maintained with isoflurane (Abbott Laboratories) in oxygen.

As previously described, a curvilinear skin incision extended from the right orbit to an area rostral to the auricle (24). A segment of zygomatic arch was resected while the temporal fascia and muscle were elevated and a craniectomy was performed exposing the local dura mater. The distal middle cerebral artery (MCA) and associated branches were permanently occluded using bipolar cautery forceps resulting in ischemic infarction. The temporalis muscle and epidermis were routinely re-apposed.

Anesthesia was discontinued and pigs were returned to their pens upon extubation and monitored every 15 minutes until vitals including temperature, heart rate, and respiratory rate returned to normal, every 4 hours for 24 hours, and twice a day thereafter until post-transplantation sutures were removed. Banamine (2.2 mg/kg IM) was administered for post-operative pain, acute inflammation, and fever management every 12 hours for the first 24 hours, and every 24 hours for 3 days post-stroke.

Magnetic resonance imaging acquisition and analysis

MRI was performed 24 hours post-stroke on a General Electric 3.0 Tesla MRI system. Pigs were sedated and maintained under anesthesia as previously described for MCAO surgery. MRI of the cranium was performed using an 8-channel torso coil with the pig positioned in supine recumbency. Multiplanar MR brain imaging sequences were acquired including T2 Fluid Attenuated Inversion Recovery (T2FLAIR), T2Weighted (T2W), T2Star (T2*), DWI, and DTI. Sequences were analyzed using Osirix software. Cytotoxic edema consistent with ischemic stroke was confirmed 24 hours post-stroke by comparing corresponding hyperintense regions in T2FLAIR and DWI sequences and hypointense regions in ADC maps.

DWI sequences were used to generate ADC maps. ADC values were calculated for each axial slice at a manually drawn region of interest (ROI) that was defined by areas of hypointensity and directly compared to an identical ROI in the contralateral hemisphere. Average ADC values were obtained by calculating the average signal intensity across all slices and reported as 10^{-3} mm^2/s. Hemisphere volume was calculated using T2W sequences for each axial slice by manually outlining the ipsilateral and contralateral hemispheres. The hemisphere areas were multiplied by the slice thickness (3mm) to obtain

total hemisphere volumes. Lesion volume was calculated using DWI sequences for each axial slice by manually outlining hyperintense ROIs. The area of each ROI was multiplied by the slice thickness (2mm) to obtain the total lesion volume. Similarly, intracerebral hemorrhage (ICH) volume was calculated by manually outlining areas of hypointensity utilizing T2* sequences. Midline shift (MLS) was calculated utilizing T2W sequences for each axial slice by measuring the distance from the natural midline along the anterior and posterior attachments of the falx cerebri to the septum pellucidum. DTI was utilized to generate FA maps. FA values of the internal capsules were calculated manually on one representative slice per pig and were expressed as a percent change in the ipsilateral hemisphere relative to the contralateral hemisphere.

Blood collection and analysis

Venous blood samples were collected pre-stroke, 4, 12, and 24 hours post-stroke into K2EDTA spray coated tubes (Patterson Veterinary). 4 μL of blood was pipetted onto the base of a ColorFrost microscope slide (ThermoScientific) approximately 1 cm from the edge. At an angle of approximately 45 degrees, a spreader slide was placed in front of the blood and retracted until the blood sample evenly spread along the width of the slide. Even pressure on the spreader slide was applied in a forward direction in order to create a smear. Care was taken to ensure each blood smear covered two-thirds of the slide and exhibited an oval feathered end. Each slide was air dried for 10 minutes, fixed with methanol for 2 minutes, air dried for 2 minutes, and then stained in Wright-Giemsa stain for 5 minutes. The stained slide was submerged in distilled water (dH_2O) for 10 minutes. Finally, the slide was rinsed, air dried, and then a cover slip was applied using Phosphate Buffered Saline (PBS). Trained, blinded personnel completed manual white blood cell counts of

lymphocytes, neutrophils, and band cells at the monolayer, beginning approximately one millimeter away from the body of the smear. The first 100 white blood cells visualized were identified and cell counts were expressed as a percentage.

Gait analysis

Pigs underwent gait analysis pre-stroke and 48 hours post-stroke to assess changes in spatiotemporal gait parameters. Data was recorded using a GAITFour® electronic, pressure-sensitive mat (CIR Systems Inc., Franklin, NJ) 7.01 m in length and 0.85 m in width with an active area that is 6.10 m in length and 0.61 m in width. In this arrangement, the active area is a grid, 48 sensors wide by 480 sensors long, totaling 23,040 sensors. 2 weeks pre-stroke, pigs were trained to travel across a gait mat at a consistent, 2-beat pace. To reinforce consistency, rewards were given at each end of the mat for successful runs. Pre-stroke gait data was collected on 3 separate days for each pig. At each time point, pigs were encouraged to move along the mat until 5 consistent trials were collected in which the pigs were not distracted and maintained a consistent pace with no more than 15 total trials collected.

Gait data was semi-automatically analyzed using GAITFour® Software to provide quantitative measurements of velocity (cm/sec) and cadence (steps/min). Additional measurements were quantified specifically for the affected front left limb, which is contralateral to the induced stroke lesion on the right side of the brain. These measurements included stride length (the distance between successive ground contact of the same hoof), swing percent of cycle (the percent of a full gait cycle in which a limb is not in contact with the ground), cycle time (the amount of time for a full stride cycle),

swing time (the amount of time a limb is in the swing phase, or not in contact with the ground) and mean pressure (the amount of pressure exerted by a limb).

Open field testing

As an additional measure of functional outcome, pigs underwent open field (OF) behavior testing pre-stroke and 48 hours post-stroke. All tests took place in a 2.7 m x 2.7 m arena lined with black rubber matting, used to provide stable footing. White curtains were hung around the arena to reduce visual distractions during testing. Trials were recorded using EthoVision video tracking software (Noldus Systems) to obtain objective and quantifiable measures of behavioral characteristics.

Pigs were individually brought to the behavior arena and allowed to explore for 10 minutes during the OF test. Behaviors automatically tracked during this test include velocity and distance traveled. Additionally, exploratory behaviors typical of pigs such as sniffing the wall (perimeter sniffing) were manually tracked and coded in the EthoVision software by trained personnel.

Statistical analysis

All quantitative data was analyzed with SAS version 9.3 (Cary, NC) and statistical significances between groups were determined by one-way analysis of variance (ANOVA) and post-hoc Tukey-Kramer Pair-Wise comparisons. Comparisons where p-values were $\leq$ 0.05 were considered significantly different.

Results

MCAO induces acute ischemic infarction and decreased diffusivity.

To confirm ischemic stroke 24 hours post-MCAO, MRI DWI (**Figure 3.1A**) and T2FLAIR sequences were assessed. Scans exhibited territorial hyperintense lesions

characteristic of an edematous injury. Hypointense lesions observed on corresponding ADC maps (**Figure 3.1B**) confirmed areas of restricted diffusion indicative of cytotoxic edema thus confirming permanent cauterization of the MCA resulted in ischemic stroke. DWI-ADC mismatch resulted in identification of potentially salvageable penumbra tissue. DWI sequences revealed an average lesion volume of 9.91±1.40 cm^3 (**Figure 3.1A**). ADC sequences revealed significantly ($p \leq 0.0001$) decreased diffusivity within ischemic lesions when compared to identical regions of interest in the contralateral hemisphere (0.34±0.02 vs. 0.62±0.03 $x10^{-3}mm^2/s$, respectively; **Figure 3.1B-C**).

Ischemic stroke results in acute hemispheric swelling, hemorrhage, and loss of white matter integrity.

Analysis of T2W sequences at 24 hours post-stroke revealed a trending ($p=0.16$) increase in ipsilateral hemisphere volume indicative of cerebral swelling when compared to the contralateral hemisphere (25.99±1.78 vs. 22.49±1.40 cm^3, respectively; **Figure 3.2A-C**) and an associated MLS of 2.48±0.55 mm (**Figure 3.2A-B**). Acute ICH was observed via T2* sequences with a consistent mean hemorrhage volume of 1.73±0.07 cm^3 (**Figure 3.2D-E**, white arrow), which suggests the ischemic infarct area underwent hemorrhagic transformation (HT). These HTs impacted basal ganglion structures as well as portions of the cerebellum, brain regions responsible for motor function. To assess changes in WM integrity, FA values of the internal capsules were evaluated 24 hours post-stroke, revealing a significant ($p<0.01$) decrease in the ipsilateral internal capsule (IC) when compared to the contralateral side (0.17±0.01 vs. 0.23±0.01 respectively; **Figure 3.3A-C**). Collectively, MRI results demonstrated MCAO led to tissue-level damage

including ischemic infarction, decreased diffusivity, hemispheric swelling, pronounced MLS, HT, and disrupted WM integrity.

Ischemic stroke increases circulating neutrophil levels and decreases circulating lymphocyte levels.

To determine changes in immune cell response to acute ischemic stroke, venous blood samples were collected pre-stroke, 4, 12, and 24 hours post-stroke. Band neutrophils (**Figure 3.4A-B**), neutrophils (**Figure 3.4C-D**), and lymphocytes (**Figure 3.4E-F**) were assessed via manual cell counts. Band neutrophils significantly ($p<0.05$) increased 12 hours post-stroke compared to pre-stroke (5.50±0.99% vs. 1.92±0.51% respectively; **Figure 3.4B**). Similarly, the number of circulating neutrophils was significantly ($p<0.05$) increased at 4- and 12-hours post-stroke when compared to pre-stroke (43.7±5.27% and 48.9±3.92% vs. 26.5±1.96%, respectively; **Figure 3.4D**). The number of circulating lymphocytes was significantly ($p<0.05$) decreased at 12- and 24-hours post-stroke compared to pre-stroke (25.60±4.01% and 26.60±4.29% vs. 44.83±3.66% respectively; **Figure 3.4F**). These results demonstrated stroke resulted in an increase in circulating band neutrophils and neutrophils and a decrease in circulating lymphocytes which indicates an acute immune response.

Ischemic stroke decreases exploratory behaviors during open field testing.

Changes in exploratory behaviors were assessed using the open field (OF) test 48 hours post-stroke. Perimeter sniffing, a typical exploratory behavior exhibited by pigs, was recorded utilizing Ethovision XT tracking software to assess differences in perimeter sniffing pre- and post-stroke (**Figure 3.5A-B**); representative 10-minute movement tracings show perimeter sniffing (red) and non-perimeter sniffing (yellow). Pigs'

perimeter sniffing frequency significantly ($p<0.05$) decreased 48 hours post-stroke compared to pre-stroke (13±2.94 vs 26±4.02 times, respectively, **Figure 3.5C**). However, no significant differences were noted for velocity and distance traveled in the OF test between pre- and 48 hours post-stroke. These results suggest that stroke impairs normal exploratory behaviors.

Ischemic stroke results in spatiotemporal gait deficits.

Key spatiotemporal gait parameters were analyzed pre-stroke and 48 hours post-stroke to detect potential impairments in motor function as an outcome of stroke. Significant ($p<0.01$) decreases were noted in the average velocity and cadence at 48 hours post-stroke compared to pre-stroke indicating the speed of the pigs decreased as a result of stroke (61.01±8.39 vs 162.9±12.73 cm/s and 61.01±5.91 vs 126.44±3.72 steps/min, respectively, **Figure 3.6A-B**). Further changes were noted in measurements of the contralateral left forelimb (LF). The limb contralateral to the stroke lesion typically has more pronounced motor deficits relative to the ipsilateral limb in humans, mice, and rats (68, 69). The swing percent of cycle significantly ($p<0.01$) decreased demonstrating pigs spent more time with the LF in contact with the ground at 48 hours post-stroke compared to pre-stroke suggesting an increased need for support (30.70±2.12 vs 48.89±2.35%, respectively, **Figure 3.6C**). A significant ($p<0.01$) decrease in stride length of the LF was observed at 48 hours post-stroke compared to pre-stroke (59.04±3.85cm vs 76.72±4.60cm, respectively, **Figure 3.6D**). Cycle time of the LF significantly ($p<0.01$) increased signifying a slower gait at 48 hours post-stroke compared to pre-stroke (1.02±.09 vs 0.48±0.013sec, respectively, **Figure 3.6E**). Finally, the mean pressure exhibited by the LF significantly ($p<0.01$) decreased at 48 hours post-stroke compared to

pre-stroke (2.62±.03 vs 2.82±.03 arbitrary units (AU), respectively, **Figure 3.6F**). Deficits in the measured gait parameters indicate stroke lead to substantial motor impairments at acute time points in pigs.

Discussion

In this study, we observed and characterized acute stroke injury severity, prognostic biomarkers, and potential therapeutic targets utilizing clinically-relevant MRI, immune, behavior, and motor function tests in the translational ischemic stroke pig model. Lesion volumes were consistent among pigs and closely replicated human lesion volumes with similar impairments in functional performance (70-73). Ischemic injury produced cerebral swelling and consequent MLS as well as notable ICH, all of which are strongly associated with stroke patient morbidity (39, 74, 75). In addition, stroke led to reduced WM integrity of the IC correlating with a contralateral deteriorations in motor function commonly seen in patients post-stroke (30, 76, 77). Also similar to human stroke patients, MCAO led to an acute immune response marked by an increase in circulating neutrophils and a corresponding decrease in circulating lymphocytes which is a key biomarker for identifying ischemic stroke patients at risk for the development of intracerebral hemorrhage thus influencing the use of tPA (78-80). Functional assessments showed impaired behavior and motor function disruptions that affected both spatiotemporal parameters and weight distribution, all of which parallel clinical functional outcomes in stroke patients (81-83). By further understanding these physiological hallmarks and exploiting the similarities between pigs and humans, the ischemic stroke pig model can be utilized to decrease the translational gap between rodent models and human stroke patients.

Early detection of ischemic infarction via DWI analysis has proven to be a critical component for both prognosis and therapeutic potentials within the narrow treatment window of acute ischemic stroke (84-86). This study showed mean lesion volumes of 9.91±3.14 cm^3 at 24 hours post-stroke. Given that pig brains are approximately 7.5 times smaller than human brains, lesion volumes were found to closely replicate patient DWI lesion volumes. Acute DWI lesion thresholds of 72 cm^3 are common in patients with major cerebral artery occlusions (26, 87-90). Often pre-clinical stroke models have relied on T1 or T2 MRI sequences which are typically delayed in early recognition of cerebral ischemia and do not account for diffusion abnormalities that may evolve into infarction (91-93). DWI lesion measurements overcome this limitation. Common pathological features of human ischemic infarction were also observed in our model including significant restricted diffusion in focal regions spanning the parietal, limbic, and temporal lobes as indicated by ADC maps (85, 94-96). Specifically, our pig model replicates characteristics of human MCA stroke by primarily demonstrating cytotoxic edema which will later evolve into vasogenic edema. In some pre-clinical stroke models, including rodent photochemical and photothromobotic models, cytotoxic edema and vasogenic edema develop simultaneously resulting in ischemic lesions lacking a penumbra (97, 98). This is a major model limitation as the penumbra is considered potentially salvagable tissue in human patients and is a coveted therapeutic intervention target. MRI-based discrimination of core from penumbra and non-ischemic tissue provides critical information for the testing of neuroprotective and restorative treatments as well as the initiation of surgical interventions within acute and sub-acute treatment windows (99, 100). For example, ischemic core volumes distinguishable from penumbra enable clinicians to consider the risk of cerebral

hemorrhage from acute revascularization therapy (101). For these reasons, evaluating the efficacy and safety of potential treatments in an animal model with similar pathophysiology of acute ischemia in terms of cytotoxic and vasogenic edema as humans is of significant value.

Cerebral edema and consequent hemispheric swelling are serious stroke complications that result in rapid neurological deterioration and a disproportionately high 30-day patient mortality rate of 60-80% (102-104). Crudely managed via osmotic diuretics and/or decompressive craniectomies, patients are in desperate need for more effective and less invasive pharmacotherapies (105-107). These needs have been met with poor therapeutic translation due to discrepencies in lissencephalic small animal stroke models including limited cerebral edema and swelling as well as variable MLS and mortality rates (108-110). Specifically in endothelin-1 (ET-1) rodent stroke models, animals exhibit a dose-dependent ischemic lesion with marginal ischemic edema making this model less suited for studying acute stroke pathophysiology (111-114). In contrast, our pig stroke model exhibited increased ipsilateral hemipshere swelling due to the development of cytotoxic edema and consquent MLS within 24 hours post-stroke. These observations are in keeping with other large animal models of stroke, in which permanent ovine MCAO demonstrated cerebral edema and MLS (115). These physiological responses post-ischemic stroke are frequently associated with different levels of consciousness and serve as a predictive indicator of patient prognosis (116, 117). Furthermore, clinical studies indicate quantification of MLS can predict cerebral herniations and subsequent death prior to clinical signs and are a clinically-relevant feature of this pig stroke model (118).

Although MRI techniques have become increasingly valuable in characterizing and refining the field's understanding of ICH, the time course and underlying mechanisms remain poorly understood due to variability in the onset, size, and location of ICH in current stroke animal models (119). Often resulting from hemorrhagic transformation (HT) in ischemic stroke patients, spontaneous ICH incidence ranges from 38-71% in autopsy studies and from 13-43% in CT studies (120, 121). Furthermore, when ICH occupies >30% of the infarct zone, it has been correlated with early neurological deterioration and a significant increase in mortality rates 90 days post-ischemic stroke (122, 123). T2* sequences showed consistent mean hemorrhage volume between stroke pigs, indicating MCAO caused loss of macro- and microvessel integrity. The classical clinical presentations of ICH were replicated in our model through the progression of neurological deficits within hours post-stroke including decreased consciousness, head-pressing, vomiting, facial paralysis, and limb weakness (120, 124, 125). Interestingly, these neurological deficits correlated with the location of ICH. For example, ICH in the cerebellum was associated with ataxia whereas ICH in basal ganglia structures were associated with limb weakness. In previous studies, early neurologic deterioration was attributed primarily to cerebral edema and lesion volume; however, recent clinical pathological, MR, and CT studies suggest hemorrhage into ischemic tissues is a major contributor to poor clinical outcome, making ICH a novel target of pre-clinical studies (126-129). By replicating both tissue-level and neurological presentations unique to ICH, our model presents an exciting new platform for testing hemostatic therapies and surgical interventions.

For the first time, it was observed MCAO led to reduced WM integrity in the IC 24 hours post-stroke in the pig model. This subcortical structure is highly involved in communication between the cerebral cortex and brainstem resulting in profound muscle weakness and inhibited perception of sensory information of the patient's face, arm, trunk, and leg post-stroke (130). Studies using Functional Ambulatory Categories found patients with IC lesions experience persistent (>6 months) functional motor deficits; requiring aids for balance and support during ambulation (131). As the right IC transmits nerve signals for movement of the left side of the body, our pig MCAO model closely replicated post-stroke deficits as seen through a decrease in spatiotemporal gait parameters of the hemiplegic limb including LF stride length and LF swing percent of cycle. Similarly, stroke patients exhibit decreases in the duration of stride length and the swing phase in the hemiplegic limb (132-135). Mean pressure of the LF limb was also decreased in stroke pigs likely as a result of overall greater weakness of the hemiplegic limb (136). Stroke pigs compensated for limb weakness and balance impairments by taking shorter, slower steps, thus reducing their velocity and cadence to better stabilize their gait. In a comparable human study utilizing the analogous GAITRite system, WM lesions corresponded with a poorer gait score as measured by step length and abnormal cadence in patients (77). These manifestations support our previous studies evaluating functional deficits post-stroke, thus providing further evidence quantitative gait analysis is a critical tool for the evaluation of stroke severity and therapeutic impact on recovery (25, 137).

Immune and inflammatory responses have been shown to play a key role in the sequela of ischemic stroke (138). Within the first few hours after stroke, neutrophils are recruited to the site of injury and release cytokines, chemokines, free oxygen radicals, and

other inflammatory mediators (139). In this study, we observed a significant increase in neutrophils at 4- and 12-hours post-stroke. Neutrophil release of inflammatory mediators has been directly associated with cell damage or death as well as damage to the vasculature and extracellular matrices (139). Neutrophils have been implicated to play a significant role in blood brain barrier disruption and HT following ischemic stroke, which may explain one potential mechanism for HT observed 24 hours post-stroke in this study (79). Conversely, acute ischemic stroke has been shown to induce a rapid and long-lasting suppression of circulating immune cells such as lymphocytes that can lead to increased susceptibility of systemic infections after stroke (140). In this study, we observed a significant decrease in lymphocytes at 12 and 24 hours post-stroke, consistent with reports that stroke in humans induces immediate loss of lymphocytes that is most pronounced at 12 hours post-stroke (141). Though the exact mechanisms by which lymphocytes mediate immunosuppression post-stroke remain unclear, clinical evidence supports that lower levels of lymphocytes are a sign of poor long-term functional outcome (142-144). The neutrophil-to-lymphocyte ratio (NLR) was determined to be a useful marker to predict neurological deterioration and short-term mortality in patients with acute ischemic stroke (145, 146). Elevated NLRs have been reported to be associated with chronic inflammation, poor functional prognosis, and larger lesion volumes in ischemic stroke patients (78, 139, 146-148). These results suggest that neutrophil recruitment in our pig model may play a significant role in inflammatory-mediated secondary injury processes that contribute to the development of functional impairments. Furthermore, similar to human stroke patients, neutrophil and lymphocyte levels in our pig model may also serve as ideal markers for stroke severity and outcome prediction.

Open field testing is regularly used to evaluate behavior in rodents after ischemic stroke (149), specifically as an indicator of changes in exploratory behaviors (150, 151). In this study, a significant decrease was noted in perimeter sniffing frequency post-stroke in open field testing. Pigs are inherently exploratory animals and perimeter sniffing is a typical exploratory behavior (152). This change in behavior may be attributed to post-stroke depression (PSD) as this behavioral disturbance has been reported to commonly develop in humans in the acute post-stroke period (153, 154). In accordance with the behavioral changes noted in the present study, PSD in humans is characterized by general apathy and lack of interest (155, 156). Evaluation and understanding of behavioral changes in a translational, large animal stroke model is crucial for future studies to assess functional outcomes of potential therapies.

In this study, we have demonstrated our pig model of ischemic stroke positively replicates cellular, tissue, and functional outcomes at acute time points similar to human stroke patients. MCAO in our pig ischemic stroke model exhibited a multifactorial effect leading to cytotoxic edema, lesioning, hemispheric swelling, and ICH, while also impairing diffusivity and WM integrity. These structural changes correlated with behavioral and motor function deficits in a similar manner to acute human stroke patients. As an effective model of acute ischemic stroke pathophysiology, the pig system is potentially an excellent tool for identifying potential treatment targets and testing novel therapeutics and diagnostics.

Acknowledgements

The authors would like to thank Brandy Winkler and our team of undergraduate researchers who were involved in various aspects of surgeries, post-operative care, pig

gait/behavioral testing, and data analysis. We would also like to thank the University of Georgia Animal Resources team for veterinary care and guidance as well as Rick Utley and Kelly Parham for their pig expertise and management skills.

Funding

This work was supported by the National Institute of Neurological Disorders and Stroke [grant number R01NS093314].

Declarations of interest

We have no declarations of interest to report.

References

1. WHO publishes definitive atlas on global heart disease and stroke epidemic. Indian J Med Sci. 2004;58(9):405-6.

2. Greenlund KJ, Croft JB, Mensah GA. Prevalence of heart disease and stroke risk factors in persons with prehypertension in the United States, 1999-2000. Arch Intern Med. 2004;164(19):2113-8.

3. Organization WH. Global status report on noncommunicable diseases 2010. 2010:176.

4. Cheng NT, Kim AS. Intravenous Thrombolysis for Acute Ischemic Stroke Within 3 Hours Versus Between 3 and 4.5 Hours of Symptom Onset. The Neurohospitalist. 2015;5(3):101-9.

5. Boyle K, Joundi RA, Aviv RI. An historical and contemporary review of endovascular therapy for acute ischemic stroke. Neurovascular Imaging. 2017;3(1):1.

6. Saver JL, Albers GW, Dunn B, Johnston KC, Fisher M, Consortium SV. Stroke Therapy Academic Industry Roundtable (STAIR) recommendations for extended window acute stroke therapy trials. Stroke. 2009;40(7):2594-600.

7. Barber PA, Darby DG, Desmond PM, Yang Q, Gerraty RP, Jolley D, et al. Prediction of stroke outcome with echoplanar perfusion- and diffusion-weighted MRI. Neurology. 1998;51(2):418-26.

8. Vilela P, Rowley HA. Brain ischemia: CT and MRI techniques in acute ischemic stroke. Eur J Radiol. 2017;96:162-72.

9. Attye A, Boncoeur-Martel MP, Maubon A, Mounayer C, Couratier P, Labrunie A, et al. [Diffusion-Weighted Imaging infarct volume and neurologic outcomes after ischemic stroke]. J Neuroradiol. 2012;39(2):97-103.

10. Beaulieu C. The basis of anisotropic water diffusion in the nervous system - a technical review. NMR Biomed. 2002;15(7-8):435-55.

11. Sotak CH. The role of diffusion tensor imaging in the evaluation of ischemic brain injury - a review. NMR Biomed. 2002;15(7-8):561-9.

12. Mousavi SA, Saadatnia M, Khorvash F, Hoseini T, Sariaslani P. Evaluation of the neuroprotective effect of dextromethorphan in the acute phase of ischaemic stroke. Archives of medical science : AMS. 2011;7(3):465-9.

13. Diener HC, Cortens M, Ford G, Grotta J, Hacke W, Kaste M, et al. Lubeluzole in acute ischemic stroke treatment: A double-blind study with an 8-hour inclusion window comparing a 10-mg daily dose of lubeluzole with placebo. Stroke. 2000;31(11):2543-51.

14. Diener HC, Lees KR, Lyden P, Grotta J, Davalos A, Davis SM, et al. NXY-059 for the treatment of acute stroke: pooled analysis of the SAINT I and II Trials. Stroke. 2008;39(6):1751-8.

15. Clark WM, Wechsler LR, Sabounjian LA, Schwiderski UE, Citicoline Stroke Study G. A phase III randomized efficacy trial of 2000 mg citicoline in acute ischemic stroke patients. Neurology. 2001;57(9):1595-602.

16. Stem Cell Therapies as an Emerging Paradigm in Stroke P. Stem Cell Therapies as an Emerging Paradigm in Stroke (STEPS): bridging basic and clinical science for cellular and neurogenic factor therapy in treating stroke. Stroke. 2009;40(2):510-5.

17. Savitz SI, Chopp M, Deans R, Carmichael T, Phinney D, Wechsler L, et al. Stem Cell Therapy as an Emerging Paradigm for Stroke (STEPS) II. Stroke. 2011;42(3):825-9.

18. Fisher M, Hanley DF, Howard G, Jauch EC, Warach S, Group S. Recommendations from the STAIR V meeting on acute stroke trials, technology and outcomes. Stroke. 2007;38(2):245-8.

19. Fisher M, Feuerstein G, Howells DW, Hurn PD, Kent TA, Savitz SI, et al. Update of the stroke therapy academic industry roundtable preclinical recommendations. Stroke. 2009;40(6):2244-50.

20. Fisher M, Stroke Therapy Academic Industry R. Recommendations for advancing development of acute stroke therapies: Stroke Therapy Academic Industry Roundtable 3. Stroke. 2003;34(6):1539-46.

21. Albers GW, Goldstein LB, Hess DC, Wechsler LR, Furie KL, Gorelick PB, et al. Stroke Treatment Academic Industry Roundtable (STAIR) recommendations for maximizing the use of intravenous thrombolytics and expanding treatment options with intra-arterial and neuroprotective therapies. Stroke. 2011;42(9):2645-50.

22. Duberstein KJ, Platt SR, Holmes SP, Dove CR, Howerth EW, Kent M, et al. Gait analysis in a pre- and post-ischemic stroke biomedical pig model. Physiology & Behavior. 2014;125:8-16.

23. Baker EW, Platt SR, Lau VW, Grace HE, Holmes SP, Wang L, et al. Induced Pluripotent Stem Cell-Derived Neural Stem Cell Therapy Enhances Recovery in an Ischemic Stroke Pig Model. Sci Rep. 2017;7(1):10075.

24. Platt SR, Holmes SP, Howerth EW, Duberstein KJ, Dove CR, Kinder HA, et al. Development and characterization of a Yucatan miniature biomedical pig permanent middle cerebral artery occlusion stroke model. Exp Transl Stroke Med. 2014;6(1):5.

25. Webb RL, Kaiser EE, Jurgielewicz BJ, Spellicy S, Scoville SL, Thompson TA, et al. Human Neural Stem Cell Extracellular Vesicles Improve Recovery in a Porcine Model of Ischemic Stroke. Stroke. 2018;49(5):1248-56.

26. Lind NM, Moustgaard A, Jelsing J, Vajta G, Cumming P, Hansen AK. The use of pigs in neuroscience: modeling brain disorders. Neurosci Biobehav Rev. 2007;31(5):728-51.

27. Nakamura M, Imai H, Konno K, Kubota C, Seki K, Puentes S, et al. Experimental investigation of encephalomyosynangiosis using gyrencephalic brain of the miniature pig: histopathological evaluation of dynamic reconstruction of vessels for functional anastomosis. Laboratory investigation. J Neurosurg Pediatr. 2009;3(6):488-95.

28. Kuluz JW, Prado R, He D, Zhao W, Dietrich WD, Watson B. New pediatric model of ischemic stroke in infant piglets by photothrombosis: acute changes in cerebral blood flow, microvasculature, and early histopathology. Stroke. 2007;38(6):1932-7.

29. Tanaka Y, Imai H, Konno K, Miyagishima T, Kubota C, Puentes S, et al. Experimental model of lacunar infarction in the gyrencephalic brain of the miniature pig: neurological assessment and histological, immunohistochemical, and physiological evaluation of dynamic corticospinal tract deformation. Stroke. 2008;39(1):205-12.

30. Baltan S, Besancon EF, Mbow B, Ye Z, Hamner MA, Ransom BR. White matter vulnerability to ischemic injury increases with age because of enhanced excitotoxicity. J Neurosci. 2008;28(6):1479-89.

31. Dewar D, Yam P, McCulloch J. Drug development for stroke: importance of protecting cerebral white matter. Eur J Pharmacol. 1999;375(1-3):41-50.

32. Rudkin S, Cerejo R, Tayal A, Goldberg MF. Imaging of acute ischemic stroke. Emerg Radiol. 2018;25(6):659-72.

33. Warach S, Gaa J, Siewert B, Wielopolski P, Edelman RR. Acute human stroke studied by whole brain echo planar diffusion-weighted magnetic resonance imaging. Ann Neurol. 1995;37(2):231-41.

34. Warach S, Chien D, Li W, Ronthal M, Edelman RR. Fast magnetic resonance diffusion-weighted imaging of acute human stroke. Neurology. 1992;42(9):1717-23.

35. Lutsep HL, Albers GW, DeCrespigny A, Kamat GN, Marks MP, Moseley ME. Clinical utility of diffusion-weighted magnetic resonance imaging in the assessment of ischemic stroke. Ann Neurol. 1997;41(5):574-80.

36. Lovblad KO, Laubach HJ, Baird AE, Curtin F, Schlaug G, Edelman RR, et al. Clinical experience with diffusion-weighted MR in patients with acute stroke. AJNR Am J Neuroradiol. 1998;19(6):1061-6.

37. Lee LJ, Kidwell CS, Alger J, Starkman S, Saver JL. Impact on stroke subtype diagnosis of early diffusion-weighted magnetic resonance imaging and magnetic resonance angiography. Stroke. 2000;31(5):1081-9.

38. Barber PA, Darby DG, Desmond PM, Gerraty RP, Yang Q, Li T, et al. Identification of major ischemic change. Diffusion-weighted imaging versus computed tomography. Stroke. 1999;30(10):2059-65.

39. Lovblad KO, Baird AE, Schlaug G, Benfield A, Siewert B, Voetsch B, et al. Ischemic lesion volumes in acute stroke by diffusion-weighted magnetic resonance imaging correlate with clinical outcome. Ann Neurol. 1997;42(2):164-70.

40. Tong DC, Yenari MA, Albers GW, O'Brien M, Marks MP, Moseley ME. Correlation of perfusion- and diffusion-weighted MRI with NIHSS score in acute (<6.5 hour) ischemic stroke. Neurology. 1998;50(4):864-70.

41. Lansberg MG, Thijs VN, O'Brien MW, Ali JO, de Crespigny AJ, Tong DC, et al. Evolution of apparent diffusion coefficient, diffusion-weighted, and T2-weighted signal intensity of acute stroke. AJNR Am J Neuroradiol. 2001;22(4):637-44.

42. Moseley ME, Cohen Y, Mintorovitch J, Chileuitt L, Shimizu H, Kucharczyk J, et al. Early detection of regional cerebral ischemia in cats: comparison of diffusion- and T2-weighted MRI and spectroscopy. Magn Reson Med. 1990;14(2):330-46.

43. Rordorf G, Koroshetz WJ, Copen WA, Cramer SC, Schaefer PW, Budzik RF, Jr., et al. Regional ischemia and ischemic injury in patients with acute middle cerebral artery stroke as defined by early diffusion-weighted and perfusion-weighted MRI. Stroke. 1998;29(5):939-43.

44. D'Olhaberriague L, Welch KM, Nagesh V, Gymnopoulos C, Mansbach HH, Hugg JW, et al. Preliminary clinical-radiological assessment of a MR tissue signature model in human stroke. J Neurol Sci. 1998;156(2):158-66.

45. Etherton MR, Wu O, Giese AK, Lauer A, Boulouis G, Mills B, et al. White Matter Integrity and Early Outcomes After Acute Ischemic Stroke. Transl Stroke Res. 2019.

46. Liu G, Dang C, Chen X, Xing S, Dani K, Xie C, et al. Structural remodeling of white matter in the contralesional hemisphere is correlated with early motor recovery in patients with subcortical infarction. Restor Neurol Neurosci. 2015;33(3):309-19.

47. Wang Y, Liu G, Hong D, Chen F, Ji X, Cao G. White matter injury in ischemic stroke. Prog Neurobiol. 2016;141:45-60.

48. Olavarria VV, Brunser A, Cabral N, Martins S, Munoz-Venturelli P, Cavada G, et al. The distribution of the modified Rankin scale scores change according to eligibility criteria in acute ischemic stroke trials: A consideration for sample size calculations when using ordinal regression analysis. Contemp Clin Trials Commun. 2017;5:133-6.

49. Martinaud O, Pouliquen D, Gerardin E, Loubeyre M, Hirsbein D, Hannequin D, et al. Visual agnosia and posterior cerebral artery infarcts: an anatomical-clinical study. PLoS One. 2012;7(1):e30433.

50. Capitani E, Laiacona M, Pagani R, Capasso R, Zampetti P, Miceli G. Posterior cerebral artery infarcts and semantic category dissociations: a study of 28 patients. Brain. 2009;132(Pt 4):965-81.

51. Park KC, Yoon SS, Rhee HY. Executive dysfunction associated with stroke in the posterior cerebral artery territory. J Clin Neurosci. 2011;18(2):203-8.

52. Weimar C, Mieck T, Buchthal J, Ehrenfeld CE, Schmid E, Diener HC, et al. Neurologic worsening during the acute phase of ischemic stroke. Arch Neurol. 2005;62(3):393-7.

53. Michael KM, Allen JK, Macko RF. Reduced ambulatory activity after stroke: the role of balance, gait, and cardiovascular fitness. Arch Phys Med Rehabil. 2005;86(8):1552-6.

54. Raghavan P. Upper Limb Motor Impairment After Stroke. Phys Med Rehabil Clin N Am. 2015;26(4):599-610.

55. Nascimento LR, de Oliveira CQ, Ada L, Michaelsen SM, Teixeira-Salmela LF. Walking training with cueing of cadence improves walking speed and stride length after stroke more than walking training alone: a systematic review. J Physiother. 2015;61(1):10-5.

56. Hak L, Houdijk H, van der Wurff P, Prins MR, Beek PJ, van Dieen JH. Stride frequency and length adjustment in post-stroke individuals: influence on the margins of stability. J Rehabil Med. 2015;47(2):126-32.

57. Peterson CL, Hall AL, Kautz SA, Neptune RR. Pre-swing deficits in forward propulsion, swing initiation and power generation by individual muscles during hemiparetic walking. J Biomech. 2010;43(12):2348-55.

58. Nolan KJ, Yarossi M, McLaughlin P. Changes in center of pressure displacement with the use of a foot drop stimulator in individuals with stroke. Clin Biomech (Bristol, Avon). 2015;30(7):755-61.

59. De Nunzio A, Zucchella C, Spicciato F, Tortola P, Vecchione C, Pierelli F, et al. Biofeedback rehabilitation of posture and weightbearing distribution in stroke: a center of foot pressure analysis. Funct Neurol. 2014;29(2):127-34.

60. Villa RF, Ferrari F, Moretti A. Post-stroke depression: Mechanisms and pharmacological treatment. Pharmacol Ther. 2018;184:131-44.

61. Ayerbe L, Ayis S, Crichton S, Wolfe CD, Rudd AG. The long-term outcomes of depression up to 10 years after stroke; the South London Stroke Register. J Neurol Neurosurg Psychiatry. 2014;85(5):514-21.

62. De Ryck A, Brouns R, Fransen E, Geurden M, Van Gestel G, Wilssens I, et al. A prospective study on the prevalence and risk factors of poststroke depression. Cerebrovasc Dis Extra. 2013;3(1):1-13.

63. Sauleau P, Lapouble E, Val-Laillet D, Malbert CH. The pig model in brain imaging and neurosurgery. Animal. 2009;3(8):1138-51.

64. Craner SL, Ray RH. Somatosensory cortex of the neonatal pig: I. Topographic organization of the primary somatosensory cortex (SI). J Comp Neurol. 1991;306(1):24-38.

65. Craner SL, Ray RH. Somatosensory cortex of the neonatal pig: II. Topographic organization of the secondary somatosensory cortex (SII). J Comp Neurol. 1991;306(1):39-48.

66. Lapchak PA, Zhang JH, Noble-Haeusslein LJ. RIGOR guidelines: escalating STAIR and STEPS for effective translational research. Translational stroke research. 2013;4(3):279-85.

67. Baker EW, Platt SR, Lau VW, Grace HE, Holmes SP, Wang L, et al. Induced Pluripotent Stem Cell-Derived Neural Stem Cell Therapy Enhances Recovery in an Ischemic Stroke Pig Model. Scientific Reports. 2017;7(1):10075.

68. Hetze S, Romer C, Teufelhart C, Meisel A, Engel O. Gait analysis as a method for assessing neurological outcome in a mouse model of stroke. J Neurosci Methods. 2012;206(1):7-14.

69. Vandeputte C, Taymans JM, Casteels C, Coun F, Ni Y, Van Laere K, et al. Automated quantitative gait analysis in animal models of movement disorders. BMC Neurosci. 2010;11:92.

70. Otero-Ortega L, Laso-Garcia F, Gomez-de Frutos MD, Rodriguez-Frutos B, Pascual-Guerra J, Fuentes B, et al. White Matter Repair After Extracellular Vesicles Administration in an Experimental Animal Model of Subcortical Stroke. Sci Rep. 2017;7:44433.

71. Xin H, Li Y, Cui Y, Yang JJ, Zhang ZG, Chopp M. Systemic administration of exosomes released from mesenchymal stromal cells promote functional recovery and neurovascular plasticity after stroke in rats. J Cereb Blood Flow Metab. 2013;33(11):1711-5.

72. Zhang Y, Chopp M, Meng Y, Katakowski M, Xin H, Mahmood A, et al. Effect of exosomes derived from multipluripotent mesenchymal stromal cells on functional recovery and neurovascular plasticity in rats after traumatic brain injury. J Neurosurg. 2015;122(4):856-67.

73. Zhang Y, Chopp M, Zhang ZG, Katakowski M, Xin H, Qu C, et al. Systemic administration of cell-free exosomes generated by human bone marrow derived mesenchymal stem cells cultured under 2D and 3D conditions improves functional recovery in rats after traumatic brain injury. Neurochem Int. 2016.

74. Schellinger PD, Jansen O, Fiebach JB, Hacke W, Sartor K. A standardized MRI stroke protocol: comparison with CT in hyperacute intracerebral hemorrhage. Stroke. 1999;30(4):765-8.

75. Jokinen H, Gouw AA, Madureira S, Ylikoski R, van Straaten EC, van der Flier WM, et al. Incident lacunes influence cognitive decline: the LADIS study. Neurology. 2011;76(22):1872-8.

76. Ahmad AS, Satriotomo I, Fazal J, Nadeau SE, Dore S. Considerations for the Optimization of Induced White Matter Injury Preclinical Models. Front Neurol. 2015;6:172.

77. Srikanth V, Beare R, Blizzard L, Phan T, Stapleton J, Chen J, et al. Cerebral white matter lesions, gait, and the risk of incident falls: a prospective population-based study. Stroke. 2009;40(1):175-80.

78. Pikija S, Sztriha LK, Killer-Oberpfalzer M, Weymayr F, Hecker C, Ramesmayer C, et al. Neutrophil to lymphocyte ratio predicts intracranial hemorrhage after endovascular thrombectomy in acute ischemic stroke. J Neuroinflammation. 2018;15(1):319.

79. Guo Z, Yu S, Xiao L, Chen X, Ye R, Zheng P, et al. Dynamic change of neutrophil to lymphocyte ratio and hemorrhagic transformation after thrombolysis in stroke. J Neuroinflammation. 2016;13(1):199.

80. Song Q, Li Y, Wang Y, Wei C, Liu J, Liu M. Increased Neutrophil-to-lymphocyte Ratios are Associated with Greater Risk of Hemorrhagic Transformation in Patients with Acute Ischemic Stroke. Curr Neurovasc Res. 2018;15(4):326-35.

81. Cappellari M, Moretto G, Bovi P. Day-7 modified Rankin Scale score as the best measure of the thrombolysis direct effect on stroke? J Thromb Thrombolysis. 2013;36(3):314-5.

82. Clark PC, Dunbar SB, Aycock DM, Courtney E, Wolf SL. Caregiver perspectives of memory and behavior changes in stroke survivors. Rehabil Nurs. 2006;31(1):26-32.

83. Alexander LD, Black SE, Patterson KK, Gao F, Danells CJ, McIlroy WE. Association between gait asymmetry and brain lesion location in stroke patients. Stroke. 2009;40(2):537-44.

84. Kumar G, Goyal MK, Sahota PK, Jain R. Penumbra, the basis of neuroimaging in acute stroke treatment: current evidence. J Neurol Sci. 2010;288(1-2):13-24.

85. Ledezma CJ, Fiebach JB, Wintermark M. Modern imaging of the infarct core and the ischemic penumbra in acute stroke patients: CT versus MRI. Expert Rev Cardiovasc Ther. 2009;7(4):395-403.

86. Saenger AK, Christenson RH. Stroke biomarkers: progress and challenges for diagnosis, prognosis, differentiation, and treatment. Clin Chem. 2010;56(1):21-33.

87. Gonzalez RG. Clinical MRI of acute ischemic stroke. J Magn Reson Imaging. 2012;36(2):259-71.

88. Sanak D, Nosal V, Horak D, Bartkova A, Zelenak K, Herzig R, et al. Impact of diffusion-weighted MRI-measured initial cerebral infarction volume on clinical outcome in acute stroke patients with middle cerebral artery occlusion treated by thrombolysis. Neuroradiology. 2006;48(9):632-9.

89. Luby M, Bykowski JL, Schellinger PD, Merino JG, Warach S. Intra- and interrater reliability of ischemic lesion volume measurements on diffusion-weighted, mean transit time and fluid-attenuated inversion recovery MRI. Stroke. 2006;37(12):2951-6.

90. Lansberg MG, O'Brien MW, Tong DC, Moseley ME, Albers GW. Evolution of cerebral infarct volume assessed by diffusion-weighted magnetic resonance imaging. Arch Neurol. 2001;58(4):613-7.

91. Huisman TA. Diffusion-weighted imaging: basic concepts and application in cerebral stroke and head trauma. Eur Radiol. 2003;13(10):2283-97.

92. Huisman TA. Diffusion-weighted and diffusion tensor imaging of the brain, made easy. Cancer Imaging. 2010;10 Spec no A:S163-71.

93. Payabvash S, Taleb S, Benson JC, Rykken JB, Oswood MC, McKinney AM, et al. The Effects of DWI-Infarct Lesion Volume on DWI-FLAIR Mismatch: Is There a Need for Size Stratification? J Neuroimaging. 2017;27(4):392-6.

94. Merino JG, Warach S. Imaging of acute stroke. Nat Rev Neurol. 2010;6(10):560-71.

95. Yoo AJ, Pulli B, Gonzalez RG. Imaging-based treatment selection for intravenous and intra-arterial stroke therapies: a comprehensive review. Expert Rev Cardiovasc Ther. 2011;9(7):857-76.

96. Assemlal HE, Tschumperle D, Brun L, Siddiqi K. Recent advances in diffusion MRI modeling: Angular and radial reconstruction. Med Image Anal. 2011;15(4):369-96.

97. Carmichael ST. Rodent models of focal stroke: size, mechanism, and purpose. NeuroRx. 2005;2(3):396-409.

98. Macrae IM. Preclinical stroke research--advantages and disadvantages of the most common rodent models of focal ischaemia. Br J Pharmacol. 2011;164(4):1062-78.

99. Stankowski JN, Gupta R. Therapeutic targets for neuroprotection in acute ischemic stroke: lost in translation? Antioxid Redox Signal. 2011;14(10):1841-51.

100. Jaffer H, Morris VB, Stewart D, Labhasetwar V. Advances in stroke therapy. Drug Deliv Transl Res. 2011;1(6):409-19.

101. Selim M, Fink JN, Kumar S, Caplan LR, Horkan C, Chen Y, et al. Predictors of hemorrhagic transformation after intravenous recombinant tissue plasminogen activator: prognostic value of the initial apparent diffusion coefficient and diffusion-weighted lesion volume. Stroke. 2002;33(8):2047-52.

102. Berrouschot J, Sterker M, Bettin S, Koster J, Schneider D. Mortality of space-occupying ('malignant') middle cerebral artery infarction under conservative intensive care. Intensive Care Med. 1998;24(6):620-3.

103. Hacke W, Schwab S, Horn M, Spranger M, De Georgia M, von Kummer R. 'Malignant' middle cerebral artery territory infarction: clinical course and prognostic signs. Arch Neurol. 1996;53(4):309-15.

104. Thrift AG, Dewey HM, Macdonell RA, McNeil JJ, Donnan GA. Stroke incidence on the east coast of Australia: the North East Melbourne Stroke Incidence Study (NEMESIS). Stroke. 2000;31(9):2087-92.

105. Arnaout OM, Aoun SG, Batjer HH, Bendok BR. Decompressive hemicraniectomy after malignant middle cerebral artery infarction: rationale and controversies. Neurosurg Focus. 2011;30(6):E18.

106. Vahedi K, Hofmeijer J, Juettler E, Vicaut E, George B, Algra A, et al. Early decompressive surgery in malignant infarction of the middle cerebral artery: a pooled analysis of three randomised controlled trials. Lancet Neurol. 2007;6(3):215-22.

107. Wang DZ, Nair DS, Talkad AV. Acute Decompressive Hemicraniectomy to Control High Intracranial Pressure in Patients with Malignant MCA Ischemic Strokes. Curr Treat Options Cardiovasc Med. 2011;13(3):225-32.

108. O'Collins VE, Macleod MR, Donnan GA, Horky LL, van der Worp BH, Howells DW. 1,026 experimental treatments in acute stroke. Ann Neurol. 2006;59(3):467-77.

109. Kotwica Z, Hardemark HG, Persson L. Intracranial pressure changes following middle cerebral artery occlusion in rats. Res Exp Med (Berl). 1991;191(2):99-104.

110. DeVries AC, Nelson RJ, Traystman RJ, Hurn PD. Cognitive and behavioral assessment in experimental stroke research: will it prove useful? Neurosci Biobehav Rev. 2001;25(4):325-42.

111. Schirrmacher R, Dea M, Heiss WD, Kostikov A, Funck T, Quessy S, et al. Which Aspects of Stroke Do Animal Models Capture? A Multitracer Micro-PET Study of Focal Ischemia with Endothelin-1. Cerebrovasc Dis. 2016;41(3-4):139-47.

112. Hughes PM, Anthony DC, Ruddin M, Botham MS, Rankine EL, Sablone M, et al. Focal lesions in the rat central nervous system induced by endothelin-1. J Neuropathol Exp Neurol. 2003;62(12):1276-86.

113. Fuxe K, Bjelke B, Andbjer B, Grahn H, Rimondini R, Agnati LF. Endothelin-1 induced lesions of the frontoparietal cortex of the rat. A possible model of focal cortical ischemia. Neuroreport. 1997;8(11):2623-9.

114. Fluri F, Schuhmann MK, Kleinschnitz C. Animal models of ischemic stroke and their application in clinical research. Drug Des Devel Ther. 2015;9:3445-54.

115. Wells AJ, Vink R, Helps SC, Knox SJ, Blumbergs PC, Turner RJ. Elevated Intracranial Pressure and Cerebral Edema following Permanent MCA Occlusion in an Ovine Model. PLoS One. 2015;10(6):e0130512.

116. Ropper AH. Lateral displacement of the brain and level of consciousness in patients with an acute hemispheral mass. N Engl J Med. 1986;314(15):953-8.

117. Treadwell SD, Thanvi B. Malignant middle cerebral artery (MCA) infarction: pathophysiology, diagnosis and management. Postgrad Med J. 2010;86(1014):235-42.

118. Walberer M, Blaes F, Stolz E, Muller C, Schoenburg M, Tschernatsch M, et al. Midline-shift corresponds to the amount of brain edema early after hemispheric stroke--an MRI study in rats. J Neurosurg Anesthesiol. 2007;19(2):105-10.

119. Alharbi BM, Tso MK, Macdonald RL. Animal models of spontaneous intracerebral hemorrhage. Neurol Res. 2016;38(5):448-55.

120. Jaillard A, Cornu C, Durieux A, Moulin T, Boutitie F, Lees KR, et al. Hemorrhagic transformation in acute ischemic stroke. The MAST-E study. MAST-E Group. Stroke. 1999;30(7):1326-32.

121. Bang OY, Saver JL, Kim SJ, Kim GM, Chung CS, Ovbiagele B, et al. Collateral flow averts hemorrhagic transformation after endovascular therapy for acute ischemic stroke. Stroke. 2011;42(8):2235-9.

122. D'Amelio M, Terruso V, Famoso G, Di Benedetto N, Realmuto S, Valentino F, et al. Early and late mortality of spontaneous hemorrhagic transformation of ischemic stroke. J Stroke Cerebrovasc Dis. 2014;23(4):649-54.

123. Fiorelli M, Bastianello S, von Kummer R, del Zoppo GJ, Larrue V, Lesaffre E, et al. Hemorrhagic transformation within 36 hours of a cerebral infarct: relationships with early clinical deterioration and 3-month outcome in the European Cooperative Acute Stroke Study I (ECASS I) cohort. Stroke. 1999;30(11):2280-4.

124. Caceres JA, Goldstein JN. Intracranial hemorrhage. Emerg Med Clin North Am. 2012;30(3):771-94.

125. Sahni R, Weinberger J. Management of intracerebral hemorrhage. Vasc Health Risk Manag. 2007;3(5):701-9.

126. Castro P, Azevedo E, Serrador J, Rocha I, Sorond F. Hemorrhagic transformation and cerebral edema in acute ischemic stroke: Link to cerebral autoregulation. J Neurol Sci. 2017;372:256-61.

127. Zhang J, Yang Y, Sun H, Xing Y. Hemorrhagic transformation after cerebral infarction: current concepts and challenges. Ann Transl Med. 2014;2(8):81.

128. Kanazawa M, Takahashi T, Nishizawa M, Shimohata T. Therapeutic Strategies to Attenuate Hemorrhagic Transformation After Tissue Plasminogen Activator Treatment for Acute Ischemic Stroke. J Atheroscler Thromb. 2017;24(3):240-53.

129. Yaghi S, Willey JZ, Cucchiara B, Goldstein JN, Gonzales NR, Khatri P, et al. Treatment and Outcome of Hemorrhagic Transformation After Intravenous Alteplase in Acute Ischemic Stroke: A Scientific Statement for Healthcare Professionals From the American Heart Association/American Stroke Association. Stroke. 2017;48(12):e343-e61.

130. Biesbroek JM, Weaver NA, Biessels GJ. Lesion location and cognitive impact of cerebral small vessel disease. Clin Sci (Lond). 2017;131(8):715-28.

131. Lee KB, Kim JS, Hong BY, Sul B, Song S, Sung WJ, et al. Brain lesions affecting gait recovery in stroke patients. Brain Behav. 2017;7(11):e00868.

132. Corriveau H, Hebert R, Raiche M, Prince F. Evaluation of postural stability in the elderly with stroke. Arch Phys Med Rehabil. 2004;85(7):1095-101.

133. Roth EJ, Merbitz C, Mroczek K, Dugan SA, Suh WW. Hemiplegic gait. Relationships between walking speed and other temporal parameters. Am J Phys Med Rehabil. 1997;76(2):128-33.

134. Dickstein R, Shefi S, Marcovitz E, Villa Y. Anticipatory postural adjustment in selected trunk muscles in post stroke hemiparetic patients. Arch Phys Med Rehabil. 2004;85(2):261-7.

135. Titianova EB, Tarkka IM. Asymmetry in walking performance and postural sway in patients with chronic unilateral cerebral infarction. J Rehabil Res Dev. 1995;32(3):236-44.

136. Hidler JM, Carroll M, Federovich EH. Strength and coordination in the paretic leg of individuals following acute stroke. IEEE Trans Neural Syst Rehabil Eng. 2007;15(4):526-34.

137. Duberstein KJ, Platt SR, Holmes SP, Dove CR, Howerth EW, Kent M, et al. Gait analysis in a pre- and post-ischemic stroke biomedical pig model. Physiol Behav. 2014;125:8-16.

138. Chamorro A, Hallenbeck J. The harms and benefits of inflammatory and immune responses in vascular disease. Stroke. 2006;37(2):291-3.

139. Kleinig TJ, Vink R. Suppression of inflammation in ischemic and hemorrhagic stroke: therapeutic options. Curr Opin Neurol. 2009;22(3):294-301.

140. Haeusler KG, Schmidt WU, Fohring F, Meisel C, Helms T, Jungehulsing GJ, et al. Cellular immunodepression preceding infectious complications after acute ischemic stroke in humans. Cerebrovasc Dis. 2008;25(1-2):50-8.

141. Vogelgesang A, Grunwald U, Langner S, Jack R, Broker BM, Kessler C, et al. Analysis of lymphocyte subsets in patients with stroke and their influence on infection after stroke. Stroke; a journal of cerebral circulation. 2008;39(1):237-41.

142. Schwartz M, Moalem G. Beneficial immune activity after CNS injury: prospects for vaccination. J Neuroimmunol. 2001;113(2):185-92.

143. Kim JY, Kawabori M, Yenari MA. Innate inflammatory responses in stroke: mechanisms and potential therapeutic targets. Curr Med Chem. 2014;21(18):2076-97.

144. Kim J, Song TJ, Park JH, Lee HS, Nam CM, Nam HS, et al. Different prognostic value of white blood cell subtypes in patients with acute cerebral infarction. Atherosclerosis. 2012;222(2):464-7.

145. Xue J, Huang W, Chen X, Li Q, Cai Z, Yu T, et al. Neutrophil-to-Lymphocyte Ratio Is a Prognostic Marker in Acute Ischemic Stroke. Journal of stroke and cerebrovascular diseases : the official journal of National Stroke Association. 2017;26(3):650-7.

146. Zhang J, Ren Q, Song Y, He M, Zeng Y, Liu Z, et al. Prognostic role of neutrophil-lymphocyte ratio in patients with acute ischemic stroke. Medicine (Baltimore). 2017;96(45):e8624.

147. Suh B, Shin DW, Kwon HM, Yun JM, Yang HK, Ahn E, et al. Elevated neutrophil to lymphocyte ratio and ischemic stroke risk in generally healthy adults. PLoS One. 2017;12(8):e0183706.

148. Lattanzi S, Cagnetti C, Provinciali L, Silvestrini M. Neutrophil-to-lymphocyte ratio and neurological deterioration following acute cerebral hemorrhage. Oncotarget. 2017;8(34):57489-94.

149. Balkaya M, Krober JM, Rex A, Endres M. Assessing post-stroke behavior in mouse models of focal ischemia. J Cereb Blood Flow Metab. 2013;33(3):330-8.

150. Crawley JN. Exploratory behavior models of anxiety in mice. Neuroscience and biobehavioral reviews. 1985;9(1):37-44.

151. Belzung C, Griebel G. Measuring normal and pathological anxiety-like behaviour in mice: a review. Behavioural brain research. 2001;125(1-2):141-9.

152. Studnitz M, Jensen MB, Pedersen LJJAabs. Why do pigs root and in what will they root?: A review on the exploratory behaviour of pigs in relation to environmental enrichment. Applied Animal Behaviour Science. 2007;107(3-4):183-97.

153. Chemerinski E, Robinson RG. The neuropsychiatry of stroke. Psychosomatics. 2000;41(1):5-14.

154. van Almenkerk S, Depla MF, Smalbrugge M, Eefsting JA, Hertogh CM. Institutionalized stroke patients: status of functioning of an under researched population. J Am Med Dir Assoc. 2012;13(7):634-9.

155. Association AP. Diagnostic and statistical manual of mental disorders (DSM-5®): American Psychiatric Pub; 2013.

156. Andersen G, Vestergaard K, Ingemann-Nielsen M, Lauritzen L. Risk factors for post-stroke depression. Acta Psychiatr Scand. 1995;92(3):193-8.

Figure 3.1: MCAO induces acute ischemic infarction and decreased diffusivity. DWI sequences exhibited territorial hyperintense lesions of 9.91±1.40 cm^3 characteristic of an edematous injury (**A**, white arrow). ADC maps revealed signal void indicative of restricted diffusion and cytotoxic edema (**B**, white arrow). Ipsilateral ROIs exhibited a significantly ($p \leq 0.0001$) lower ADC value relative to the contralateral hemisphere (0.34±0.02 vs. 0.62±0.03 $x10^{-3}mm^2/s$, respectively; **C**). ***** indicates significant difference between hemispheres.

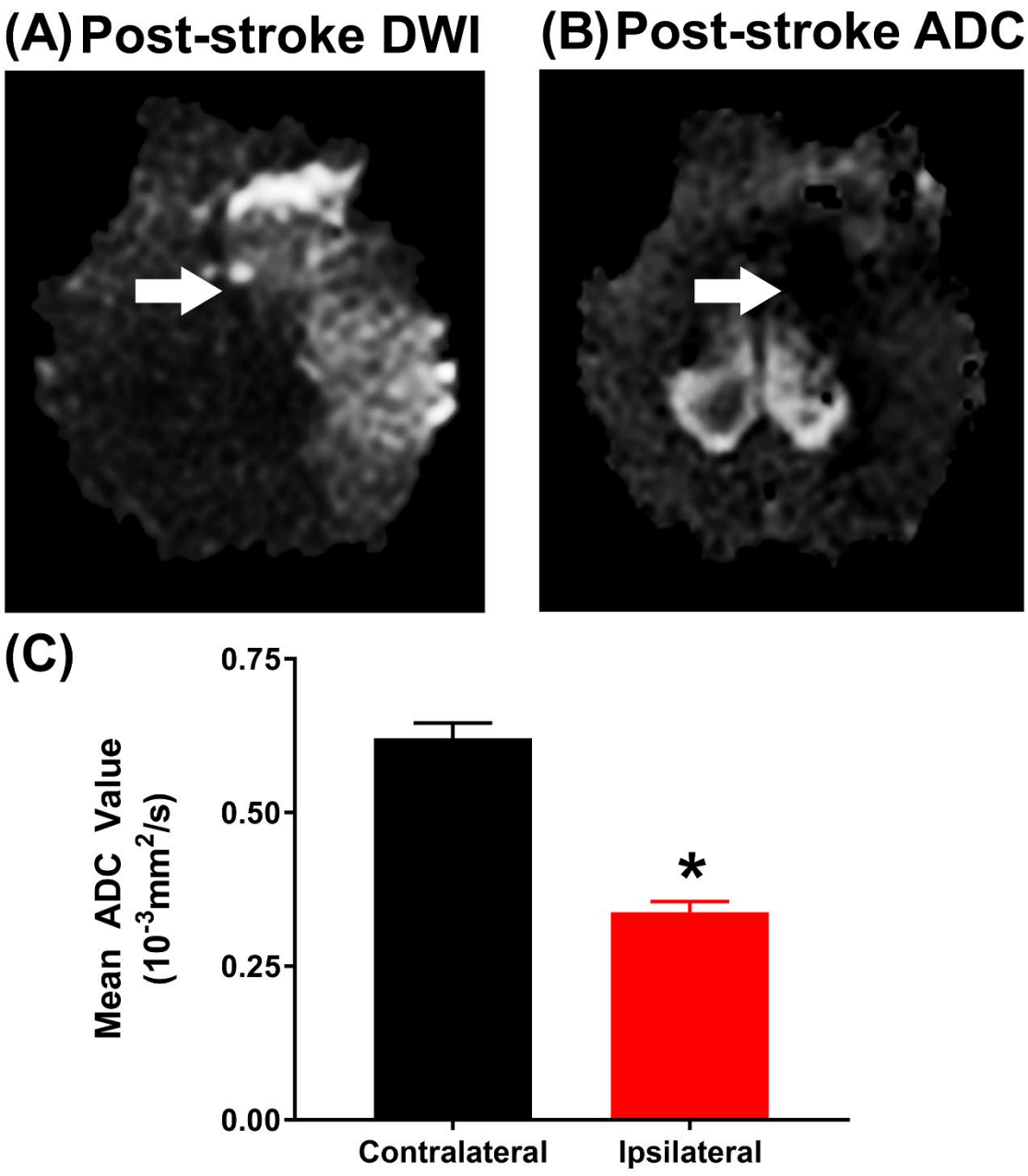
(A) Post-stroke DWI
(B) Post-stroke ADC
(C)
Mean ADC Value
($10^{-3}mm^2/s$)
0.75
0.50
0.25
0.00
*
Contralateral
Ipsilateral

Figure 3.2: Ischemic stroke results in hemispheric swelling, consequent midline shift, and intracerebral hemorrhage. T2W sequences revealed increased swelling of the ipsilateral hemisphere (25.99±1.78 vs. 22.49±1.40 cm^3; **A-C**) resulting in a pronounced MLS of 2.48±0.55 mm compared to pre-stroke imaging (**A** and **B**, red lines). Characteristic hypointense ROIs indicated the presence of ipsilateral ICH when compared to pre-stroke T2* sequences (1.73±0.17 cm^3, **D** and **E**, white arrow).

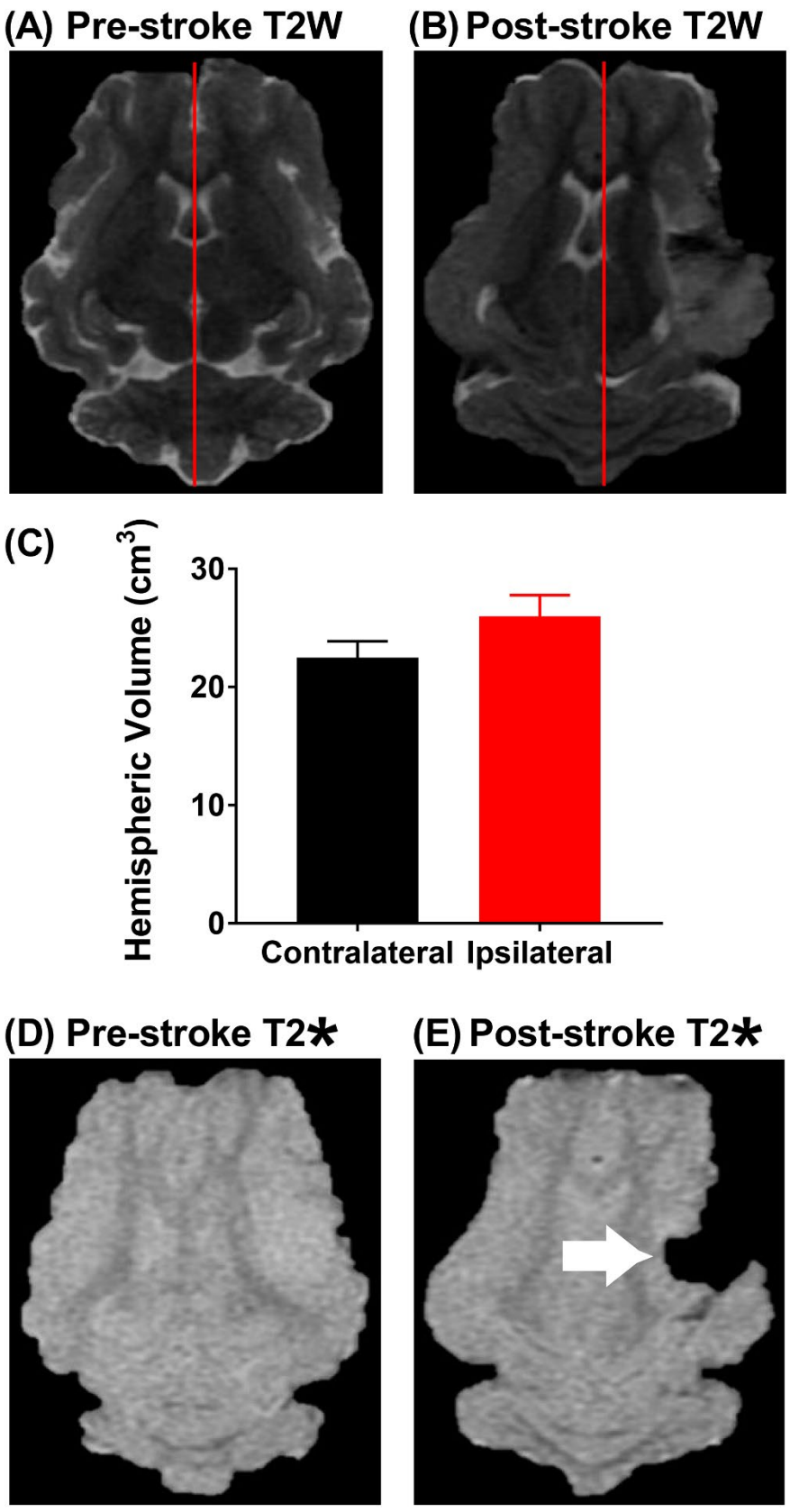
(A) Pre-stroke T2W
(B) Post-stroke T2W
(C)
Hemispheric Volume (cm3)
30
20
10
0
Contralateral
Ipsilateral
(D) Pre-stroke T2*
(E) Post-stroke T2*

Figure 3.3: Ischemic stroke diminishes white matter integrity of the internal capsule. Pre-stroke the left and right IC possess similar WM integrity (**A**). 24 hours post-stroke, the ipsilateral IC exhibited a disruption in WM integrity (**B**, white arrow). Further analysis revealed a significant ($p<0.01$) decrease in the ipsilateral IC FA value when compared to the contralateral IC (0.17±0.01 vs. 0.23±0.01 respectively; **C**). * indicates significant difference between hemispheres.

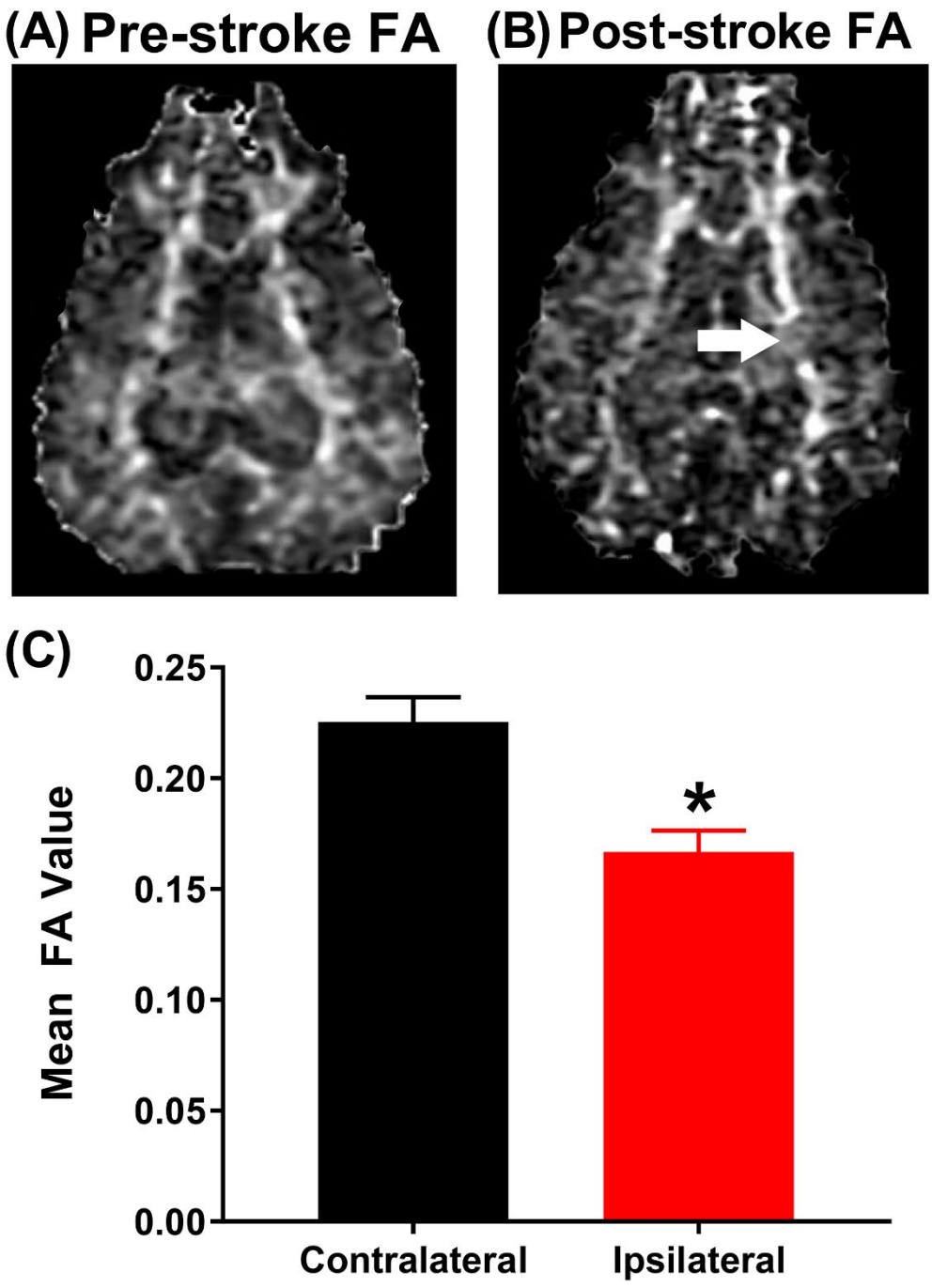
(A) Pre-stroke FA
(B) Post-stroke FA
(C)
Mean FA Value
0.25
0.20
0.15
0.10
0.05
0.00
*
Contralateral
Ipsilateral

Figure 3.4: Ischemic stroke leads to increases in circulating neutrophil levels and decreases in circulating lymphocyte levels. Band neutrophils showed a significant ($p<0.05$) increase 12 hours post-stroke when compared to pre-stroke (5.50±0.99 vs. 1.92±0.51% respectively; **A, B**). Circulating neutrophils were significantly ($p<0.05$) increased at 4- and 12-hours post-stroke relative to pre-stroke (43.7±5.27 and 48.9±3.92% vs. 26.5±1.96%, respectively; **C, D**). Circulating lymphocytes were significantly ($p<0.05$) decreased at 12- and 24-hours post-stroke compared to pre-stroke (25.60±4.01 and 26.60±4.29% vs. 44.83±3.66% respectively; **E, F**). * indicates significant difference between pre-stroke and post-stroke time points.

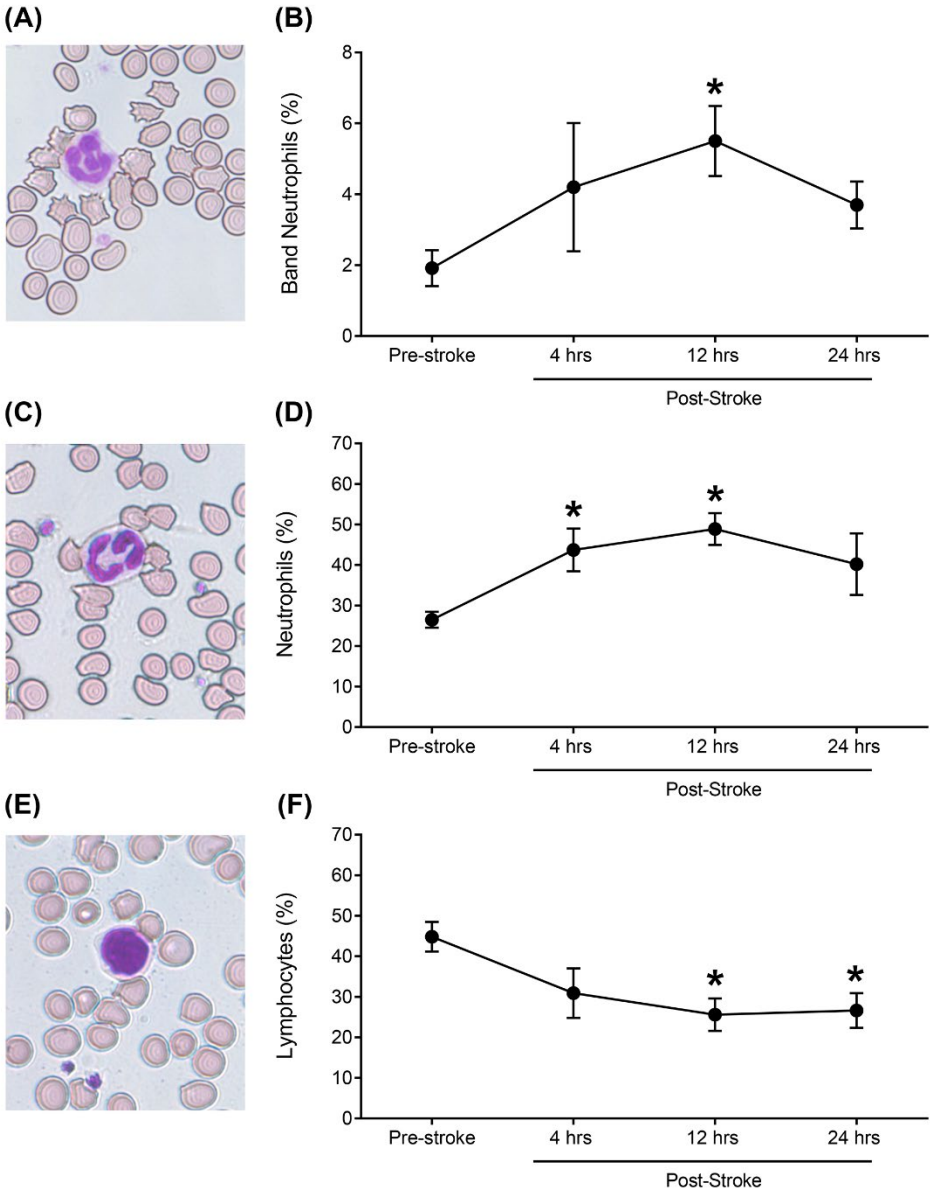
(A)
(B)
Band Neutrophils (%)
8
6
4
2
0
*
Pre-stroke
4 hrs
12 hrs
24 hrs
Post-Stroke
(C)
(D)
Neutrophils (%)
70
60
50
40
30
20
10
0
*
*
Pre-stroke
4 hrs
12 hrs
24 hrs
Post-Stroke
(E)
(F)
Lymphocytes (%)
70
60
50
40
30
20
10
0
*
*
Pre-stroke
4 hrs
12 hrs
24 hrs
Post-Stroke

Figure 3.5: MCAO leads to functional disabilities and behavioral abnormalities. Ethovision XT tracking software was used during OF testing to automatically assess differences in perimeter sniffing (red line) versus OF arena exploration (yellow line) pre-stroke (**A**) and post-stroke (**B**). Exploratory perimeter sniffing frequencies were significantly ($p<0.05$) reduced at 48 hours post-stroke compared to pre-stroke observations (13.0±2.94 vs 26.0±4.02, respectively; **C**). * indicates a significant difference from pre-stroke.

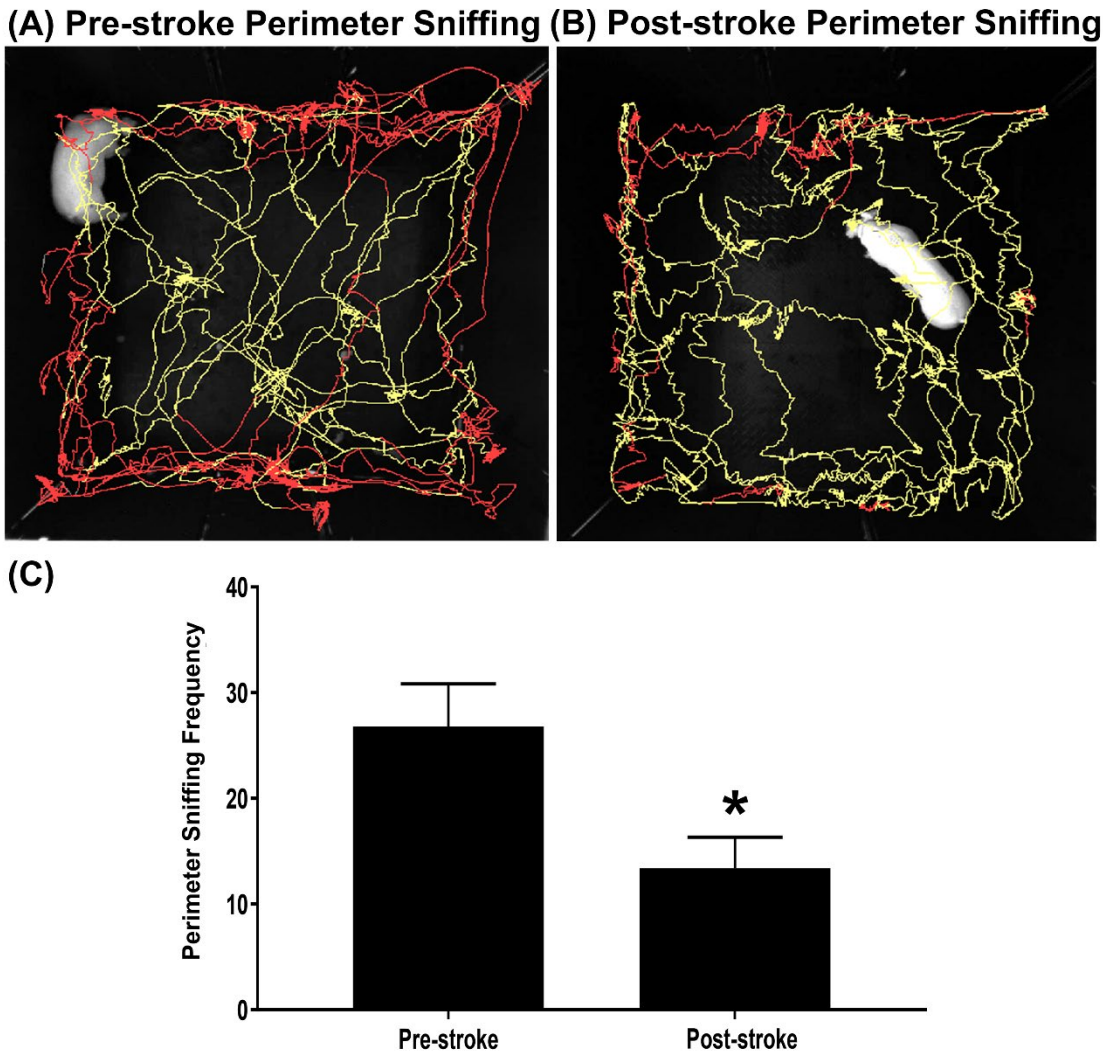
(A) Pre-stroke Perimeter Sniffing
(B) Post-stroke Perimeter Sniffing
(C)
Perimeter Sniffing Frequency
40
30
20
10
0
*
Pre-stroke
Post-stroke

Figure 3.6: Ischemic stroke results in spatiotemporal gait deficits. Velocity and cadence significantly ($p< 0.01$) decreased post-stroke (61.01±8.39 vs 162.9±12.73 cm/s and 61.01±5.91 vs 126.44±3.72 steps/min, respectively, **A-B**). The LF swing percent of cycle significantly ($p<0.01$) decreased compared to pre-stroke (30.70±2.12 vs 48.89±2.35%, respectively, **C**). A significant ($p<0.01$) decrease in LF stride length was observed post-stroke compared to pre-stroke (59.04±3.85 vs 76.72±4.60cm, respectively, **D**). LF cycle time significantly ($p<0.01$) increased relative to pre-stroke (1.02±.09 vs 0.48±0.013sec, respectively, **E**). The mean pressure exhibited by the LF significantly ($p<0.01$) decreased at post-stroke compared to pre-stroke (2.62±.03 vs 2.82±.03 arbitrary units (A.U.), respectively, **F**). * indicates significant difference between pre-stroke and post-stroke time points.

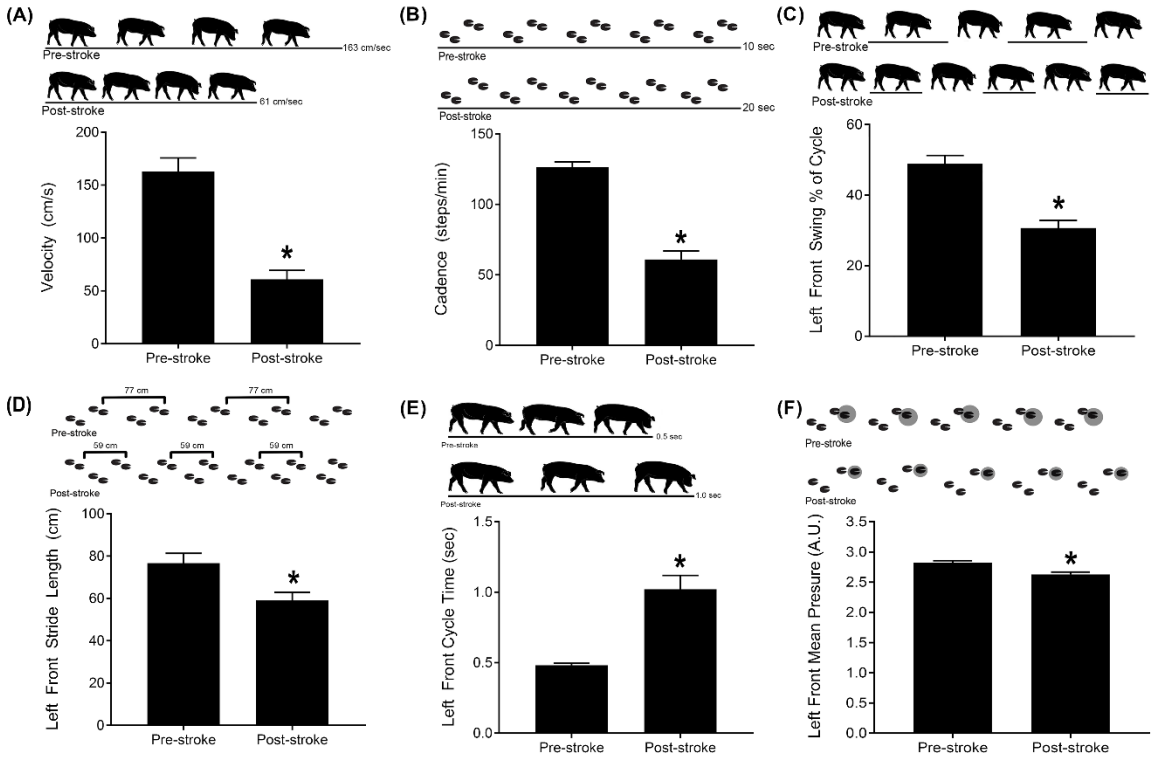
(A)
Pre-stroke
163 cm/sec
Post-stroke
61 cm/sec
Velocity (cm/s)
200
150
100
50
0
*
Pre-stroke
Post-stroke
(B)
Pre-stroke
10 sec
Post-stroke
20 sec
Cadence (steps/min)
150
100
50
0
*
Pre-stroke
Post-stroke
(C)
Pre-stroke
Post-stroke
Left Front Swing % of Cycle
60
40
20
0
*
Pre-stroke
Post-stroke
(D)
77 cm
77 cm
Pre-stroke
59 cm
59 cm
59 cm
Post-stroke
Left Front Stride Length (cm)
100
80
60
40
20
0
*
Pre-stroke
Post-stroke
(E)
Pre-stroke
0.5 sec
Post-stroke
1.0 sec
Left Front Cycle Time (sec)
1.5
1.0
0.5
0.0
*
Pre-stroke
Post-stroke
(F)
Pre-stroke
Post-stroke
Left Front Mean Presure (A.U.)
3.5
3.0
2.5
2.0
1.5
1.0
0.5
0.0
*
Pre-stroke
Post-stroke

CHAPTER 4

HUMAN NEURAL STEM CELL EXTRACELLULAR VESICLES IMPROVE RECOVERY IN A PORCINE MODEL OF ISCHEMIC STROKE[1]

---

[1]Webb, R.L.†, Kaiser, E.E.†, Jurgielewicz, B.J., Spellicy, S.E., Scoville, S.L., Thompson, T.A., Swetenburg, R.L., Hess, D.C., West, F.D., and Stice, S.L. *Stroke*. 2018; 49:1248–1256. Reprinted here with permission of the publisher.

† these authors equally contributed to this work

Abstract

Background and Purpose:

Recent work from our group suggests human neural stem cell derived extracellular vesicle (NSC EV) treatment improves both tissue and sensorimotor function in a preclinical thromboembolic (TE) mouse model of stroke. In this study, NSC EVs were evaluated in a pig ischemic stroke model, where clinically-relevant endpoints were utilized to assess recovery in a more translational large animal model.

Methods

Ischemic stroke was induced by permanent middle cerebral artery occlusion (MCAO), and either NSC EV or PBS treatments were administered intravenously (IV) at 2, 14, and 24 hours post-MCAO. NSC EV effects on tissue level recovery were evaluated via magnetic resonance imaging (MRI) at 1 and 84 days post-MCAO. Effects on functional recovery were also assessed through longitudinal behavior and gait analysis testing.

Results

NSC EV treatment was neuroprotective and led to significant improvements at the tissue and functional levels in stroked pigs. NSC EV treatment eliminated intracerebral hemorrhage (ICH) in ischemic lesions in NSC EV pigs (0/7) versus control pigs (7/8). NSC EV treated pigs exhibited a significant decrease in cerebral lesion volume and decreased brain swelling relative to control pigs 1-day post-MCAO. NSC EVs significantly reduced edema in treated pigs relative to control pigs, as assessed by improved diffusivity through Apparent Diffusion Coefficient (ADC) maps. NSC EVs preserved white matter (WM) integrity with increased corpus callosum fractional anisotropy (FA) values 84 days post-MCAO. Behavior and mobility improvements paralleled structural changes, as NSC EV

treated pigs exhibited improved outcomes including increased exploratory behavior and faster restoration of spatiotemporal gait parameters.

Conclusions

This study demonstrated for the first time in a large animal model novel NSC EVs significantly improved neural tissue preservation and functional levels post-MCAO, suggesting NSC EVs may be a paradigm changing stroke therapeutic.

Introduction

Food and Drug Administration (FDA) approved therapies for stroke (tissue plasminogen activator and endovascular thrombectomy) are currently only available to a small subpopulation of stroke victims [1, 2]. Following a litany of failed treatments, assessment by the Stem Cell Emerging Paradigm in Stroke (STEPS) consortium meetings identified major needs including 1) a regenerative therapy, and 2) testing in translational animal models more reflective of human pathology [3, 4]. Similarly, the Stroke Therapy Academic Industry Roundtable (STAIR) encouraged 1) testing in higher-order gyrencephalic species, 2) evaluating clinically-relevant routes of administration, and 3) longitudinal behavior assessment [5, 6]. These recommendations prompted our therapeutic evaluation of intravenously (IV) administered human neural stem cell extrecellular vesicles (NSC EVs) in a translational pig ischemic stroke model.

One of the most promising emerging therapeutics capable of addressing the need for a neuroprotective and/or regenerative therapy are extracellular vesicles (EVs) sourced from stem cells cultures [7]. EVs are heterogeneous populations of both 50-1,000 nm plasma membrane shed microvesicles, and 40-150 nm exosomes derived from the endocytic pathway. These EVs are enriched in transmembrane proteins, bioactive lipids, and miRNAs, and are produced by virtually all cell types [8, 9]. Recently, the therapeutic potential of these cell signaling vesicles has been explored from several cell sources and for varied applications [10]. The vast majority of previously reported neural injury studies evaluating stem cell derived EVs have utilized mesenchymal stem cell (MSC) derived EVs [11-13]. However, in vivo biodistribution of EVs is highly dependent on cell source, suggesting EVs will display specific biodistribution patterns in vivo reflecting their parent cell line [14].

We compared the neuroprotective and regenerative properties of NSC EVs versus isogenically derived MSC EVs in a mouse thromboembolic (TE) stroke model. MSC EV treatments trended towards decreasing stroke lesion volume whereas NSC EVs signifincantly decreased lesion size, preserved motor function, and improved episodic memory[15]. These findings collectively warrant further rigorous testing of NSC EVs in a secondary pig ischemic stroke model.

Following the STEPs and STAIR committees' recommendations, NSC EV therapeutic benefits should be extensively tested using clinically-relevant routes of administration, treatment regimen, and endpoints in a large animal model of ischemic stroke. The porcine permanent middle cerebral artery occlusion (MCAO) model possesses several advantages including brain anatomy and physiology comparable to humans [16-18]. Both human and porcine brains are gyrencephalic and are composed of >60% white matter (WM), while rodent brains are lissencephalic and are composed of <10% WM [19-22]. These similar attributes in cytoarchitecture are critically important as WM is highly vulnerable to pathological processes that follow ischemic stroke [22]. Since pigs are of similar body size to humans and their brains are only 7.5 times smaller than human brains, compared to the 650 times smaller rodent brain, pigs are a more direct assessment of dosing in a preclinical model [18]. These similarities in brain composition, cytoarchitecture, and size collectively support the use of a pig ischemic stroke model to better predict outcomes between preclinical rodent models and human clinical trials.

The objectives of this study were to evaluate the therapeutic potential of NSC EVs through magnetic resonance imaging (MRI) at 1 and 84 days post-MCAO, and to longitudinally assess changes in motor function via gait analysis and open field testing. In

this study we present for the first time, evidence NSC EVs promote extensive tissue and functional level recovery in a large animal preclinical stroke model.

Materials and Methods

Data that support the findings of this study are available from the corresponding author upon reasonable request.

Study design

The overarching aim of these studies were to evaluate NSC EV efficacy as a potential acute stroke therapy in a preclinical, biologically relevant porcine MCAO model of ischemic stroke. Endpoints were selected to evaluate tissue and functional level changes in response to treatment. We employed a split plot experimental design, where all treatment groups were conducted within one day to control for and reduce experimental variation. The sample size for this study was determined by a power calculation based on our previously published work using the pig MCAO model with lesion volume changes by MRI imaging being the primary endpoint[23]. The power analysis was calculated using a two-tailed ANOVA test, α=0.05, and an 80% power of detection, effect size of 1.19 and a standard deviation of 44.63. Initially, 14 pigs were randomly assigned to the treated and control groups. However, due to high mortality rates within the control group, 2 additional pigs were added to the control group for a total 9 pigs in the control group and 7 pigs in the treated group (physiological data, and mortality information included in online-only data supplement Table I and II, respectively). While a greater percentage of NSC EV pigs survived relative to control pigs, there were no statistically significant survival rate differences between treatment groups (online-only data supplement Fig. I). Ischemic stroke was induced by a blinded surgeon and EVs were delivered as single use aliquots by

investigators. To control for potential day effects, one treated and one control pig were assigned to each surgical day except for one surgical day in which the two additional control pig surgeries were performed. Due to the timing of the first treatment, it was not possible to show proof of identical lesion sizes prior to NSC EV administration or account for progression rate of lesions. However, a one-way ANOVA and post-hoc Tukey-Kramer pair-wise test comparing the lesion volumes of pigs within each treatment group between the first and second half of the study resulted in no significant difference (treated $p= 0.9994$, non-treated $p= 0.7804$). This consistency in lesion volumes suggests there was no significant difference in time dependent variables including the effect of surgical procedures over the course of the study. All endpoints and functional measurements were prospectively planned and underwent unblinded analysis. Predefined exclusion criteria from all endpoints included instances of infection in the injury site, self-inflicted injuries that required euthanasia, inability to thermoregulate, uncontrolled seizure activity, and/or respiratory distress. 1 control pig was excluded from MRI collection due to post-operative complications and premature death (online-only data supplement Table II). Data collection from 1 treated pig was retrospectively excluded from all assessments due to a Trueperella (Arcanobacterium) pyogenes abscess and was determined to be the result of the surgery by pathologists and veterinarians. No outliers were removed from the data.

Results

NSC EV manufacture consistently produced biologically active and reproducible vesicles.

EVs were harvested from NSC basal culture medium according to standard production protocol and with reproducible size profile with over 90% of EVs under 200 nm in diameter as determined by Nanosight (Supplemental methods) [15]. To determine

cellular uptake of NSC EVs, a critical component of EV function, uptake of DiI labeled NSC EVs was evaluated using an interferometric technique known as spatial light interference microscopy (SLIM) [24]. Time lapse imaging (18-hour time point shown) indicated NSC EVs were taken up by cells and were visualized while being transported within the cell (**Figure 4.1A-C**, online-only data Supplemental Movie S1). NSC EVs may ultimately exert their efficacy through uptake by various cell types when in circulation. NSC EVs were analyzed using a commercially available MACSPlex exosome kit and displayed a consistent EV marker profile (**Figure 4.1D**). Along with the recently published physical size evaluation this data supported a consistent profile and bioactivity of NSC EVs derived from separate purifications [15].

NSC EVs decreased lesion volume and mitigated cerebral swelling 1-day post-MCAO.

To confirm ischemic stroke 1-day post-MCAO, MRI T2 Weighted Fluid Attenuated Inversion Recovery (T2FLAIR), and Diffusion Weighted Imaging (DWI) sequences were assessed and exhibited territorial hyperintense lesions characteristic of an edematous injury (**Figure 4.2A**, white arrows). Hypointense lesions observed on corresponding Apparent Diffusion Coefficient (ADC) maps confirmed areas of restricted diffusion indicative of cytotoxic edema (**Figure 4.2A**, white arrows), thus confirming permanent cauterization of the middle cerebral artery (MCA) resulted in ischemic stroke. T2 Weighted (T2W) sequences at 1-day post-MCAO revealed characteristic hyperintense lesions indicative of acute ischemic stroke (**Figure 4.2B**). To account for the space-occupying effect of brain edema, edema-corrected lesion volume (LVc) was calculated utilizing T2W and corresponding ADC maps revealing a significant ($p<0.05$) decrease in LVc in NSC EV treated pigs when compared to controls (6.0±1.4 vs. 10.7±1.4

cm^3 respectively, **Figure 4.2C**). T2W based results also indicated significantly ($p \leq 0.01$) decreased swelling of the affected ipsilateral hemisphere resulting in a less pronounced midline shift in NSC EV treated pigs relative to control pigs 1-day post-MCAO (113.7±2.6 vs. 126.8±3.4 % respectively, **Figure 4.2B, D**). Despite these acute changes, there were no significant differences in lesion volume or brain atrophy between treatment groups 84 days post-MCAO (**Supplemental Figure 4.3**). The occurrence of intracerebral hemorrhage (ICH) was also substantially reduced in NSC EV treated pigs relative to controls (0/7 and 7/8 pigs, respectively, **Figure 4.2B**, white arrows, **Supplemental Figure 4.2**).

NSC EVs promoted increased diffusivity and white matter integrity 1 and 84 days post-MCAO.

Cerebral diffusivity was evaluated utilizing DWI sequences and derived ADC maps. Signal void, consistent with restricted diffusion and indicative of cytotoxic edema was quantified (**Figure 4.3A**, white arrows). Mean ADC values in the affected ipsilateral hemisphere were compared to the contralateral hemisphere with calculated percent changes closer to zero being more similar to normal tissue. NSC EV treated pigs exhibited a significantly ($p<0.01$) reduced percent change in ADC values when compared to control pigs 1-day post-MCAO (-18.7±2.6 vs. -32.3±1.5 % respectively; **Figure 4.3C**). To assess long-term changes in WM integrity, the corpus callosum was examined 84 days post-MCAO. Changes in FA in the affected ipsilateral hemisphere were again compared to the contralateral hemisphere. FA maps depicted a decrease in the corpus callosum of the ipsilateral hemisphere of control pigs 84 days post-MCAO (**Figure 4.3B**, white arrow), while NSC EV treated pigs exhibited a significantly ($p<0.01$) lower percent decrease in FA values (-13.9±3.2% vs. -43.3±6.7 %, respectively; **Figure 4.3D**). Collectively, MRI results

offered compelling evidence NSC EV treatment provided neuroprotection and promoted tissue level recovery by decreasing cerebral lesion volume, swelling, incidence of ICH, and preserving diffusivity and WM integrity.

NSC EVs resulted in increased motor activity and exploratory behavior.

Exploratory behavior and motor activity pre- and post-MCAO were assessed by open field testing. NSC EV treated pigs did not significantly decrease their distance traveled, while control pigs were less active, compared to pre-MCAO time points (113.6±12.0 vs. 42.0±12.7 m; $p<0.01$; **Figure 4.4A**). Interestingly, longitudinal analysis at 84 days post-MCAO revealed NSC EV treated pigs exhibited a significant increase in distance traveled compared to their pre-MCAO time points (107.3±9.9 vs. 217.0±29.6 m; $p<0.05$), however this trend was not observed in control pigs. Together, these findings suggest NSC EVs preserved normal exploratory behaviors and motor activity post-MCAO.

NSC EV treatment led to faster and improved recovery of spatiotemporal gait parameters

In addition to exploratory activity, there were several key differences in measured temporal gait parameters between treatment groups. Velocity (distance traveled/second), cadence (strides/minute), and swing percent of cycle (percentage of one full gait cycle in which the contralateral hind limb was in the noncontact phase) significantly decreased 1-day post-MCAO for both NSC EV treated and control pigs. However, by 7 days post-MCAO, NSC EV treated pigs recovered when compared to pre-MCAO performance (**Figure 4.4B**). In contrast, control pigs' deficits in velocity, cadence and swing percent of cycle persisted through 7 days post-MCAO. By 28 days post-MCAO, NSC EV treated pigs exhibited a significant increase in temporal gait parameters relative to control pigs, thus demonstrating substantial improvement.

Similar functional outcomes in spatial gait parameters were also observed. Stride length (distance between consecutive hoof prints of the contralateral forelimb), hoof print area (measured by the number of activated sensors of the contralateral forelimb), and total scaled pressure (the sum of peak pressure values recorded from each activated sensor by a hoof during contact) decreased similarly in both groups 1-day post-MCAO (**Figure 4.4C**). However, NSC EV treated pigs recovered by 7 days post-MCAO while control pigs remained significantly impaired at the same time points for these spatial parameters, indicating faster recovery.

Discussion

This pivotal study presents the first experimental evidence IV administration of NSC EVs improved tissue and functional level outcomes in a translational porcine ischemic stroke model while adhering to the STEPS and STAIR committee recommendations for developing and testing novel stroke therapeutics [3-6, 25, 26]. NSC EV intervention led to significant decreases in lesion volume, which has never been observed before in EV-related neural injury studies and has been considered a key biomarker for recovery [12, 13, 27, 28]. Although EVs were harvested from human NSC EVs, no overt negative immune responses were detected in the porcine model. These data support our recently published data in a thromboembolic mouse model where the injury response to stroke was dampened while augmenting a reparative systemic response favoring macrophage polarization toward anti-inflammatory M2 cells, increasing Treg cells, and decreasing proinflammatory TH17 cells [15]. In addition, NSC EV therapy led to preserved diffusivity and sustained WM integrity, which strongly correlates with improvements in executive function, cognitive decline, and sensorimotor deterioration, as well as decreased

hemispheric swelling and ICH incidence, which are intimately associated with stroke patient morbidity [22, 29-33].

Significant decreases in hemispheric swelling and decreased incidence of ICH indicated NSC EV treatment not only preserved cellular integrity in the ischemic site, but also preserved the integrity of microvessels and associated capillary beds 1-day post-MCAO. A recent study of MSC EVs post-MCAO reported increased vascular remodeling in the ischemic boundary zone of rats [12]. The NSC EV marker profile (Fig. 1D) indicated consistent presence of integrins, including integrin beta-1 (CD29) and integrin alpha 2b (CD41b). Integrin beta-1 is known to mediate cell-to-cell and cell-to-matrix interactions, and regulate cell migration [34, 35]. Similarly, integrin alpha-2b is a receptor known to bind a variety of ligands leading to rapid platlet aggregation as well as positive regulation of leukocyte migration and megakaryocyte differentiation [36, 37]. In addition, blockade of integrin alpha-2b (CD41) increases ICH incidence and mortality after transient MCAO in a dose-dependent manner [38]. By altering the processes of coagulation and vascular function, IV administered NSC EVs may protect the integrity of the blood brain barrier through inherent intercellular signaling components. While the exact molecular mechanism of action is currently unknown, whether dependent on one or multiple EV components or direct action at the systemic level or on the brain directly, this data, in addition to our published rodent study, supports that NSC EVs are biologically active and elicit a positive neuroprotective response in vivo in both rodent and large animal preclinical stroke models [15].

A frequently used predictive indicator of patient prognosis is acute lesion volume due to the high correlation between neurological deficits and long-term functional

outcomes [39-42]. Although multiple MSC EV related rodent models of stroke have observed improvements in tissue and functional recovery, the extent of neural protection seen with NSC EV treatment is unprecedented. Previous rodent stroke studies assessing the efficacy of MSC EVs showed no changes in lesion volume [12, 13, 27, 28]. In comparison, our recently published data indicated a ~35% reduction in lesion volume in the mouse TE-stroke model. Comparatively, our data in the porcine model possessed a significant 44% decrease in lesion volume at 1-day post-MCAO, suggesting NSC EVs are potentially more protective and thus more therapeutically relevant than MSC EVs.

Restoring motor function in stroke patients is critical for improvement in quality of life and is a robust measure of therapeutic potential [43-47]. Most stroke patients exhibit hemiparesis with correlative asymmetries, decreased velocity, stride length, and other spatiotemporal parameters, therefore it was vital to determine whether these cellular benefits resulted in functional benefits at the organismal level [48, 49]. To date, no exosome efficacy study has performed a comprehensive assessment of changes in gait function post-stroke. Previous studies have relied on gross measurements (foot fault tests, rotarod), which do not account for fine motor changes in gait as do relative pressure, swing percent, and stride length [11, 12]. In this study, we found significant changes and decreased recovery time in these and other translational parameters that are critical readouts for human patients. The pig is also likely a more representative model of human gait changes post-stroke when compared to rodents, despite being a quadruped, as weight (pigs in this study were between 72 and 104 kg), limb, and body length are more comparable to humans and are more similarly affected by biomechanical forces generated during normal movement.

In this study, we have demonstrated NSC EVs are a potent biological treatment that positively impact both molecular and functional outcomes post-stroke, while abiding by STEP and STAIR committee recommendations for rigorously developing and testing therapeutics. NSC EVs in our porcine ischemic stroke model exhibited a multifactorial effect leading to decreased lesion volume, hemispheric swelling, and ICH, while also promoting diffusivity, WM integrity, and functional performance in a large animal model with similar cerebral architecture and WM composition to humans. As an effective treatment in both rodent and porcine stroke models, NSC EVs possess inherent biological characteristics suitable for translation into human stroke therapeutics.

Supplemental

Materials and Methods

Supplemental Table 4.1. Physiological Data

Supplemental Table 4.2. Death Summary

Supplemental Figure 4.1. Kaplan Meyer survival curve

Supplemental Figure 4.2. Representative images of ICH 1-day post-MCAO

Supplemental Figure 4.3. 1 and 84-day post-MCAO lesion volumes

Supplemental Movie S1. EV visualization by SLIM

Acknowledgments

The authors would like to thank Simon R. Platt, DVM, who performed the pig permanent occlusion surgeries, as well as Caroline Jackson, Justin Sharma, Austin Passaro, and Viviana Martinez who were involved with various aspects of the EV manufacturing process, pig gait/behavioral testing, and figure preparation. We would also like to thank Tracey Stice for project management guidance. We would also like to thank Julie Nelson at the UGA CTEGD Flow Cytometry Core and Phi Optics for use of the SLIM system.

Funding

This work was supported by ArunA Biomedical, Inc., NINDS grant R43NS103596, NINDS grant R01NS093314, Science and Technology Center Emergent Behaviors of Integrated Cellular Systems (EBICS) Grant No. CBET-0939511, and the Georgia Research Alliance.

Disclosures

R.L.W. and S.L.S. have submitted a patent filing on the NSC EVs, and this technology is licensed from the UGA Research Foundation by ArunA Biomedical, Inc. All authors affiliated with ArunA Biomedical, Inc. own equity in the company.

References

1. Cheng NT, Kim AS. Intravenous thrombolysis for acute ischemic stroke within 3 hours versus between 3 and 4.5 hours of symptom onset. *The Neurohospitalist*. 2015;5:101-109
2. Boyle K, Joundi RA, Aviv RI. An historical and contemporary review of endovascular therapy for acute ischemic stroke. *Neurovascular Imaging*. 2017;3:1
3. Stem Cell Therapies as an Emerging Paradigm in Stroke P. Stem cell therapies as an emerging paradigm in stroke (steps): Bridging basic and clinical science for cellular and neurogenic factor therapy in treating stroke. *Stroke*. 2009;40:510-515
4. Savitz SI, Chopp M, Deans R, Carmichael T, Phinney D, Wechsler L, et al. Stem cell therapy as an emerging paradigm for stroke (steps) ii. *Stroke*. 2011;42:825-829
5. Fisher M, Feuerstein G, Howells DW, Hurn PD, Kent TA, Savitz SI, et al. Update of the stroke therapy academic industry roundtable preclinical recommendations. *Stroke*. 2009;40:2244-2250
6. Saver JL, Albers GW, Dunn B, Johnston KC, Fisher M, Consortium SV. Stroke therapy academic industry roundtable (stair) recommendations for extended window acute stroke therapy trials. *Stroke*. 2009;40:2594-2600
7. Lener T, Gimona M, Aigner L, Börger V, Buzas E, Camussi G, et al. Applying extracellular vesicles based therapeutics in clinical trials – an isev position paper. *Journal of Extracellular Vesicles*. 2015;4:30087
8. Basso M, Bonetto V. Extracellular vesicles and a novel form of communication in the brain. *Frontiers in Neuroscience*. 2016;10:127

9. Raposo G, Stoorvogel W. Extracellular vesicles: Exosomes, microvesicles, and friends. *The Journal of Cell Biology*. 2013;200:373

10. György B, Hung ME, Breakefield XO, Leonard JN. Therapeutic applications of extracellular vesicles: Clinical promise and open questions. *Annual review of pharmacology and toxicology*. 2015;55:439-464

11. Doeppner TR, Herz J, Gorgens A, Schlechter J, Ludwig AK, Radtke S, et al. Extracellular vesicles improve post-stroke neuroregeneration and prevent postischemic immunosuppression. *Stem Cells Transl Med*. 2015;4:1131-1143

12. Xin H, Li Y, Cui Y, Yang JJ, Zhang ZG, Chopp M. Systemic administration of exosomes released from mesenchymal stromal cells promote functional recovery and neurovascular plasticity after stroke in rats. *J Cereb Blood Flow Metab*. 2013;33:1711-1715

13. Zhang Y, Chopp M, Zhang ZG, Katakowski M, Xin H, Qu C, et al. Systemic administration of cell-free exosomes generated by human bone marrow derived mesenchymal stem cells cultured under 2d and 3d conditions improves functional recovery in rats after traumatic brain injury. *Neurochem Int*. 2016

14. Wiklander OPB, Nordin JZ, O'Loughlin A, Gustafsson Y, Corso G, Mäger I, et al. Extracellular vesicle in vivo biodistribution is determined by cell source, route of administration and targeting. *J extracell vesicles*. 2015.

15. Webb RL, Kaiser EE, Scoville SL, Thompson TA, Fatima S, Pandya C, et al. Human neural stem cell extracellular vesicles improve tissue and functional recovery in the murine thromboembolic stroke model. *Translational Stroke Research*. 2017

16. Platt SR, Holmes SP, Howerth EW, Duberstein KJJ, Dove CR, Kinder HA, et al. Development and characterization of a yucatan miniature biomedical pig permanent middle cerebral artery occlusion stroke model. *Experimental & Translational Stroke Medicine*. 2014;6:5

17. Duberstein KJ, Platt SR, Holmes SP, Dove CR, Howerth EW, Kent M, et al. Gait analysis in a pre- and post-ischemic stroke biomedical pig model. *Physiology & Behavior*. 2014;125:8-16

18. Lind NM, Moustgaard A, Jelsing J, Vajta G, Cumming P, Hansen AK. The use of pigs in neuroscience: Modeling brain disorders. *Neurosci Biobehav Rev*. 2007;31:728-751

19. Nakamura M, Imai H, Konno K, Kubota C, Seki K, Puentes S, et al. Experimental investigation of encephalomyosynangiosis using gyrencephalic brain of the miniature pig: Histopathological evaluation of dynamic reconstruction of vessels for functional anastomosis. Laboratory investigation. *J Neurosurg Pediatr*. 2009;3:488-495

20. Kuluz JW, Prado R, He D, Zhao W, Dietrich WD, Watson B. New pediatric model of ischemic stroke in infant piglets by photothrombosis: Acute changes in cerebral blood flow, microvasculature, and early histopathology. *Stroke*. 2007;38:1932-1937

21. Tanaka Y, Imai H, Konno K, Miyagishima T, Kubota C, Puentes S, et al. Experimental model of lacunar infarction in the gyrencephalic brain of the miniature pig: Neurological assessment and histological, immunohistochemical,

and physiological evaluation of dynamic corticospinal tract deformation. *Stroke*. 2008;39:205-212

22. Baltan S, Besancon EF, Mbow B, Ye Z, Hamner MA, Ransom BR. White matter vulnerability to ischemic injury increases with age because of enhanced excitotoxicity. *The Journal of neuroscience : the official journal of the Society for Neuroscience*. 2008;28:1479-1489

23. Baker EW, Platt SR, Lau VW, Grace HE, Holmes SP, Wang L, et al. Induced pluripotent stem cell-derived neural stem cell therapy enhances recovery in an ischemic stroke pig model. *Scientific Reports*. 2017;7:10075

24. Mir M, Kim T, Majumder A, Xiang M, Wang R, Liu SC, et al. Label-free characterization of emerging human neuronal networks. 2014;4:4434

25. Fisher M, Stroke Therapy Academic Industry R. Recommendations for advancing development of acute stroke therapies: Stroke therapy academic industry roundtable 3. *Stroke*. 2003;34:1539-1546

26. Albers GW, Goldstein LB, Hess DC, Wechsler LR, Furie KL, Gorelick PB, et al. Stroke treatment academic industry roundtable (stair) recommendations for maximizing the use of intravenous thrombolytics and expanding treatment options with intra-arterial and neuroprotective therapies. *Stroke*. 2011;42:2645-2650

27. Otero-Ortega L, Laso-Garcia F, Gomez-de Frutos MD, Rodriguez-Frutos B, Pascual-Guerra J, Fuentes B, et al. White matter repair after extracellular vesicles administration in an experimental animal model of subcortical stroke. *Sci Rep*. 2017;7:44433

28. Zhang Y, Chopp M, Meng Y, Katakowski M, Xin H, Mahmood A, et al. Effect of exosomes derived from multipluripotent mesenchymal stromal cells on functional recovery and neurovascular plasticity in rats after traumatic brain injury. *Journal of neurosurgery*. 2015;122:856-867

29. Lovblad KO, Baird AE, Schlaug G, Benfield A, Siewert B, Voetsch B, et al. Ischemic lesion volumes in acute stroke by diffusion-weighted magnetic resonance imaging correlate with clinical outcome. *Ann Neurol*. 1997;42:164-170

30. Schellinger PD, Jansen O, Fiebach JB, Hacke W, Sartor K. A standardized mri stroke protocol: Comparison with ct in hyperacute intracerebral hemorrhage. *Stroke*. 1999;30:765-768

31. Ahmad AS, Satriotomo I, Fazal J, Nadeau SE, Dore S. Considerations for the optimization of induced white matter injury preclinical models. *Front Neurol*. 2015;6:172

32. Jokinen H, Gouw AA, Madureira S, Ylikoski R, van Straaten EC, van der Flier WM, et al. Incident lacunes influence cognitive decline: The ladis study. *Neurology*. 2011;76:1872-1878

33. Srikanth V, Beare R, Blizzard L, Phan T, Stapleton J, Chen J, et al. Cerebral white matter lesions, gait, and the risk of incident falls: A prospective population-based study. *Stroke*. 2009;40:175-180

34. Li J, Ballif BA, Powelka AM, Dai J, Gygi SP, Hsu VW. Phosphorylation of acap1 by akt regulates the stimulation-dependent recycling of integrin β1 to control cell migration. *Developmental Cell*. 2005;9:663-673

35. Bax DV, Bernard SE, Lomas A, Morgan A, Humphries J, Shuttleworth CA, et al. Cell adhesion to fibrillin-1 molecules and microfibrils is mediated by α5β1 and αvβ3 integrins. *Journal of Biological Chemistry*. 2003;278:34605-34616

36. Ma YQ, Qin J, Plow EF. Platelet integrin αiibβ3: Activation mechanisms. *Journal of Thrombosis and Haemostasis*. 2007;5:1345-1352

37. Webb DJ, Parsons JT, Horwitz AF. Adhesion assembly, disassembly and turnover in migrating cells – over and over and over again. *Nature Cell Biology*. 2002;4:E97

38. Kleinschnitz C, Pozgajova M, Pham M, Bendszus M, Nieswandt B, Stoll G. Targeting platelets in acute experimental stroke: Impact of glycoprotein ib, vi, and iib/iiia blockade on infarct size, functional outcome, and intracranial bleeding. *Circulation*. 2007;115:2323-2330

39. Borsody M, Warner Gargano J, Reeves M, Jacobs B, Group MI-SS. Infarction involving the insula and risk of mortality after stroke. *Cerebrovasc Dis*. 2009;27:564-571

40. Huisa BN, Neil WP, Schrader R, Maya M, Pereira B, Bruce NT, et al. Clinical use of computed tomographic perfusion for the diagnosis and prediction of lesion growth in acute ischemic stroke. *J Stroke Cerebrovasc Dis*. 2014;23:114-122

41. Schiemanck SK, Kwakkel G, Post MW, Prevo AJ. Predictive value of ischemic lesion volume assessed with magnetic resonance imaging for neurological deficits and functional outcome poststroke: A critical review of the literature. *Neurorehabil Neural Repair*. 2006;20:492-502

42. Tong DC, Yenari MA, Albers GW, O'Brien M, Marks MP, Moseley ME. Correlation of perfusion- and diffusion-weighted mri with nihss score in acute (<6.5 hour) ischemic stroke. *Neurology*. 1998;50:864-870

43. Nascimento LR, de Oliveira CQ, Ada L, Michaelsen SM, Teixeira-Salmela LF. Walking training with cueing of cadence improves walking speed and stride length after stroke more than walking training alone: A systematic review. *J Physiother*. 2015;61:10-15

44. Hak L, Houdijk H, van der Wurff P, Prins MR, Beek PJ, van Dieen JH. Stride frequency and length adjustment in post-stroke individuals: Influence on the margins of stability. *J Rehabil Med*. 2015;47:126-132

45. Peterson CL, Hall AL, Kautz SA, Neptune RR. Pre-swing deficits in forward propulsion, swing initiation and power generation by individual muscles during hemiparetic walking. *J Biomech*. 2010;43:2348-2355

46. Nolan KJ, Yarossi M, McLaughlin P. Changes in center of pressure displacement with the use of a foot drop stimulator in individuals with stroke. *Clin Biomech (Bristol, Avon)*. 2015;30:755-761

47. De Nunzio A, Zucchella C, Spicciato F, Tortola P, Vecchione C, Pierelli F, et al. Biofeedback rehabilitation of posture and weightbearing distribution in stroke: A center of foot pressure analysis. *Funct Neurol*. 2014;29:127-134

48. Ng YS, Stein J, Ning M, Black-Schaffer RM. Comparison of clinical characteristics and functional outcomes of ischemic stroke in different vascular territories. *Stroke*. 2007;38:2309-2314

49. Patterson KK, Parafianowicz I, Danells CJ, Closson V, Verrier MC, Staines WR, et al. Gait asymmetry in community-ambulating stroke survivors. *Arch Phys Med Rehabil*. 2008;89:304-310

Figure 4.1: NSC EV manufacture produces biologically active, consistent vesicles. DiI labeled vesicles (**B**) were added into the culture medium of human umbilical MSCs (**A**) and imaged over 24 hours (**A-C**). Vesicles are taken up by the cells (**C**) and can be seen being actively transported within the cell. Flow cytometry is routinely used for batch analysis of NSC EVs (using the commercially available MACSPlex kit) and indicates NSC EVs have a consistent marker profile (**D**).

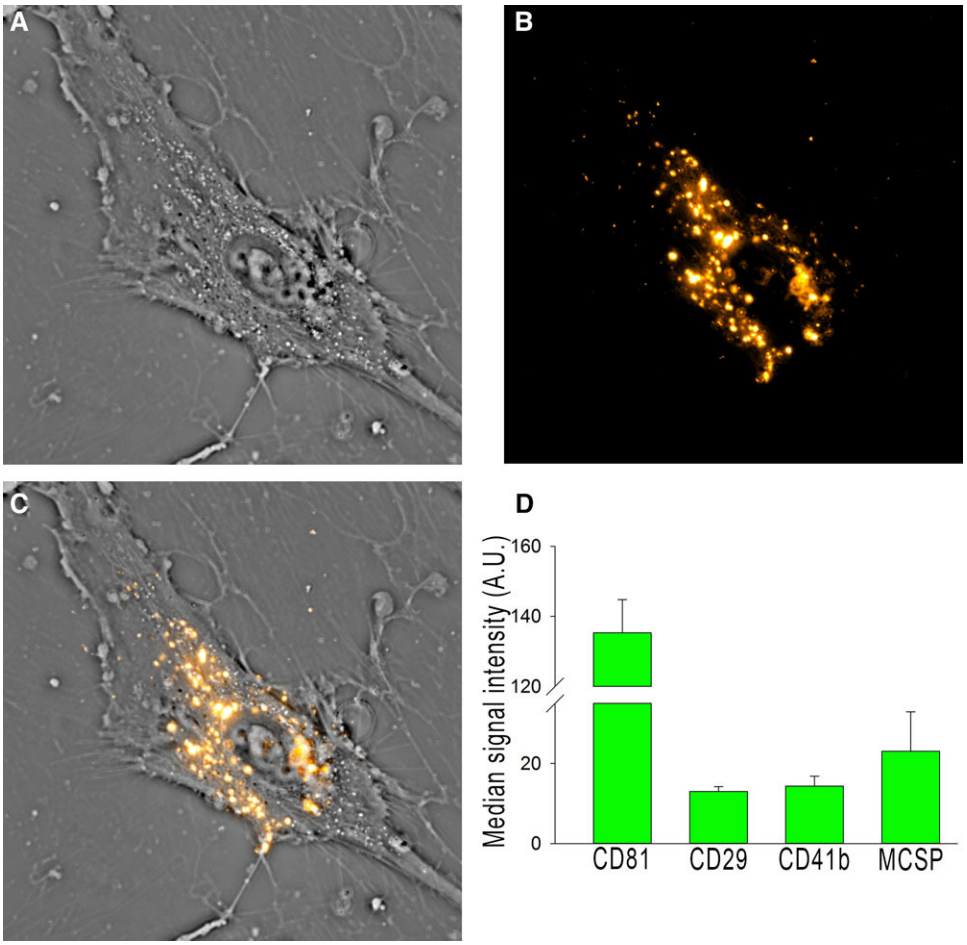
A
B
C
D
Median signal intensity (A.U.)
160
140
120
20
0
CD81
CD29
CD41b
MCSP

Figure 4.2: NSC EV treatment decreases intracerebral hemorrhage, lesion volume, and hemispheric swelling 1-day post-MCAO. T2W and DWI sequences revealed territorial hyperintense lesions characteristic of an edematous injury (**A**, white arrows). Hypointense lesions observed on corresponding ADC maps confirmed areas of restricted diffusion indicative of cytotoxic edema (**A**, white arrow). These resulting hallmarks demonstrated permanent cauterization of the ventral aspect of the MCA resulted in bona fide, repeatable ischemic stroke in all pigs. NSC EV treated pigs exhibited a reduced incidence of ICH (**B**, white arrows). NSC EV treated pigs also demonstrated a significant ($p<0.05$) decrease in LVc when compared to control pigs at 1 day post-MCAO (6.0±1.4 vs. 10.7±1.4 cm^3 respectively; **C**) and a significantly ($p<0.01$) lower percent increase in hemisphere volume resulting in a less pronounced midline shift relative to control pigs at 1 day post-MCAO (113.77±2.571 vs. 126.83±3.41 % respectively; **D**). * indicates significant difference between treatment groups.

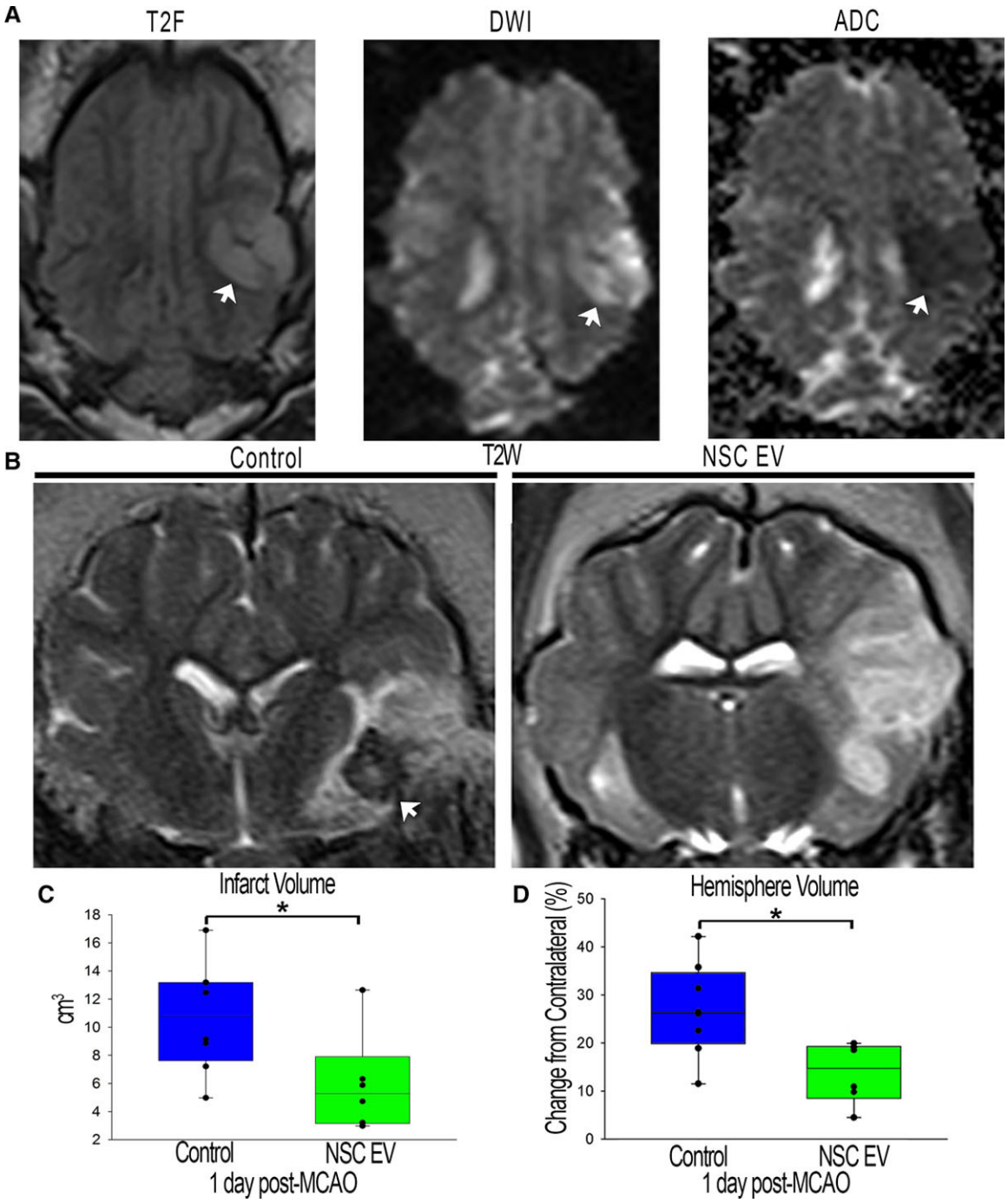
A
T2F
DWI
ADC
B
Control
T2W
NSC EV
C
Infarct Volume
*
cm3
18
16
14
12
10
8
6
4
2
Control
NSC EV
1 day post-MCAO
D
Hemisphere Volume
*
Change from Contralateral (%)
50
40
30
20
10
0
Control
NSC EV
1 day post-MCAO

Figure 4.3: NSC EV treatment promotes increased diffusivity of ischemic lesions and preserved white matter integrity of the corpus callosum. ADC maps derived from DWI sequences revealed signal void indicative of restricted diffusion and cytotoxic edema. NSC EV treated pigs exhibited a significantly ($p<0.01$) lower percent decrease in ADC values relative to control pigs 1-day post-MCAO (-18.72±2.55 vs. -32.35±1.54 % respectively; **A, C**, white arrows) suggesting improved diffusivity in ischemic lesions. Color-coded FA maps depicted territorial changes in the corpus callosum 84 days post-MCAO. NSC EV treated pigs exhibited a significantly ($p<0.01$) lower percent decrease in FA values (-13.94±3.18 vs. -43.29±6.65 % respectively; **B, D**, white arrows) when compared to control pigs, suggesting preserved white matter integrity. * indicates significant difference between treatment groups.

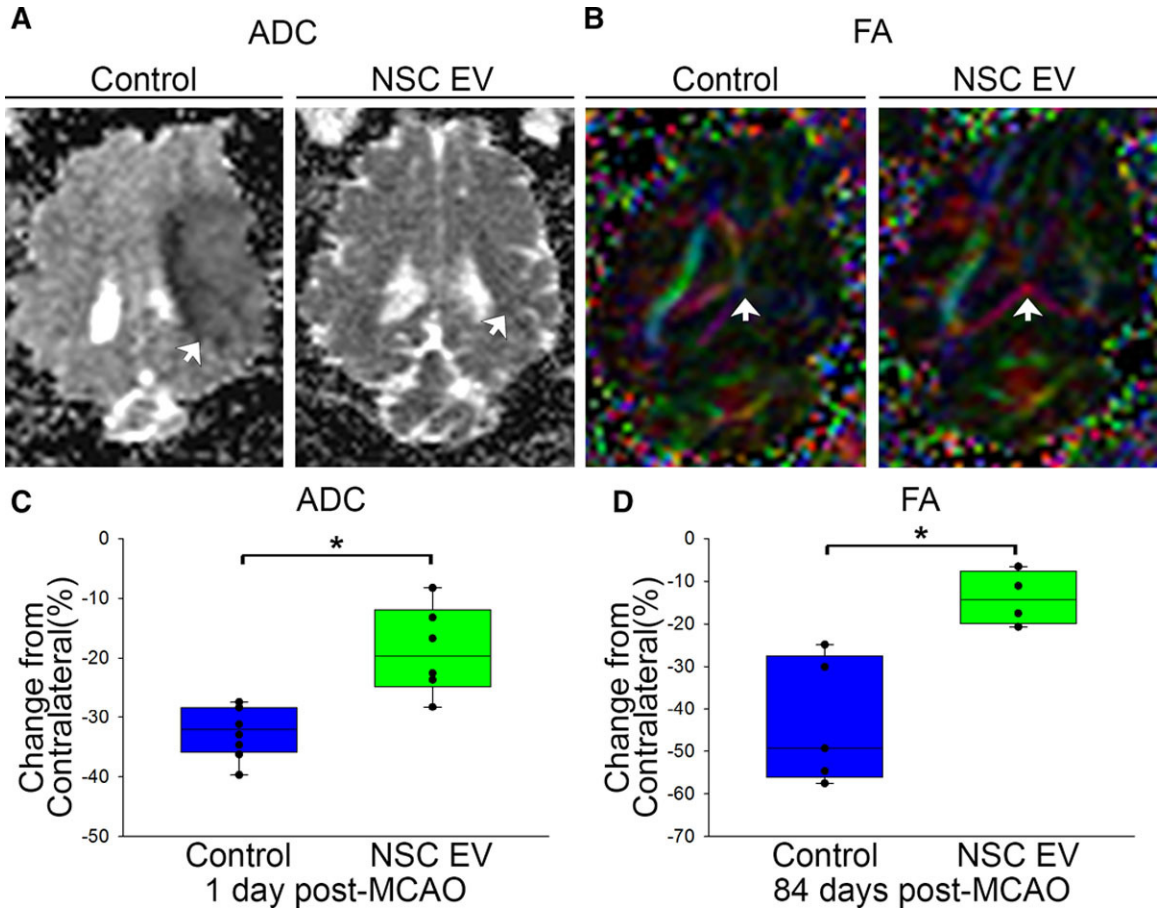
A
ADC
Control
NSC EV
B
FA
Control
NSC EV
C
ADC
Change from Contralateral(%)
0
-10
-20
-30
-40
-50
*
Control
NSC EV
1 day post-MCAO
D
FA
Change from Contralateral(%)
0
-10
-20
-30
-40
-50
-60
-70
*
Control
NSC EV
84 days post-MCAO

Figure 4.4: NSC EV treatment results in increased motor activity and improved recovery of spatiotemporal gait parameters. Ethovision™ XT tracking software was utilized during open field testing to automatically assess differences in distance traveled between treatment groups; representative 10-minute movement tracings shown for control (**A**, blue) and NSC EV treated (**A**, green) pigs. Control pigs experienced a significant decrease in distance traveled at 7 days post-MCAO while treated pigs did not. Both groups increased distance traveled over 28 days, however treated pigs traveled significantly further than their pre-MCAO distance while control pigs did not. At 1-day post-MCAO, NSC EV treated and control pigs exhibited significant decreases in temporal gait parameters including velocity, cadence, and swing percent pigs (**B**). By 7 days post-MCAO, NSC EV treated pigs recovered these parameters while control pigs did not recover until 28 days. At 28 days the NSC EV treated pigs performed significantly better in velocity, cadence, and swing percent than control pigs. Differences in spatial gait parameters were also noted between NSC EV treated and control pigs in terms of stride length, hoof print area, and relative pressure (**C**). By 7 days post-MCAO, NSC EV treated pigs had recovered from deficits in stride length, hoof print area, and relative pressure, whereas control pigs remained impaired. In addition, NSC EV treated pigs performed significantly better in terms of stride length when compared to control pigs at the same time point. *, # indicates significant ($p<0.01$) difference between pre- and post-MCAO timepoints. a indicates significant ($p<0.01$) difference between treatment groups.

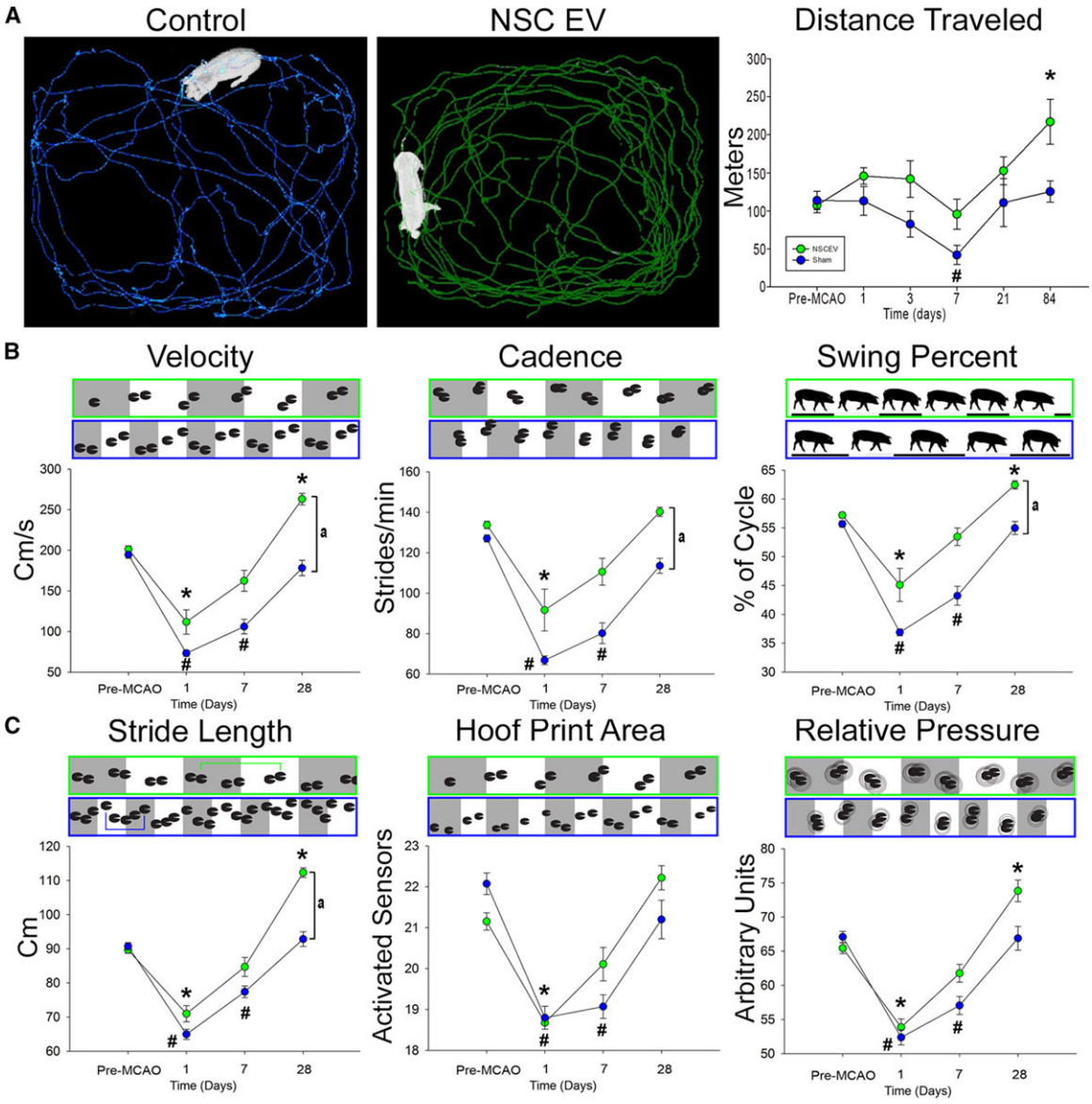
A
Control
NSC EV
Distance Traveled
Meters
NSCEV
Sham
Pre-MCAO
1
3
7
21
84
Time (days)
B
Velocity
Cadence
Swing Percent
Cm/s
Strides/min
% of Cycle
Pre-MCAO
1
7
28
Time (Days)
C
Stride Length
Hoof Print Area
Relative Pressure
Cm
Activated Sensors
Arbitrary Units

Supplemental Material

Materials and Methods

Animals and housing

All work performed in this study was approved by the University of Georgia Institutional Animal Care and Use Committee guidelines. Sexually mature, castrated male Landrace pigs, 5-6 months old and 72-104 kg were obtained from the biosecure University of Georgia Swine farm, original seed stock was from one commercial entity. Young, healthy male pigs were used in accordance with the STAIR guidelines that suggests initial therapeutic evaluations should be performed with young, healthy male animals, and further studies should be performed in females, aged animals, and animals with co-morbidities such as hypertension and diabetes [1]. Pigs were individually housed at a room temperature of 27ºC with a 12-hour light/dark cycle. All pigs were fed standard grower diets ad libitum prior to stroke induction, and only feed restricted prior to anesthetic events.

Middle cerebral artery occlusion (MCAO) surgical procedure

MCAO was induced as previously described with minor adjustments [2]. The day of surgery pigs were administered antibiotics (Ceftiofur sodium (Naxcel®; 4 mg/kg IM) and non-steroidal anti-inflammatory Flunixin Meglumine (Banamine-S; 2.2mg/kg IM). Pre-induction analgesia and sedation was achieved using xylazine (7 mg/kg IM), butorphanol (0.3 mg/kg IM) and midazolam (0.3 mg/kg IM). Anesthesia was induced with IV propofol to effect, and prophylactic lidocaine (0.5 to 1.0 mL of 2% lidocaine) was administered topically to the laryngeal folds to facilitate intubation. Anesthesia was maintained with 1.5% inhalational isoflurane (Abbott Laboratories) in oxygen.

As previously described, neural injury was induced by making a curvilinear skin incision extending superiorly from the right orbit to an area rostral to the auricle. A portion of zygomatic arch was resected with the rostral aspect extended from the insertion point of the orbital ligament caudally 3-4 cm. The temporal fascia and muscle were elevated and a craniectomy was generated exposing the local dura mater. The distal middle cerebral artery (MCA) and associated branches were permanently occluded using bipolar cautery forceps thus resulting in ischemic infarction spanning the most caudal aspect of the frontal lobe, significant areas of the temporal lobe, and portions of the parietal and occipital lobes. The exposed brain was covered with a sterile biograft made of porcine small intestine submucosa (MatriStem, ACell) and the temporalis muscle was routinely reattached along the temporalis line and the skin was routinely reapposed.

Anesthesia was discontinued and pigs were returned to their pens upon extubation and monitored every 4 hours for the next 24 hours. Heart rate, respiratory rate, and temperature were recorded at each time point. Banamine (2.2 mg/kg) was administered IM for postoperative pain, acute inflammation, and fever management every 12 hours for the first 24 hours, and every 24 hours for 3 days post-MCAO. Naxcel (4 mg/kg) was administered IM as an antibiotic every 24 hours for 3 days post-MCAO.

Cell culture, EV enrichment, and characterization

H9 cells were differentiated into NSCs using standard operating procedures previously published [3-5]. Media was harvested off NSC cultures when cells reached ~80% confluence. Media was filtered through a 0.22 μm filter and further enriched by ultrafiltration using a 100 kDa regenerated cellulose Amicon or Centricon ultra-centrifugal filter units or the Amicon stirred cell system, and washed twice with PBS**.** Enriched EVs

were stored in single use aliquots 52 ml for pigs (2.7 x 10^{10} ± 10% vesicles/kg) and stored at -20°C. Labeled EVs were incubated with 10 uM DiI for 30 minutes before washes. DiI labeled EVs were applied to differentiated NSCs or MSCs and visualized by SLIM as previously described.

NSC EV and PBS +/+ administration

A total of 50 mLs of either PBS with calcium and magnesium (PBS+/+) or NSC EVs suspended in PBS +/+ IV access were administered via peripheral ear vein. PBS +/+ or NSC EVs treatment was administered 2, 14, and 24 hours post-MCAO.

MRI acquisition and analysis

MRI was performed 1 and 84 days post-MCAO on a Siemens 3.0 Tesla Magnetom Avanto MRI system. Utilizing the previously described surgical anesthesia protocol, MRI of the cranium was performed using a 12-channel head coil, 25 cm in diameter with the pig positioned in supine recumbency. Standard multiplanar magnetic resonance (MR) brain imaging sequences were acquired including T2FLAIR, T2W, DWI, and DTI. T2FLAIR, T2W, DWI, and ADC maps were analyzed using Osirix software whereas DTI and computed FA values were analyzed using ImageJ software. Cytotoxic edema consistent with ischemic stroke was confirmed at 1-day post-MCAO by comparing corresponding hyperintense regions in T2FLAIR and DWI sequences, and hypointense regions in ADC maps. To control for the space-occupying effect of brain edema, hemisphere volumes were calculated utilizing T2W sequences while ischemic lesion volumes were calculated via ADC maps as previously described by Gerriets et al [6]. Corrected lesion volumes were calculated according to the following formula modified from Loubinoux et al. where LVc

and LVu indicate corrected and uncorrected lesion volume, respectively, and HVc and HVi indicate volume of the contralateral and ipsilateral hemisphere, respectively [7].

$$LV^c = HV_C+HV_i-(HV_C+HV_i-LV^u)\cdot\frac{HV_C+HV_i}{2HV_C}$$

DWI sequences were utilized to identify hypointense regions of interest (ROI) in the ipsilateral hemisphere and directly compared to identical ROIs in the contralateral hemisphere at each coronal plane. Average ADC values were calculated for each coronal slice, and changes in mean ADC value of the ipsilateral hemisphere were expressed as a percentage change relative to the contralateral hemisphere. DTI was utilized to generate FA values in the corpus callosum and was expressed as a percent change in the ipsilateral hemisphere relative to the contralateral hemisphere.

Behavior assessment and analysis

Open field testing occurred pre-MCAO, 1, 7, and 21 days post-MCAO. Pigs were permitted to enter the open field arena via two starting gates according to a predetermined pseudorandomized pattern. Pigs were recorded utilizing Ethovision™ XT tracking software (Noldus) while exploring the novel 14ft x 16ft open field arena for 10 minutes. All surfaces of the open field arena were cleaned thoroughly with ethanol between pigs.

Gait data was collected pre-MCAO, 1, 7, and 28 days post-MCAO. Analysis was performed using an automated computer software program (GaitFour 4.9x9i, GaitRite, New Jersey) to objectively evaluate multiple spatiotemporal gait parameters [8]. Predefined inclusion criteria included a consistent gait with less than a 10% velocity variation, a minimum of 12 consecutive footfalls or 3 gait cycles, and no external distractions within each individual trial. The surfaces of the gait track were cleaned thoroughly with ethanol between pigs.

Statistical analysis

All quantitative data was analyzed with SAS version 9.3 (Cary, NC) and statistical significances between groups were determined by one-way analysis of variance and post-hoc Tukey-Kramer Pair-Wise comparisons. Treatments where p-values were ≤ 0.05 were considered significantly different.

Supplemental references

1. Lapchak PA, Zhang JH, Noble-Haeusslein LJ. Rigor guidelines: Escalating stair and steps for effective translational research. *Translational stroke research*. 2013;4:279-285
2. Platt SR, Holmes SP, Howerth EW, Duberstein KJJ, Dove CR, Kinder HA, et al. Development and characterization of a yucatan miniature biomedical pig permanent middle cerebral artery occlusion stroke model. *Experimental & Translational Stroke Medicine*. 2014;6:5
3. Boyd NL, Robbins KR, Dhara SK, West FD, Stice SL. Human embryonic stem cell–derived mesoderm-like epithelium transitions to mesenchymal progenitor cells. *Tissue Engineering. Part A*. 2009;15:1897-1907
4. Dhara SK, Hasneen K, Machacek DW, Boyd NL, Rao RR, Stice SL. Human neural progenitor cells derived from embryonic stem cells in feeder-free cultures. *Differentiation*. 2008;76:454-464
5. Shin S, Mitalipova M, Noggle S, Tibbitts D, Venable A, Rao R, et al. Long-term proliferation of human embryonic stem cell–derived neuroepithelial cells using defined adherent culture conditions. *STEM CELLS*. 2006;24:125-138
6. Gerriets T, Stolz E, Walberer M, Muller C, Kluge A, Bachmann A, et al. Noninvasive quantification of brain edema and the space-occupying effect in rat stroke models using magnetic resonance imaging. *Stroke*. 2004;35:566-571
7. Loubinoux I, Volk A, Borredon J, Guirimand S, Tiffon B, Seylaz J, et al. Spreading of vasogenic edema and cytotoxic edema assessed by quantitative

diffusion and t2 magnetic resonance imaging. *Stroke*. 1997;28:419-426; discussion 426-417

8. Duberstein KJ, Platt SR, Holmes SP, Dove CR, Howerth EW, Kent M, et al. Gait analysis in a pre- and post-ischemic stroke biomedical pig model. *Physiol Behav*. 2014;125

Supplemental Table 4.1: Physiological data. There were no statistical differences in any physiological parameters between groups.

	Control			NSC EV		
	HR (bpm)	Temp (°F)	RR (bpm)	HR (bpm)	Temp (°F)	RR (bpm)
Average 0 hours	73.78	97.90	25.33	65.33	96.92	28.00
Standard Deviation 0 hours	36.99	1.09	8.94	17.28	1.65	6.69
Average 13 hours	100.44	100.68	36.78	92.67	100.68	35.33
Standard Deviation 13 hours	26.64	1.85	33.00	35.09	1.50	14.18

Supplement Table 4.2: Death summary.

Pig #	**Treatment Group**	**Survival Post-MCAO**	**Cause of Death**
4	Control	1 day	Seizure
5	NSC EV treated	7 days	Non-stroke related post-operative injury; broken leg
6	Control	3 days	Seizure
8	Control	0 days	Non-stroke related post-operative complication
11	NSC EV treated	21 days	Idiopathic; possibly endocarditis
13	Control	2 days	Seizure

Supplemental Figure 4.1: NSC EVs do not alter post-stroke survival rate. Although a greater percentage of treated pigs survived to the endpoint, there were not statistically significant differences in survival rate between groups.

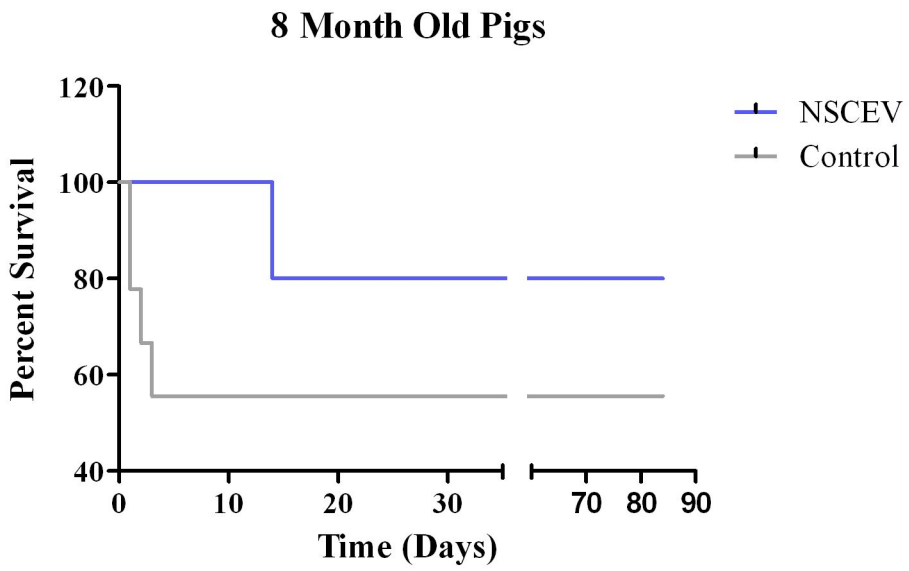
8 Month Old Pigs
Percent Survival
120
100
80
60
40
0
10
20
30
70
80
90
Time (Days)
NSCEV
Control

Supplemental Figure 4.2: NSC EVs resulted in decreased ICH. T2W sequences revealed characteristic hyperintense lesions indicative of acute ischemic stroke. Control pigs exhibited significantly ($p=0.0100$) greater hemorrhage indicated by hypointense areas in the infarct region relative to NSC EV treated pigs at 1-day post-MCAO.

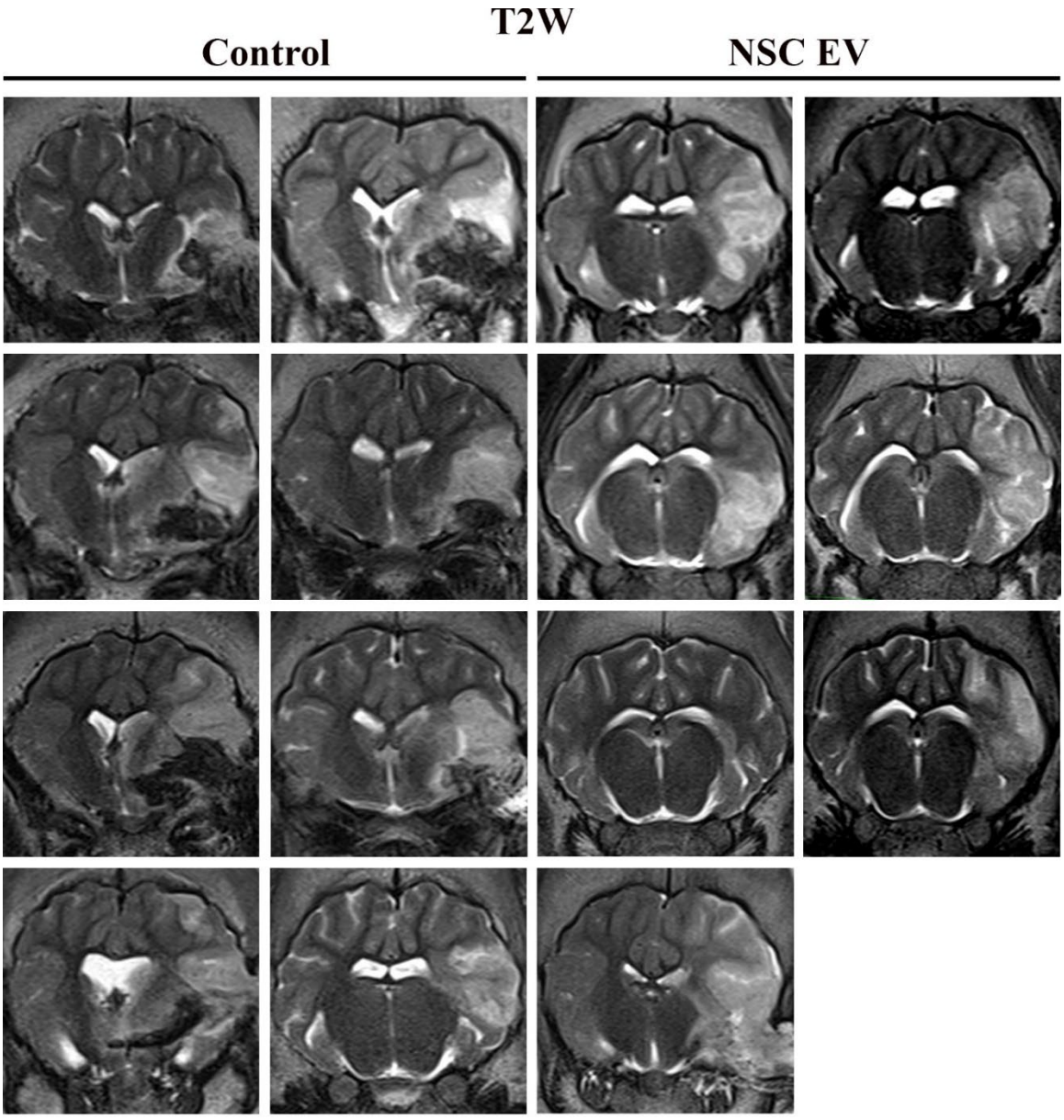
T2W
Control
NSC EV

Supplemental Figure 4.3: NSC EVs do not alter lesion volume and brain atrophy at 84 days post-MCAO. There were no significant differences in lesion volume or brain atrophy between groups 84 days post-MCAO.

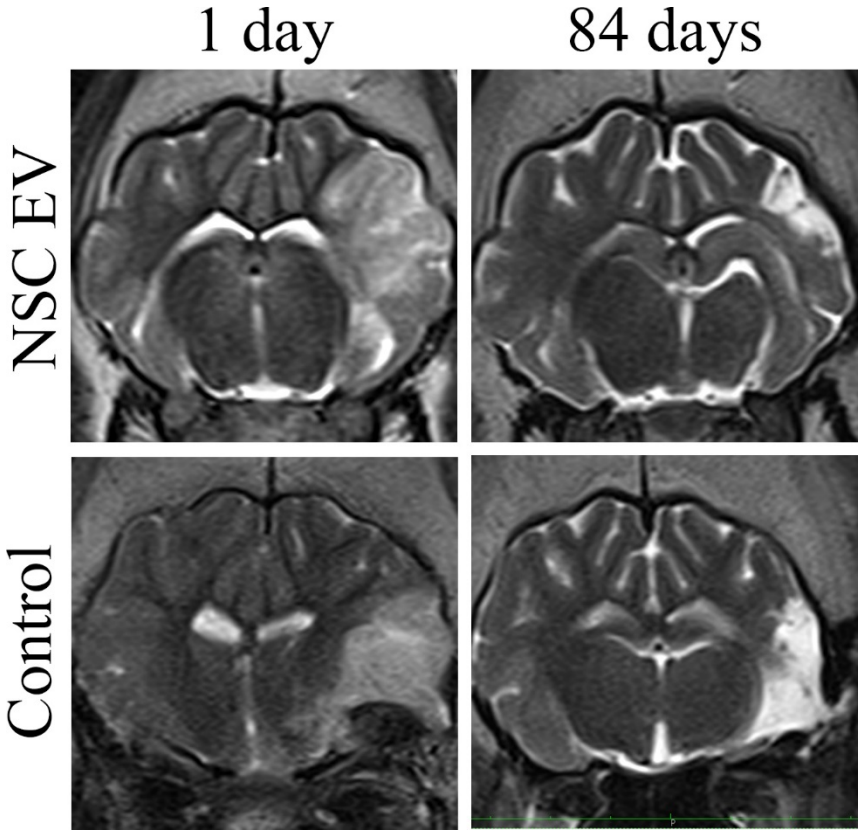
1 day
84 days
NSC EV
Control

CHAPTER 5

INTRACISTERNAL ADMINISTRATION OF TANSHINONE IIA-LOADED NANOPARTICLES LEADS TO REDUCED TISSUE INJURY AND FUNCTIONAL DEFICITS IN A PORCINE MODEL OF ISCHEMIC STROKE [1]

---

[1]Kaiser, E.E. †, Waters E.S. †, Yang, X. †, Fagan, M.M., Scheulin K.M., Jeon J.H., Shin S.K., Kinder H.A., Kumar, A., Platt S.R., Duberstein K.J., Park H.J., Xie, J., and West, F.D. Submitted to *Theranostics*, 08/30/19.

† these authors equally contributed to this work

Abstract

Rationale

Although the absolute number of new stroke patients has increased every year, few Food and Drug Administration approved treatments are available to patients. Tanshinone-IIA (Tan IIA) is a promising potential therapeutic for ischemic stroke that has shown success in preclinical rodent studies, but led to inconsistent efficacy results in human patients. The physical properties of Tan IIA, including short half-life and low solubility, suggest that poly (lactic-*co*-glycolic acid) (PLGA) nanoparticle (NP) delivery may lead to improved and consistent therapeutic effects. The objective of this study was to develop Tan IIA-loaded nanoparticles (Tan IIA-NPs) and evaluate their therapeutic effects on cerebral pathological changes and consequent motor function deficits in a translational pig ischemic stroke model.

Methods

Tan IIA-NPs were synthesized through a nanoprecipitation method and assessed for NP characteristics, cytotoxicity (MTT assay), antioxidative (SOD assay), and anti-inflammatory (TNF-α and IFN-γ ELISA assays) properties in vitro. Ischemic stroke was induced by permanent middle cerebral artery occlusion in male Landrace pigs. At 1-hour post-stroke, Tan IIA-NPs or vehicle only was administered via intracisternal injection. Magnetic resonance imaging (MRI) was performed at 24 hours post-stroke to assess brain pathology and blood was collected pre-stroke, 4, 12, and 24 hours post-stroke to evaluate immune responses. Gait analysis was performed pre- and post-stroke to measure changes in spatiotemporal gait parameters.

Results

Tan IIA-NPs treated cells showed a reduction in SOD activity and TNF-α and IFN-γ inflammatory cytokines in in vitro assays demonstrating antioxidative and anti-inflammatory effects. MRI results demonstrated that ischemic stroke pigs treated with Tan IIA-NPs had reduced hemispheric swelling (7.85 vs. 16.83 %), midline shift (1.72 vs. 2.91 mm), and lesion volumes (9.54 vs. 12.01 cm^3). Treatment also lead to reduced change in diffusivity (-37.30 vs. -46.33 %), white matter damage (-19.66 vs. -30.11 %), and hemorrhage (0.84 vs. 2.90 cm^3) 24 hours post-stroke. Tan IIA-NPs also lead to a reduced percentage of circulating band neutrophils at 12 (7.75 vs. 14.00 %) and 24 (4.25 vs. 5.75 %) hours post-stroke suggesting a mitigated immune response. Spatiotemporal gait deficits including cadence, cycle time, step time, swing percent of cycle, and stride length, as well as changes in relative mean pressure were also less severe post-stroke in Tan IIA-NP treated pigs relative to control pigs.

Conclusion

The findings of this study demonstrate administration of Tan IIA-NPs in the acute phase post-stroke mitigates cerebral injury leading to less severe gait deficits in a translational pig ischemic stroke model. With stroke being the leading cause of functional disability in the United States, and gait deficits being a major component, these promising results suggest acute Tan IIA-NP administration may improve functional outcomes and the quality of life of many future stroke patients.

Introduction

The absolute number of new stroke patients has increased to an estimated 10.3 million people a year [1, 2]. Unfortunately, there are few Food and Drug Administration (FDA)-approved treatments for ischemic stroke with each presenting potential risks. Tissue plasminogen activator (tPA), for example, has a limited administration window with potentially deadly risk factors including intracerebral hemorrhage (ICH) [3-7]. The limited therapeutic time window results in relatively low administration rates (<5% patients) of tPA. There is a clear need for further investigation of novel stroke therapies and delivery approaches that lead to robust recovery. Therapeutic approaches that modulate key processes in the secondary injury cascade including inflammation and oxidative stress are promising neuroprotective options [8]. Tanshinone IIA (Tan IIA) is one such neuroprotectant that acts as a free-radical scavenger and has antioxidant and anti-inflammatory effects post-stroke [9, 10]. Similar to many other neuroprotective therapeutics, administration of Tan IIA has resulted in reduced lesion volumes, mortality, and improved neurological function in preclinical rodent studies [11-13]. However, Tan IIA and many other neuroprotective therapies have demonstrated limited efficacy in human clinical trials [14, 15]. One potential way to improve the efficacy of Tan IIA in humans is through the use of a nanoparticle (NP) delivery system. NP drug delivery can improve drug circulation time and control release over extended periods of time while simultaneously reducing toxicity [16, 17]. The disconnect in neuroprotectant success between preclinical rodent studies and human clinical trials is likely in part due to major differences in size, cytoarchitecture, and physiology between rodent and human brains leading to dissimilar therapeutic responses [18-21]. These inherent anatomical differences have led to a demand

from the stroke therapeutic community for the development and testing of novel treatments in more representative translational animal models, such as the pig, that more closely resemble human brain anatomy and physiology [22, 23].

Following the primary ischemic insult, a secondary injury cascade is initiated with the release of the excitatory neurotransmitter, glutamate, from dying neurons causing excitotoxicity, peri-infarct depolarizations, production of reactive oxygen species (ROS), and inflammation [24, 25]. Generated ROS leads to the damage of DNA, RNA, and critical cellular machinery leading to cell death. The increase in ROS, the release of damaged-associated molecular patterns (DAMPS), and hypoxia triggers an immune response including an increase in neutrophils and the production of inflammatory cytokines such as tumor necrosis factor α (TNF-α) and interleukin 6 (IL-6) [26, 27]. The secondary injury cascade leads to rapid and substantial brain damage. Therefore, inhibiting ROS production and inflammation may be a promising therapeutic target.

Tan IIA has been shown to have antioxidant and anti-inflammatory effects in rodent and human stroke studies [28, 29]. Rodent studies showed Tan IIA was effective in reducing brain edema and infarct volume in response to ischemic injury [11, 13, 28]. Reduced brain edema and lesioning correlated with rodent improvements in overall neurological function post-stroke including limb mobility, ambulation, righting reflexes, and reduced circling behavior [11]. Human clinical trials testing Tan IIA in its purified or crude form (dried *Salvia miltiorhiza* root) has led to mixed efficacy results with studies showing significant to no improvements in clinical outcomes (e.g. cerebral blood flow, neurological symptoms, and muscle strength) of ischemic stroke patients [14, 15, 30, 31]. Conflicting results between rodent and human outcomes suggest Tan IIA may be a

potentially effective treatment, yet further optimization is needed to achieve improved consistency in post-stroke outcomes.

In its purified form, Tan IIA has a short circulation half-life and poor solubility, which limits systemic drug concentrations and consequent pharmacological responses [32, 33]. Furthermore, the hydrophobic properties of Tan IIA reduces permeability and bioavailability, thus requiring higher administration doses [33]. Poly (lactic-*co*-glycolic acid) (PLGA) NPs are an FDA-approved copolymer made of lactic acid and glycolic acid. PLGA or the PEGylated derivative, polyethylene glycol–poly lactic acid-*co*-glycolic acid (PEG–PLGA), can encapsulate large amounts of hydrophobic molecules, like Tan IIA, and release them at a controlled rate [34]. A sustained drug release improves drug bioavailability and reduces the frequency of drug administration. The controlled release, low toxicity, high biodegradability, low immunogenicity, and significant clinical experience makes PLGA a favorable nanoplatform for drug delivery [35]. Extensive preclinical and clinical studies confirm PLGA NPs are a safe and efficient delivery system [17, 34, 36]. A PLGA NP delivery system could significantly improve the bioavailability, solubility, and pharmacological efficacy of Tan IIA in ischemic stroke patients. NP treatments are commonly delivered intravenously (IV), however this limits the therapeutic effects of NP delivered drugs for ischemic stroke as NPs cannot freely transverse the blood brain barrier (BBB). Intracisternal delivery of NPs may overcome this challenge as NPs do not need to cross the BBB due to direct administration into the cerebral spinal fluid (CSF) of the central nervous system (CNS). Additionally, intracisternal NP treatments are not diluted in the circulatory system, removed by filtering organs such as the liver, thus lower

NP concentrations are required, and the potential of off target effects in other organ systems is reduced.

The Stroke Therapy Academic and Industry Roundtable (STAIR) recommended preclinical testing of potential therapeutics in gyrencephalic species to increase the possibility of translating therapies to the clinic [22]. The use of large animal models is an important step in the translational framework as most therapies that have reached and failed in clinical trials have been successfully tested in rodent models, indicating a need for a more predictive model. The pig has anatomical and physiological similarities to humans making it a robust model for studying novel therapeutics for ischemic stroke [37]. While rodent brains are lissencephalic and composed of <10% white matter (WM), both human and pig brains are gyrencephalic and composed of >60% WM [38]. These differences have proven critically important in ischemic stroke pathology as WM and gray matter (GM) exhibit differing sensitivities to hypoxia, with WM more consistently injured in most stroke cases [39-41]. The pathology of GM is believed to differ from WM in terms of lymphocyte infiltration, macrophage activity, and BBB alterations in response to injury [42]. WM also has a greater dependence on Na^+ and Ca^{2+} exchange, γ-aminobutyric acid (GABA), and adenosine with an autoprotective feed-back loop [43]. These anatomical similarities support that stroke pathophysiology in the pig model is likely more representative of the human condition and therefore more predictive of human outcomes compared to traditional rodent models.

In this study, Tan IIA PLGA NPs (Tan IIA-NPs) were characterized and demonstrated antioxidative and anti-inflammatory capabilities in vitro. Acute testing of Tan IIA-NPs in a pig model of ischemic stroke showed Tan IIA-NPs have a

neuroprotective effect leading to reduced cerebral swelling, lesion volume, and improved WM integrity. These tissue level improvements corresponded with improved motor function suggesting Tan IIA-NPs may be an effective treatment for ischemic stroke.

Methods and Materials

Synthesis of PLGA-b-PEG-OH

PLGA acid (PLGA-COOH;1.0 g, 0.170 mmol; Lactel), polyethylene glycol (HO-PEG-OH;2.29 g, 0.684 mmol; Sigma Aldrich), and deoxyadenosine monophosphate (dMAP; 0.023 g, 0.187 mmol; Alfa Aesar) were dissolved in 30 mL of anhydrous dichloromethane (CH_2Cl_2; Sigma Aldrich). Next, a 10 mL CH_2Cl_2 solution of dicyclohexylmethanediimine (DCC; 0.141 g or 0.684 mmol; Sigma Aldrich) was added dropwise to the reaction mixture at 0 °C with magnetic stirring. The mixture was warmed up to room temperature and stirred overnight. Insoluble dicyclohexylurea ($C_{13}H_{24}N_2O$) was filtered out. The raw product was precipitated out by adding 50 mL of 50:50 diethyl ether ($(C_2H_5)_2O$; Sigma Aldrich) and methanol (CH_3OH; Sigma Aldrich) to the mixture. The mixture was centrifuged for 15 minutes at 4 °C. The purification step was repeated 4-5 times, followed by ^1H NMR analysis that was performed on a Varian Mercury Plus 400 system.

NP synthesis

PLGA NPs were synthesized through a nanoprecipitation method. Briefly, poly (lactide-*co*-glycolide)-b-poly (ethylene glycol)-maleimide (PLGA-b-PEG-OH) was first dissolved in dimethylformamide (DMF) at a concentration of 50 mg/mL. 100 μL of the polymer solution was mixed with drug-to-be-loaded (150 μL, 0.15 mg; Tan IIA, TCI America; Pioglitazone (Piog), Sigma Aldrich; Baicalin (Baic), Sigma Aldrich; Puerarin

(Puer), Sigma Aldrich; Edaravone (Edar), Sigma Aldrich; Resveratrol (Resv), Sigma Aldrich) for 30 % feeding and diluted with DMF (Fisher Scientific) to a final polymer concentration of 5 mg/mL. The mixture was added dropwise to sterile nanopure water with constant stirring, and the resulting solution was agitated in a fume hood for 2 hours. Drug loaded NPs were collected on an amicon ultracentrifugation unit (100 kDa cut-off) and were washed 3-4 times with water. Finally, the NPs were resuspended in sterilized nanopure water.

NP characterization

A drop of diluted NP solution was deposited onto a transmission electron microscopy (TEM) grid, followed by staining with 2% uranyl acetate. TEM images were taken on a FEI Tecnai 20 transmission electron microscope operating at an accelerating voltage of 200 kV. Hydrodynamic size and surface charge of NPs were analyzed on a Malvern Zetasizer Nano ZS system.

Drug loading and release

For drug loading analysis, a 50 μL aqueous solution of NPs was diluted to 900 μL and 100 μL 0.1 mM sodium hydroxide (NaOH; Sigma Adrich) was added to the solution. The mixture was incubated at room temperature overnight. Next, the solution was sonicated for 30 minutes and centrifugated at 5000 rpm for 10 minutes. 100 μL supernatant was transferred into a 96-well UV transparent plate and its absorbance at the relevant wavelength was measured (Tan IIA: 258 nm; Baic: 320 nm; Piog: 270 nm).

Drug release study

For the drug release study, 100 μL NP solution was loaded onto a dialysis unit and allowed to float on a 1.1 mL phosphate buffered saline (PBS) solution (pH: 5.5, 6.5,

or 7.4; Gibco). The system was put on an Eppendorf shaker set at 37 °C. At each time point (0.5, 1, 2, 4, 8, 12, 24, 36, and 48 hours), 100 μL PBS solution was transferred to a 96-well UV transparent plate. The drug content was assessed by measuring the relevant absorbance (Tan IIA: 258 nm; Baic: 320 nm; Piog: 270 nm) and compared to a standard curve. 100 μL of fresh PBS solution was added back to the dialysis system.

Cell culture

Neural stem cells (NSCs; HIP™ hNSC BC1, GlobalStem) were maintained on Matrigel-coated (Corning) tissue culture treated plates in NSC media composed of Neurobasal medium (Gibco), 2% B-27 Supplement (Gibco), 1% non-essential amino acids (Gibco) 2 mM L-glutamine (Gibco), 1% penicillin/streptomycin (Gibco), 20 ng/mL basic fibroblast growth factor (bFGF; R&D Systems). NSCs were incubated at 37 °C with 5% CO_2 and a complete media change was performed every other day. When NSCs reached confluence, cells were enzymatically passaged using Accutase (Gibco).

Microglia cells (ATCC) were maintained on tissue culture treated plates in microglia media composed of Eagle's Minimum Essential Medium (ATCC), 11% fetal bovine serum (ATCC) 1% penicillin/streptomycin (Gibco). Microglia were incubated at 37 °C with 5% CO_2 and a complete media change was performed every other day. When microglia reached confluence, cells were enzymatically passaged using 0.05% trypsin (Gibco).

MTT assay

The MTT assay was performed according to the manufacturer's protocol (Sigma Aldrich). Briefly, $8x10^3$ NSCs were seeded into each well of a 96 well plate. After 8 hours of incubation at 37 °C in a humidified atmosphere with 5% CO_2, a gradient of the tested

drugs or NPs were added into the wells. After 24 hours of incubation, the medium was removed and cells were washed. 10 μL MTT solution (10 mg/mL) was added into each well and incubated with cells for 4 hours. The absorbance at 570 nm was measured on a plate reader. Viability was calculated by computing relative absorbance with regard to PBS treated cells.

SOD activity assay

The superoxide dismutase (SOD) activity assay was performed according to the manufacturer's protocol (Cayman). Briefly, 1×10^6 NSCs were seeded into each well of a 6-well plate. After 24 hours, the cells were incubated with 250 μM hydrogen peroxide (H_2O_2) to induce oxidative stress. After 30 minutes, the cells were washed with PBS and then incubated with drugs or drug-containing NPs at different concentrations for 24 hours. The cells were then detached from plate using a cell scraper, collected by centrifugation, and washed 3 times with PBS. The resultant cells were homogenized by sonication and then centrifuged at 3600 rpm at 4 °C for 10 minutes. The supernatant was immediately collected and diluted with assay buffers by 4 times the supernatant amount. The diluted solutions were transferred into a 96-well plate at a volume of 200 μL per well. 20 μL of diluted xanthine oxidase was added into the solution and the plate was covered with foil and shaken at room temperature for 30 minutes. The absorbance at 450 nm was then read on a plate reader. The SOD activity was calculated as U/mL of protein by comparing to SOD standards.

ELISA assays

Anti-inflammatory efficacy was tested by TNF-α and IFN-γ enzyme-linked immunosorbent assay (ELISA) assays according to the manufacturer's protocol

(Invitrogen). Briefly, $2x10^4$ microglia cells in microglia media were seeded in 12 well plates overnight. To induce an inflammatory response in microglia cells, 150 ng/mL lipopolysaccharide (LPS) was added in each well and incubated at 37 °C with 5% CO_2. After 24 hours, cells were washed with PBS 2 times and then incubated with either drugs or at each respective drug's inhibitory concentration (IC) 20, IC 6.7, IC 2.2, IC 0.74, IC 0.25 or 0 based on the previously performed MTT assay and 150 ng/mL LPS. Negative control samples were not treated with LPS or drug. After 24 hours, supernatant was collected from each well, processed and absorbance was read at 450nm. Cytokine values were calculated as pg/mL.

Animals and housing

All work performed in this study was approved by the University of Georgia Institutional Animal Care and Use Committee (IACUC) guidelines. Sexually mature, castrated male Landrace pigs, 5-6 months old and 48-56 kg were enrolled in this study. Male pigs were used in accordance with the STAIR guidelines that suggests initial therapeutic evaluations should be performed with young, healthy male animals [44]. Pigs were individually housed at a room temperature approximately 27 ºC with a 12-hour light/dark cycle. All pigs were fed standard grower diets.

MCA Occlusion and NP delivery

One day prior to surgery, antibiotics and pain medication were administered (Excede; 5 mg/kg intramuscular (IM) and fentanyl patch; 100 mg/kg/hr transdermal (TD)). Pre-induction analgesia and sedation were achieved using xylazine (2 mg/kg IM) and midazolam (0.2 mg/kg IM). Anesthesia was induced with IV propofol to effect and

prophylactic lidocaine (1.0 mL 2% lidocaine) topically to the laryngeal folds to facilitate intubation. Anesthesia was maintained with isoflurane (Abbott Laboratories) in oxygen.

As previously described, a curvilinear skin incision extended from the right orbit to an area rostral to the auricle [45]. A segment of the zygomatic arch was resected while the temporal fascia and muscle were elevated and a craniectomy was performed exposing the local dura mater. Following a local durectomy, the distal middle cerebral artery (MCA) and associated branches were permanently occluded using bipolar cautery forceps resulting in ischemic infarction. The temporalis muscle and epidermis were routinely re-apposed.

At 1 hour post-stroke, PBS (n=2) or Tan IIA-NPs (n=2) were intracisternally delivered via a 20 gauge, 3.5 or 6" spinal needle inserted through the skin on the midline of the dorsal neck, at an anatomical intersection of a vertical line created by the rostral aspect of the wings of the first vertebral body and a horizontal line connecting the dorsal arch of C2 with the occipital protuberance. Once the needle was through the cutaneous tissues, the stylet was removed and advanced until CSF appeared in the needle hub confirming entry into the cistern. A small volume (3-5 mLs) of CSF was removed while the spinal needle was in place and the volume removed was replaced with PBS or Tan IIA-NPs. The volume of NPs delivered was determined by the NP loading efficiency and each animal received a dose of 133μg/kg Tan IIA.

Anesthesia was discontinued, pigs were returned to their pens upon extubation, and monitored every 15 minutes until vitals including temperature, heart rate, and respiratory rate returned to normal. Monitoring was reduced to every 4 hours for 24 hours, and then twice a day thereafter until post-transplantation sutures were removed. Banamine (2.2

mg/kg IM) was administered for post-operative pain and fever management every 12 hours for the first 24 hours post-stroke and then every 24 hours for 3 days.

MRI acquisition and analysis

MRI was performed 24 hours post-stroke on a General Electric 3.0 Tesla MRI system. Pigs were sedated and maintained under anesthesia as previously described for MCA occlusion surgery. MRI of the cranium was performed using an 8-channel torso coil with pigs positioned in supine recumbency. Multiplanar MRI sequences were acquired including T2 Fluid Attenuated Inversion Recovery (T2FLAIR), T2Weighted (T2W), T2Star (T2*), Diffusion-Weighted Imaging (DWI), and Diffusion Tensor Imaging (DTI). Sequences were analyzed using Osirix software (Version 5.6). Cytotoxic edema consistent with ischemic stroke was confirmed 24 hours post-stroke by comparing hyperintense regions in T2FLAIR and DWI sequences to corresponding hypointense regions in DWI generated Apparent Diffusion Coefficient (ADC) maps.

Hemisphere volume was calculated using T2W sequences for each axial slice by manually outlining the ipsilateral and contralateral hemispheres, while excluding the ventricles. The hemisphere areas were multiplied by the T2W slice thickness (3 mm) to obtain total hemisphere volumes. Lesion volume was calculated using DWI sequences for each axial slice by manually outlining hyperintense regions of interest (ROI). The area of each ROI was multiplied by the DWI slice thickness (2 mm) to obtain the total lesion volume. ADC values were calculated for each axial slice based on hypointense ROI and directly compared to identical ROI in the contralateral hemisphere. DTI was utilized to generate fractional anisotropy (FA) maps. FA values of the internal capsules were manually calculated on the slice where the internal capsules and the splenium of the corpus callosum

were visualized. FA values were expressed as a percent change in the ipsilateral hemisphere relative to the contralateral hemisphere. ICH volume was calculated based on hypointense ROIs in T2* sequences and multiplied by the slice thickness (2 mm).

Blood collection and analysis

Venous blood samples were collected pre-stroke, 4 hours, 12 hours, and 24 hours post-stroke into K2EDTA spray coated tubes (Patterson Veterinary). Samples were stored at room temperature for 30 minutes. 4μL of blood was then pipetted onto a ColorFrost microscope slide (ThermoScientific) approximately 1 cm from the bottom. A spreader slide was placed in front of the blood at a 45° angle and retracted while maintaining even pressure until the blood sample spread evenly along the width of the slide. Care was taken to ensure each blood smear covered approximately two-thirds of the slide and exhibited an oval feathered end. Each slide was air-dried for 10 minutes and fixed with methanol for 2 minutes. Once dry, the slide was stained with Rowmanosky stain for 5 minutes. The stained slide was then submerged in double-distilled water (ddH_2O) for 10 minutes. Finally, the slide was rinsed and allowed to air dry prior to applying a cover slip. Trained, blinded personnel completed manual cell counts of lymphocytes and band neutrophils at the monolayer, beginning approximately 1 mm away from the body of the smear. The first 100 cells visualized were identified and cell counts were expressed as a percentage.

Gait analysis

Pre- and post-stroke, all pigs underwent gait analysis to measure differences in spatiotemporal and relative pressure gait parameters between treatment groups. 2 weeks prior to stroke induction, all pigs were trained to travel across a gait mat at a consistent, two-beat pace. Pigs received food rewards at each end of the mat for each successful run

in which the pig was not distracted and moved at a consistent pace. For each pig, pre-stroke data was collected on 3 separate days. At each time point, pigs moved across the mat until 5 consistent repetitions were achieved, with no more than 15 total repetitions collected.

All data was automatically captured using a GAITFour® electronic, pressure-sensitive mat (CIR Systems Inc., Franklin, NJ) that is 7.01 m in length and 0.85 m in width with an active area that is 6.10 m in length and 0.61 m in width. In this arrangement, the active area is a grid, 48 sensors wide by 480 sensors long, totaling 23,040 sensors. Gait data was then semi-automatically analyzed using the GAITFour® Software. All resulting data was analyzed for cadence (steps/min). Further measurements were quantified for the left forelimb, contralateral to the stroke lesion. These measurements included stride length (distance between successive ground contact of the left forelimb), swing percent of cycle (percent of a full gait cycle in which the left forelimb is not in contact with the ground), cycle time (amount of time for a full stride cycle), and mean pressure (amount of pressure exerted by the left forelimb).

Statistical analysis

All quantitative data was analyzed with SAS version 9.3 (Cary, NC) and statistical significances between groups were determined by one-way analysis of variance (ANOVA) and post-hoc Tukey-Kramer Pair-Wise comparisons. Treatments where p-values ≤ 0.05 were considered significantly different. Only two animals were included in each treatment group for in vivo studies, therefore statistical analysis was limited to in vitro studies.

Results

Tan IIA and Baic drug characteristics enable NP drug delivery.

Six neuroprotective drugs with antioxidative and/or anti-inflammatory properties were identified, Baic, Piog, Tan IIA, Puer, Edar, and Resv, and were selected for testing as a NP based ischemic stroke therapy. These drugs were selected based on preclinical success in treating ischemic stroke, with some advancing and proving unsuccessful in human clinical trials, while also having biological characteristics that could benefit from the use of a NP delivery system such as a short half-life [11-15, 46-55]. Puer, Edar, and Resv showed very low NP loading efficiency, due to their relatively high hydrophilicity, and therefore these drugs were eliminated from the study. Baic, Piog, and Tan IIA showed higher loading efficiencies of 17.01, 4.90, and 15.90 %, respectively. Baic, Piog, and Tan IIA loaded NPs (henceforth referred to as Baic-NPs, Piog-NPs, and Tan IIA-NPs) were imaged using TEM and had an average size of 60.80, 74.20, and 52.20 nm, respectively (**Figure 5.1A**). Baic-NPs, Piog-NPs, and Tan IIA-NPs size was also assessed by dynamic light scattering (DLS), which found the hydrodynamic sizes to be 89.28±1.8, 122.40±2.3, and 91.34±1.3 nm, respectively (**Figure 5.1B**). The relative increase of hydrodynamic sizes is attributed to surface PEGylation and hydration. Assessment of zeta potential showed that all three NPs have a negatively charged surface, -31.91, -27.39, -28.98 mV, respectively, which is due to the hydroxyl termini of the PEG chains (**Figure 5.1C**). For all three formulations, the drug molecules were slowly released from NPs at acidic and more neutral pH levels (pH 5.5, 6.5, and 7.4; **Figure 5.1D**), which is beneficial from a sustained delivery perspective. However, while Tan IIA-NPs and Baic-NPs afford good colloidal stability, Piog-NPs showed a relatively high degree of aggregation after dispersing in PBS for 2-3 hours. Hence, subsequent cellular tests focused on Baic-NPs and Tan IIA-NPs.

Tan IIA-NPs and Baic-NPs suppress oxidative stress in NSCs and inflammation in microglia.

Tan IIA and Baic have been previously shown to be effective in ischemic stroke animal models at a dose range of 15 mg/kg and 90 mg/kg, respectively [56, 57]. Therefore, Tan IIA-NPs, Baic-NPs and corresponding free drugs were tested for cytotoxicity and efficacy in a comparable dose range. MTT assays were performed to determine the relative cytotoxicity of Tan IIA-NPs, Baic-NPs and corresponding free drugs on NSCs. MTT assays at 24 hours showed the IC_{50} values of Tan IIA-NPs and Baic-NPs were 33 μM and over 672 μM, respectively (**Figure 5.2A-B**). Notably, while Baic-NPs showed very similar profiles to the Baic free molecules, Tan IIA-NPs showed significantly ($p<0.05$) less toxicity compared to free Tan IIA at IC_{50}: 6.6 μM. This may be attributed to NP-mediated, slow release of Tan IIA at early timepoints.

To study the antioxidative efficacy of Tan IIA-NPs and Baic-NPs, NSCs were treated with H_2O_2 (250 μM) and incubated with drug-loaded NPs and corresponding free drugs. A series of dilutions (determined from respective IC_{20} doses) were tested. Oxidative stress was tested by measuring SOD activity at 24 hours (**Figure 5.2**). Both Tan IIA-NPs and Baic-NPs showed a concentration-dependent reduction of SOD activity, indicating an antioxidative effect (**Figure 5.2C-D**). Tan IIA-NPs resulted in a greater reduction in SOD levels than Baic-NPs at their respective IC_{20} (2 vs. 672 μM, respectively) and $IC_{2.5}$ (0.25 vs. 84 μM, respectively) doses.

To assess the potential anti-inflammatory effect of Tan IIA-NPs and Baic-NPs, microglia cells were treated with LPS and then incubated with drug-loaded NPs and free drugs. The inflammatory response was assessed by measuring TNF-α and IFN-γ. Positive

controls treated with LPS showed a significant ($p<0.05$) increase in TNF- α and IFN-γ levels (128.03±26.21 and 45.92±1.02 pg/ml, respectively). Treatment of microglia with Tan IIA-NPs and Baic-NPs at IC_{20} and $IC_{2.5}$ doses resulted in undetectable levels of TNF-α and IFN-γ demonstrating an anti-inflammatory response (data not shown). Based on these combined cytotoxicity, oxidative stress, and inflammatory test results, Tan IIA-NPs were selected for further testing in an ischemic stroke pig model.

Tan IIA-NPs reduce hemispheric swelling, consequent MLS, and ischemic lesion volumes post-ischemic stroke.

T2W sequences collected 24 hours post-stroke revealed Tan IIA-NP treated pigs (**Figure 5.3B**) exhibited a reduced percent change in ipsilateral hemispheric swelling when compared to PBS controls (**Figure 5.3A**) (7.85 vs. 16.83 %, respectively; **Figure 5.3C**). This mitigation of hemispheric swelling resulted in a decreased MLS (1.72 vs. 2.91 mm; red lines; **Figure 5.3D**). Acute ischemic lesion volumes were also reduced in Tan IIA-NP treated pigs 24 hours post-stroke (9.54 vs. 12.01 cm^3; **Figure 5.3E**), which suggests a reduction in acute tissue injury.

Tan IIA-NP treatment leads to reduced cytotoxic edema, WM damage, and ICH post-ischemic stroke.

Hypointense lesioned areas were observed on ADC maps, which are indicative of restricted diffusion and cytotoxic edema (**Figure 5.4A-B**, white arrows). Tan IIA-NP treated pigs (**Figure 5.4B**) had a reduced percent change in mean ADC values when compared PBS control pigs (**Figure 5.4A**) (-37.30 vs. -46.33 %; **Figure 5.4C**). To determine the neuroprotective effect of Tan IIA-NPs on cerebral WM, internal capsule FA values were evaluated in Tan IIA-NP and PBS treated animals at 24 hours post-stroke. Tan

IIA-NP treated animals showed a decreased reduction in FA value relative to PBS treated animals (-19.66 vs. -30.11 %; **Figure 5.4D**). T2* sequences showed hypointense acute ICH in PBS and Tan IIA-NP treated pigs 24 hours post-stroke (**Figure 5.5A-B**, respectively). However, Tan IIA-NP treated pigs had smaller hemorrhage volumes compared to PBS treated pigs (0.85 vs. 2.91 cm^3; **Figure 5.5C**). This data supports that Tan IIA-NPs lead to a reduction in restricted diffusion, cytotoxic edema, WM damage, and ICH in ischemic stroke animals.

Tan IIA-NPs reduce circulating band neutrophils in post-stroke pigs.

To assess changes in the stroke immune response, band neutrophil and lymphocyte populations were measured in blood samples collected pre-stroke, 4, 12, and 24 hours post-stroke. At 12 hours post-stroke, the percentage of circulating band neutrophils was lower in Tan IIA-NP treated animals than in the PBS control animals at 12 (7.75 vs. 14%) and 24 (4.25 vs. 5.75 %) post-stroke (**Figure 5.6A-B**). Conversely, the percentage of circulating lymphocytes was similar in both treatment groups at all assessed time points (**Figure 5.6C-D**).

Spatiotemporal and kinetic gait deficits are less severe post-stroke in Tan IIA-NP treated pigs.

Changes in key spatiotemporal and kinetic gait parameters were measured to detect differences in functional outcomes post-Tan IIA-NP treatment. A decrease was noted for both treatment groups in the average cadence of the pigs from pre-stroke to post-stroke indicating a decrease in speed. However, the decrease in cadence was more severe for the PBS treated pigs compared to Tan IIA-NP treated pigs (133.9 to 64.8 steps/min vs. 135.7 to 116.9 steps/min, respectively, **Figure 5.7A**). The limb contralateral to the stroke lesion

is often more affected as compared to the ipsilateral limb, which in this study are the limbs of the left side. In addition, pigs typically carry more weight on the forehand, typically making deficits more severe in the left forelimb. Deficits were noted for the left forelimb in both treatment groups for multiple gait parameters. The cycle time of the left front limb increased post-stroke for both treatment groups, with a more drastic increase in cycle time noted for the PBS treatment group as compared to the Tan IIA-NP treated pigs (0.46 to 0.93 vs. 0.44 to 0.55 sec, respectively, **Figure 5.7B**). Similarly, the left front step time increased post-stroke in both groups, with a greater increased step time in PBS pigs compared to Tan IIA-NP pigs (0.24 to 0.49 vs. 0.22 to 0.27 sec, respectively, **Figure 5.7C**). Decreases in cycle time and step time indicated an overall slower gait post-stroke, opposed to pre-stroke performance. The swing percent of cycle decreased for the left front limb of all pigs, with PBS pigs decreasing further than Tan IIA-NP pigs (49.4 to 33.3 vs. 49.1 to 43.2 %, respectively, **Figure 5.7D**). A reduction was noted in the left front stride length of all animals, with PBS pigs displaying a greater reduction in stride length relative to Tan IIA-NP pigs (78.38 to 63.18 vs. 84.87 to 77.44 cm, respectively, **Figure 5.7E**). Finally, the mean pressure of the left front limb decreased in both treatment groups with a larger decrease in pressure noted for the PBS pigs opposed to the Tan IIA-NP pigs (2.93 to 2.76 vs. 2.87 to 2.88 arbitrary units (AU), respectively, **Figure 5.7F**). Post-stroke deficits were noted for all parameters in both treatment groups, however more pronounced deficits were seen in the gait of PBS pigs, thus indicating administration of Tan IIA-NP in the acute phase post-stroke leads to less severe gait deficits.

Discussion

In this study, we demonstrate for the first time Tan IIA-NP treatment leads to improvements in clinically relevant MRI-based stroke tissue injury parameters and functional deficits in a translational ischemic stroke pig model. Tan IIA-NP therapy was selected from a number of drug candidates based on in vitro assessment of biochemical properties that augment NP delivery of a drug and efficacy in antioxidative and anti-inflammatory studies. Tan IIA-NP therapy resulted in considerable reductions in MLS, lesion volumes, WM damage, and ICH in the pig stroke model; parameters that closely correlate with functional deficits and mortality in human patients [41, 58, 59]. Tan IIA-NP treatment and associated reduction in overall brain injury corresponded with less severe spatiotemporal and relative pressure gait deficits including parameters that are often affected in human patients including stride length and cadence [60, 61]. These promising preclinical results in the pig model suggest that Tan IIA-NP therapy is ready for the next step in the STAIR criteria for translating pre-clinical studies into human clinical trials including expanded studies with additional animals of both genders and therapeutic window and dose finding studies.

To improve drug bioavailability, Tan IIA was encapsulated into PLGA-PEG NPs. The nanoplatform allows for controlled release of Tan IIA, potentially leading to prolonged ant-inflammatory and oxidative effects. In addition, Tan IIA-NPs were injected intracisternal into the subarachnoid space rather than IV. This injection route bypasses the BBB that would otherwise prevent the delivery of therapeutics to the ischemic areas. Combining NP delivery and intracisternal administration represents a novel approach in drug delivery. A recent study performed in mice also observed efficient distribution and

good tolerance of NPs after intracisternal injection [62]. Because the entire central nervous system (CNS) can be accessed through the CSF, this approach may be extended for the treatment of other CNS diseases.

Infarct volume, cerebral swelling, and consequent MLS have been shown to play a key role in the development of neurological deficits and high patient mortality rates [13, 58, 59, 63]. In the present study, the acute treatment window of Tan IIA-NPs demonstrated potential in mitigating these clinical presentations by decreasing hemisphere and lesion volumes. In a study of free form Tan IIA, Tang et al. provided evidence that lesion volumes were significantly reduced in 1 and 4 hour post-stroke Tan IIA treatment groups versus 6 and 12 hour Tan IIA treatment groups [28]. Additional studies have indicated Tan IIA possesses a neuroprotective effect in cerebral ischemia-reperfusion rodent models, whereby encephaledema and hemispheric swelling were relieved, infarction volumes decreased, and neurobehavior scores were significantly improved [64, 65].

Measures of ICH and ADC and are also strong predictors of clinical outcomes with increased hemorrhage and decreased ADC values being closely associated with poor clinical outcomes and higher mortality rates [66-68]. In the current study, Tan IIA-NP treated animals showed a decreased hemorrhage volume and a decreased percent change in ADC values relative to PBS treated animals. A recent study in a MCAO ischemic stroke mouse model showed that free form Tan IIA has a protective effect on the BBB, which would result in reduced hemorrhage [65]. This study demonstrated increased presence of the tight junction protein claudin-5 and reduced BBB leakage in Tan IIA treated animals. In a study assessing the ability of Tan IIA to maintain vascular integrity in a rat aneurysm model, researchers demonstrated Tan IIA reduced aneurysm size and increased vascular

wall thickness improving vascular integrity relative to control animals [69]. Zhou et al. showed in an ICH zebrafish model, Tan IIA reduced ICH area and incidence [70]. In a follow-up in vitro study with human umbilical vein endothelial cells, they demonstrated that Tan IIA inhibits actin depolymerization near cell borders and cell contraction, which would result in destabilization of cell-cell adheren junctions critical to maintaining the BBB. These results in multiple unique disease models across three different species demonstrates Tan IIA leads to increased stability in intracerebral vasculature that would result in reduced ICH as observed in this study. Preservation of diffusivity observed in this study is likely a direct result of decreased injury due to acute Tan IIA-NP treatment. This corresponds with previous Tan IIA studies in rodent models showing improved cerebral blood flow, reduced free radical formation, inflammation, and a decrease in infarcted brain tissue [11, 28].

Gait deficits constitute a significant portion of disabilities related to stroke. Unsurprisingly, many patients report improvement in mobility as a main goal for post-stroke recovery, making this an important benchmark for stroke therapeutic treatment potential [71]. Human stroke patients are often left with hemiparesis resulting in gait deficits including decreased cadence and stride length with associated increased swing percent of cycle and cycle time [60, 61, 72]. Similarly, pigs in the current study exhibited a post-stroke decrease in stride length and cadence with an associated increase in cycle time and step time in the left forelimb. These alterations in gait patterns mirror what is seen in humans and are likely reflective of the decreased velocity that typically accompanies postural instability following stroke. Further, pigs in the current study showed decreased swing percent of cycle of the affected contralateral forelimb post-stroke. While this is

opposite of what is often seen in human stroke patients, a decrease in relative swing and increase in relative stance has been reported as a hallmark gait change in pig models for both stroke and traumatic brain injury and is likely due to an increased need for ground contact to stabilize the gait along with decreased propulsion [73-75]. In the present study, changes in spatiotemporal gait properties were noted in all pigs in the acute time frame following stroke, however a more pronounced deficit was noted in the gait of PBS pigs as compared to Tan IIA-NP pigs post-stroke. Additionally, PBS pigs in this study also showed a reduction in mean hoof pressure of the contralateral forelimb, indicating compensatory balance mechanisms to distribute weight away from the affected contralateral side, while Tan IIA-NP pigs showed no kinetic changes. Several studies have demonstrated Tan IIA administration in rodent stroke models led to a reduction in severity of functional neurologic deficits (determined by factors such as failure to extend the forepaw of the contralateral limb, circling, lack of balance, or inability to walk) as compared to control animals [11, 76, 77]. The results of the present study are in agreement with these rodent models and suggest the administration of Tan IIA-NPs in the acute phase post-stroke mitigates cerebral injury and thereby results in less severe functional deficits.

Conclusion

This study demonstrated Tan IIA-NPs have notable potential to be a novel treatment for ischemic stroke. Utilizing a highly translatable pig model of ischemic stroke, Tan IIA-NP treatment leads to reduced hemispheric swelling, MLS, lesion volumes, cytotoxic edema, WM damage, and ICH 24 hours post-stroke. These manifested improvements in acute ischemic stroke pathophysiology led to marked improvements in a number of spatiotemporal and kinetic gait parameters. These promising results support the

idea Tan IIA-NPs are ready for further preclinical studies assessing safety and efficacy in a larger cohort of animals in both sexes in order to evaluate dosing and administration windows in accordance with the STAIR criteria for therapeutic translation to clinical trials.

Acknowledgments

The authors would like to thank Brandy Winkler and our team of undergraduate researchers who were involved in various aspects of surgeries, post-operative care, pig gait/behavioral testing, and data analysis. We would also like to thank the University of Georgia Animal Resources team for veterinary care and guidance as well as Rick Utley and Kelly Parham for their pig expertise and management skills. We would like to thank Samantha Spellicy for her assistance with midline shift and blood analysis. This work was supported by the National Institutes of Health, National Institute of Neurological Disorders and Stroke grant R01NS093314.

References

1. Feigin, V.L., B. Norrving, and G.A. Mensah, *Global Burden of Stroke.* Circ Res, 2017. **120**(3): p. 439-448.

2. Benjamin, E.J., et al., *Heart Disease and Stroke Statistics-2019 Update: A Report From the American Heart Association.* Circulation, 2019. **139**(10): p. e56-e528.

3. Schwamm, L.H., et al., *Temporal trends in patient characteristics and treatment with intravenous thrombolysis among acute ischemic stroke patients at Get With The Guidelines-Stroke hospitals.* Circ Cardiovasc Qual Outcomes, 2013. **6**(5): p. 543-9.

4. Macrae, I.M. and S.M. Allan, *Stroke: The past, present and future.* Brain Neurosci Adv, 2018. **2**: p. 2398212818810689.

5. Jilani, T.N. and A.H. Siddiqui, *Tissue Plasminogen Activator*, in *StatPearls*. 2019: Treasure Island (FL).

6. National Institute of Neurological, D. and P.A.S.S.G. Stroke rt, *Tissue plasminogen activator for acute ischemic stroke.* N Engl J Med, 1995. **333**(24): p. 1581-7.

7. Gravanis, I. and S.E. Tsirka, *Tissue-type plasminogen activator as a therapeutic target in stroke.* Expert Opin Ther Targets, 2008. **12**(2): p. 159-70.

8. Durukan, A. and T. Tatlisumak, *Acute ischemic stroke: overview of major experimental rodent models, pathophysiology, and therapy of focal cerebral ischemia.* Pharmacol Biochem Behav, 2007. **87**(1): p. 179-97.

9. Han, J.Y., et al., *Ameliorating effects of compounds derived from Salvia miltiorrhiza root extract on microcirculatory disturbance and target organ injury by ischemia and reperfusion.* Pharmacol Ther, 2008. **117**(2): p. 280-95.

10. Chen, H.S., S.H. Qi, and J.G. Shen, *One-Compound-Multi-Target: Combination Prospect of Natural Compounds with Thrombolytic Therapy in Acute Ischemic Stroke.* Curr Neuropharmacol, 2017. **15**(1): p. 134-156.

11. Lam, B.Y., et al., *Neuroprotective effects of tanshinones in transient focal cerebral ischemia in mice.* Phytomedicine, 2003. **10**(4): p. 286-91.

12. Xia, W.J., et al., *Partial neuroprotective effect of pretreatment with tanshinone IIA on neonatal hypoxia-ischemia brain damage.* Pediatr Res, 2005. **58**(4): p. 784-90.

13. Tang, C., et al., *The effects of Tanshinone IIA on blood-brain barrier and brain edema after transient middle cerebral artery occlusion in rats.* Phytomedicine, 2010. **17**(14): p. 1145-9.

14. Sze, F.K., et al., *Does Danshen improve disability after acute ischaemic stroke?* Acta Neurol Scand, 2005. **111**(2): p. 118-25.

15. Wu, B., M. Liu, and S. Zhang, *Dan Shen agents for acute ischaemic stroke.* Cochrane Database Syst Rev, 2007(2): p. CD004295.

16. Cheng, J., et al., *Formulation of functionalized PLGA-PEG nanoparticles for in vivo targeted drug delivery.* Biomaterials, 2007. **28**(5): p. 869-876.

17. Danhier, F., et al., *PLGA-based nanoparticles: an overview of biomedical applications.* J Control Release, 2012. **161**(2): p. 505-22.

18. Cai, B. and N. Wang, *Large Animal Stroke Models vs. Rodent Stroke Models, Pros and Cons, and Combination?* Acta Neurochir Suppl, 2016. **121**: p. 77-81.

19. Kaur, H., A. Prakash, and B. Medhi, *Drug therapy in stroke: from preclinical to clinical studies.* Pharmacology, 2013. **92**(5-6): p. 324-34.

20. Gladstone, D.J., et al., *Toward wisdom from failure: lessons from neuroprotective stroke trials and new therapeutic directions.* Stroke, 2002. **33**(8): p. 2123-36.

21. Cheng, Y.D., L. Al-Khoury, and J.A. Zivin, *Neuroprotection for ischemic stroke: two decades of success and failure.* NeuroRx, 2004. **1**(1): p. 36-45.

22. Stroke Therapy Academic Industry, R., *Recommendations for standards regarding preclinical neuroprotective and restorative drug development.* Stroke, 1999. **30**(12): p. 2752-8.

23. Baker, E.W., et al., *Induced Pluripotent Stem Cell-Derived Neural Stem Cell Therapy Enhances Recovery in an Ischemic Stroke Pig Model.* Sci Rep, 2017. **7**(1): p. 10075.

24. Endres, M., U. Dirnagl, and M.A. Moskowitz, *The ischemic cascade and mediators of ischemic injury.* Handb Clin Neurol, 2009. **92**: p. 31-41.

25. Bernstock, J.D., et al., *Neural stem cell transplantation in ischemic stroke: A role for preconditioning and cellular engineering.* J Cereb Blood Flow Metab, 2017. **37**(7): p. 2314-2319.

26. Dirnagl, U., C. Iadecola, and M.A. Moskowitz, *Pathobiology of ischaemic stroke: an integrated view.* Trends Neurosci, 1999. **22**(9): p. 391-7.

27. Rothwell, N.J. and S.J. Hopkins, *Cytokines and the nervous system II: Actions and mechanisms of action.* Trends Neurosci, 1995. **18**(3): p. 130-6.

28. Tang, Q., et al., *Protective effect of tanshinone IIA on the brain and its therapeutic time window in rat models of cerebral ischemia-reperfusion.* Exp Ther Med, 2014. **8**(5): p. 1616-1622.

29. *Danshen in ischemic stroke.* Chin Med J (Engl), 1977. **3**(4): p. 224-6.

30. Zhou, L., Z. Zuo, and M.S. Chow, *Danshen: an overview of its chemistry, pharmacology, pharmacokinetics, and clinical use.* J Clin Pharmacol, 2005. **45**(12): p. 1345-59.

31. Adams, J.D., et al., *Preclinical and clinical examinations of Salvia miltiorrhiza and its tanshinones in ischemic conditions.* Chin Med, 2006. **1**: p. 3.

32. Chen, X., et al., *Role of P-glycoprotein in restricting the brain penetration of tanshinone IIA, a major active constituent from the root of Salvia miltiorrhiza Bunge, across the blood-brain barrier.* Xenobiotica, 2007. **37**(6): p. 635-78.

33. Savjani, K.T., A.K. Gajjar, and J.K. Savjani, *Drug solubility: importance and enhancement techniques.* ISRN Pharm, 2012. **2012**: p. 195727.

34. Locatelli, E. and M. Comes Franchini, *Biodegradable PLGA-b-PEG polymeric nanoparticles: synthesis, properties, and nanomedical applications as drug delivery system.* Journal of Nanoparticle Research, 2012. **14**(12).

35. Govender, T., et al., *PLGA nanoparticles prepared by nanoprecipitation: drug loading and release studies of a water soluble drug.* Journal of Controlled Release, 1999. **57**(2): p. 171-185.

36. Jain, R.A., *The manufacturing techniques of various drug loaded biodegradable poly(lactide-co-glycolide) (PLGA) devices.* Biomaterials, 2000. **21**(23): p. 2475-2490.

37. Lind, N.M., et al., *The use of pigs in neuroscience: modeling brain disorders.* Neurosci Biobehav Rev, 2007. **31**(5): p. 728-51.

38. Nakamura, M., et al., *Experimental investigation of encephalomyosynangiosis using gyrencephalic brain of the miniature pig: histopathological evaluation of dynamic reconstruction of vessels for functional anastomosis. Laboratory investigation.* J Neurosurg Pediatr, 2009. **3**(6): p. 488-95.

39. McKay, S.M., et al., *Distinct types of microglial activation in white and grey matter of rat lumbosacral cord after mid-thoracic spinal transection.* J Neuropathol Exp Neurol, 2007. **66**(8): p. 698-710.

40. Baltan, S., et al., *White matter vulnerability to ischemic injury increases with age because of enhanced excitotoxicity.* J Neurosci, 2008. **28**(6): p. 1479-89.

41. Falcao, A.L., et al., *The resistance to ischemia of white and gray matter after stroke.* Ann Neurol, 2004. **56**(5): p. 695-701.

42. Mallucci, G., et al., *The role of immune cells, glia and neurons in white and gray matter pathology in multiple sclerosis.* Prog Neurobiol, 2015. **127-128**: p. 1-22.

43. Fern, R., S.G. Waxman, and B.R. Ransom, *Modulation of anoxic injury in CNS white matter by adenosine and interaction between adenosine and GABA.* J Neurophysiol, 1994. **72**(6): p. 2609-16.

44. Lapchak, P.A., J.H. Zhang, and L.J. Noble-Haeusslein, *RIGOR guidelines: escalating STAIR and STEPS for effective translational research.* Transl Stroke Res, 2013. **4**(3): p. 279-85.

45. Platt, S.R., et al., *Development and characterization of a Yucatan miniature biomedical pig permanent middle cerebral artery occlusion stroke model.* Exp Transl Stroke Med, 2014. **6**(1): p. 5.

46. Tu, X.K., et al., *Effect of baicalin on matrix metalloproteinase-9 expression and blood-brain barrier permeability following focal cerebral ischemia in rats.* Neurochem Res, 2011. **36**(11): p. 2022-8.

47. Tu, X.K., et al., *Neuroprotective effect of baicalin in a rat model of permanent focal cerebral ischemia.* Neurochem Res, 2009. **34**(9): p. 1626-34.

48. Yaghi, S., et al., *Pioglitazone Prevents Stroke in Patients With a Recent Transient Ischemic Attack or Ischemic Stroke: A Planned Secondary Analysis of the IRIS Trial (Insulin Resistance Intervention After Stroke).* Circulation, 2018. **137**(5): p. 455-463.

49. Blankenship, D., et al., *Oral pioglitazone reduces infarction volume and improves neurologic function following MCAO in rats.* Adv Exp Med Biol, 2011. **701**: p. 157-62.

50. Chang, Y., et al., *Neuroprotective mechanisms of puerarin in middle cerebral artery occlusion-induced brain infarction in rats.* J Biomed Sci, 2009. **16**: p. 9.

51. Zheng, Q.H., et al., *Efficacy and safety of puerarin injection in curing acute ischemic stroke: A meta-analysis of randomized controlled trials.* Medicine (Baltimore), 2017. **96**(1): p. e5803.

52. Kobayashi, S., et al., *Effect of Edaravone on Neurological Symptoms in Real-World Patients With Acute Ischemic Stroke.* Stroke, 2019. **50**(7): p. 1805-1811.

53. Lee, X.R. and G.L. Xiang, *Effects of edaravone, the free radical scavenger, on outcomes in acute cerebral infarction patients treated with ultra-early thrombolysis of recombinant tissue plasminogen activator.* Clin Neurol Neurosurg, 2018. **167**: p. 157-161.

54. Hermann, D.M., et al., *Sustained neurological recovery induced by resveratrol is associated with angioneurogenesis rather than neuroprotection after focal cerebral ischemia.* Neurobiol Dis, 2015. **83**: p. 16-25.

55. Koronowski, K.B., et al., *Neuronal SIRT1 (Silent Information Regulator 2 Homologue 1) Regulates Glycolysis and Mediates Resveratrol-Induced Ischemic Tolerance.* Stroke, 2017. **48**(11): p. 3117-3125.

56. Liang, W., X.B. Huang, and W.Q. Chen, *The Effects of Baicalin and Baicalein on Cerebral Ischemia: A Review.* Aging and Disease, 2017. **8**(6): p. 850-867.

57. Shang, Y.H., et al., *Progress on the protective effect of compounds from natural medicines on cerebral ischemia.* Chinese Journal of Natural Medicines, 2013. **11**(6): p. 588-595.

58. Berrouschot, J., et al., *Mortality of space-occupying ('malignant') middle cerebral artery infarction under conservative intensive care.* Intensive Care Med, 1998. **24**(6): p. 620-3.

59. Hacke, W., et al., *'Malignant' middle cerebral artery territory infarction: clinical course and prognostic signs.* Arch Neurol, 1996. **53**(4): p. 309-15.

60. Hsu, A.L., P.F. Tang, and M.H. Jan, *Analysis of impairments influencing gait velocity and asymmetry of hemiplegic patients after mild to moderate stroke.* Arch Phys Med Rehabil, 2003. **84**(8): p. 1185-93.

61. Balaban, B. and F. Tok, *Gait disturbances in patients with stroke.* PM R, 2014. **6**(7): p. 635-42.

62. Householder, K.T., et al., *Fate of nanoparticles in the central nervous system after intrathecal injection in healthy mice.* Sci Rep, 2019. **9**(1): p. 12587.

63. Thrift, A.G., et al., *Stroke incidence on the east coast of Australia: the North East Melbourne Stroke Incidence Study (NEMESIS).* Stroke, 2000. **31**(9): p. 2087-92.

64. Liu, L., et al., *The neuroprotective effects of Tanshinone IIA are associated with induced nuclear translocation of TORC1 and upregulated expression of TORC1, pCREB and BDNF in the acute stage of ischemic stroke.* Brain Res Bull, 2010. **82**(3-4): p. 228-33.

65. Wang, L., et al., *Tanshinone II A down-regulates HMGB1, RAGE, TLR4, NF-kappaB expression, ameliorates BBB permeability and endothelial cell function, and protects rat brains against focal ischemia.* Brain Res, 2010. **1321**: p. 143-51.

66. Fiehler, J., et al., *Predictors of apparent diffusion coefficient normalization in stroke patients.* Stroke, 2004. **35**(2): p. 514-9.

67. Terruso, V., et al., *Frequency and determinants for hemorrhagic transformation of cerebral infarction.* Neuroepidemiology, 2009. **33**(3): p. 261-5.

68. Beslow, L.A., et al., *Hemorrhagic transformation of childhood arterial ischemic stroke.* Stroke, 2011. **42**(4): p. 941-6.

69. Ma, J., et al., *Tanshinone IIA attenuates cerebral aneurysm formation by inhibiting the NFkappaBmediated inflammatory response.* Mol Med Rep, 2019. **20**(2): p. 1621-1628.

70. Zhou, Z.Y., et al., *Sodium tanshinone IIA sulfonate promotes endothelial integrity via regulating VE-cadherin dynamics and RhoA/ROCK-mediated cellular contractility and prevents atorvastatin-induced intracerebral hemorrhage in zebrafish.* Toxicol Appl Pharmacol, 2018. **350**: p. 32-42.

71. Cress, R.H. and W.C. Fleming, *Treatment goals and selection of patients for rehabilitation with hemiplegia.* Ala J Med Sci, 1966. **3**(3): p. 307-11.

72. Woolley, S.M., *Characteristics of gait in hemiplegia.* Top Stroke Rehabil, 2001. **7**(4): p. 1-18.

73. Duberstein, K.J., et al., *Gait analysis in a pre- and post-ischemic stroke biomedical pig model.* Physiol Behav, 2014. **125**: p. 8-16.

74. Baker, E.W., et al., *Controlled Cortical Impact Severity Results in Graded Cellular, Tissue, and Functional Responses in a Piglet Traumatic Brain Injury Model.* J Neurotrauma, 2019. **36**(1): p. 61-73.

75. Kinder, H.A., et al., *Traumatic Brain Injury Results in Dynamic Brain Structure Changes Leading to Acute and Chronic Motor Function Deficits in a Pediatric Piglet Model.* J Neurotrauma, 2019.

76. Chen, Y., et al., *Neuroprotective capabilities of Tanshinone IIA against cerebral ischemia/reperfusion injury via anti-apoptotic pathway in rats.* Biol Pharm Bull, 2012. **35**(2): p. 164-70.

77. Dong, K., et al., *Neuroprotective effects of Tanshinone IIA on permanent focal cerebral ischemia in mice.* Phytother Res, 2009. **23**(5): p. 608-13.

Figure 5.1: Baic, Piog, and Tan IIA are capable of undergoing NP packaging. TEM images of drug loaded PLGA NPs (**A**). The average NP sizes were 60.8, 74.2, and 52.2 nm for Baic-NPs, Piog-NPs, and Tan IIA-NPs, respectively. Hydrodynamic sizes of NPs were 89.28±1.8, 122.4 ±2.3, and 91.34± 1.3 nm for Baic-NPs, Piog-NPs, and Tan IIA-NPs, respectively (**B**). NPs zeta potentials were -31.91, -27.39, and -28.98 mV for Baic-NPs, Piog-NPs, and Tan IIA-NPs, respectively (**C**). Drug release profiles for Baic-NPs, Piog-NPs, and Tan IIA-NPs (**D**).

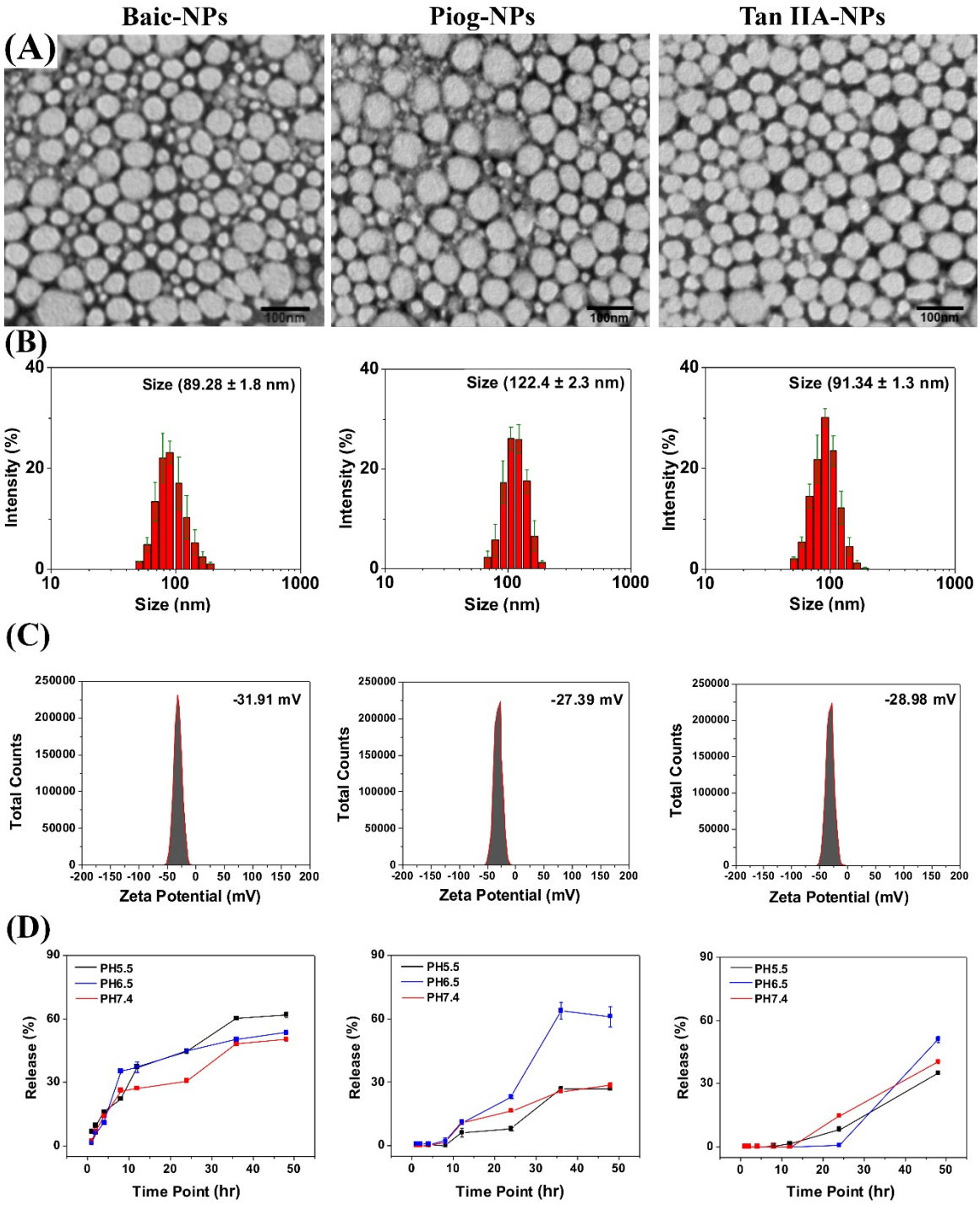
Baic-NPs
Piog-NPs
Tan IIA-NPs
(A)
100nm
100nm
100nm
(B)
Size (89.28 ± 1.8 nm)
Size (122.4 ± 2.3 nm)
Size (91.34 ± 1.3 nm)
Intensity (%)
Size (nm)
(C)
-31.91 mV
-27.39 mV
-28.98 mV
Total Counts
Zeta Potential (mV)
(D)
PH5.5
PH6.5
PH7.4
Release (%)
Time Point (hr)

Figure 5.2. Tan IIA-NPs and Baic-NPs reduce oxidative stress in NSCs. MTT assay results showed Tan IIA-NPs (**A**) and Baic-NPs (**B**) or free drugs IC_{50} values were over 33 μM and 672 μM, respectively. * or # indicates a significant difference between vehicle only control and treatment. & indicates a significant difference between drug only and drug loaded NP. SOD assay results showed a significant reduction in SOD at 2 μM and 336 μM for Tan IIA-NPs (**C**) and Baic-NPs (**D**), respectively. * or # indicates a significant difference between positive control and treatment. & indicates a significant difference between drug only and drug loaded NP.

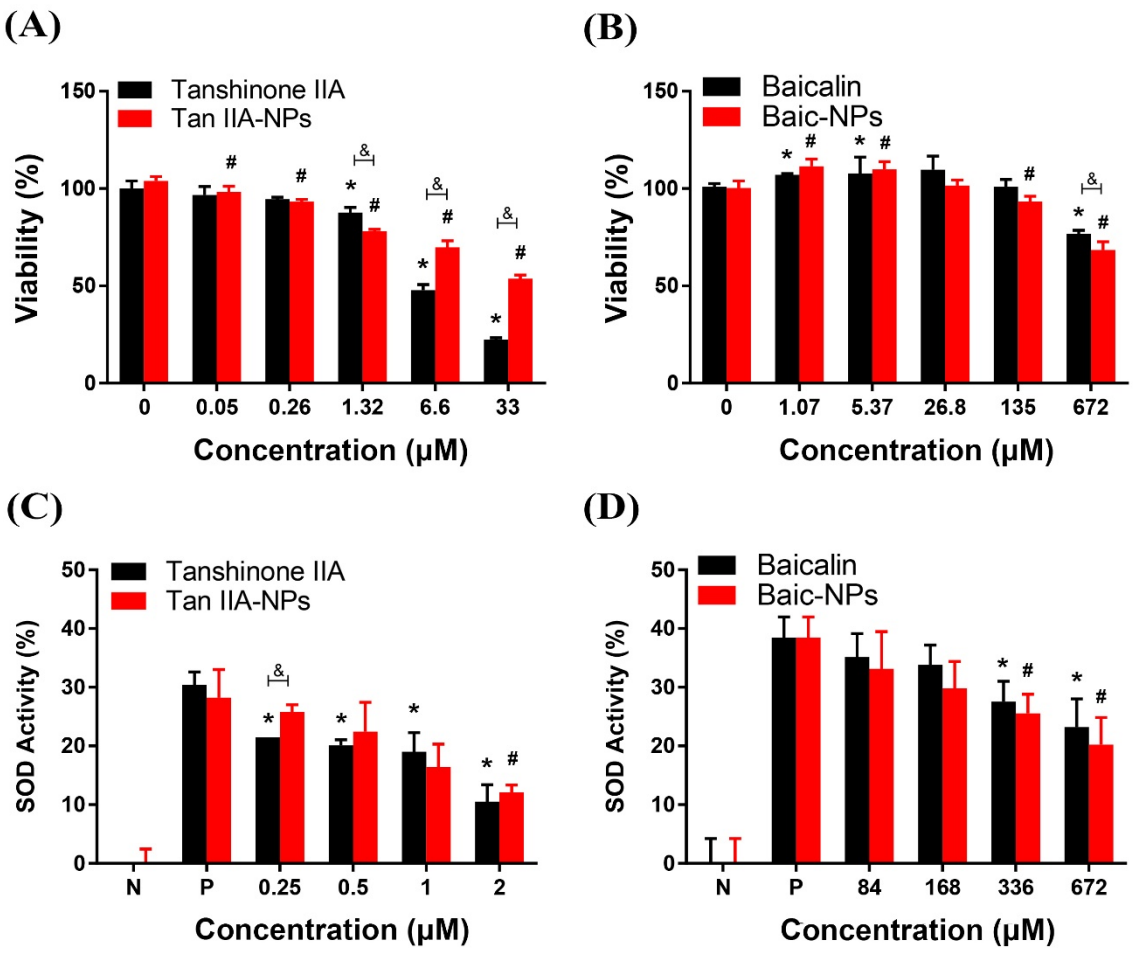
(A)
Tanshinone IIA
Tan IIA-NPs
Viability (%)
150
100
50
0
0
0.05
0.26
1.32
6.6
33
Concentration (μM)
(B)
Baicalin
Baic-NPs
Viability (%)
150
100
50
0
0
1.07
5.37
26.8
135
672
Concentration (μM)
(C)
Tanshinone IIA
Tan IIA-NPs
SOD Activity (%)
50
40
30
20
10
0
N
P
0.25
0.5
1
2
Concentration (μM)
(D)
Baicalin
Baic-NPs
SOD Activity (%)
50
40
30
20
10
0
N
P
84
168
336
672
Concentration (μM)

Figure 5.3: Tan IIA-NPs reduce hemispheric swelling, MLS, and ischemic lesion volumes. Compared to PBS pigs (**A**), Tan IIA-NP treated pigs (**B**) exhibited a reduction in ipsilateral hemispheric swelling (7.85 vs. 16.83 %, respectively; **C**), MLS (1.72 vs. 2.91 mm, respectively, red lines; **D**), and lesion volumes (9.54 vs. 12.01 cm^3, respectively; **E**) at 24 hours post-stroke.

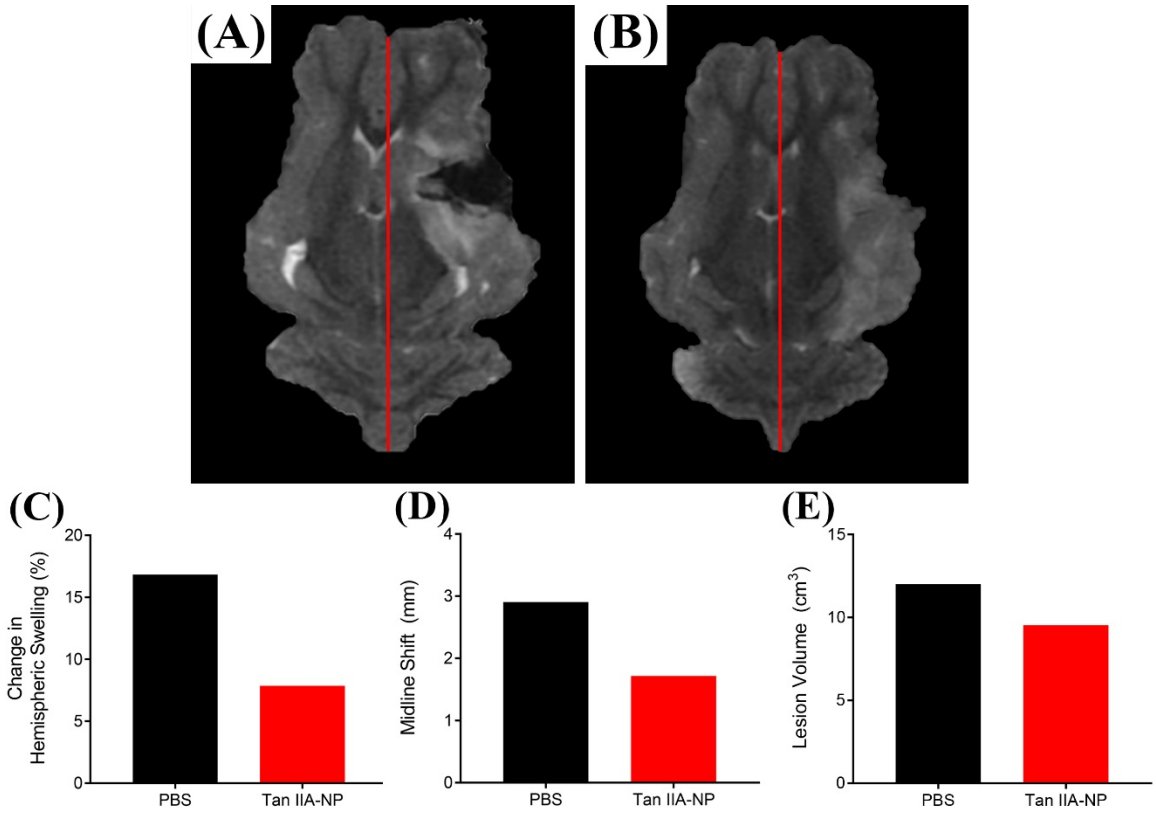
(A)
(B)
(C)
Change in Hemispheric Swelling (%)
20
15
10
5
0
PBS
Tan IIA-NP
(D)
Midline Shift (mm)
4
3
2
1
0
PBS
Tan IIA-NP
(E)
Lesion Volume (cm3)
15
10
5
0
PBS
Tan IIA-NP

Figure 5.4: Tan IIA-NPs lead to reduced cytotoxic edema and WM damage post-ischemic stroke. Hypointense lesioned areas were observed on ADC maps in PBS (**A**) and Tan IIA-NP (**B**) treated pigs. Tan IIA-NP treated pigs had a smaller percent change in mean ADC relative to PBS treated pigs (-37.30 vs. -46.33 %, respectively; **C**). Treated pigs showed a decreased reduction in FA values relative to PBS treated pigs (-19.66 vs. -30.11%, respectively; **D**).

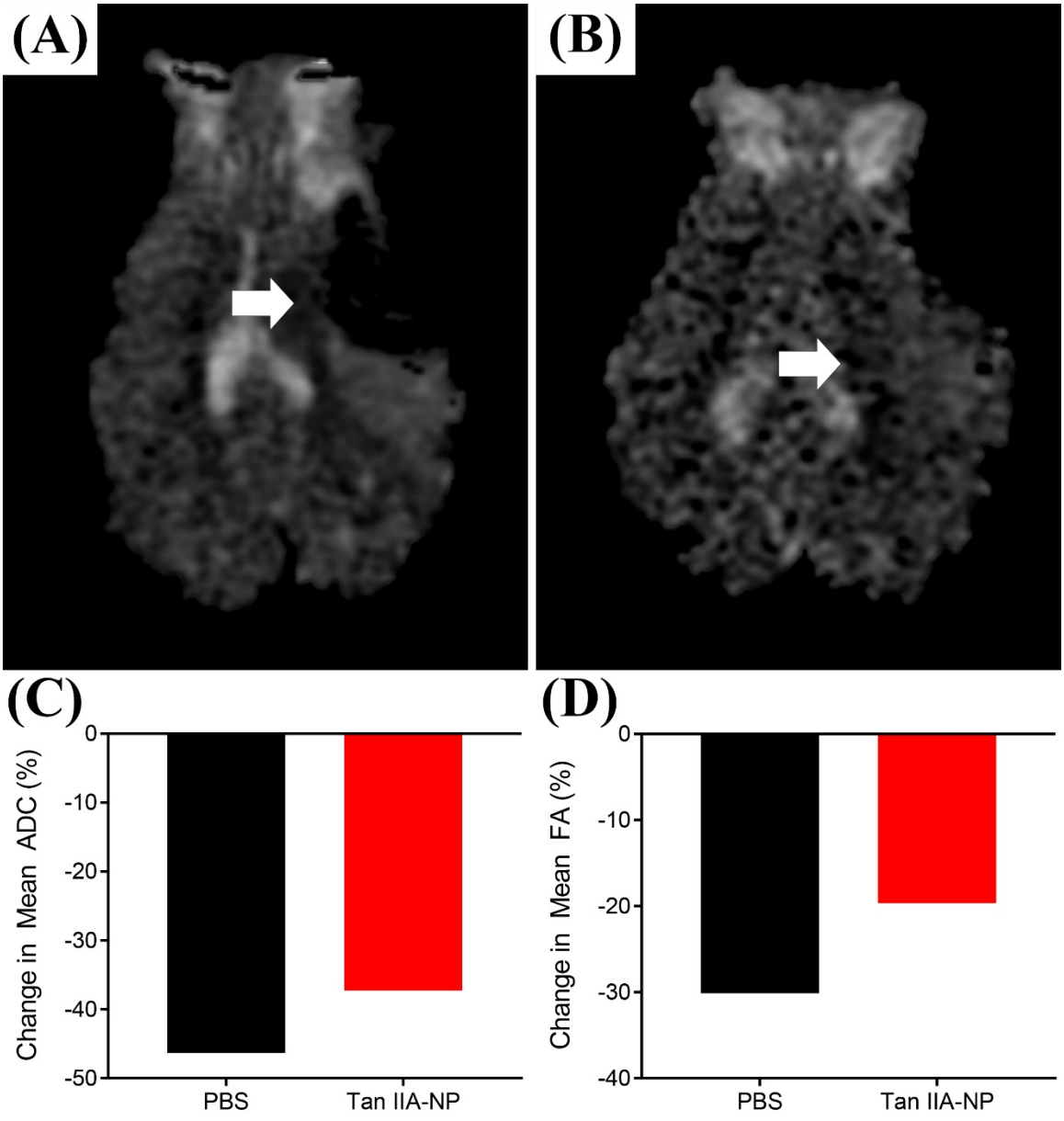
(A)
(B)
(C)
(D)
Change in Mean ADC (%)
0
-10
-20
-30
-40
-50
PBS
Tan IIA-NP
Change in Mean FA (%)
0
-10
-20
-30
-40
PBS
Tan IIA-NP

Figure 5.5: Tan IIA-NPs lead to reduced hemorrhage post-ischemic stroke. T2* sequences showed acute ICH in PBS (**A**) and Tan IIA-NP (**B**) treated pigs 24 hours post-stroke. Tan IIA-NP treated pigs had smaller hemorrhage volumes compared to PBS treated pigs (0.84 vs. 2.90 cm^3, respectively; **C**).

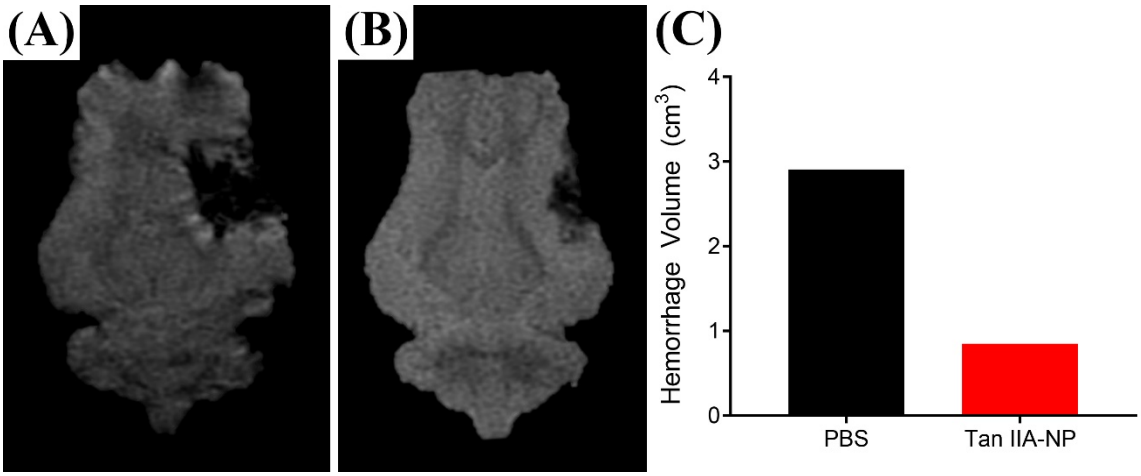
(A)
(B)
(C)
Hemorrhage Volume (cm3)
4
3
2
1
0
PBS
Tan IIA-NP

Figure 5.6: Tan IIA-NPs reduce circulating band neutrophils. Band neutrophil (**A**) and lymphocyte (**C**) populations were determined in blood samples collected pre-stroke, 4, 12, and 24 hours post-stroke. At 12 hours post-stroke the percentage of circulating band neutrophils was lower in Tan IIA-NP treated pigs than in the PBS control pigs (7.75 vs. 14.00 %, respectively; **B**). The percentage of circulating lymphocytes was similar in both treatment groups at all assessed time points (**D**).

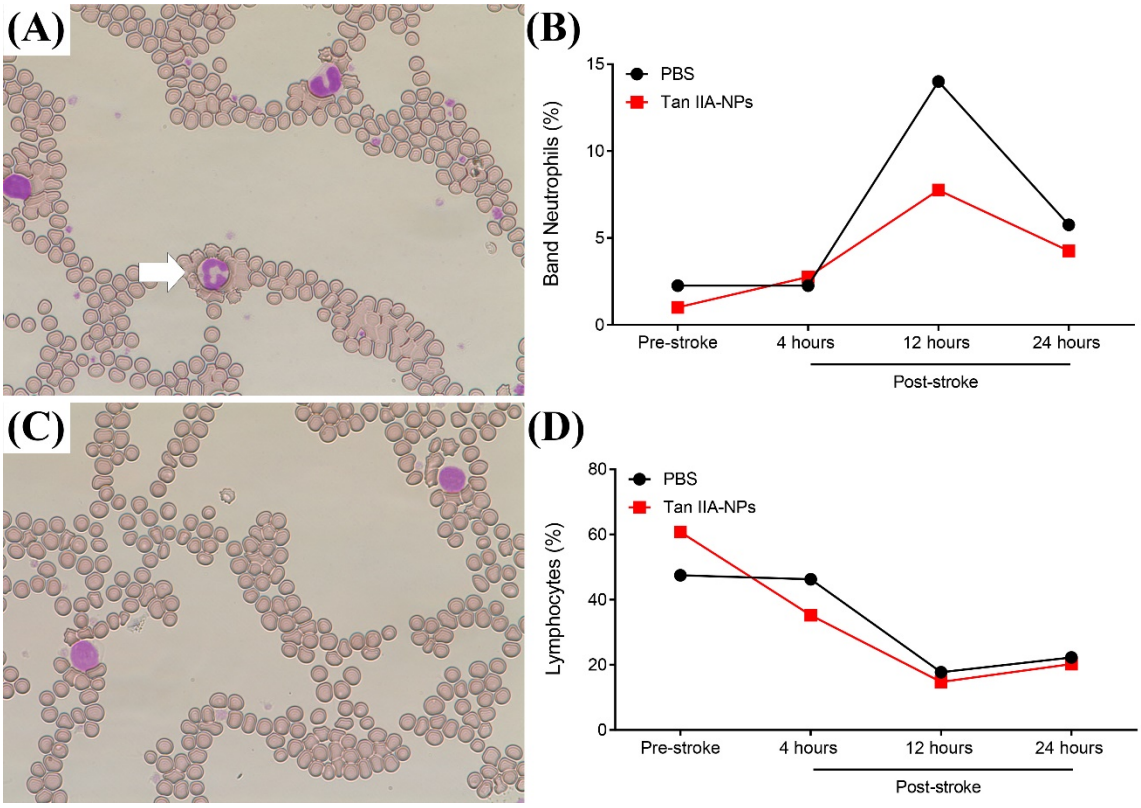
(A)
(B)
PBS
Tan IIA-NPs
Band Neutrophils (%)
15
10
5
0
Pre-stroke
4 hours
12 hours
24 hours
Post-stroke
(C)
(D)
PBS
Tan IIA-NPs
Lymphocytes (%)
80
60
40
20
0
Pre-stroke
4 hours
12 hours
24 hours
Post-stroke

Figure 5.7: Spatiotemporal and kinetic gait deficits are less severe post-stroke in Tan IIA-NP treated pigs. A decrease in the average cadence of the pigs from pre-stroke to post-stroke was more severe in PBS control pigs opposed to Tan IIA-NP treated pigs (133.9-64.8 vs. 135.7-116.9 steps/min, respectively; **A**). The cycle time of the left front limb increased more drastically in PBS control pigs as compared to Tan IIA-NP treated pigs (0.46-0.93 vs. 0.44-0.55 sec, respectively; **B**). The left front step time increased post-stroke in PBS pigs more so than Tan IIA-NP pigs (0.24-0.49 vs. 0.22-0.27 sec, respectively; **C**). The swing percent of cycle decreased more for the left front limb of PBS control pigs than Tan IIA-NP pigs (49.40-33.30 vs. 49.10-43.20 %, respectively; **D**). The left front stride length of pigs treated with PBS displaying a greater reduction in stride length relative to Tan IIA-NP pigs (78.38-63.18 vs. 84.87-77.44 cm, respectively; **E**). A larger decrease in mean pressure of the left front limb was noted for PBS control pigs but not Tan IIA-NP treated pigs (2.93-2.76 vs. 2.87-2.88 AU, respectively; **F**).

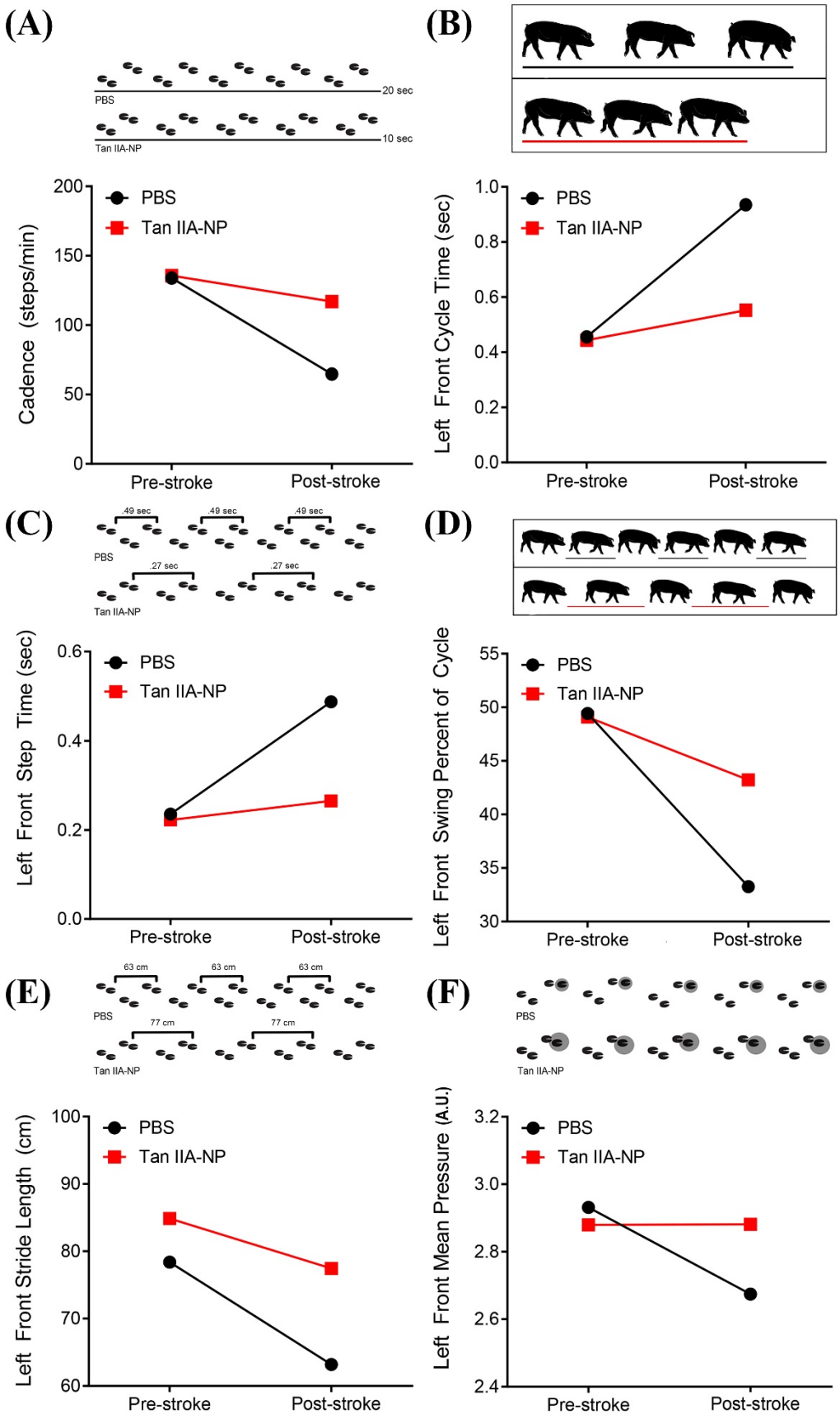
(A)
PBS
20 sec
Tan IIA-NP
10 sec
(B)
Cadence (steps/min)
200
150
100
50
0
PBS
Tan IIA-NP
Pre-stroke
Post-stroke
Left Front Cycle Time (sec)
1.0
0.8
0.6
0.4
0.2
0.0
PBS
Tan IIA-NP
Pre-stroke
Post-stroke
(C)
.49 sec
.49 sec
.49 sec
PBS
.27 sec
.27 sec
Tan IIA-NP
(D)
Left Front Step Time (sec)
0.6
0.4
0.2
0.0
PBS
Tan IIA-NP
Pre-stroke
Post-stroke
Left Front Swing Percent of Cycle
55
50
45
40
35
30
PBS
Tan IIA-NP
Pre-stroke
Post-stroke
(E)
63 cm
63 cm
63 cm
PBS
77 cm
77 cm
Tan IIA-NP
(F)
PBS
Tan IIA-NP
Left Front Stride Length (cm)
100
90
80
70
60
PBS
Tan IIA-NP
Pre-stroke
Post-stroke
Left Front Mean Pressure (A.U.)
3.2
3.0
2.8
2.6
2.4
PBS
Tan IIA-NP
Pre-stroke
Post-stroke

CHAPTER 6

TANSHINONE IIA-LOADED NANOPARTICLES AND INDUCED PLURIPOTENT STEM CELL-DERIVED NEURAL STEM CELL THERAPIES ENHANCE RECOVERY IN A TRANSLATIONAL PIG ISCHEMIC STROKE MODEL[1]

[1]Kaiser, E.E., Waters E.S., Yang, X., Fagan, M.M., Scheulin K.M., Jeon J.H., Shin S.K., Kinder H.A., Kumar, A., Platt S.R., Duberstein K.J., Park H.J., Xie, J., and West, F.D. To be submitted to *Stroke*.

Abstract

Background

Tissue plasminogen activator (tPA) continues to be the gold standard for treatment of ischemic stroke. However, due to the restrictive treatment window and potentially deadly risk factors, clinical application of tPA is limited. Combination therapies, both pharmacological and non-pharmacological, have been hypothesized as a logical approach to enhancing the development of novel stroke therapies. To test this hypothesis, the combined effects of administration of Tanshinone IIA drug-loaded nanoparticles (Tan IIA-NPs) and transplanted induced pluripotent stem cell-derived neural stem cells (iNSCs) were evaluated in a translational pig ischemic stroke model.

Methods

Eighteen male pigs underwent middle cerebral artery occlusion (MCAO) surgery with six pigs randomly assigned to the following treatment groups: PBS+PBS, PBS+iNSC, and iNSC+Tan IIA-NP. PBS or Tan IIA-NPs were administered intracisternally 1-hour post-stroke and either PBS or iNSCs were transcranially transplanted into the parenchyma 5 days post-stroke. Multiparametric magnetic resonance imaging (MRI) was collected at 24 hours post-stroke and 12 weeks post-transplantation.

Results

MRI assessments demonstrated Tan IIA-NP administration reduced lesion and intracerebral hemorrhage volumes and swelling-induced midline shift. Diffusivity within ischemic lesions was also preserved. iNSC transplantation attenuated changes in white matter integrity at chronic time points.

Conclusion

Collectively, Tan IIA-NPs and iNSCs possess significant potential as a multifaceted neuroprotective and regenerative treatment for ischemic stroke patients. The robust preservation of cerebral tissues and associated neural recovery responses to Tan IIA-NP and iNSC therapies in a large animal model with increased predicative value strongly supports the continued evaluation of this novel combination therapy.

Key words Ischemia, Neural stem cells, Tanshinone IIA, Nanoparticles, Pig, Magnetic resonance

Introduction

Projections show that by 2030 an additional 3.4 million Americans will have had a stroke – a 20.5% increase from 2012 [1]. The lack of vital oxygen and nutrients to cerebral tissues results in the destruction of 1.9 million neurons, 14 billion synapses, and 12 kilometers of myelinated fibers each minute a patient goes without treatment [2]. Food and Drug Administration (FDA) approved stroke therapies, tissue plasminogen activator (tPA) and endovascular thrombectomy, are currently available to only a small subpopulation of stroke victims due to short administration windows and associated risk factors [3, 4]. Furthermore, these therapies possess no direct regenerative potentials to enhance the replacement of damaged cerebral tissue and associated improvements in functional recovery [5]. As a result, substantial efforts have been made to develop novel therapeutics that are capable of mitigating cerebral damage through neuroprotectant and regenerative mechanisms. This need prompted the combined therapeutic evaluation of Tanshinone IIA nanoparticles (Tan IIA-NPs) and induced pluripotent stem cell-derived neural stem cells (iNSCs) in a translational pig ischemic stroke model.

One of the most promising therapeutics capable of addressing the need for a regenerative therapy are iNSCs. Recent investigations have shown induced pluripotent stem cells (iPSCs) can be successfully generated from patient somatic cells and differentiated into neural stem cells (iNSCs). This is critical for clinical translation as these autologous cells avoid the need for patient immunosuppression and consequent post-stroke infection susceptibility [6, 7]. Upon transplantation in rodent models of ischemic stroke, iNSCs have been found to differentiate into neural cell types (e.g. neurons and glia), thus serving as a cell replacement therapy while simultaneously producing

synergistic angiogenic (e.g. VEGF) and neuroprotective (e.g. BDNF) factors that promote endogenous repair of the damaged parenchyma [8-10]. Specifically, many of the grafted cells have showed GABA immunoreactivity with mature neuronal electrophysiological properties capable of receiving synaptic input from host neurons [11, 12]. Transplanted cells within the center of the graft also revealed a symmetrical glia-like current-voltage relationship according to whole-cell patch recordings [13]. Collectively, these effects have led to reduced lesion volumes as well as improvements in beam walking, grasping tasks, and Morris water maze performance [14, 15]. Over the years neural stem cell-based therapies have progressed from testing in preclinical models to clinical trials with promising results. In a recent clinical trial, improved neurological function as indicated by NIHSS scores with no adverse outcomes (e.g. immunological response, tumor formation) was demonstrated following engraftment of an immortalized human neural stem cell (NSC) line [16]. In order to provide additional support for the clinical application of stem cell transplantation, further testing of iNSCs therapies are required.

An increasing body of research suggests pretreatment with a neuroprotectant agent may bolster the effectiveness of iNSCs and improve patient outcomes post-stroke [17]. Tanshinone IIA (Tan IIA) is one such potential therapeutic with antioxidant and anti-inflammatory effects post-stroke [18, 19]. Similar to many other neuroprotective therapeutics, administration of Tan IIA has resulted in reduced lesion volumes and improved neurological function in preclinical rodent studies [20-22]. Recent studies have confirmed Tan IIA mediates nerve cell apoptosis by inhibiting caspase-3, caspase-8, and macrophage migration inhibitory factor (MIF) [23-25]. Tang et al. provided evidence Tan IIA may also attenuate blood-brain barrier (BBB) damage through the reduction of matrix

metallopeptidase 9 (MMP-9) expression [26]. Interestingly, these results were replicated in a recent clinical trial in which patients who received both tPA and Tan IIA administration also exhibited significant reductions in MMP-9 [27]. This resulted in ameliorated blood-brain barrier (BBB) damage and excellent functional outcome indicated by a 90-day modified Rankin scale (mRS) scores ≤1. Nanoparticle delivery of Tan IIA with an FDA-approved poly lactic-*co*-glycolic acid (PLGA) nanoparticle (NP) may further improve the therapeutic potential of Tan IIA by increasing its bioavailability and reducing cytotoxicity [28]. The sustained pharmacological release associated with NP biodegradability also reduces drug administration frequencies [29]. By mediating post-stroke inflammatory responses and decreasing levels of endogenous cytotoxicity, pretreatment with Tanshinone IIA nanoparticles (Tan IIA-NPs) may improve iNSC regenerative effects and promote enhanced neurobehavioral and functional recovery in patients.

To increase the translational potential of a Tan IIA and iNSC combination therapy, preclinical testing should be performed in a large animal model of ischemic stroke- such as the pig model. Compared to commonly used rodent models, pigs possess inherent anatomical similarities to humans that directly affect ischemic severity, penumbra evolution, and tissue recovery including gyrification, white to gray matter ratios, and collateral blood flow [30-33]. Comparable cerebral volumes between pigs and humans (~10% larger) also allows for a more direct assessment of Tan IIA and iNSC dosing [34, 35]. These attributes collectively support the use of a preclinical pig model to better predict treatment efficacy and consequent pathophysiological outcomes between rodent studies and clinical trials. Furthermore, comparable body size between pigs and

humans permits the use of clinically relevant magnetic resonance technologies which may provide critical insight into Tan IIA and iNSC mediated tissue-level changes across acute and chronic time points [10, 36, 37].

The objective of this study was to evaluate the therapeutic potential of a Tan IIA-NPs and iNSCs through magnetic resonance imaging (MRI) at 24 hours post-stroke and 12 weeks post-iNSC transplantation. Prior to iNSC transplantation, Tan IIA-NP administration preserved diffusivity and reduced acute lesion volumes. iNSC treatment decreased chronic lesion volumes and preserved white matter (WM). The results demonstrate that a Tan IIA-NP and iNSC transplantation combination therapy possess significant potential as a neuroprotective and cell replacement therapy in a robust gyrencephalic large animal model, thus providing further support for the use of these novel therapies in clinical trials.

Materials and methods

Animals and housing

This study was performed in accordance with the Guide for the Care and Use of Laboratory Animals guidelines and approved by the University of Georgia Institutional Animal Care and Use Committee (Protocol Number: 2017-07-019Y1A0). 9 months old, sexually mature, castrated Yucatan miniature swine 31-41 kg were purchased from the Lonestar™ Laboratory Swine. Pigs were group housed prior to stroke induction in a Public Health Service (PHS) and AAALAC approved facility at a room temperature approximately 27°C with a 12-hour light/dark cycle. Pigs were given access to water and fed standard grower diets with provision of enrichment through daily human contact and toys.

Study design

6 pigs were randomly assigned to each respective treatment group. The sample size for this study was determined by a power calculation based on our routine use of the middle cerebral artery occlusion model with lesion volume changes by MRI imaging being the primary endpoint. The power analysis was calculated using a two-tailed ANOVA test, α=0.05, and an 80% power of detection effect size of 1.19 and a standard deviation of 44.63. This was a randomized study in which 2 pigs were assigned to each surgical and MRI day. All endpoints and functional measurements were prospectively planned and underwent blinded analysis. Predefined exclusion criteria from all endpoints included instances of infection at the incision site, self-inflicted injuries that required euthanasia, inability to thermoregulate, uncontrolled seizure activity, and/or respiratory distress. No outliers were removed from the data.

Synthesis of Poly(lactide-co-glycolide)-b-poly(ethylene glycol)-maleimide (PLGA-b-PEG-OH)

Poly(D,L-lactide-*co*-glycolide)-COOH (PLGA-COOH, 1.0 g, 0.170 mmol, Lactel), poly(ethylene glycol) (OH-PEG-OH, 2.29 g, 0.684 mmol, Sigma Aldrich), and 4-(Dimethylamino)pyridine (DMAP, 0.023 g, 0.187 mmol, Alfa Aesar) were dissolved in 30 mL of anhydrous dichloromethane (CH_2Cl_2). 10 mL CH_2Cl_2 solution of N, N'-Dicyclohexylcarbodiimide (DCC, 0.141 g, 0.684 mmol, Sigma Aldrich) was added dropwise to the reaction mixture at 0°C and continuously stirred with a magnetic stir bar. The reaction mixture was warmed to 23°C and stirred overnight. Insoluble dicyclohexylurea ($C_{13}H_{24}N_2O$) was filtered out. The raw product was precipitated out by adding 50 mL of 50:50 diethyl ether ($(C_2H_5)_2O$) and methanol (CH_3OH) to the reaction

mixture. The mixture was centrifuged for 15 minutes at 4°C. The purification step was repeated 4-5 times, followed by ^{1}H NMR analysis (Varian Mercury Plus 400).

Tanshinone-IIa nanoparticle (Tan-IIa NP) synthesis and characterization

Poly(lactide-*co*-glycolide (PLGA) nanoparticles (NPs) were synthesized through a nanoprecipitation method. Briefly, PLGA-b-PEG-OH was dissolved in dimethylformamide (DMF) at a concentration of 50 mg/mL. A 100 μL of the polymer solution was mixed with Tanshinone-IIa (Tan-IIa, 150 μL, 0.15 mg) for 30 % feeding and diluted with DMF to a final polymer concentration of 5 mg/mL. The mixture was added dropwise to sterilized nanopure water with constant stirring, and the resulting solution was agitated in a fume hood for 2 hours. Tan-IIa NPs were collected on an amicon ultracentrifugation unit (100 kDa cut-off) and were washed 3-4 times with water. Finally, the NPs were resuspended in sterilized nanopure water.

A drop of diluted NP solution was deposited onto a transmission electron microscopy (TEM) grid, followed by staining with 2% uranyl acetate ($UO_2(CH_3COO)$ $2H_2O$). A TEM image was taken on a FEI Tecnai 20 transmission electron microscope operating at an accelerating voltage of 200 kV. Hydrodynamic size and surface charge of NPs were analyzed on a Malvern Zetasizer Nano ZS system.

For drug loading analysis, a 50 μL aqueous solution of NPs was diluted to 900 μL. 100 μL 0.1 mM sodium hydroxide (NaOH) was added to the solution and left at 23°C overnight. Afterwards, the solution was sonicated for 30 minutes and centrifugated at 5000 rpm for 10 minutes. 100 μL supernatant was transferred into a 96-well ultraviolent (UV) transparent plate and its absorbance at 258 nm was measured.

Human Induced Pluripotent Stem Cell-Derived Neural Stem Cells (iNSC) culture

iNSCs were maintained on Matrigel-coated (Corning) tissue culture plates and maintained in neural stem cell media composed of Neurobasal medium (Gibco), 2% B-27 Supplement (Gibco), 1% non-essential amino acids (Gibco) 2 mM L-glutamine (Gibco), 1% penicillin/streptomycin (Gibco), 32 and 20 ng/mL bFGF (R&D Systems). A complete media change was performed every other day. When iNSCs reached confluence, cells were enzymatically passaged using Accutase (Gibco) and removed from the dish using a cell scraper.

Labeling of iNSCs

3 days prior to transplantation, 1.4x107 iNSCs were labeled with 1,1′-dioctadecyl-3,3,3′,3′-tetramethylindotricarbocyanine iodide (DiR) at a concentration of 2 μg/mL diluted in phosphate buffered saline (PBS). After incubation at 37°C for 5 minutes, iNSCs were washed twice with PBS, then washed once with media via centrifugation at 250 x g. Cells were re-plated on Matrigel-coated (Corning) tissue culture treated plates at 7 million cells per 150 mm plate and maintained in neural stem cell media as described above until transplantation day.

Pre-surgical and anesthetic protocol

1 day prior to surgical induction, pigs were administered Excede (5 mg/kg, intramuscular (IM)) and fentanyl (100 mg/kg/hr, transdermal (TD)) for infection prevention and pain management. Pre-induction analgesia and sedation were achieved using xylazine (2 mg/kg, IM) and midazolam (0.2 mg/kg, IM). Anesthesia was induced with intravenous (IV) propofol to effect and 1 mL prophylactic 2% lidocaine topically to the laryngeal folds to facilitate intubation. Lactated ringers solution was administrated as well (5 ml/kg/hour, IV).

Anesthesia was maintained with isoflurane (Abbott Laboratories) in oxygen. Artificial ventilation was maintained at 8-12 breaths per minute with tidal volume of 5–10 ml/kg. Heart rate was monitored by Doppler probe placement on the ventral tail artery while blood pressure was monitored by sphygmomanometer (Riester). Rectal temperature was recorded every 15 minutes using a digital thermometer.

Following surgical procedures, anesthesia was discontinued and pigs were returned to their pens upon extubation and monitored every 15 minutes until vitals including temperature, heart rate, and respiratory rate returned to normal, every 4 hours for 24 hours, and twice a day thereinafter until post-transplantation sutures were removed. Banamine (2.2 mg/kg IM) was administered for post-operative pain, acute inflammation, and fever management every 12 hours for the first 24 hours, and every 24 hours for 3 days post-stroke.

Middle cerebral artery occlusion (MCAO) surgical procedures

As previously described by Platt et al. a right transcranial approach was utilized to access the MCA [36]. Briefly, a curvilinear skin incision enabled the temporal fascia and muscle to be reflected from skin flap. The zygomatic arch was partially resected exposing the ventral aspect of the calvaria. A surgical defect was generated in the calvaria and the visible dura mater was reflected. The arachnoid was opened exposing the distal portion of the MCA for permanent cauterization utilizing bipolar cautery forceps resulting in ischemic infarction. The exposed brain was then covered with a sterile biograft made of porcine small intestine submucosa (MatriStem, ACell) and the temporalis muscle and epidermis were routinely re-apposed.

Tan IIa NP administration

At 1 hour post-stroke, PBS or Tan IIA-NPs were delivered via a 20 gauge, 3.5 or 6” spinal needle inserted through the skin on the midline of the dorsal neck, at an anatomical intersection of a vertical line created by the rostral aspect of the wings of the first vertebral body and a horizontal line connecting the dorsal arch of C2 with the occipital protuberance. Once the needle was through the cutaneous tissues, the stylet was removed and advanced until cerebral spinal fluid (CSF) appeared in the needle hub confirming entry into the cistern. A small volume (3-5 mLs) of CSF was removed while the spinal needle was in place and the volume removed was replaced with PBS or Tan IIA-NPs. The volume of NPs delivered was determined by the NP loading efficiency and each animal received a dose of 133μg/kg Tan IIA.

iNSC transplantation surgical procedures

5 days post-stroke, all pigs received either iNSC treatment or vehicle only PBS transplantation. Pigs were anesthetized according to the aforementioned pre-surgical and anesthetic protocol. Transplantation surgeries were performed as previously described by Baker et al. utilizing a stereotaxic frame (David Kopf Instruments) with pig specific modifications [10]. A mounted quintessential stereotaxic injector (Stoelting Company) was utilized to inject $1.2x10^7$ DiR-labeled iNSCs at a rate of 2 μL/minute to prevent backflow. Immediately prior to injection, approximately 80 μL of iNSCs suspended in PBS or vehicle control were sterilely loaded into a glass micro-pipette syringe with a 26-gauge needle (Hamilton Co, Reno, NV) and attached to the stereotaxic apparatus.

Transplantation depth at the most dorsal aspect of the craniectomy site within the perilesional region was determined by 24-hour post-stroke MRI analysis of each pig. This transplantation depth was equally subdivided into four separate injection depths to permit

the injection of 4 boli, approximately 20 µL each, into both white and gray matter compartments spanning inferior to superior relative to the cortex. After transplantation was complete, the needle retracted at a rate of 1 mm/minute to prevent backflow. Anesthesia was discontinued and the pigs were returned to their pens upon extubation.

Magnetic resonance imaging (MRI) acquisition and analysis

MRI was performed 24 hours post-stroke and 12 weeks post-transplantation on a General Electric 3.0 Tesla MRI system. Pigs were sedated and maintained under anesthesia as previously described for surgical procedures. Following acquisition of 12-week post-transplantation MRI, pigs were not recovered from anesthesia and euthanized via lethal IV injection of euthanasia solution (1mL/10 lbs). MRI of the cranium was performed using an 8-channel torso coil with the pig positioned in supine recumbency. Multiplanar MR brain imaging sequences were acquired including T2Weighted (T2W), T2 Fluid Attenuated Inversion Recovery (T2FLAIR), T2Star (T2*), Diffusion Weighted Imaging (DWI), and Diffusion Tensor Imaging (DTI). Sequences were analyzed using Osirix software. Ischemic stroke was confirmed by comparing corresponding hyperintense regions in T2FLAIR and DWI sequences and hypointense regions in ADC maps.

Hemisphere volume was calculated using T2W sequences for each axial slice by manually outlining the ipsilateral and contralateral hemispheres. The hemisphere areas were multiplied by the slice thickness (3 mm) to obtain total hemisphere volumes. Changes in the ipsilateral hemisphere were expressed as a percentage change relative to the contralateral hemisphere. Lesion volume was calculated using T2W sequences for each axial slice by manually outlining hyperintense ROIs. The area of each ROI was

multiplied by the slice thickness (3 mm) to obtain the total lesion volume and is reported as cm^3.

To control for the space-occupying effect of brain edema, hemisphere volumes were calculated utilizing T2W sequences while lesion volumes were also calculated via ADC maps as previously described by Gerriets et al [38]. Corrected lesion volumes were calculated according to the following formula modified from Loubinoux et al. where LVc and LVu indicate corrected and uncorrected lesion volume, respectively, and HVc and HVi indicate volume of the contralateral and ipsilateral hemisphere, respectively [39].

$$LV^c = HV_C + HV_i - (HV_C + HV_i - LV^u) \cdot \frac{HV_C + HV_i}{2HV_C}$$

Midline shift (MLS) was calculated utilizing T2W sequences for each axial slice by measuring the distance from the natural midline along the anterior and posterior attachments of the falx cerebri to the septum pellucidum. The distance between the exact midpoint of the length of the septum pellucidum and the ideal midline was measured and is reported in mm.

DWI sequences were used to generate ADC maps. ADC values were calculated for each axial slice at a manually drawn region of interest (ROI) that was defined by areas of hypointensity and directly compared to an identical ROI in the contralateral hemisphere. Average ADC values were obtained by calculating the average signal intensity across all slices, while changes in the ipsilateral hemisphere were expressed as a percentage change relative to the contralateral hemisphere and is reported as 10^{-3} mm^2/s.

DTI sequences were utilized to generate fractional anisotropy (FA) maps. FA values were calculated for the internal capsule that was defined by an area of hyperintensity and directly compared to internal capsule in the contralateral hemisphere.

Changes in the ipsilateral internal capsule were expressed as a percentage change relative to the contralateral internal capsule.

Intracerebral hemorrhage (ICH) volume was calculated by manually outlining areas of hypointensity utilizing T2* sequences for each axial slice by manually outlining hypointense ROIs. The area of each ROI was multiplied by the slice thickness (3 mm) to obtain the total ICH volume and is reported as cm^3.

Statistical analysis

All quantitative data was analyzed with SAS version 9.3 (Cary, NC). Statistical significances between groups were determined by one-way analysis of variance (ANOVA) and post-hoc Tukey-Kramer Pair-Wise comparisons with p-values ≤ 0.05 considered significantly different.

Results

Tan IIA-NP+iNSC treatment decreased chronic lesion volume and consequential MLS.

T2W sequences revealed significantly ($p<0.05$) reduced hyperintense lesion volumes in Tan IIA-NP+iNSC treated pigs when compared to PBS+iNSC and PBS+PBS control pigs 24 hours post-stroke (7.34±1.27 vs. 14.71±1.23 and 13.07±1.12 cm^3 respectively; **Figure 6.1A-C,** white arrows, **6.1D**). As iNSCs were not transplanted until day 5, this suggests that Tan IIA-NP nanoparticles have a significant therapeutic effect. At 12 weeks post-transplantation, Tan IIA-NP+iNSC treated pigs exhibited significantly ($p<0.01$) reduced lesion volumes compared to PBS+PBS control pigs (2.35±0.66 vs. 5.68±0.53 cm^3 respectively; **Figure 6.1E-G,** white arrows, **6.1D**). All treatment groups demonstrated significantly ($p<0.05$) reduced lesion volumes at 12 weeks post-

transplantation relative to 24 hours post-stroke (5.68±0.53 vs. 13.07±1.12; 3.40±0.65 vs. 14.72±1.23; 2.35±0.66 vs. 7.34±1.27 cm^3 respectively; **Figure 6.1D**).

Although Tan IIA-NP administration at 24 hours post-stroke had no significant effect on MLS (**Figure 6.1A-C**, red lines, **6.1H**), T2W imaging results indicated significantly ($p<0.01$) reduced MLS in Tan IIA-NP+iNSC treated pigs relative to PBS+PBS control pigs 12 weeks post-transplantation (0.81±0.21 vs. 2.60±0.42 mm respectively) suggesting reduced tissue atrophy in the affected ipsilateral hemisphere (**Figure 6.1E-G,** red lines**, 6.1H**). Tan IIA-NP+iNSC and PBS+iNSC treated pigs also exhibited significant ($p<0.05$) changes between time points (0.81±0.21 vs. 1.99±0.29 mm; 1.31±0.28 vs. 1.99±0.29 mm respectively; **Figure 6.1H**).

Tan IIA-NPs preserved diffusivity and reduced edema-corrected lesion volumes.

Cerebral diffusivity was evaluated utilizing DWI sequences and derived ADC maps. Signal void, consistent with restricted diffusion and indicative of cytotoxic edema was quantified (**Figure 6.2A-C**, white arrows). Mean ADC values in the affected ipsilateral hemisphere were compared to the contralateral hemisphere with calculated percent changes closer to zero being more similar to normal tissue. Tan IIA-NP+iNSC treated pigs exhibited a significantly ($p<0.05$) reduced percent change in ADC values when compared to PBS+iNSC and PBS+PBS control pigs 24 hours post-stroke (-17.11±2.90 vs. -41.81±4.94 and 31.58±3.43 % respectively; **Figure 6.2D**). To account for the space-occupying effect of brain edema, edema-corrected lesion volumes (LVc) were calculated utilizing to ADC maps revealing a significant ($p<0.05$) decrease in LVc in Tan IIA-NP+iNSC treated pigs when compared to controls (2.11±0.76 vs. 7.39±1.74 and 7.17±0.76 cm^3 respectively, **Figure 6.2E**).

iNSCs prevented chronic WM degradation.

To assess long-term changes in WM integrity, the internal capsules were examined 24 hours post-stroke and 12 weeks post-transplantation. Changes in fractional anisotropy (FA) in the affected ipsilateral internal capsule were compared to the contralateral internal capsule with similar percent increases in FA values being observed between treatment groups 24 hours post-stroke (**Figure 6.3A-C,** white arrows, **6.3D**). At 12 weeks post-transplantation, Tan IIA-NP+iNSC and PBS+iNSC treated pigs exhibited a lower percent decrease in FA values compared to PBS+PBS control pigs with trending ($p=0.1$) differences between Tan IIA-NP+iNSC and PBS+PBS control pigs (**Figure 6.3E-G,** white arrows**, 6.3D**). Although PBS+iNSC treated pigs exhibited the greatest percent change in FA values at 24 hours post-stroke, they show comparable FA values to Tan IIA-NP+iNSC treated pigs 12 weeks post-transplantation. This suggests iNSC transplantation may help prevent WM degradation following ischemic injury. This hypothesis is reinforced as PBS+PBS control pigs demonstrated a significant ($p<0.01$) difference in percent change between time points (-42.25±4.31 vs. 23.01±2.96 %, respectively; **Figure 6.3D)** whereas Tan IIA-NP+iNSC and PBS+iNSC treated pigs did not.

Tan IIA-NPs mitigated acute ICH volumes.

Acute ICH was observed via hypointense abnormalities on T2* sequences 24 hours post-stroke (**Figure 6.4A-C**, white arrows). The occurrence of ICH was significantly reduced in Tan IIA-NP+iNSC treated pigs relative to PBS+PBS control pigs (0.73±0.15 vs. 1.52±0.12 cm^3 respectively, **Figure 6.4D**). These results suggest Tan IIA-NPs may help reduce ICH volumes during the acute phase post-stroke. Collectively, these MRI based results offer compelling evidence Tan IIA and iNSC treatments provided neuroprotection

and promoted tissue level recovery by decreasing lesion and ICH volumes, consequent MLS while also preserving diffusivity and WM integrity.

Discussion

This pivotal study presents the first experimental evidence that intracisternal administration of Tan IIA-NPs and intraparenchymal transplantation of iNSCs improved MRI tissue-level outcomes in a translational pig ischemic stroke model. These therapies attenuated tissue degradation and promoted neural recovery processes as seen through reductions in lesion volumes, MLS, WM damage, and ICH; critical predicative indicators of patient prognosis due to the high correlation between neurological deficits and functional outcomes [40-43]. Consequently, these results suggested Tan IIA-NP and iNSC intervention could be a potent therapeutic for patients with ischemic stroke.

Delivering therapeutic compounds to target tissues is a major challenge in the treatment of stroke. To potentially improve Tan IIA's pharmacological responses, Tan IIA was encapsulated into PLGA-PEG NPs. This nano-delivery platform protects drugs from rapid degradation and enhances drug concentration in target tissues [44]. Furthermore, physiochemical and biological properties of NPs permit increased cellular uptake when compared to free-form larger molecules [45]. These properties could therefore induce controlled, extended release of Tan IIA that may result in prolonged anti-inflammatory and antioxidative effects while reducing potential cytotoxicity. Intracisternal injection of Tan IIA-NPs into the subarachnoid space rather than IV eliminates filtering by peripheral organs and allows for the administration of lower Tan IIA doses (10-30 mg/kg intraperitoneal in rodents vs. 0.133 mg/kg intracisternal in pigs) and decreased dosage frequency [22, 26]. Intracisternal injection also bypasses the BBB that would otherwise prevent

the delivery of therapeutics to ischemic areas. NP delivery and intracisternal administration of Tan IIA was well tolerated by pigs and represents a novel approach in drug delivery.

A frequently utilized predictor of patient prognosis is acute lesion volumes due to the high correlation between functional outcomes and neurological deficits [40, 41, 46, 47]. Here, acute treatment with Tan IIA-NPs demonstrated potential in mitigating these clinical outcomes by significantly decreasing T2W and edema-corrected lesion volumes at acute and chronic time points which was not observed in pig stroke studies with iNSC transplantation alone [10]. In similar rodent studies, Tan IIA treatment resulted in significantly reduced lesion volumes in the striatum and lateral cortex [20, 26]. Tang et al. further compared the effect of Tan IIA administration times on lesion volumes reporting 1- and 4-hour post-stroke delivery of Tan IIA resulted in the greatest reduction in lesion volumes [25]. Similar to human correlations between lesion volumes and functional outcomes, additional studies have indicated the neuroprotective effect of Tan IIA in cerebral ischemia-reperfusion rodent models leads to significantly improved neurobehavior scores [22, 48]. Reduced rodent lesion volumes were also accompanied by decreased motor function deficits including extension of the forepaw, circling, and imbalanced walking/righting reflexes following Tan IIA administration [20, 25].

ICH and diffusivity also possess prognostic value with increased hemorrhage volumes and decreased ADC values being closely associated with early neurological deterioration and a significant increase in mortality rates 90 days post-ischemia [49-52]. In the current study, T2* and DWI sequences showed reduced ICH and preserved diffusivity in Tan IIA-NP treated pigs 24 hours post-stroke. In zebrafish, Tan IIA effectively reduced the occurrence and area of cerebral hemorrhage while restoring motor function impairments in

a dose dependent manner [53]. Comparatively, Tan IIA administration in rodents successfully maintained vascular integrity observed through increased vessel wall thickness relative to control animals [54]. Reduced changes in diffusivity observed in this study corresponded with previous Tan IIA studies in rodent models presenting evidence of improved cerebral blood flow, increased anti-oxygen radical and anti-inflammatory activities, and decreased infarcted brain tissue [20, 25]. Liu et al. credited Tan IIA's influence on the TORC1 signal pathway for reductions in brain water content [22]. This signaling pathway has also been found to influence protein synthesis, cell growth, and neurotransmission and thus remains a potential therapeutic target for ischemic cerebrovascular diseases [55, 56].

Tan IIA effects in reducing post-stroke tissue damage may be in part due to its capabilities in ameliorating blood-brain barrier (BBB) damage. In humans, disruption of the BBB occurs within hours of ischemic onset followed by an increase in matrix metallopeptidase (MMP)-9 levels, edema formation, and hemorrhagic transformation within 24-72 hours [57, 58]. Likewise, elevated levels of MMPs following transient ischemia in rodents resulted in the degradation of tight junction proteins, claudin-5 and occludin, that are integral components of the BBB [59]. Interestingly, Tan IIA-NP treated pigs demonstrated reductions in cytotoxic edema and ICH 24 hours post-stroke, thus suggesting BBB breakdown may be somewhat preserved in these animals. Tang et al. reported Tan IIA administration mediated BBB breakdown by significantly decreasing MMP-9 levels while restoring occludin expression in a dose-dependent manner [26]. Wang et al. also demonstrated reduced BBB leakage in Tan IIA treated animals was associated with significant increases in the presence of claudin-5 [48]. Patients who received tPA and daily

IV injections of Tan IIA exhibited ameliorated BBB damage with significant differences in claudin-5 and MMP-9 expression and impressive functional outcomes as indicated by 90-day modified Rankin scale (mRS) scores ≤1 when compared to the placebo group [27]. Tan IIA's protective effects in multiple species demonstrates increased BBB stability and remains an important treatment target that should be further investigated.

Although it has been shown that Tan IIA possess antioxidant and anti-inflammatory neuroprotective effects, chronic reductions in WM damage and MLS in iNSC treated pigs suggests iNSCs are a critical component of neural recovery as treatment effects were greater in PBS+iNSC and Tan IIA+iNSC groups 12 weeks post-transplantation [25, 60]. Disruption of WM axonal bundles often leads to cognitive, behavioral, and motor dysfunctions, thus studying stroke induced WM changes in a model with comparable WM volumes is critically important for the testing of novel therapeutics [32]. In a similar study by Baker et al., transplantation of iNSCs resulted in significant improvements in pig FA values 12 weeks post-transplantation [10]. Human neural stem cells transplanted into chronic stroke patients also resulted in increased FA values [16]. Rodent research endeavors aimed at further understanding WM repair processes found transplantation of stem cells enhanced WM reorganization and connectivity through increased myelination, WM bundle thickness, and axonal sprouting within ischemic tissues [61-63]. Reductions in tissue atrophy and consequent MLS suggested iNSC treatment also enhanced cellular survival. Neurotrophic factors meditated by iNSCs may induce tissue recovery through the expression of BDNF, GDNF, and NTF3 which have been shown to protect neurons from ischemic injury in both small and large animal models [10, 64, 65]. Acute treatment with Tan IIA may also supplement neuronal survival by inhibiting NF-κB binding activity

through the suppression of the NF-κB inducing kinase-IκB kinase (NIK–IKK) pathway [48]. Recent research suggested persistent activation of the NF-κB complex rendered neurons vulnerable to ischemic insult and attenuation of this activation by Tan IIA provided a potential mechanism that explained the anti-inflammatory and neuroprotective activity of Tan IIA [24, 66]. Collectively, these longitudinal effects of combined Tan IIA-NP and iNSC treatment warrants further investigation.

Conclusion

For the first time, this study demonstrated administration of Tan IIA-NPs and iNSCs mitigated ischemic injury responses, thus leading to improved tissue recovery in a translational pig ischemic stroke model. Acute Tan IIA-NP macro-level changes were mechanistically supported by iNSC cellular level changes, resulting in multifaceted effects including decreased lesion and ICH volumes, preserved diffusivity, and attenuated WM damage and MLS. These findings collectively support the continued investigation of this novel combination therapy for translation into human clinical trials.

Acknowledgments

The authors would like to thank Savannah Cheek, RVT, Brandy Winkler, and our team of undergraduate researchers who were involved in various aspects of surgeries, post-operative care, MRI acquisition, pig gait/behavioral testing, and data analysis. We would also like to thank the University of Georgia Animal Resources team for veterinary care and expertise.

Funding

This work was supported by the National Institutes of Health, National Institute of Neurological Disorders and Stroke grant R01NS093314. The funders had no role in study

design, data collection and analysis, decision to publish, or preparation of the manuscript.

Disclosures

The authors declare that they have no disclosures to report.

References

1. Mackay J, Mensah GA, Mendis S, Greenlund K, World Health Organization. *The atlas of heart disease and stroke*. Geneva: World Health Organization; 2004.

2. Saver JL. Time is brain--quantified. *Stroke*. 2006;37:263-266

3. Balami JS, White PM, McMeekin PJ, Ford GA, Buchan AM. Complications of endovascular treatment for acute ischemic stroke: Prevention and management. *Int J Stroke*. 2018;13:348-361

4. Gravanis I, Tsirka SE. Tissue-type plasminogen activator as a therapeutic target in stroke. *Expert Opin Ther Targets*. 2008;12:159-170

5. Paul CL, Ryan A, Rose S, Attia JR, Kerr E, Koller C, et al. How can we improve stroke thrombolysis rates? A review of health system factors and approaches associated with thrombolysis administration rates in acute stroke care. *Implement Sci*. 2016;11:51

6. Amabile G, Meissner A. Induced pluripotent stem cells: Current progress and potential for regenerative medicine. *Trends Mol Med*. 2009;15:59-68

7. Santos Samary C, Pelosi P, Leme Silva P, Rieken Macedo Rocco P. Immunomodulation after ischemic stroke: Potential mechanisms and implications for therapy. *Crit Care*. 2016;20:391

8. Polentes J, Jendelova P, Cailleret M, Braun H, Romanyuk N, Tropel P, et al. Human induced pluripotent stem cells improve stroke outcome and reduce secondary degeneration in the recipient brain. *Cell Transplant*. 2012;21:2587-2602

9. Laterza C, Uoshima N, Tornero D, Wilhelmsson U, Stokowska A, Ge R, et al. Attenuation of reactive gliosis in stroke-injured mouse brain does not affect neurogenesis from grafted human ipsc-derived neural progenitors. *PLoS One*. 2018;13:e0192118

10. Baker EW, Platt SR, Lau VW, Grace HE, Holmes SP, Wang L, et al. Induced pluripotent stem cell-derived neural stem cell therapy enhances recovery in an ischemic stroke pig model. *Sci Rep*. 2017;7:10075

11. Oki K, Tatarishvili J, Wood J, Koch P, Wattananit S, Mine Y, et al. Human-induced pluripotent stem cells form functional neurons and improve recovery after grafting in stroke-damaged brain. *Stem Cells*. 2012;30:1120-1133

12. Daadi MM, Li Z, Arac A, Grueter BA, Sofilos M, Malenka RC, et al. Molecular and magnetic resonance imaging of human embryonic stem cell-derived neural stem cell grafts in ischemic rat brain. *Mol Ther*. 2009;17:1282-1291

13. Hemmer K, Zhang M, van Wullen T, Sakalem M, Tapia N, Baumuratov A, et al. Induced neural stem cells achieve long-term survival and functional integration in the adult mouse brain. *Stem Cell Reports*. 2014;3:423-431

14. Jensen MB, Yan H, Krishnaney-Davison R, Al Sawaf A, Zhang SC. Survival and differentiation of transplanted neural stem cells derived from human induced pluripotent stem cells in a rat stroke model. *J Stroke Cerebrovasc Dis*. 2013;22:304-308

15. Yuan T, Liao W, Feng NH, Lou YL, Niu X, Zhang AJ, et al. Human induced pluripotent stem cell-derived neural stem cells survive, migrate, differentiate, and improve neurologic function in a rat model of middle cerebral artery occlusion. *Stem Cell Res Ther*. 2013;4:73

16. Kalladka D, Sinden J, Pollock K, Haig C, McLean J, Smith W, et al. Human neural stem cells in patients with chronic ischaemic stroke (pisces): A phase 1, first-in-man study. *Lancet*. 2016;388:787-796

17. Dwaine F. Emerich GO. *Cell therapy: Current status and future directions*. Springer; 2017.

18. Han JY, Fan JY, Horie Y, Miura S, Cui DH, Ishii H, et al. Ameliorating effects of compounds derived from salvia miltiorrhiza root extract on microcirculatory disturbance and target organ injury by ischemia and reperfusion. *Pharmacol Ther*. 2008;117:280-295

19. Chen HS, Qi SH, Shen JG. One-compound-multi-target: Combination prospect of natural compounds with thrombolytic therapy in acute ischemic stroke. *Curr Neuropharmacol*. 2017;15:134-156

20. Lam BY, Lo AC, Sun X, Luo HW, Chung SK, Sucher NJ. Neuroprotective effects of tanshinones in transient focal cerebral ischemia in mice. *Phytomedicine*. 2003;10:286-291

21. Xia WJ, Yang M, Fok TF, Li K, Chan WY, Ng PC, et al. Partial neuroprotective effect of pretreatment with tanshinone iia on neonatal hypoxia-ischemia brain damage. *Pediatr Res*. 2005;58:784-790

22. Liu L, Zhang X, Wang L, Yang R, Cui L, Li M, et al. The neuroprotective effects of tanshinone iia are associated with induced nuclear translocation of torc1 and upregulated expression of torc1, pcreb and bdnf in the acute stage of ischemic stroke. *Brain Res Bull*. 2010;82:228-233

23. Zhoua L, Bondy, SC, .Jian, L, Wen, P, Yang, F, Luo, H, Li, W, Zhou, J. Tanshinone iia attenuates the cerebral ischemic injury-induced increase in levels of gfap and of caspases-3 and -8. *Neuroscience*. 2015;288:105-111

24. Chen Y, Wu X, Yu S, Lin X, Wu J, Li L, et al. Neuroprotection of tanshinone iia against cerebral ischemia/reperfusion injury through inhibition of macrophage migration inhibitory factor in rats. *PLoS One*. 2012;7:e40165

25. Tang Q, Han R, Xiao H, Li J, Shen J, Luo Q. Protective effect of tanshinone iia on the brain and its therapeutic time window in rat models of cerebral ischemia-reperfusion. *Exp Ther Med*. 2014;8:1616-1622

26. Tang C, Xue H, Bai C, Fu R, Wu A. The effects of tanshinone iia on blood-brain barrier and brain edema after transient middle cerebral artery occlusion in rats. *Phytomedicine*. 2010;17:1145-1149

27. Ji B, Zhou F, Han L, Yang J, Fan H, Li S, et al. Sodium tanshinone iia sulfonate enhances effectiveness rt-pa treatment in acute ischemic stroke patients associated with ameliorating blood-brain barrier damage. *Transl Stroke Res*. 2017;8:334-340

28. Locatelli E, Comes Franchini M. Biodegradable plga-b-peg polymeric nanoparticles: Synthesis, properties, and nanomedical applications as drug delivery system. *Journal of Nanoparticle Research*. 2012;14

29. Govender T, Stolnik S, Garnett MC, Illum L, Davis SS. Plga nanoparticles prepared by nanoprecipitation: Drug loading and release studies of a water soluble drug. *J Control Release*. 1999;57:171-185

30. Gralla J, Schroth G, Remonda L, Fleischmann A, Fandino J, Slotboom J, et al. A dedicated animal model for mechanical thrombectomy in acute stroke. *AJNR Am J Neuroradiol*. 2006;27:1357-1361

31. Kobayashi E, Hishikawa S, Teratani T, Lefor AT. The pig as a model for translational research: Overview of porcine animal models at jichi medical university. *Transplant Res*. 2012;1:8

32. Ahmad AS, Satriotomo I, Fazal J, Nadeau SE, Dore S. Considerations for the optimization of induced white matter injury preclinical models. *Front Neurol*. 2015;6:172

33. Meng S, Qiao M, Foniok T, Tuor UI. White matter damage precedes that in gray matter despite similar magnetic resonance imaging changes following cerebral hypoxia-ischemia in neonatal rats. *Exp Brain Res*. 2005;166:56-60

34. Conrad MS, Dilger RN, Johnson RW. Brain growth of the domestic pig (sus scrofa) from 2 to 24 weeks of age: A longitudinal mri study. *Dev Neurosci*. 2012;34:291-298

35. Allen JS, Damasio H, Grabowski TJ. Normal neuroanatomical variation in the human brain: An mri-volumetric study. *Am J Phys Anthropol*. 2002;118:341-358

36. Platt SR, Holmes SP, Howerth EW, Duberstein KJ, Dove CR, Kinder HA, et al. Development and characterization of a yucatan miniature biomedical pig permanent middle cerebral artery occlusion stroke model. *Exp Transl Stroke Med*. 2014;6:5

37. Webb RL, Kaiser EE, Jurgielewicz BJ, Spellicy S, Scoville SL, Thompson TA, et al. Human neural stem cell extracellular vesicles improve recovery in a porcine model of ischemic stroke. *Stroke*. 2018;49:1248-1256

38. Gerriets T, Stolz E, Walberer M, Muller C, Kluge A, Bachmann A, et al. Noninvasive quantification of brain edema and the space-occupying effect in rat stroke models using magnetic resonance imaging. *Stroke*. 2004;35:566-571

39. Loubinoux I, Volk A, Borredon J, Guirimand S, Tiffon B, Seylaz J, et al. Spreading of vasogenic edema and cytotoxic edema assessed by quantitative diffusion and t2 magnetic resonance imaging. *Stroke*. 1997;28:419-426; discussion 426-417

40. Huisa BN, Neil WP, Schrader R, Maya M, Pereira B, Bruce NT, et al. Clinical use of computed tomographic perfusion for the diagnosis and prediction of lesion growth in acute ischemic stroke. *J Stroke Cerebrovasc Dis*. 2014;23:114-122

41. Schiemanck SK, Kwakkel G, Post MW, Prevo AJ. Predictive value of ischemic lesion volume assessed with magnetic resonance imaging for neurological deficits and functional outcome poststroke: A critical review of the literature. *Neurorehabil Neural Repair*. 2006;20:492-502

42. Falcao AL, Reutens DC, Markus R, Koga M, Read SJ, Tochon-Danguy H, et al. The resistance to ischemia of white and gray matter after stroke. *Ann Neurol*. 2004;56:695-701

43. Berrouschot J, Sterker M, Bettin S, Koster J, Schneider D. Mortality of space-occupying ('malignant') middle cerebral artery infarction under conservative intensive care. *Intensive Care Med*. 1998;24:620-623

44. Nevozhay D, Kanska U, Budzynska R, Boratynski J. [current status of research on conjugates and related drug delivery systems in the treatment of cancer and other diseases]. *Postepy Hig Med Dosw (Online)*. 2007;61:350-360

45. Suri SS, Fenniri H, Singh B. Nanotechnology-based drug delivery systems. *J Occup Med Toxicol*. 2007;2:16

46. Borsody M, Warner Gargano J, Reeves M, Jacobs B, Group MI-SS. Infarction involving the insula and risk of mortality after stroke. *Cerebrovasc Dis*. 2009;27:564-571

47. Tong DC, Yenari MA, Albers GW, O'Brien M, Marks MP, Moseley ME. Correlation of perfusion- and diffusion-weighted mri with nihss score in acute (<6.5 hour) ischemic stroke. *Neurology*. 1998;50:864-870

48. Wang L, Zhang X, Liu L, Cui L, Yang R, Li M, et al. Tanshinone ii a down-regulates hmgb1, rage, tlr4, nf-kappab expression, ameliorates bbb permeability and endothelial cell function, and protects rat brains against focal ischemia. *Brain Res*. 2010;1321:143-151

49. Fiehler J, Knudsen K, Kucinski T, Kidwell CS, Alger JR, Thomalla G, et al. Predictors of apparent diffusion coefficient normalization in stroke patients. *Stroke*. 2004;35:514-519

50. Terruso V, D'Amelio M, Di Benedetto N, Lupo I, Saia V, Famoso G, et al. Frequency and determinants for hemorrhagic transformation of cerebral infarction. *Neuroepidemiology*. 2009;33:261-265

51. D'Amelio M, Terruso V, Famoso G, Di Benedetto N, Realmuto S, Valentino F, et al. Early and late mortality of spontaneous hemorrhagic transformation of ischemic stroke. *J Stroke Cerebrovasc Dis*. 2014;23:649-654

52. Fiorelli M, Bastianello S, von Kummer R, del Zoppo GJ, Larrue V, Lesaffre E, et al. Hemorrhagic transformation within 36 hours of a cerebral infarct: Relationships with early clinical deterioration and 3-month outcome in the european cooperative acute stroke study i (ecass i) cohort. *Stroke*. 1999;30:2280-2284

53. Zhou ZY, Huang B, Li S, Huang XH, Tang JY, Kwan YW, et al. Sodium tanshinone iia sulfonate promotes endothelial integrity via regulating ve-cadherin

dynamics and rhoa/rock-mediated cellular contractility and prevents atorvastatin-induced intracerebral hemorrhage in zebrafish. *Toxicol Appl Pharmacol*. 2018;350:32-42

54. Ma J, Hou D, Wei Z, Zhu J, Lu H, Li Z, et al. Tanshinone iia attenuates cerebral aneurysm formation by inhibiting the nfkappabmediated inflammatory response. *Mol Med Rep*. 2019;20:1621-1628

55. Xie R, Wang P, Ji X, Zhao H. Ischemic post-conditioning facilitates brain recovery after stroke by promoting akt/mtor activity in nude rats. *J Neurochem*. 2013;127:723-732

56. Pastor MD, Garcia-Yebenes I, Fradejas N, Perez-Ortiz JM, Mora-Lee S, Tranque P, et al. Mtor/s6 kinase pathway contributes to astrocyte survival during ischemia. *J Biol Chem*. 2009;284:22067-22078

57. Fishman RA. Brain edema. *N Engl J Med*. 1975;293:706-711

58. Montaner J, Alvarez-Sabin J, Molina C, Angles A, Abilleira S, Arenillas J, et al. Matrix metalloproteinase expression after human cardioembolic stroke: Temporal profile and relation to neurological impairment. *Stroke*. 2001;32:1759-1766

59. Yang Y, Estrada EY, Thompson JF, Liu W, Rosenberg GA. Matrix metalloproteinase-mediated disruption of tight junction proteins in cerebral vessels is reversed by synthetic matrix metalloproteinase inhibitor in focal ischemia in rat. *J Cereb Blood Flow Metab*. 2007;27:697-709

60. Danshen in ischemic stroke. *Chin Med J (Engl)*. 1977;3:224-226

61. Jiang Q, Zhang ZG, Ding GL, Silver B, Zhang L, Meng H, et al. Mri detects white matter reorganization after neural progenitor cell treatment of stroke. *Neuroimage*. 2006;32:1080-1089

62. van Velthoven CT, Dzietko M, Wendland MF, Derugin N, Faustino J, Heijnen CJ, et al. Mesenchymal stem cells attenuate mri-identifiable injury, protect white matter, and improve long-term functional outcomes after neonatal focal stroke in rats. *J Neurosci Res*. 2017;95:1225-1236

63. van Velthoven CT, Sheldon RA, Kavelaars A, Derugin N, Vexler ZS, Willemen HL, et al. Mesenchymal stem cell transplantation attenuates brain injury after neonatal stroke. *Stroke*. 2013;44:1426-1432

64. Cheng B, Mattson MP. Nt-3 and bdnf protect cns neurons against metabolic/excitotoxic insults. *Brain Res*. 1994;640:56-67

65. Wang Y, Lin SZ, Chiou AL, Williams LR, Hoffer BJ. Glial cell line-derived neurotrophic factor protects against ischemia-induced injury in the cerebral cortex. *J Neurosci*. 1997;17:4341-4348

66. Jang SI, Kim HJ, Kim YJ, Jeong SI, You YO. Tanshinone iia inhibits lps-induced nf-kappab activation in raw 264.7 cells: Possible involvement of the nik-ikk, erk1/2, p38 and jnk pathways. *Eur J Pharmacol*. 2006;542:1-7

Figure 6.1: Tan IIA-NP+iNSC treatment decreased lesion volume and consequential MLS. Tan IIA-NP+iNSC treated pigs exhibited a significant decrease in hyperintense lesion volumes when compared to PBS+iNSC and PBS+PBS groups at 24 hours (24 HPS) post-stroke (**A-C**, white arrows, **D**) and compared to PBS+PBS control pigs at 12 weeks post-transplantation (12 WPT) (**E&G**, white arrows, **D**). All treatment groups possessed significantly reduced lesion volumes compared to 24 hours post-stroke values (**D**). Tan IIA-NP+iNSC treated pigs demonstrated a significantly less pronounced MLS 12 weeks post-transplantation compared to PBS+PBS control pigs (**E&G**, red lines, **H**) while Tan IIA-NP+iNSC and PBS+iNSC treated pigs also exhibited significant changes between time points (0.81±0.21 vs. 1.99±0.29 mm; 1.31±0.28 vs. 1.99±0.29 mm respectively; **H**). * indicates significant difference between treatment groups; # indicates significant difference between time points.

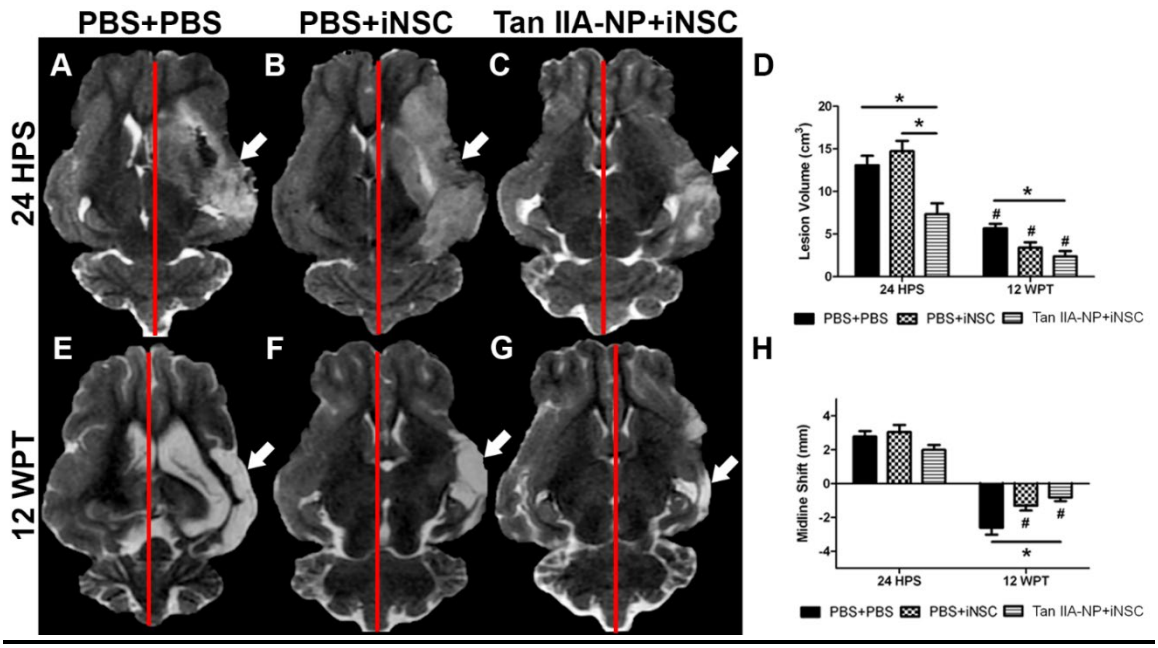
PBS+PBS
PBS+iNSC
Tan IIA-NP+iNSC
24 HPS
12 WPT
A
B
C
D
E
F
G
H
Lesion Volume (cm3)
20
15
10
5
0
*
*
*
#
#
#
24 HPS
12 WPT
PBS+PBS
PBS+iNSC
Tan IIA-NP+iNSC
Midline Shift (mm)
4
2
0
-2
-4
#
#
*
24 HPS
12 WPT
PBS+PBS
PBS+iNSC
Tan IIA-NP+iNSC

Figure 6.2: Tan IIA-NP+iNSC treatment preserved diffusivity and reduced edema-corrected lesion volumes. Tan IIA-NP+iNSC treated pigs exhibited significant conservation of diffusivity 24 HPS relative to PBS+iNSC and PBS+PBS control pigs (**A-D**, white arrows). Tan IIA-NP+iNSC treated pigs also demonstrated a significant decrease in LVc in when compared to control groups 24 hours post-stroke (**E**). * indicates significant difference between treatment groups.

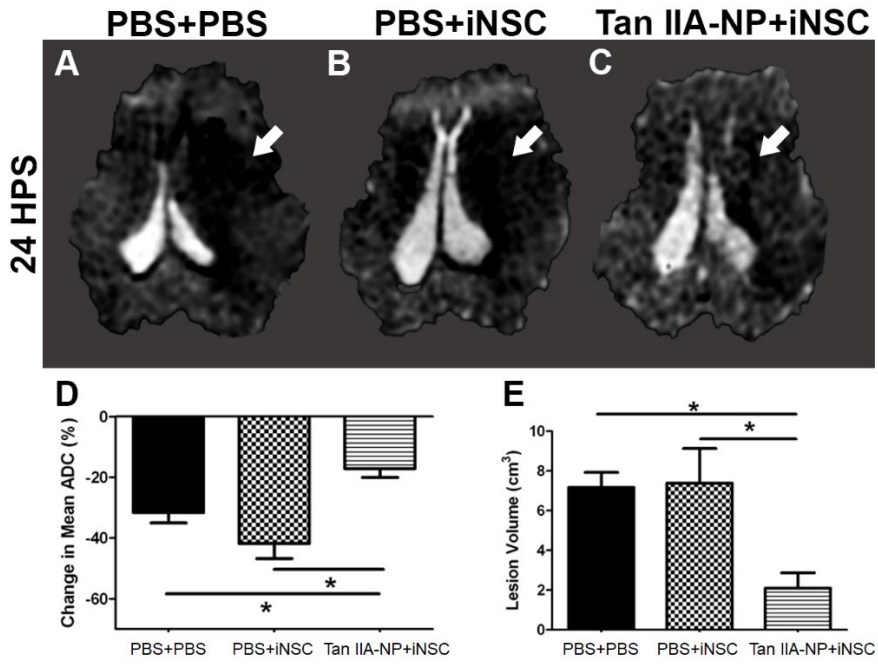
PBS+PBS
PBS+iNSC
Tan IIA-NP+iNSC
A
B
C
24 HPS
D
Change in Mean ADC (%)
0
-20
-40
-60
*
*
PBS+PBS
PBS+iNSC
Tan IIA-NP+iNSC
E
Lesion Volume (cm3)
10
8
6
4
2
0
*
*
PBS+PBS
PBS+iNSC
Tan IIA-NP+iNSC

Figure 6.3: iNSC treatment prevented chronic WM degradation. Tan IIA-NP+iNSC and PBS+iNSC treated pigs exhibited a lower percent decrease in FA values compared to PBS+PBS control pigs at 12 WPT. PBS+PBS control pigs demonstrated a significant percent change between time points (**A-G**) whereas Tan IIA-NP+iNSC and PBS+iNSC treated pigs did not. # indicates significant difference between time points.

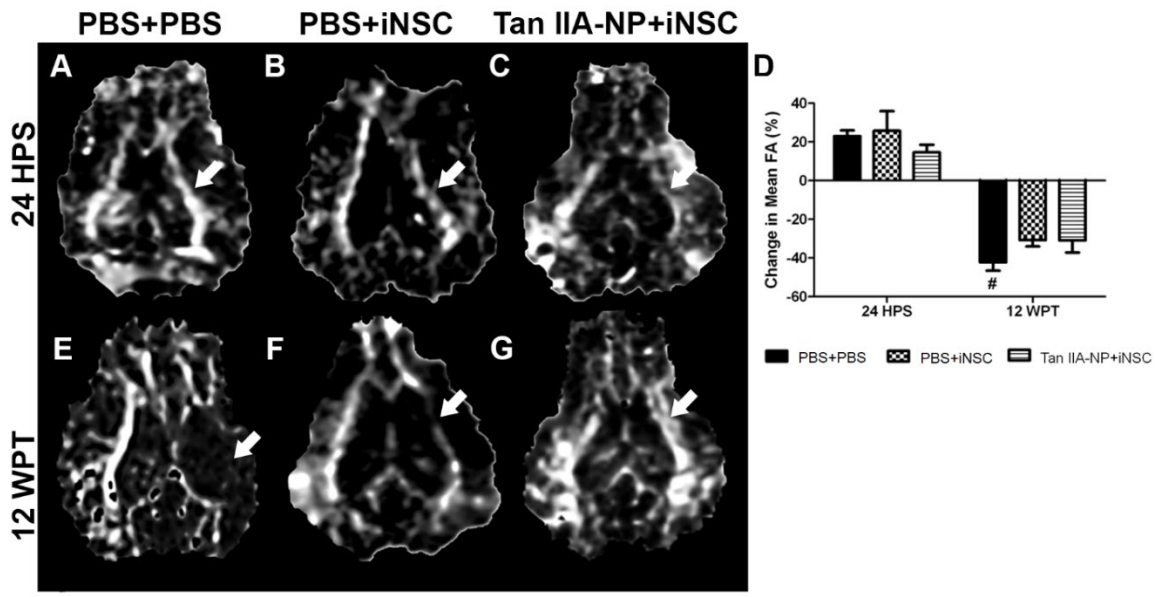
PBS+PBS
PBS+iNSC
Tan IIA-NP+iNSC
A
B
C
D
E
F
G
24 HPS
12 WPT
Change in Mean FA (%)
40
20
0
-20
-40
-60
#
24 HPS
12 WPT
PBS+PBS
PBS+iNSC
Tan IIA-NP+iNSC

Figure 6.4: Tan-IIA NPs reduced acute ICH volumes. T2* sequences 24 hours post-stroke revealed ICH in all treatment groups (**A-C**, white arrows). ICH was significantly reduced in Tan IIA-NP+iNSC treated pigs relative to PBS+PBS control pigs (0.73±0.15 vs. 1.52±0.12 cm3 respectively, **D**).

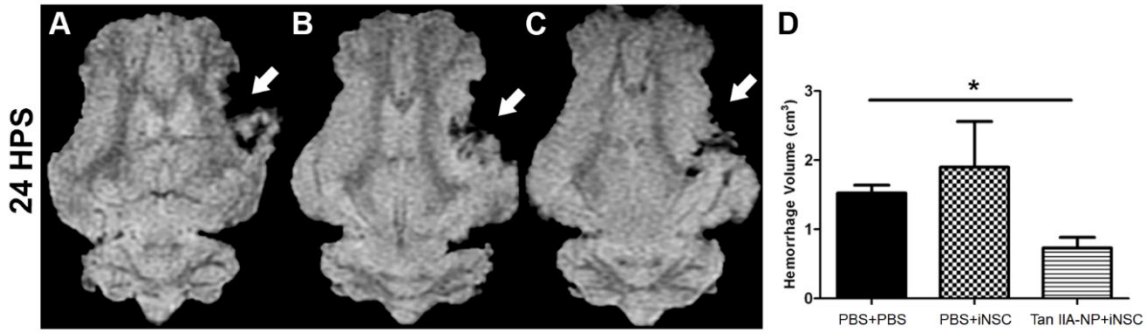
24 HPS
A
B
C
D
Hemorrhage Volume (cm³)
3
2
1
0
*
PBS+PBS
PBS+iNSC
Tan IIA-NP+iNSC

CHAPTER 8

CONCLUSION

The only Food and Drug Administration (FDA)-approved therapies currently available to ischemic stroke patients include tissue plasminogen activator (tPA), a thrombolytic agent, and thrombectomy surgical procedures [1, 2]. Limitations in pharmacological administration intervals (< 4.5 hours) and potentially deadly hemorrhagic consequences, highlight the need for safer and more inclusive patient treatment options that are capable of reducing ischemic damage and promoting neuroregenerative processes [3, 4]. A potential opportunity to hasten the speed at which novel therapeutics are developed and tested is through the use of translational animal models that are more predictive of the human condition. Compared to other large animal models, pigs are an attractive alternative for preclinical testing due to lower costs, reduced ethical concerns as well as inherent neuroanatomical similarities to humans (i.e. gyral pattern, brain size, white matter composition) that frequently correlate with neuronal network complexity and ischemic injury progression [5-7]. Furthermore, therapeutic dosing can be more accurately assessed in a pig model as humans and pigs share similarities in body size and metabolism. In order to expand the current knowledge on pig post-stroke physiological outcomes and to bolster therapeutic development and assessment strategies, the studies that comprise this dissertation 1) further characterized pig ischemic stroke using clinically-relevant and quantifiable modalities and 2) tested the efficacy of neural stem cell derived-extracellular vesicles (NSC EVs), Tanshinone IIA

nanoparticles (Tan IIA-NPs), and induced pluripotent stem cell-derived neural stem cells (iNSCs).

The first study characterized acute ischemic stroke injury severity, prognostic biomarkers, and therapeutic targets utilizing magnetic resonance imaging (MRI), immune, and motor function tests in a translational pig middle cerebral artery occlusion (MCAO) model. Lesion volumes closely replicated human lesion volumes with similar impairments in functional performance [8-11]. Ischemic injury produced cerebral swelling and consequent midline (MLS) as well as notable intracerebral hemorrhage (ICH), which are often associated with poor patient prognosis and premature mortality [12-14]. In addition, MCAO led to reduced white matter (WM) integrity as seen through fractional anisotropy (FA) maps and contralateral deteriorations in pig motor function frequently observed in patients [15-17]. MCAO led to an acute systemic immune response marked by an increase in circulating neutrophils and a corresponding decrease in circulating lymphocytes, which is a key biomarker for the development of ICH in patients and influences the use of anticoagulants [18-20]. Functional assessments paralleled clinical functional outcomes in stroke patients with impairments in motor function that affected spatiotemporal parameters and weight distribution [21-23]. By further understanding these physiological hallmarks and exploiting the similarities between pig and human post-stroke responses, the pig ischemic stroke model can be utilized to test novel therapeutics with increased predicative power of clinical efficacy.

Next, the pig ischemic stroke model was utilized to test NSC EV potency in mitigating the aforementioned pathophysiological responses. This pivotal study presents the first experimental evidence of intravenous (IV) administration of NSC EVs

improving tissue and functional level outcomes while adhering to the Stem Cell Emerging Paradigm in Stroke (STEPS) and Stroke Therapy Academic Industry Roundtable (STAIR) committee recommendations for developing and testing novel stroke therapeutics [24-27]. NSC EV intervention significantly decreased lesion volume, which has never been observed before in EV-related neural injury studies [8-11]. In addition, NSC EV therapy led to decreased hemispheric swelling and ICH incidence coupled with preserved diffusivity and WM integrity. These results strongly correlate with stroke patient cognitive decline, sensorimotor deterioration, and morbidity [12-17]. Experimental recovery in relative pressure, swing percent, stride length, and other translational pig gait parameters are critical readouts for human patients and are a robust measure of NSC EV therapeutic potential [28-32]. Collectively, these results suggest acute NSC EV administration may improve functional outcomes and the quality of life of many future stroke patients.

Finally, the therapeutic potential of intracisternal Tan IIA-NPs and intraparenchymal iNSCs were assessed via MRI tissue-level measurements. Here, acute treatment with Tan IIA-NPs demonstrated potential in mitigating post-stroke outcomes by significantly decreasing T2Weighted (T2W) and edema-corrected lesion volumes at acute and chronic time points which was not observed in pig stroke studies with iNSC transplantation alone [7]. The effect of Tanshinone IIA (Tan IIA) in reducing acute tissue damage is likely due to its capabilities in ameliorating blood-brain barrier (BBB) damage by suppressing levels of matrix metallopeptidase (MMPs), and thus preventing the degradation of tight junction proteins, claudin-5 and occludin, that are critical components of the BBB [33-35]. Acute Tan IIA-NP macro-level changes were mechanistically

supported by iNSC cellular-level changes, resulting in multifaceted effects including attenuated WM damage and MLS. iNSC effects on WM repair processes are supported by recent studies in which human neural stem cells transplanted into chronic stroke patients resulted in increased FA values [36]. Reductions in tissue atrophy and consequent MLS also suggests iNSC treatment enhances cellular survival through the secretion of neurotrophic factors which have been shown to protect neurons from ischemic injury in both small and large animal models [7, 37, 38]. These findings collectively support the continued investigation of this novel combination therapy for translation into human clinical trials.

Future studies

Although these studies further enhanced preclinical evaluation of novel therapies, there are a number of translational concerns that remain to be addressed. A common limitation of utlizing pig models of ischemic stroke is the presence of an anatomical structure known as the rete mirable. This dense network of small diameter arteries renders endovascular methods of ischemic induction unfeasible, thus necessitating rather complex transcranial surgical approaches to induce middle cerebral artery (MCA) occlusion. Consequent damage to the cranium and dura results in uncharacteristic intracranial dynamics and cerebrovascular pathophysiological changes post-stroke [39]. Furthermore, surgical craniectomy permits the loss of CSF upon dural excision and minimizes the pathological development of elevated intracranial pressure following MCA occlusion [40]. These implications do not fully replicate human post-stroke progression and therefore therapeutic efficacy of potential treatments in pig models may not be fully representative of efficacy in human patients.

In support of previously conducted rodent research, NSC EVs significantly improved neural tissue preservation and functional outcomes post-stroke. However, further studies should be conducted to investigate the mitigation of immune responses following NSC EV administration in a pig model. Although, mice treated with NSC EVs showed a dampened injury response while augmenting a reparative systemic response favoring macrophage polarization toward anti-inflammatory M2 cells, increasing Treg cells, and decreasing proinflammatory TH17 cells, this has yet to be shown in pig studies [41]. Furthermore, NSC EVs were administered systemically potentially leading to therapeutic effects in other tissues, such as the spleen, and having less to do with a direct effect on the brain. Although it is likely that a reduced number of NSC EVs reached the target brain tissues due to BBB breakdown following ischemic injury. Additional studies are needed to further explore whether the improvements observed where due to a direct effect on the brain or mediated through changes in other organ systems.

Tan IIA delivery via nanoparticle (NP) encapsulation is a novel administration platform that requires additional investigation. Despite the current developments in NP research, the use of NPs for ischemic stroke treatment is still under development. It is important to also evaluate differences in therapeutic potency between free-form Tan IIA and Tan IIA-NP in a pig model of ischemic stroke to characterize cytotoxicity and anti-inflammatory alterations in both in vitro and in vivo systems. An additional Tan IIA-NP+PBS treatment group in future studies may also provide additional information on sustained Tan IIA-NP effects at chronic time points post-stroke. Lastly, Tan IIA-NP administration via intranasal or intravenous applications would more easily permit

administration of multiple Tan IIA-NPs doses, however efficiency in reaching targeted ischemic tissues may be hindered.

In the future, a more in-depth assessment of iNSC effects on endogenous tissue recovery will be performed. Specifically, endogenous improvements through the sercetion of trophic factors remain to be investigated including iNSC influences on neuronal survivabilty, neuroblast migration, and glial scar formation. The ability of transplanted cells to differentiate in vivo into morphologically mature, regionally competent cell types will be evaluated at chronic time points. Whether these cells undergo synaptogeneis and send axons to appropriate targets, for example, remains to be elucidated. From a functional perspective, mature iNSC neurons should possess preserved electrophysiological properties and receive synaptic input from host neurons, thus improving neural network connectivity. Beyond iNSC integration characteristics, additional studies evaluating differences in transplantation times, iNSC cell numbers and vehicle solution (ie PBS vs. basal media), and co-transplantation within a biodegradable construct will be conducted to maximize iNSC efficacy and long-term survivability.

In conclusion, these studies have major implications to the stroke community by strengthening preclinical testing strategies in a large animal model with similar stroke pathologies to those observed in humans. Novel NSC EV therapy could represent a clinically feasible and cell-free paradigm with advantages in low tumorigenicity, scalable production, and high transport efficiency via intravous administration. Combined therapeutic potential of Tan IIA-NPs and iNSCs may also possess neuroprotective effects in patients through antioxidant and anti-inflammatory mechanisms with the pontential of cell replacement. Although additional studies are required to further explore therapeutic

mechanisms and to improve treatment efficacy, the findings within this dissertation could augment the chances for succesful clinical trials and improve acute and chronic recovery in stroke patients worldwide.

References

1. Cheng, N.T. and A.S. Kim, *Intravenous Thrombolysis for Acute Ischemic Stroke Within 3 Hours Versus Between 3 and 4.5 Hours of Symptom Onset.* The Neurohospitalist, 2015. **5**(3): p. 101-109.
2. Boyle, K., R.A. Joundi, and R.I. Aviv, *An historical and contemporary review of endovascular therapy for acute ischemic stroke.* Neurovascular Imaging, 2017. **3**(1): p. 1.
3. Balami, J.S., et al., *Complications of endovascular treatment for acute ischemic stroke: Prevention and management.* Int J Stroke, 2018. **13**(4): p. 348-361.
4. Gravanis, I. and S.E. Tsirka, *Tissue-type plasminogen activator as a therapeutic target in stroke.* Expert Opin Ther Targets, 2008. **12**(2): p. 159-70.
5. Lind, N.M., et al., *The use of pigs in neuroscience: modeling brain disorders.* Neurosci Biobehav Rev, 2007. **31**(5): p. 728-51.
6. Platt, S.R., et al., *Development and characterization of a Yucatan miniature biomedical pig permanent middle cerebral artery occlusion stroke model.* Exp Transl Stroke Med, 2014. **6**(1): p. 5.
7. Baker, E.W., et al., *Induced Pluripotent Stem Cell-Derived Neural Stem Cell Therapy Enhances Recovery in an Ischemic Stroke Pig Model.* Sci Rep, 2017. **7**(1): p. 10075.
8. Otero-Ortega, L., et al., *White Matter Repair After Extracellular Vesicles Administration in an Experimental Animal Model of Subcortical Stroke.* Sci Rep, 2017. **7**: p. 44433.

9. Xin, H., et al., *Systemic administration of exosomes released from mesenchymal stromal cells promote functional recovery and neurovascular plasticity after stroke in rats.* J Cereb Blood Flow Metab, 2013. **33**(11): p. 1711-5.

10. Zhang, Y., et al., *Effect of exosomes derived from multipluripotent mesenchymal stromal cells on functional recovery and neurovascular plasticity in rats after traumatic brain injury.* J Neurosurg, 2015. **122**(4): p. 856-67.

11. Zhang, Y., et al., *Systemic administration of cell-free exosomes generated by human bone marrow derived mesenchymal stem cells cultured under 2D and 3D conditions improves functional recovery in rats after traumatic brain injury.* Neurochem Int, 2016.

12. Lovblad, K.O., et al., *Ischemic lesion volumes in acute stroke by diffusion-weighted magnetic resonance imaging correlate with clinical outcome.* Ann Neurol, 1997. **42**(2): p. 164-70.

13. Schellinger, P.D., et al., *A standardized MRI stroke protocol: comparison with CT in hyperacute intracerebral hemorrhage.* Stroke, 1999. **30**(4): p. 765-8.

14. Jokinen, H., et al., *Incident lacunes influence cognitive decline: the LADIS study.* Neurology, 2011. **76**(22): p. 1872-8.

15. Baltan, S., et al., *White matter vulnerability to ischemic injury increases with age because of enhanced excitotoxicity.* J Neurosci, 2008. **28**(6): p. 1479-89.

16. Ahmad, A.S., et al., *Considerations for the Optimization of Induced White Matter Injury Preclinical Models.* Front Neurol, 2015. **6**: p. 172.

17. Srikanth, V., et al., *Cerebral white matter lesions, gait, and the risk of incident falls: a prospective population-based study.* Stroke, 2009. **40**(1): p. 175-80.

18. Pikija, S., et al., *Neutrophil to lymphocyte ratio predicts intracranial hemorrhage after endovascular thrombectomy in acute ischemic stroke.* J Neuroinflammation, 2018. **15**(1): p. 319.

19. Guo, Z., et al., *Dynamic change of neutrophil to lymphocyte ratio and hemorrhagic transformation after thrombolysis in stroke.* J Neuroinflammation, 2016. **13**(1): p. 199.

20. Song, Q., et al., *Increased Neutrophil-to-lymphocyte Ratios are Associated with Greater Risk of Hemorrhagic Transformation in Patients with Acute Ischemic Stroke.* Curr Neurovasc Res, 2018. **15**(4): p. 326-335.

21. Cappellari, M., G. Moretto, and P. Bovi, *Day-7 modified Rankin Scale score as the best measure of the thrombolysis direct effect on stroke?* J Thromb Thrombolysis, 2013. **36**(3): p. 314-5.

22. Clark, P.C., et al., *Caregiver perspectives of memory and behavior changes in stroke survivors.* Rehabil Nurs, 2006. **31**(1): p. 26-32.

23. Alexander, L.D., et al., *Association between gait asymmetry and brain lesion location in stroke patients.* Stroke, 2009. **40**(2): p. 537-44.

24. Fisher, M., et al., *Update of the stroke therapy academic industry roundtable preclinical recommendations.* Stroke, 2009. **40**(6): p. 2244-50.

25. Albers, G.W., et al., *Stroke Treatment Academic Industry Roundtable (STAIR) recommendations for maximizing the use of intravenous thrombolytics and expanding treatment options with intra-arterial and neuroprotective therapies.* Stroke, 2011. **42**(9): p. 2645-50.

26. Stem Cell Therapies as an Emerging Paradigm in Stroke, P., *Stem Cell Therapies as an Emerging Paradigm in Stroke (STEPS): bridging basic and clinical science for cellular and neurogenic factor therapy in treating stroke.* Stroke, 2009. **40**(2): p. 510-5.

27. Savitz, S.I., et al., *Stem Cell Therapy as an Emerging Paradigm for Stroke (STEPS) II.* Stroke, 2011. **42**(3): p. 825-9.

28. Nascimento, L.R., et al., *Walking training with cueing of cadence improves walking speed and stride length after stroke more than walking training alone: a systematic review.* J Physiother, 2015. **61**(1): p. 10-5.

29. Hak, L., et al., *Stride frequency and length adjustment in post-stroke individuals: influence on the margins of stability.* J Rehabil Med, 2015. **47**(2): p. 126-32.

30. Peterson, C.L., et al., *Pre-swing deficits in forward propulsion, swing initiation and power generation by individual muscles during hemiparetic walking.* J Biomech, 2010. **43**(12): p. 2348-55.

31. Nolan, K.J., M. Yarossi, and P. McLaughlin, *Changes in center of pressure displacement with the use of a foot drop stimulator in individuals with stroke.* Clin Biomech (Bristol, Avon), 2015. **30**(7): p. 755-61.

32. De Nunzio, A., et al., *Biofeedback rehabilitation of posture and weightbearing distribution in stroke: a center of foot pressure analysis.* Funct Neurol, 2014. **29**(2): p. 127-34.

33. Yang, Y., et al., *Matrix metalloproteinase-mediated disruption of tight junction proteins in cerebral vessels is reversed by synthetic matrix metalloproteinase*

inhibitor in focal ischemia in rat. J Cereb Blood Flow Metab, 2007. **27**(4): p. 697-709.

34. Ji, B., et al., *Sodium Tanshinone IIA Sulfonate Enhances Effectiveness Rt-PA Treatment in Acute Ischemic Stroke Patients Associated with Ameliorating Blood-Brain Barrier Damage.* Transl Stroke Res, 2017. **8**(4): p. 334-340.

35. Wang, L., et al., *Tanshinone II A down-regulates HMGB1, RAGE, TLR4, NF-kappaB expression, ameliorates BBB permeability and endothelial cell function, and protects rat brains against focal ischemia.* Brain Res, 2010. **1321**: p. 143-51.

36. Kalladka, D., et al., *Human neural stem cells in patients with chronic ischaemic stroke (PISCES): a phase 1, first-in-man study.* Lancet, 2016. **388**(10046): p. 787-96.

37. Cheng, B. and M.P. Mattson, *NT-3 and BDNF protect CNS neurons against metabolic/excitotoxic insults.* Brain Res, 1994. **640**(1-2): p. 56-67.

38. Wang, Y., et al., *Glial cell line-derived neurotrophic factor protects against ischemia-induced injury in the cerebral cortex.* J Neurosci, 1997. **17**(11): p. 4341-8.

39. Imai, H., et al., *A new model of focal cerebral ischemia in the miniature pig.* J Neurosurg, 2006. **104**(2 Suppl): p. 123-32.

40. Boltze, J., et al., *Permanent middle cerebral artery occlusion in sheep: a novel large animal model of focal cerebral ischemia.* J Cereb Blood Flow Metab, 2008. **28**(12): p. 1951-64.

41. Webb, R.L., et al., *Human Neural Stem Cell Extracellular Vesicles Improve Tissue and Functional Recovery in the Murine Thromboembolic Stroke Model.* Transl Stroke Res, 2017.

APPENDIX A

HUMAN NEURAL STEM CELL EXTRACELLULAR VESICLES IMPROVE TISSUE AND FUNCTIONAL RECOVERY IN THE MURINE THROMBOEMBOLIC STROKE MODEL

---

[1]Webb, R.L.†, Kaiser, E.E.†, Scoville, S.L., Thompson, Fatima, S., Pandya, C., Sriram, K., Swetenburg, R.L., Vaibhav, K., Arbab, A.S., Baban, B., Dhandapani, K.M., Hess, D.C., West, Hoda, M.N., and Stice, S.L. *Translational Stroke Research*. 2018; 9:530–539. Reprinted here with permission of the publisher.

† these authors equally contributed to this work

Abstract

Over 700 drugs have failed in stroke clinical trials, an unprecedented rate thought to be attributed in part to limited and isolated testing often solely in “young” rodent models and focusing on a single secondary injury mechanism. Here, extracellular vesicles (EVs), nanometer-sized cell signaling particles, were tested in a mouse thromboembolic (TE) stroke model. Neural stem cell (NSC) and mesenchymal stem cell (MSC) EVs derived from the same pluripotent stem cell (PSC) line were evaluated for changes in infarct volume as well as sensorimotor function. NSC EVs improved cellular, tissue, and functional outcomes in middle-aged rodents, whereas MSC EVs were less effective. Acute differences in lesion volume following NSC EV treatment were corroborated by MRI in 18-month-old aged rodents. NSC EV treatment has a positive effect on motor function in the aged rodent as indicated by beam walk, instances of foot faults, and strength evaluated by hanging wire test. Increased time with a novel object also indicated that NSC EVs improved episodic memory formation in the rodent. The therapeutic effect of NSC EVs appears to be mediated by altering the systemic immune response. These data strongly support further preclinical development of an NSC EV-based stroke therapy and warrant their testing in combination with FDA-approved stroke therapies.

Key words Neural stem cell extracellular vesicles, Thromboembolic stroke, Preclinical stroke model

Introduction

Despite the overwhelming global need, intravenous tissue plasminogen activator (IV-tPA) and endovascular thrombectomy (ET) are the only two FDA-approved stroke therapies to date [1, 2]. Both of the above "reperfusion" therapies target opening of major blood vessels in a carefully diagnosed, yet a very small sub-population of stroke victims. While reperfusion could itself trigger a secondary injury, neither of the FDA-approved stroke therapies are directly neuroprotective or neuroregenerative. Moreover, the use of IV-tPA and/or ET is improbable as a field therapy and both are limited to state-of-the-art facilities [3, 4]. Therefore, a larger population of stroke patients with limited access to these facilities (e.g., rural populations) still remain untreated and often rely on later neurorehabilitation and endogenous neuroregeneration mechanisms [5, 6].

Ideally, an implementable therapy would protect the brain in acute stroke and enhance long-term functional outcomes among stroke survivors. Along these lines, the Stroke Treatment Academic Industry Roundtable (STAIR) recommends development of stroke therapies, which could reduce reperfusion injury and promote neurovascular plasticity and recovery later. An assessment of the litany of failed treatments by the Stem Cell Emerging Paradigm in Stroke Consortium meetings (STEPS I, II, and III) resulted in identifying major treatment deficiencies including (1) lack of a regenerative therapy that will not only protect cells from ischemic injury but stimulate regeneration of lost and damaged tissues and (2) translational animal models more reflective of human pathology and improved predictive testing of treatments [7, 8].

One of the most promising therapeutic avenues capable of addressing this need for a neuroprotective and/or regenerative therapy is the use of extracellular vesicles (EVs)

[9]. EVs are membrane shed microvesicles (50–1000 nm) and exosomes (40–150 nm) produced by all cells of the central nervous system (CNS) [10, 11]. The therapeutic development of EVs is being explored for multiple regenerative therapeutic scenarios, as EVs overcome many of the limitations of cell therapies, including but not limited to the ability to deliver multiple doses, as well as the ability to store and administer EVs without specialized equipment or advanced training for medical personnel [12].

While reports on EV therapeutic benefits in rodent studies of mechanically occluded stroke (both transient suture and permanent electrocauterization models) are encouraging, optimal therapeutic EV sources have not been explored [13, 14]. Previously published stroke studies utilized non-neural sourced mesenchymal stem cell (MSC) EVs administered systemically into rodent models and produced behavioral improvements without significant reductions in infarct volume [13–15]. However, there are many indications that EV cargoes are cell type specific and the parental cell line plays a prodigious role in the biological properties of the resultant EV [14]. Therefore, EVs derived from different sources (MSC vs. NSC cells) may have unique properties relative to cell type. Also, the context under which EVs are produced directly influences the signal that the resultant EVs communicate [16, 17]. For example, EVs extracted from sera of stroke patients induced inflammatory cytokine expression in vitro [18]. Together, cell specific activity and systemic immunological activation are novel multifaceted means by which EVs may provide beneficial effects in both local and systemic processes post-ischemic insult [19]. While specific mechanism(s) of action are still being investigated, the potential therapeutic mechanisms of EVs appear to include anti-oxidative, pro-angiogenic, immunomodulatory, and/or neural plasticity regulating processes [20, 21].

Additionally, since the majority of stroke (~ 87%) occurs due to a thromboembolic (TE) occlusion and a larger population of victims remains untreated with the FDA-approved reperfusion therapies, it is critical to validate this promising therapy in a physiologically relevant TE model of stroke [9, 22, 23].

The objective of this study was to evaluate the therapeutic potential of human neural stem cell-derived EVs in a highly relevant preclinical stroke model without immunosuppression. NSC EV treatment significantly decreased neural injury in the murine model of TE stroke and also resulted in decreased behavioral and motor function deficits.

Results

Pluripotent stem cell-derived NSC and MSC EVs were similar in structural and protein marker expression, but not in size.

To eliminate the potential confounding variable of genetic differences, NSC and MSC were isogenically derived from H9 pluripotent stem cells using processes previously developed [24–26]. NSC and MSC EVs were quantified and evaluated for size differences using Nanosight's nanoparticle tracking analysis. NSC and MSC EVs have overlapping, but distinct size and concentration profiles, with a broader peak present in the MSC EV profile indicating presence of a range of vesicles up to 300 nm in size, while the vast majority of NSC EVs were under 200 nm (**Figure A.1A**). Evaluation of NSC EVs by electron microscopy (EM) revealed the presence of disperse multivesicular bodies (MVBs; **Figure A.1B**, left panel) and purified vesicles (**Figure A.1B**, right panel) could be visualized by EM after transfer to the electron microscopy grid. Differentiated neural cells were cultured with NSC EVs labeled with DiI and EVs were taken up by the

neural cells in vitro, as shown in super resolution confocal microscopy projection images (**Figure A.1C** and enlarged inset). Analysis of EVs by flow cytometry revealed that both cell types produced EVs that contained similar amounts of commonly reported EV markers such as CD63 and CD81, which are both members of the highly conserved tetraspanin superfamily.

NSC EVs provided significant benefits in the murine embolic model.

In order to compare the therapeutic efficacy of isogenically derived NSC and MSC EVs side by side, EV biodistribution was first evaluated. Indium-111 (In-111)-labeled EVs were injected 1 h post-TE-MCAO. Animals were imaged by single photon emission computed tomography (SPECT) at 1 and 24 h post-injection (**Figure A.2B**) [27]. SPECT results demonstrated systemic distribution not only in the lungs, liver, and spleen, as reported in other EV biodistribution studies [16, 28], but were also present in the infarcted hemisphere by 1 h post-TE-MCAO. By 24 h, EVs were largely cleared from the infarct site, although still present in the other organs. These results suggest that EVs preferentially accumulate in the penumbra of the injury. Based on this clearance from the infarct, animals received a three-dose treatment regimen of either EVs or PBS vehicle by tail vein injection at 2, 14, and 38 h post TE-MCAO. Animals were evaluated (after confirming no difference in cerebral blood flow; **Figure A.S1A**) by neurological deficit score (NDS) at 48 h and adhesive tape test (ATT) at 96 h post-TE-MCAO followed by blood collection and tissue analysis (**Figure A.2A**). NSC EV-treated animals during NDS assessment demonstrated a decrease in deficits compared to controls as evaluated by lower scores ($p \leq 0.055$) **Figure A.2C**). NSC EV-treated animals performed significantly ($p \leq 0.001$) faster on ATT (96.17 ± 11.57 vs. 162.53 ± 6.3 s, respectively), indicating

enhanced sensorimotor function, when compared to controls or MSC EV-treated animals (**Figure A.2D**). Analysis of metabolically active tissue by 2,3,5-triphenyltetrazolium chloride (TTC) staining versus dead tissue (colorless) indicated significantly decreased tissue loss in NSC EV-treated animals compared to the MSC EV treatment group (27.97 ± 2.78 vs. 48.19 ± 5.79 mm^2, **Figure A.2E, F**). Since EVs are present in bodily fluids and they could affect the systemic immune response via both direct and indirect antigen presentation, we next checked the peripheral immune response after EV treatment. Quantitative flow cytometry analysis of freshly collected blood samples at 96 h post-stroke indicated that NSC EV treatment significantly promoted macrophage polarization toward an anti-inflammatory M2 phenotype (**Figure A.3A–C, J**) and increased the regulatory T cell (**Figure A.3D–F, K**) population resulting in the downregulation of pro-inflammatory effector Th17 cells (**Figure A.3G–I, L**). Thus, our data indicates that NSC EV treatment after stroke is capable of dampening injury responses while augmenting a reparative systemic immune response (**Figure A.3**). In summary, this data indicates PSC-derived NSC EVs provide molecular and behavioral benefits, while PSC-derived MSC EV treatment resulted in more variable results in both infarct size and behavioral outcome assessment indicating a clear NSC EV benefit in the middle-aged embolic model. While overall survival was not significantly different between the groups, 55% of animals in the MSC EV and PBS groups survived to the endpoint, while 65% of NSC EV treated mice survived (**Figure A.S1**). For these reasons, NSC EVs were further explored as a candidate treatment, while evaluation of MSC EVs was discontinued.

NSC EV treatment reduced lesion volume and improved behavioral outcomes in aged mice.

Stroke therapeutics are often tested in young animals within a narrow time range post-stroke. NSC EVs were further explored in aged mice (18 ± 1 months), starting approximately 6 h post-stroke, to fall outside the time window of traditional tPA administration in humans. Dosage in the embolic model was maintained constant; however, the administration window was shifted to 6, 24, and 48 h post-stroke. (**Figure A.4A**). Blinded investigators randomly divided mice into non-stroked (sham) and stroked with either PBS vehicle (control) or NSC EV in PBS treatment groups (N = 24 animals/group). Analysis of T2-weighted (T2W) sequences 2 days post-TEMCAO indicated a significant decrease in lesion volume in NSC EV-treated animals (58.2 ± 5.03 and 37.9 ± 2.84 mm^3, respectively) (**Figure A.4B, C**), while ex vivo Q-ball MRI (performed on the fixed brain post-euthanasia) indicated that NSC EV treatment attenuated the post-stroke cerebral atrophy and significantly decreased it compared to the vehicle-treated group (22.8 ± 0.40 and 10.6 ± 1.94% of contralateral hemisphere) (**Figure A.4D**). Diffusion tensor imaging (DTI) and fractional anisotropy (FA) analysis was also performed after Q-ball imaging; however, no significant differences in diffusivity or white matter integrity were observed between the two groups subjected to TE stroke, which is likely due to less white matter content in small rodents. Behavioral characteristics and motor function were evaluated 14 days post-TE-MCAO. NSC EV-treated animals exhibited significantly improved coordination on the balance beam relative to control, with NSC EV-treated animals crossing in 18.9 ± 1.36 s and control animals crossing in 28.0 ± 0.45 s (**Figure A.4E**). Significantly fewer foot slips while

crossing the beam (2.21 ± 0.18 vs. 1.25 ± 0.21-foot slips) were also observed in NSC EV-treated animals (Figure A.4F). Grasping ability and forelimb strength were evaluated by the hanging wire test. NSC EV-treated animals could hang an average of 28.47 ± 1.18 s, while control animals grasping was significantly shorter (5.1 ± 0.91 s) (**Figure A.4G**). Episodic memory was evaluated by novel object recognition (NOR) testing. NSC EV-treated mice spent significantly more time exploring the novel object (NO; 36.92 ± 1.48 s) than the control group that spent only 26.50 ± 3.29 s on average with the NO. There were no significant differences in time spent with the familiar object between groups. Novel object discrimination index (DI) indicated NSC EV-treated animals performed significantly better than control group (0.26 ± 0.04 and 0.0005 ± 0.05, respectively; **Figure A.4I**). Finally, depressive phenotype was assessed by tail suspension test 28 days post-TE-MCAO. Controls were immobile for a significantly longer time period (178.13 ± 9.96 s) as compared to NSC EV-treated animals (123.08 ± 9.58 s) (**Figure A.4H**). The NSC EV group was not statistically different from the sham group in survival rates, while fewer animals survived to the endpoint in the control group (**Figure A.S1A**; $p \leq 0.319$). Collectively, this data indicates an early neuroprotective effect of NSC EV in aged mice as indicated by reduced lesion volume and improvements in functional outcomes as measured by grasping ability, forelimb strength, motor coordination, and memory consolidation.

Discussion

We present here the first experimental evidence that NSC EVs improve cellular, tissue, and functional outcomes in the murine TE-MCAO models. Mitigating the secondary injury cascades, particularly the immune response, NSC EV intervention led to

significantly decreases in infarct size and brain atrophy, which has never been observed acutely in previous studies of exosome treatment for stroke [13–15]. Although various cell therapies have improved stroke recovery in preclinical models, NSC EVs possess a number of advantages over cell-based therapeutics including decreased tumorigenicity, limited immunogenicity, enhanced biodistribution, and BBB permeability [13, 29–31]. In addition, vesicles are involved in many biological processes with the potential to serve as a neuroprotective and translatable therapeutic for neural disabilities including ischemic stroke and, importantly, can likely be used in conjunction with currently available tPA and/or endovascular therapies [32, 33]. Tissue level changes generated large-scale reductions in neural injury and rapid recovery of neurological and motor function outcomes in vivo, thus suggesting NSC EVs are a promising therapeutic for human patients.

Functional benefits following MSC EV treatment for stroke has been evaluated using several different cell lines, with varying degrees of MSC marker definition and EV dose [13, 14, 34]. However, benefits in the infarct, including evidence of axonal remodeling and angiogenesis in the ischemic boundary zone were achieved using EVs from cells modified by a lentivirus, indicating that modification can influence therapeutic potential of the resultant EVs [34]. Uniquely, the MSC EVs tested were of PSC origin and differentiated in vivo. We have shown previously that although these cells have many of the common markers (CD73, CD93, andCD105), they can have unique differentiation potential and methylation patterns [35]. MSC sourced using different tissue origins, isolation methods, and in vitro culture conditions can alter the immunosuppression potency of MSC [36]. Thus, the results here may not represent results obtained by all

sources of MSCs. However, these findings do elude to unknown subtleties of screening complex biologics, like EVs, for therapeutic potential in humans.

Stroke is unpredictable and the degree of neuroprotection provided by EVs may likely vary by the efficiency of their delivery into the ischemic brain. Therefore, we tested NSC EVs in two different treatment regimens in murine TE stroke. NSC EVs therapy, as early as 2 h after TE stroke in middle-aged (12 months old) mice, not only improved the neurological outcomes and profoundly reduced the infarction volume but also downregulated the systemic inflammatory response in the blood. It is well established that following stroke, immune cells such as leukocytes infiltrate the brain as a result of increased adhesion phenomena and resultant BBB permeability, leading to a brain localized neuroimmune response [37]. Circulating macrophages can also trigger a long-term adaptive immune response causing chronic neurodegeneration and subsequent neuropsychiatric dysfunction even after closure of the BBB [38]. Naïve immune cells such as macrophages and T lymphocytes are highly plastic in nature, which can adapt to a context-specific functional phenotype depending upon the microenvironment. Activated macrophages can also traverse into the draining cerebro-meningeal lymphatic system to trigger an adaptive immune response, which can decide the fate of outgoing T lymphocytes targeting the injured brain [39]. Since EVs carry a number of proteins, various RNA species, and bioactive lipids capable of diverse signaling, we looked into the systemic immune response 96 h after stroke. Mice treated with repeated doses of NSC EV showed increased M2-type macrophages and Treg populations, with a concurrent decrease in Th17 lymphocytes. Since macrophage activation precedes T lymphocyte proliferation and activation, it is likely that acute treatment with NSC EVs promoted a

conducive microenvironment resulting in alternatively (but not classically) activated M2-type polarization. This likely skews T lymphocytes to their regulatory phenotype, (Treg) with concurrent suppression of pro-inflammatory Th17 (an effector phenotype which releases IL-17 and causes long term neurodegeneration after stroke) [40]. Although these mechanistically novel findings in response to NSC EV therapy need further investigation, it is probable that such responses could have translational importance (Fig. 2); as such, circulating immune cells from the blood could possibly be used as a convenient biomarker to follow chronic effects of disease progression and the therapeutic effect of NSC EV in stroke during long-term follow-up.

Chronic neuropsychiatric dysfunctions such as the exacerbation of depression, anxiety, and dementia in aged individuals are very common after stroke [41]. Therefore, we next evaluated the delayed NSC EV therapy in the reproductively senescent aged (18 months old) mice subjected to TE stroke model and followed them for both acute and chronic outcomes. NSC EV therapy, even in an extended treatment window, reduced the acute lesion volume and cerebral atrophy at 28 days post-stroke. NSC EV-treated stroke mice performed better in various behavioral tasks related to motor function, muscular strength, depression, and learning/memory. Taken together, our data in murine TE stroke strongly supports further development of NSC EV-based stroke therapy.

MRI assessments of infarct volume, atrophy, and brain swelling are pivotal predictors of clinical severity and prognosis and are critical readouts in assessing the efficacy of stroke therapies [42, 43]. NSC EVs administered both within and outside the tPA therapeutic window resulted in a significant decrease in infarct volume in our murine model. In addition, MRI results suggest NSC EVs also resulted in a significant reduction

in tissue loss 28 days post-TE-MCAO in aged mice. These findings directly support recent reports in which MSC EVs were found to promote tissue preservation and neurovascular remodeling through proposed paracrine effectors [15, 44, 45].

NSC EVs may promote increases in vascular density and angiogenic processes by mediating specific gene regulation. For example, emerging data suggests downregulation of miR15a in cerebral vessels in a murine model of ischemic stroke promotes angiogenesis in the peri-infarct region by increasing FGF-2 and VEGF levels [46, 47]. Many MSC EV-related studies have observed improvements in functional recovery, neurogenesis, and angiogenesis in rodent models of ischemic stroke [14, 15, 48, 49]. However, these studies have yet to report a significant difference in acute infarct volume as we have shown here. These results suggest that NSC EVs maybe therapeutically more potent than their MSC EV counterparts. While the exact molecular mechanism(s) responsible for these effects are currently unknown, it is possible that they are mediated by tetraspanin superfamily proteins. We routinely detect tetraspanins CD63 and CD81 in NSC EVs. Tetraspanins affect cell adhesion, motility, proliferation, and coagulation [50], which we believe may improve stroke outcomes.

It is imperative for the success of translational research to also incorporate behavioral tests that are sensitive to both the area of brain damage and the interventions that are being applied [51]. Neurological deficit scores and adhesive tape removal times revealed significant improvements in NSC EV-treated mice 2 and 4 days post-TE-MCAO, respectively. Furthermore, NSC EVs promoted significant improvements in balance beam walking, the number of footfalls, hanging wire, and tail suspension performance 14 days post-TEMCAO in aged rodents. In comparison, similar studies

evaluating rodent MSC EVs also reported significant behavioral improvements in comparatively young animals, in the absence of changes in infarct volume [14, 34, 52]. However, how rodent MSC EVs evaluated in young adult animals translate to the therapeutic potential of human MSC EVs and how those compare to NSC EVs are frequently not addressed—leaving plausible gaps in our knowledge of how these resources inform further development in preclinical programs for evaluation of EVs for therapeutic use in humans.

In addition to sensorimotor tests, we also evaluated NSC EV effects on declarative memory. Fourteen days post-TEMCAO, our NSC EVs induced a significant improvement not only in NOR but also in associated NO discrimination performance. This suggests NSC EVs may also support the conservation of key brain regions associated with declarative memory and discrimination, like the dorsolateral prefrontal cortex and the medial temporal lobe [53, 54]. Advanced imaging and pharmacological inactivation studies in multiple animal models have also confirmed this theory by providing evidence that the prefrontal cortex plays a critical role during remote memory recall by regulating the hippocampus [55]. Stroke-induced injury to white matter tracts (including connections to the frontal and temporal cortices) has been linked to lasting deficits in episodic and declarative memory in both rodent models, as well as human patients [55–58].

This study uniquely encompassed a direct comparison of human MSC and NSC EVs while abiding by STEP and STAIR committee recommendations for developing stroke therapeutics. The extensive testing of NSC EVs has shown impressive biological relevance in the TE-MCAO model of ischemic stroke. By not only decreasing

hemispheric swelling, atrophy, and infarct volume but also improving functional performance in vivo, NSC EVs possess potent and translatable therapeutic potential that with further testing may change the current therapeutic paradigm of ischemic stroke. Further testing in large animal models of stroke, as well as studies evaluating the use in conjunction with tPA and endovascular therapies, will further inform the therapeutic development potential of NSC EVs.

Acknowledgements

The authors would like to thank Caroline Jackson, Justin Sharma, Austin Passaro, and Viviana Martinez who were involved with various aspects of the EV manufacturing process and figure preparation. We would also like to thank Tracey Stice for the project management guidance as well as Beth Richardson and Mary Ard at the University of Georgia Electron Microscopy Core for their technical assistance and expertise.

Funding

This work was supported by ArunA Biomedical, Inc., and R.L.S. was partially supported by the Science and Technology Center Emergent Behaviors of Integrated Cellular Systems (EBICS) Grant No. CBET-0939511.

Conflict of Interest

R.L.W. and S.L.S. have submitted a patent filing on the NSC EVs, and this technology is licensed from the UGA Research Foundation by ArunA Biomedical, Inc. R.L.W., S.L.S., T.A.T., R.L.S., and S.L.S. are affiliated with ArunA Biomedical, Inc. and own equity in the company. E.E.K., S.F., C.P., K.S., K.V., A.S.A., B.B., K.M.D., D.C.H., and M.N.H. declare that they have no conflict of interest.

Ethical Approval

All animal procedures were approved by the Institutional Animal Care and Use Committee of Augusta University. This article does not contain any studies with human participants performed by any of the authors.

References

1. Cheng NT, Kim AS. Intravenous thrombolysis for acute ischemic stroke within 3 hours versus between 3 and 4.5 hours of symptom onset. Neurohospitalist. 2015;5(3):101–9. https://doi.org/10.1177/ 1941874415583116.

2. Boyle K, Joundi RA, Aviv RI. An historical and contemporary review of endovascular therapy for acute ischemic stroke. Neurovasc Imaging. 2017;3(1):1. https://doi.org/10.1186/s40809- 016-0025-2.

3. Adams HP, del Zoppo G, Alberts MJ, Bhatt DL, Brass L, Furlan A, et al. Guidelines for the early management of adults with ischemic stroke. A guideline from the American Heart Association/American Stroke Association Stroke Council, Clinical Cardiology Council, Cardiovascular Radiology and Intervention Council, and the Atherosclerotic Peripheral Vascular Disease and Quality of Care Outcomes in Research Interdisciplinary Working Groups: The American Academy of Neurology affirms the value of this guideline as an educational tool for neurologists. 2007;115(20): e478– 534. https://doi.org/10.1161/circulationaha.107.181486.

4. Duncan PW, Zorowitz R, Bates B, Choi JY, Glasberg JJ, Graham GD, et al. Management of adult stroke rehabilitation care. A Clinical Practice Guideline. Stroke. 2005;36(9): e100–e43. https:// doi.org/10.1161/01.str.0000180861.54180.ff.

5. Kapral MK, Wang H, Mamdani M, Tu JV. Effect of socioeconomic status on treatment and mortality after stroke. Stroke. 2002;33(1): 268–75. https://doi.org/10.1161/hs0102.101169.

6. Mendis S. Stroke disability and rehabilitation of stroke: World Health Organization perspective. Int J Stroke. 2013;8(1):3–4. https://doi.org/10.1111/j.1747-4949.2012.00969.x.

7. Stem Cell Therapies as an Emerging Paradigm in Stroke (STEPS): bridging basic and clinical science for cellular and neurogenic factor therapy in treating stroke. Stroke. 2009;40(2):510–5. https://doi. org/10.1161/STROKEAHA.108.526863.

8. Savitz SI, Chopp M, Deans R, Carmichael ST, Phinney D, Wechsler L. Stem Cell Therapy as an Emerging Paradigm for Stroke (STEPS) II. Stroke. 2011;42(3):825–9. https://doi.org/10. 1161/STROKEAHA.110.601914.

9. Chopp M, Zhang ZG. Emerging potential of exosomes and noncoding microRNAs for the treatment of neurological injury/diseases. Expert Opin Emerg Drugs. 2015;20(4):523–6. https://doi. org/10.1517/14728214.2015.1061993.

10. Basso M, Bonetto V. Extracellular vesicles and a novel form of communication in the brain. Front Neurosci. 2016; 10:127. https:// doi.org/10.3389/fnins.2016.00127.

11. Raposo G, Stoorvogel W. Extracellular vesicles: exosomes, microvesicles, and friends. J Cell Biol. 2013;200(4):373–83. https://doi.org/10.1083/jcb.201211138.

12. Gimona M, Pachler K, Laner-Plamberger S, Schallmoser K, Rohde E. Manufacturing of human extracellular vesicle-based therapeutics for clinical use. Int J Mol Sci. 2017;18(6) https://doi.org/10.3390/ ijms18061190.

13. Doeppner TR, Herz J, Görgens A, Schlechter J, Ludwig A-K, Radtke S, et al. Extracellular vesicles improve post-stroke neuroregeneration and prevent postischemic immunosuppression. Stem Cells Transl Med. 2015;4(10):1131–43. https://doi.org/10. 5966/sctm.2015-0078.

14. Xin H, Li Y, Cui Y, Yang JJ, Zhang ZG, Chopp M. Systemic administration of exosomes released from mesenchymal stromal cells promote functional recovery and neurovascular plasticity after stroke in rats. J Cereb Blood Flow Metab. 2013;33(11):1711–5. https://doi.org/10.1038/jcbfm.2013.152.

15. Zhang Y, Chopp M, Zhang ZG, Katakowski M, Xin H, Qu C, et al. Systemic administration of cell-free exosomes generated by human bone marrow derived mesenchymal stem cells cultured under 2D and 3D conditions improves functional recovery in rats after traumatic brain injury. Neurochem Int. 2016; https://doi.org/10.1016/j. neuint.2016.08.003.

16. Wiklander OPB, Nordin JZ, O'Loughlin A, Gustafsson Y, Corso G, Mäger I et al. Extracellular vesicle in vivo biodistribution is determined by cell source, route of administration and targeting. J Extracell Vesicles. 2015;4. https://doi.org/10.3402/jev.v4.26316

17. Morel L, Regan M, Higashimori H, Ng SK, Esau C, Vidensky S, et al. Neuronal exosomal miRNA-dependent translational regulation of astroglial glutamate transporter GLT1. J Biol Chem. 2013;288(10):7105–16. https://doi.org/10.1074/jbc.M112.410944.

18. Couch Y, Akbar N, Davis S, Fischer R, Dickens AM, Neuhaus AA, et al. Inflammatory stroke extracellular vesicles induce macrophage activation. Stroke. 2017;48(8):2292–6. https://doi.org/10.1161/ strokeaha.117.017236.

19. Zhang ZG, Chopp M. Exosomes in stroke pathogenesis and therapy. J Clin Invest. 2016;126(4):1190–7. https://doi.org/10.1172/ JCI81133.

20. Lener T, Gimona M, Aigner L, Börger V, Buzas E, Camussi G, et al. Applying extracellular vesicles based therapeutics in clinical trials—an ISEV position paper. J Extracell Vesicles. 2015;4(1): 30087. https://doi.org/10.3402/jev.v4.30087.

21. Kordelas L, Rebmann V, Ludwig AK, Radtke S, Ruesing J, Doeppner TR, et al. MSC-derived exosomes: a novel tool to treat therapy-refractory graft-versus-host disease. Leukemia. 2014;28(4):970–3. https://doi.org/10.1038/leu.2014.41.

22. Hoda MN, Fagan SC, Khan MB, Vaibhav K, Chaudhary A, Wang P, et al. A 2 × 2 factorial design for the combination therapy of minocycline and remote ischemic perconditioning: efficacy in a preclinical trial in murine thromboembolic stroke model. Exp Transl Stroke Med. 2014;6(1):10. https://doi.org/10.1186/2040-7378-6-10. 23. Hoda MN, Li W, Ahmad A, Ogbi S, Zemskova MA, Johnson MH, et al. Sex-independent neuroprotection with minocycline after experimental thromboembolic stroke. Exp Transl Stroke Med. 2011;3(1):16. https://doi.org/10.1186/2040-7378-3-16.

24. Shin S, Mitalipova M, Noggle S, Tibbitts D, Venable A, Rao R, et al. Long-term proliferation of human embryonic stem cell derived neuroepithelial cells using defined adherent culture conditions. Stem Cells. 2006;24(1):125–38. https://doi.org/10.1634/ stemcells.2004-0150.

25. Dhara SK, Hasneen K, Machacek DW, Boyd NL, Rao RR, Stice SL. Human neural progenitor cells derived from embryonic stem cells in feeder-free cultures. Differentiation. 2008;76(5):454–64. https://doi.org/10.1111/j.1432-0436.2007.00256.x.

26. Boyd NL, Robbins KR, Dhara SK, West FD, Stice SL. Human embryonic stem cell-derived mesoderm-like epithelium transitions to mesenchymal progenitor cells. Tissue Eng A. 2009;15(8):1897– 907. https://doi.org/10.1089/ten.tea.2008.0351.

27. Hwang DW, Choi H, Jang SC, Yoo MY, Park JY, Choi NE, et al. Noninvasive imaging of radiolabeled exosome-mimetic nanovesicle using (99m)Tc-HMPAO. Sci Rep. 2015;5(1):15636. https://doi.org/10.1038/srep15636.

28. Lai CP, Mardini O, Ericsson M, Prabhakar S, Maguire C, Chen JW, et al. Dynamic biodistribution of extracellular vesicles in vivo using a multimodal imaging reporter. ACS Nano. 2014;8(1):483–94. https://doi.org/10.1021/nn404945r.

29. Wiklander OP, Nordin JZ, O'Loughlin A, Gustafsson Y, Corso G, Mager I,etal.Extracellularvesiclein vivobiodistributionisdetermined by cell source, route of administration and targeting. J Extracell Vesicles. 2015;4(1):26316. https://doi.org/10.3402/jev.v4.26316.

30. Yang T, Fogarty B, LaForge B, Aziz S, Pham T, Lai L, et al. Delivery of smallinterferingRNAtoinhibit vascular endothelial growth factor in zebrafish using natural brain endothelia cell-secreted exosome nanovesicles for the treatment of brain cancer. AAPS J. 2017;19(2): 475–86. https://doi.org/10.1208/s12248-016-0015-y.

31. Saari H, Lazaro-Ibanez E, Viitala T, Vuorimaa-Laukkanen E, Siljander P, Yliperttula M. Microvesicle- and exosome-mediated drug delivery enhances the cytotoxicity of paclitaxel in autologous prostate cancer cells. J Control Release. 2015;220(Pt B):727–37. https://doi.org/10.1016/j.jconrel.2015.09.031.

32. Paschon V, Takada SH, Ikebara JM, Sousa E, Raeisossadati R, Ulrich H, et al. Interplay between exosomes, microRNAs and toll-like receptors in brain disorders. Mol Neurobiol. 2016;53(3): 2016–28. https://doi.org/10.1007/s12035-015-9142-1.

33. Thery C, Zitvogel L, Amigorena S. Exosomes: composition, biogenesis and function. Nat Rev Immunol. 2002;2(8):569–79. https:// doi.org/10.1038/nri855.

34. Xin H, Li Y, Liu Z, Wang X, Shang X, Cui Y, et al. MiR-133b promotes neural plasticity and functional recovery after treatment of stroke with multipotent mesenchymal stromal cells in rats via transfer of exosome-enriched extracellular particles. Stem Cells. 2013;31(12):2737–46. https://doi.org/10.1002/stem.1409.

35. Sorensen AL, Timoskainen S, West FD, Vekterud K, Boquest AC, Ahrlund-Richter L, et al. Lineage-specific promoter DNA methylation patterns segregate adult progenitor cell types. Stem Cells Dev. 2010;19(8):1257–66. https://doi.org/10.1089/scd.2009.0309.

36. Klinker MW, Marklein RA, Lo Surdo JL, Wei CH, Bauer SR. Morphological features of IFN-gamma-stimulated mesenchymal stromal cells predict overall immunosuppressive capacity. Proc Natl Acad Sci U S A. 2017;114(13):E2598–E607. https://doi.org/ 10.1073/pnas.1617933114.

37. Grønberg NV, Johansen FF, Kristiansen U, Hasseldam H. Leukocyte infiltration in experimental stroke. J Neuroinflammation. 2013;10:115. https://doi.org/10.1186/1742-2094-10-115.

38. Chen Y, Garcia GE, Huang W, Constantini S. The involvement of secondary neuronal damage in the development of neuropsychiatric disorders following brain insults. Front Neurol. 2014;5:22. https:// doi.org/10.3389/fneur.2014.00022.

39. Prinz M, Erny D, Hagemeyer N. Ontogeny and homeostasis of CNS myeloid cells. Nat Immunol. 2017;18(4):385–92. https://doi. org/10.1038/ni.3703.

40. Shichita T, Sugiyama Y, Ooboshi H, Sugimori H, Nakagawa R, Takada I, et al. Pivotal role of cerebral interleukin-17-producing [gamma][delta]T cells in the delayed phase of ischemic brain injury. Nat Med. 2009;15(8):946–50. http://www.nature.com/nm/journal/ v15/n8/suppinfo/nm.1999_S1.html

41. Gottesman RF, Hillis AE. Predictors and assessment of cognitive dysfunction resulting from ischaemic stroke. Lancet Neurol. 2010;9(9):895–905. https://doi.org/10.1016/S1474-4422(10) 70164-2.

42. Lovblad KO, Baird AE, Schlaug G, Benfield A, Siewert B, Voetsch B, et al. Ischemic lesion volumes in acute stroke by diffusionweighted magnetic resonance imaging correlate with clinical outcome. Ann Neurol. 1997;42(2):164–70. https://doi.org/10.1002/ana.410420206.

43. Schellinger PD, Jansen O, Fiebach JB, Hacke W, Sartor K. A standardized MRI stroke protocol: comparison with CT in hyperacute intracerebral hemorrhage. Stroke. 1999;30(4):765–8. https://doi. org/10.1161/01.STR.30.4.765.

44. Otero-Ortega L, Gomez de Frutos MC, Laso-Garcia F, RodriguezFrutos B, Medina-Gutierrez E, Lopez JA, et al. Exosomes promote restoration after an experimental animal model of intracerebral hemorrhage. J Cereb Blood Flow Metab. 2017; https://doi.org/10.1177/0271678X17708917.

45. Chopp M, Li Y. Treatment of neural injury with marrow stromal cells. Lancet Neurol. 2002;1(2):92–100. https://doi.org/10.1016/ S1474-4422(02)00040-6.

46. Yin KJ, Hamblin M, Chen YE. Angiogenesis-regulating microRNAs andischemic stroke.CurrVascPharmacol.2015;13(3):352–65.https://doi.org/10.2174/15701611113119990016.

47. Teng H, Zhang ZG, Wang L, Zhang RL, Zhang L, Morris D, et al. Coupling of angiogenesis and neurogenesis in cultured endothelial cells and neural progenitor cells after stroke. J Cereb Blood Flow Metab. 2008;28(4):764–71. https://doi.org/10.1038/sj.jcbfm. 9600573.

48. Zhang Y, Chopp M, Meng Y, Katakowski M, Xin H, Mahmood A, et al. Effect of exosomes derived from multipluripotent mesenchymal stromal cells on functional recovery and neurovascular plasticity in rats after traumatic brain injury. J Neurosurg. 2015;122(4): 856–67. https://doi.org/10.3171/2014.11.JNS14770.

49. Otero-Ortega L, Laso-Garcia F, Gomez-de Frutos MD, RodriguezFrutos B, Pascual-Guerra J, Fuentes B, et al. White matter repair after extracellular vesicles administration in an experimental animal model of subcortical stroke. Sci Rep. 2017;7:44433. https://doi.org/ 10.1038/srep44433.

50. Charrin S, Jouannet S, Boucheix C, Rubinstein E. Tetraspanins at a glance. J Cell Sci. 2014;127(17):3641–8. https://doi.org/10.1242/ jcs.154906.

51. Schaar KL, Brenneman MM, Savitz SI. Functional assessments in the rodent stroke model. Exp Transl Stroke Med. 2010;2(1):13. https://doi.org/10.1186/2040-7378-2-13.

52. Xin H, Wang F, Li Y, QE L, Cheung WL, Zhang Y, et al. Secondary release of exosomes from astrocytes contributes to the increase in neural plasticity and improvement of functional recovery after stroke in rats treated with exosomes harvested from microRNA 133b-overexpressing multipotent mesenchymal stromal cells. Cell Transplant. 2017;26(2):243–57. https://doi.org/10.3727/ 096368916X693031.

53. Blum S, Hebert AE, Dash PK. A role for the prefrontal cortex in recall of recent and remote memories. Neuroreport. 2006;17(3): 341–4. https://doi.org/10.1097/01.wnr.0000201509.53750.bc.

54. Halgren E, Babb TL, Crandall PH. Activity of human hippocampal formation and amygdala neurons during memory testing. Electroencephalogr Clin Neurophysiol. 1978;45(5):585–601. https://doi.org/10.1016/0013-4694(78)90159-1.

55. Frankland PW, Bontempi B. The organization of recent and remote memories. Nat Rev Neurosci. 2005;6(2):119–30. https://doi.org/10. 1038/nrn1607.

56. Lockhart SN, Mayda AB, Roach AE, Fletcher E, Carmichael O, Maillard P, et al. Episodic memory function is associated with multiple measures of white matter integrity in cognitive aging. Front Hum Neurosci. 2012;6:56. https://doi.org/10.3389/fnhum.2012.00056.

57. Tulving E, Markowitsch HJ. Episodic and declarative memory: role of the hippocampus. Hippocampus. 1998;8(3):198–204. https://doi. org/10.1002/(SICI)1098-1063(1998)8:3<198::AID-HIPO2> 3.0.CO;2-G.

58. Lundy-Ekman L. Neuroscience : fundamentals for rehabilitation. 4th ed. St. Louis: Elsevier; 2013.

Figure A.1: NSCs and MSCs produce EVs containing commonly reported EV biomarkers. EVs produced by NSCs and MSCs have overlapping, but distinct size profiles, with a greater presence of larger vesicles present in the MSC EV profile (~ 124 nm (**A**). Electron microscopy of NSC revealed the presence of disperse multivesicular bodies (**B**, left panel), while EV enrichment resulted in presence of purified EVs (**B**, right panel). Labeled NSC EVs (DiI) were taken up by differentiated neural cells in vitro (**C**), with single projection super resolution confocal images shown; z-stack in supplemental movie S1.

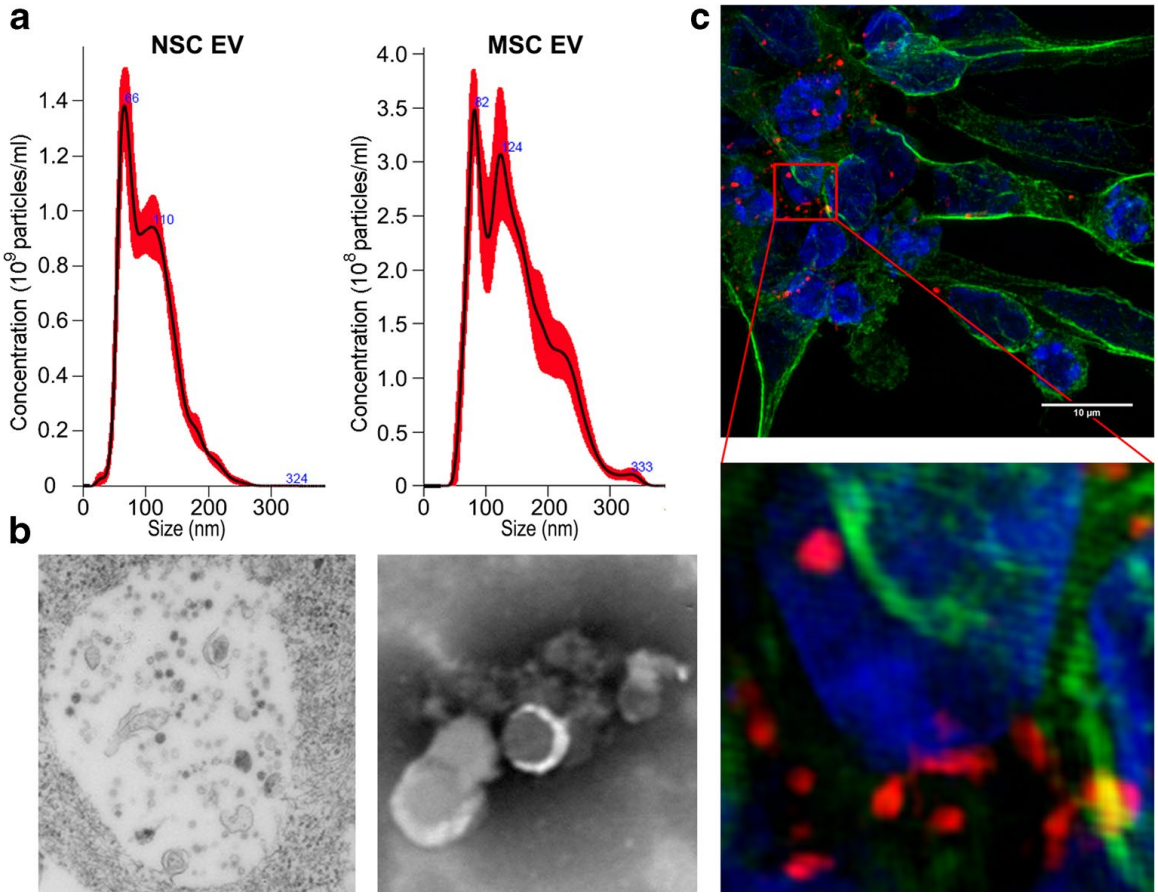
a
NSC EV
MSC EV
Concentration (10^9 particles/ml)
Concentration (10^8 particles/ml)
Size (nm)
Size (nm)
86
110
324
82
124
333
b
c
10 µm

Figure A.2: NSC EVs outperform MSC EVs in the murine embolic stroke model and indicate acute benefits may be modulated by augmenting the systemic immune response. One hour after stroke induction either free In111 or labeled EVs (**B**, left and right, respectively) were administered into mice via tail vein injection and analyzed by SPECT. EVs were present in the infarct region 1 h after injection (**B**, red circles, left brain panels), but were largely cleared by 24 h (**B**, red circles, right brain panels). Systemic presence in the lungs, liver, and spleen are in agreement with other EV biodistribution studies (**B**, body panels). Based on rapid clearance, animals received three doses of EVs (MSC EV, NSC EV, or vehicle control; N = 12/group), at 2, 14, and 28 h after TE-MCAO, (as outlined in **A**). Neurological deficit 48 h post-TE-MCAO (**C**) indicated that animals that received MSC EVs were indistinguishable from controls, while NSC EV evaluation trended toward significance ($p = 0.055$). Adhesive tape test indicated improved somatosensory function after NSC EV treatment compared to either MSC EV or control (**D**) Acute effects on neural tissue were analyzed by 2,3,5-triphenyltetrazolium Chloride (TTC) differentiated metabolically active (live, red) and inactive (dead, colorless) tissue indicated significantly decreased injury and infarct following NSC EV treatment (**E, F**).

Figure A.3: NSC EV treatment augments the systemic immune response to TE stroke. Cells in circulation that were analyzed for immune cell presence indicated an increase in functional M2 macrophages associated with tissue repair (**A-C, J**) and increased immunosuppressive Tregs (**D-F, K**), as well as a decrease in pro-inflammatory Th17 (CD4+, IL-17+) cells compared to MSC EVs and control (**G-I, L**). Asterisks (*) indicate statistical differences from sham group while the number sign (#) indicates significant statistical differences between control and NSC EV groups; *; #p value ≤ 0.05; **, ##p value ≤ 0.01; ***, ###p value ≤ 0.001.

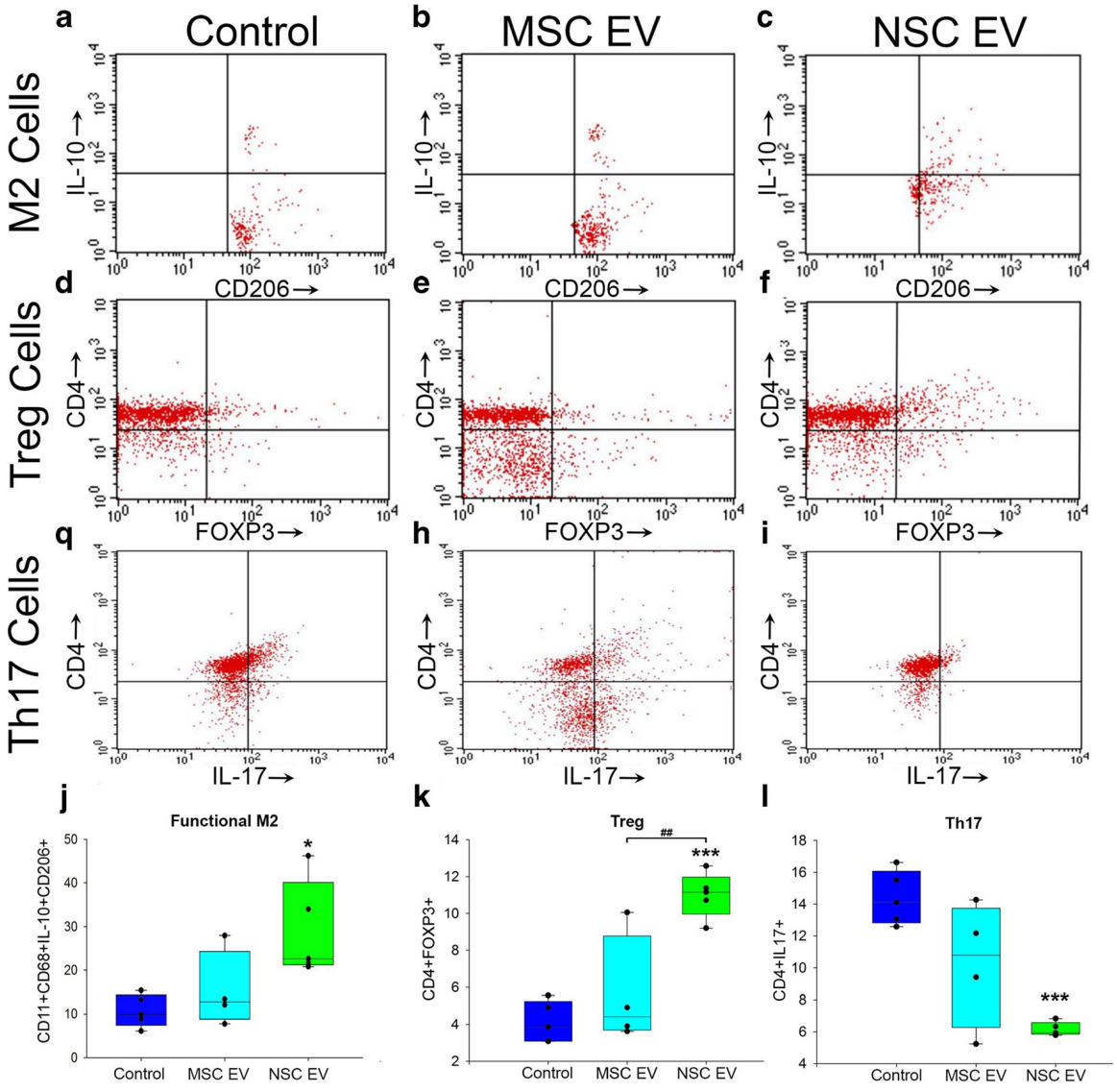
a
Control
b
MSC EV
c
NSC EV
M2 Cells
IL-10→
CD206→
d
e
f
Treg Cells
CD4→
FOXP3→
q
h
i
Th17 Cells
IL-17→
j
Functional M2
CD11+CD68+IL-10+CD206+
k
Treg
CD4+FOXP3+
##
***
l
Th17
CD4+IL17+
***
*
Control
MSC EV
NSC EV

Figure A.4: NSC EV treatment resulted in molecular and behavioral benefits in aged rodents. Based on increased benefit from NSC EV treatment, aged C57BL/6 animals (N = 24/group) were randomly split into control (PBS vehicle) and NSC EV treatment groups by blinded investigators, who delivered treatments at 6, 28, and 48 h as outlined in **A**. Analysis of T2 W images (**B**, lesion shown in white) demonstrated a significant reduction in lesion size in NSC EV-treated aged mice relative to control mice at 48 h (**C**). Volumetric analysis of T2 intensity (**B**) sequences revealed a significant reduction in ipsilateral hemisphere atrophy in NSC EV-treated mice relative to non-treated mice at 30 days (**D**). DTI sequences showed no significant differences in FA between NSC EV treated and control mice at 28 days (**B**). Balance and coordination were evaluated by beam walk, where both TE-MCAO groups took longer to cross the beam than sham animals, but NSC EV-treated animals were significantly faster at performing the task than controls (**E**). The number of foot slips during beam walk also indicated improved coordination in treated animals vs. control (**F**). Forelimb coordination was further analyzed by hanging wire test, where NSC EV animals significantly outperformed control animals (**G**). Tail suspension test revealed that control animals were immobile for significantly longer than NSC EV-treated animals (**H**). Non-spatial memory of animals was evaluated by novel object recognition test, where NOR discriminatory index indicated that both TE-MCAO groups had detectable deficits, but NSC EV-treated mice performed significantly better than controls, as a result of treated animals spending more time with the novel object, compared to the familiar object (**I**). Asterisks (*) indicate statistical differences from sham group while the number sign (#) indicates significant

statistical differences between control and NSC EV groups; *; #p value ≤ 0.05; **, ##p value ≤ 0.01; ***, ###p value ≤ 0.001.

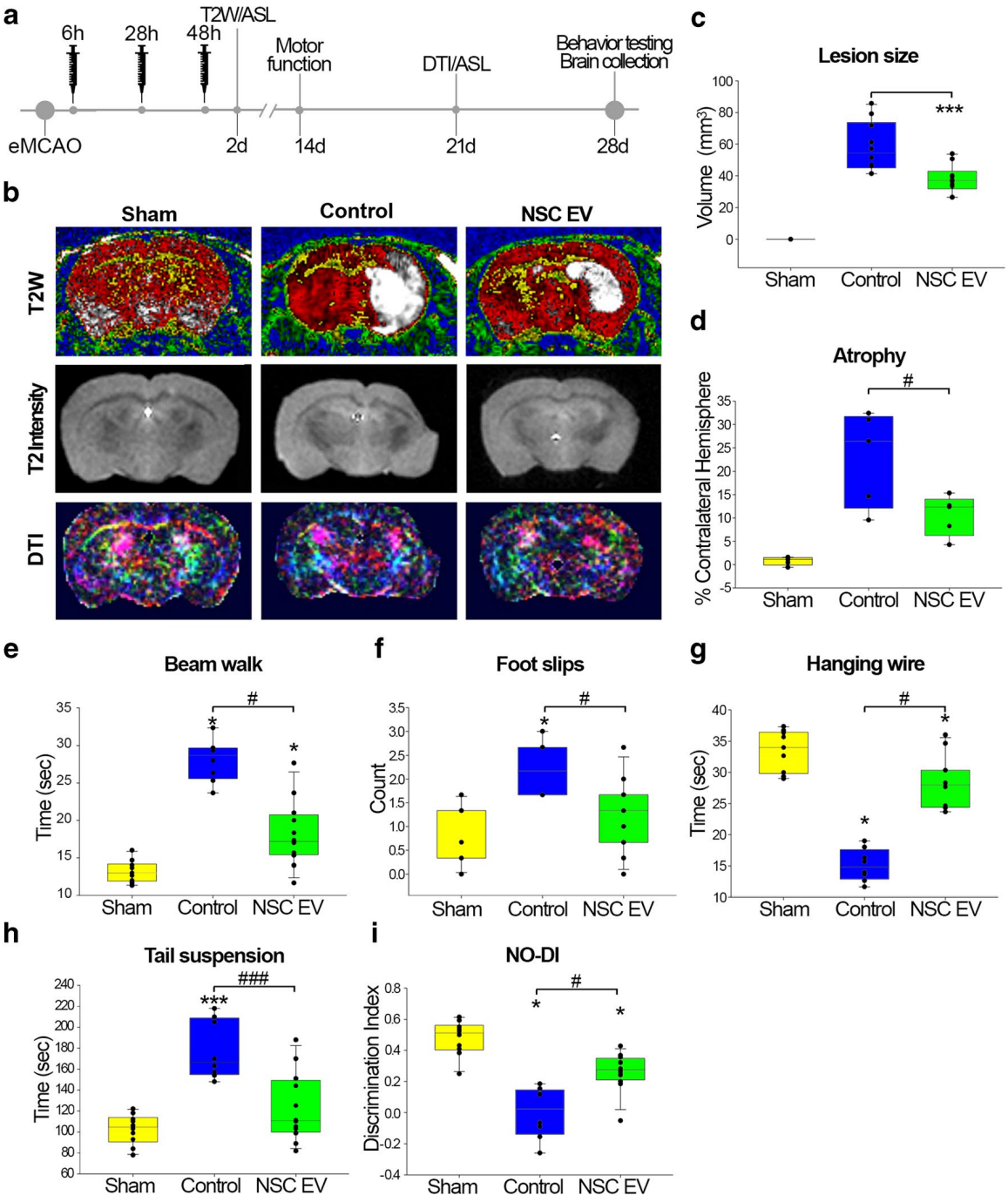
a
6h
28h
T2W/ASL
48h
Motor function
DTI/ASL
Behavior testing
Brain collection
eMCAO
2d
14d
21d
28d
b
Sham
Control
NSC EV
T2W
T2 Intensity
DTI
c
Lesion size
Volume (mm³)
***
Sham
Control
NSC EV
d
Atrophy
% Contralateral Hemisphere
#
e
Beam walk
Time (sec)
f
Foot slips
Count
g
Hanging wire
Time (sec)
h
Tail suspension
Time (sec)
###
i
NO-DI
Discrimination Index